The Application of Remotely Sensed Data to a Catchment-Scale Nutrient Transport Model

Thesis submitted for the degree of

Doctor of Philosophy

At the University of Leicester

By

Barry Shepherd B.Sc. (London)

Department of Biology

University of Leicester

April 2003

This thesis is dedicated to my gorgeous Suzanne and our two wonderful children Bethany and Hope.

Marriage and parenthood are team efforts, and whilst I have failed badly in both over the last six years there should be two names on the spine of this thesis.

"For nitrates are not the land, nor phosphates; and the length of fibre in the cotton is not the land. Carbon is not a man, nor salt nor water nor calcium. He is all these, but he is much more, much more; and the land is so much more than its analysis. The man who is more than his chemistry, walking on the earth, turning his plough-point for a stone, dropping his handles to slide over an outcropping, kneeling in the earth to eat his lunch; that man who is more than his elements knows the land that is more than its analysis."

John Steinbeck
The Grapes of Wrath, 1939

"Modelling is rather like masturbation – a pleasurable and harmless pastime, just so long as you don't mistake it for the real thing."

Felix Franks
British Physical Chemist

"....our technological successes have simply made us more efficient at being stupid"

John F. Welles
The Survival Advantage of Stupidity, 1984

Abstract

Nutrient transport models are being used increasingly as a tool for the research and management of nutrient enrichment (eutrophication) of freshwaters. Phosphorus is seen as the main cause of freshwater eutrophication. A nutrient transport model was acquired that could simulate the movement of phosphorus through a catchment. The SWAT model from the US Department of Agriculture, Agricultural Research Service, appeared to suit the requirements of a catchment-scale, continual time model that was distributed in nature. It is based on physical processes in order that predictions could be made for land management practices or environmental conditions that had been absent in calibration processes.

Remote sensing technology has the potential to improve on estimates of distributed variables based on spot measurements and interpolative techniques. The initial intention of this project was to estimate several parameters from remote sensing images and use them as input to the chosen nutrient transport model. The SWAT model is only able to utilise mapped data for soil types and land cover. Whilst the latter can be extracted from various remote-sensing devices the former cannot. Synthetic aperture radar (SAR) has the potential to estimate several of the parameters considered influential to the movement of nutrients in a catchment. This study utilised five SAR images to investigate the potential of extracting: (i) land cover data, (ii) soil moisture, (iii) soil surface roughness, (iv) soil organic matter content (v) oilseed rape leaf area index and (vi) oilseed rape biomass. No significant relationships were found between any of the soil parameters and radar backscatter using linear regression. It is thought that this may be due to the excessive moisture levels at the time of sampling, but sampling intensity could also have been better. Likewise no significant relationships were found between the botanical parameters and radar backscatter. Wheat and oilseed rape characteristics were also collected and applied to the MIMICS model to assess the technology of radiative transfer models in the UK. There was a significant correlation between the backscatter values obtained through the MIMICS model and the backscatter from mature wheat to the SAR images to but not to green wheat or oilseed rape.

A land cover map was generated using a multi date composite of three of the SAR images. The images were acquired in May, July and August of 1999. Land-classes were assigned using supervised maximum likelihood estimation (MLE) and unsupervised training. Out of 11 classes of land cover found on the Stonton Brook, 11 were identified using the supervised training and MLE and only seven using the unsupervised training. The former method acquired a total accuracy of 46 % against the latter's 53%. On applying the classification schemes to a field boundary map the total accuracies improved to 58 % and 54 % respectively. Both maps were regarded as moderately accurate and both were used in the SWAT model.

A high frequency instream sampling regime was conducted to measure flow and phosphorus levels within the river to ensure adequate data existed to compare with the modelling output. Flow was sampled every 30 minutes, and total phosphorus was sampled every 3.5-7 hours for the duration of the field campaign. Further meteorological data and field measurements were taken from crops and soils to help in parameterisation of the SWAT model and to assess the potential of remote sensing for the given parameters.

Finally, the SWAT model was chosen to model hydrology and nutrient transport in the Stonton Brook. Three versions of the model were parameterised using collected data and a field map produced from ground survey. Hydrology was modelled inadequately by AVSWAT99, but adequately by AVSWAT2000 and the revised AVSWAT2000 as shown by percent bias (PBIAS) and persistence model efficiency (PME) analyses. Underlying land management and plant growth factors were shown to work inadequately in AVSWAT2000 and supported the revisions made to the revised model. The revised model gave better results in the underlying components but problems still existed. Better flow results were obtained when specifying land cover using maps derived from SAR images. The map produced from unsupervised training attained the best estimates of accuracy using PBIAS and PME, but ironically contained the greatest amount of error compared to the other two maps. SAR-derived land cover data has been shown to be adequate in specifying land cover for catchment scale hydrological modelling.

All three versions failed to model phosphorus transport adequately. All versions overestimated phosphorus loss by at least a factor of two and at most a factor of 13. It is shown that that the overestimation of phosphorus was due to overestimation of mineral and organic phosphorus to surface flow events.

Contents

Acknowledgements

This thesis has been the effort of many more people than are normally involved in a Ph.D. I can only take credit whilst standing besides all those who gave and offered help. I alone take full credit for any errors.

Firstly, I would like to thank my wife Suzanne for her undying support throughout the last twenty years, without which I would never have had the confidence to embark upon a Ph.D. To my parents for life itself, and the family I had so much encouragement from. Also from Suzanne's family – Cindy and Rob for their full encouragement and play time with the kiddies. Thirdly, I must thank David and Andy for the opportunity and trust in me. Special thanks from Suzanne and myself go to Gaynor, David, Maureen, Cathy, Clare, Jon and Tess for their friendship and support during times of stress. Jo, Ben, Emma, Dave, John, John, Ted, Frank, Malcolm, Dave, Munir, Kitaika, Helen, Noosie, Sarah, Geoff, Bev for just being in the lab with a smile and sense of humour. Special thanks go to Gaynor and Rory for their exquisite sense of humour and dedication to pranks. Matt, Shona, Emma, Willem and Gaynor for their diligence in the analyses. Extra special thanks for the dedication shown by Matt for falling in the river as well as sampling it. Special thanks to Steve, Leslie, Penny and Yvonne without whose technical and admin support I would have floundered. To the Geography crew: Marianne, Jane, Kevin, Bill, Jo, Frazer, Tony, Mike, Dave and especially Peter for his advice on RS. Thanks go to Steven Anthony and Paul Quinn of ADAS for their modelling experience. Thanks Jon for the mathematical advice over beers – best way by far! John Cook of NERC for his dogged desire for good photographs. Thanks to Bill, Peter and David of the Environment Agency for their support and guidance and to Nick of Quest Environmental. To Paul for your help in field work and the MIMICS stuff we had a laff over. To the SWAT crew: Jeff, Mauro, Nancy, Srini for the supply of weaponry and patience over my questioning. Special thanks also to the SWAT crew at Silsoe, especially Kannan. I thank Mark and Pat from Royal Holloway for their support in the preceding three years.

Thanks go to NERC and the EA who funded this Ph.D. project under grant Ref GT22/96/EO/3, and the additional money for the extensive fieldwork. Thanks also to the European Space Agency for their generous supply of SAR images under the 3rd Announcement of Opportunity.

List of Figures

List of Plates

List of Tables

Chapter 1 Introduction

1.1 Study Overview

Water is one of the most important considerations in human health, welfare, development and maintenance of nations (OECD, 1982; ICWE, 1992; The World Bank, 1993). Clean available water is required to maintain and improve economies and to alleviate poverty in developing nations. Freshwater is already a heavily pressurised resource throughout the world, and is potentially a source of conflict between interested parties whose borders the resource crosses (OECD, 1982; ICWE, 1992; The World Bank, 1993; Newson, 1996). Further pressures only add to the current concerns on the provision of freshwater. Nutrient enrichment or eutrophication is one of the most problematic factors affecting water quality and availability of this invaluable resource. Eutrophication has been declared an environmental problem of "major concern" (OECD, 1985; EEA, 1995; EEA 1999; EA, 2000). Although it has been identified as a growing problem in many countries and action taken to mitigate the problem (ICWE, 1992; Harper and Pacini, 1995; Tim, 1996a), Withers *et al.* (2000) have reported that the number of UK rivers, canals and lakes sensitive to eutrophication nearly doubled between 1994 and 1998.

Intensive agriculture is considered one of the main causes of eutrophication (De Willigen *et al.*, 1990; Heathwaite *et al.*, 1990; Golterman and de Oude, 1991; Burt and Heathwaite, 1993; Morse *et al.*, 1993; Moss *et al.*, 1996; Gibson, 1998; Haygarth and Jarvis, 1997; Sharpley *et al.*, 2000; Withers *et al.*, 2000). Mitigation of the problem therefore must include close scrutiny of agricultural land and practices and subsequent action if rivers and lakes are to be returned to more natural nutrient levels. A river system involves the whole of the catchment area and large-scale modelling of the hydrology and nutrient transport of catchments needs to be investigated for this purpose. Large-scale models require widespread data collection and remote sensing can provide such data (Schultz, 1988; de Jong, 1994; Beven, 1996; de Troch *et al.*, 1996; Tim, 1996a). This project describes the use of a catchment-scale nutrient export model parameterised with remotely sensed data and field survey data for a catchment in lowland UK. The model is based within a geographic information system (GIS) for efficient data management which also allows better visual representation of the system modelled. This project involves one piece of experimental work on the modelling process with several other areas of work that contain their own analyses.

1.1.1 What is eutrophication?

The Environment Agency (EA) defines eutrophication as:

> *"The enrichment of water by nutrients, stimulating an array of symptomatic changes including increased production of algae and/or higher plants, which can adversely affect the diversity of the biological system, the quality of the water and the uses to which the water may be put"* (Environment Agency, 2000).

There are extensive reviews of eutrophication in Golterman and de Oude (1991), Harper (1992) and Harper and Pacini (1995). Nutrient enrichment can occur naturally (Odum, 1971), and over the short term can have desirable effects such as increased productivity (Golterman and de Oude, 1991). Natural systems have an inherent resilience to perturbations including those created by nutrients. Self-purifying processes occur in river and lake systems (Fox and Malati, 1985; Moss *et al.*, 1988; Elosegui *et al.*, 1995), but they are limited in their capacity to utilise large amounts of additional nutrients or xenobiotics either as acute or chronic events. Rivers that have naturally low nutrient levels of around 10μg P l^{-1} (oligotrophic) will adsorb or utilise added nutrients quickly and efficiently without significant effects. If nutrient input is maintained or levels are already high; in excess of 100μg P l^{-1} (eutrophic), the river system will be limited in its ability to fix further additions of nutrients and will become incorporated in excessive planktonic algal growth (McColl, 1974). Systems with intermediate levels of nutrients (60μg P l^{-1}) are termed mesotrophic (Fox and Malati, 1985). The above values defining the various trophic levels of rivers systems have been taken from Moss (1988) but are accepted as being somewhat arbitrary. P-levels as low as 47μg P l^{-1} have been measured in rivers showing signs of eutrophication (McGarrigle, 1993)

Eutrophication is the term given to nutrient enrichment associated with anthropogenic activities and can have deleterious effects on water quality, ecosystems and aquatic management. Nutrient enrichment is not in itself limited to aquatic environments. Any ecosystem that undergoes an increase in nutrients that is then monopolised by a few species to the detriment of others is considered enriched. Effects of aquatic eutrophication occur in three sectors:

1) Ecological

2) Recreational

3) Water resource

Although lake eutrophication has received more attention than river eutrophication, rivers are more widely affected than lakes (Harper, 1992). The effects are similar in both rivers and lakes but are expressed more dramatically in lakes due to the still water and lack of purging during high flow. River communities of plants and animals that are associated with the lower stretches tend to be found further upstream in eutrophic conditions (Hynes, 1969 in: Harper, 1992). Aquatic eutrophication is manifested in the direct effects on primary producers with secondary repercussions expressed throughout the rest of the ecosystem (Harper, 1992). The first direct ecological effect of aquatic eutrophication is an increase in algal biomass, which is followed by a shift in algal population composition (Golterman and de Oude, 1991). This latter point is caused by the release of the flora from nutrient-limited growth and competition (Odum, 1971). Diatoms, Cyanobacteria and unicellular green algae start to dominate and are more tolerant to low light and oxygen levels (Harper, 1992). They are also smaller than flora associated with oligotrophic or mesotrophic waters and are not so readily grazed (Brook, 1964). In chronic cases of lake enrichment, the eukaryotic algae are dominated or replaced by the prokaryotic Cyanobacteria.

Secondary effects are caused by the shift in algal species as a food source, and the effects of increased primary biomass. Increased biomass of the nuisance species of algae increase turbidity of the water and reduce light penetration of the water column. Mineralisation of decaying bloom species also increases, thus raising the biological oxygen demand (BOD) through the respiration of the decomposition bacteria. This causes a reduction in oxygen near the bottom of the river and in the slower river stretches, and especially so at night when photosynthesis does not occur. The most important of the secondary effects is the reduction in biodiversity of the flora and invertebrate and vertebrate communities (Brooks, 1969): macrophyte plant species decline through reduced light and oxygen levels; certain zooplankton species favour the change of available algal species but to the detriment of other zooplankton species, and this leads to a decline in food availability for most invertebrate and fish species. Reductions in macrophyte numbers and diversity will also reduce the niches available for invertebrate and fish species and further declines will occur (Golterman and de Oude, 1991). Many invertebrates and vertebrates found in oligotrophic rivers are intolerant to low oxygen levels and those that are become more dominant. Dominance of chironomid midge larvae and oligochaete worms (bloodworms) are indicators of advanced eutrophic conditions (Harper, 1992), combined with losses of snails and damselfly species (Moss, 1988). Effects in the vertebrate communities can be seen through the replacement of game fish e.g. trout with coarse fish species such as carp (Brooks, 1969; Golterman and de Oude, 1991). Although the repercussions of reduced fish diversity have been demonstrated in the bird communities associated with lakes in other parts of the world (Harper, 1992), similar effects have not been reported in the UK. Water shrews (*Neomys fodiens*) and water voles (*Arvicola terrestris*) require clear and clean water in the rivers they inhabit. Habitat losses through increased turbidity have been shown to be a component of their decline in the UK (Anon., 1984; MacDonald, 2001).

In lakes and rivers certain planktonic algae such as *Mycrocystis* and *Anabaena* genera can bloom under extreme conditions of eutrophication and release toxic secondary metabolites into the surrounding water. These secondary metabolites become problematic to fish and mammalian species (Golterman and de Oude, 1991; Harper 1992; Lee, 1992; Bowling and Baker, 1996). Although Golterman and de Oude (1991) do not consider this a significant ecological effect, it could have dire repercussions on rare mammalian species in the UK such as otters (*Lutra lutra*) (R. Strachan, WildCRU, Oxford University).

Eutrophication can affect the use of river systems for recreation (Campbell and Whitney, 1970). Changes in fish communities have impacts upon the use of rivers for angling. Fish species of the Salmonidae family such as brown trout (*Salmo trutta*) and grayling (*Thymallus thymallus*), associated with clear, oxygen-rich lowland rivers have financial implications for rivers. Their replacement with coarse fish species such as carp (*Cyprinus carpio*) and tench (*Tinca tinca*) that have resilience to low oxygen levels, will alter the economics of sports fisheries owners or managers (Brooks, 1969; Sharpley and Rekolainen, 1998; Uunk, 1991). Additionally, mats caused by blooms and turbidity are unsightly and can smell, thus reducing the aesthetic quality of rivers (Sharpley and Rekolainen, 1998).

Water resource managers have to contend with the quality of river water from the paradoxical uses of potable water and as a waste sink: they are at the same time polluting the river and cleaning the water (Gill, 1996). As eutrophication increases so does the needs of cleansing, placing more pressure on filtration systems and thus raising costs (Moss, 1988; Uunk, 1991). Taste and odour of water is affected and requires rectifying. Extraction licence-owners pay for a certain quality of water, and water from eutrophic systems can fall below their requirements (Gill, 1996).

1.1.2 Nutrient elements and compounds

Factors that affect the growth of plants are light, temperature and nutrients (Golterman and de Oude, 1991; EA, 2000). When one or more of these are in short supply and restrict growth, it is termed the limiting factor (Moss, 1998). This would be light or temperature in temperate climates in late early spring, autumn, and winter. Otherwise the limiting factor is often a nutrient. Approximately 15 elements are required for plant growth. The main ones are: carbon, hydrogen, oxygen, nitrogen, sulphur, phosphorus and iron (Golterman and de Oude, 1991). Carbon, hydrogen, oxygen, sulphur and iron are normally available in quantities in excess of the needs of plants. In certain ecosystems silica (Si) can be limiting during a diatom bloom (Heathwaite *et al.*, 1990; Harper, 1992; Foy and Withers, 1995), but the most commonly considered limiting nutrients are nitrogen (N) and phosphorus (P). P is generally considered to be the most limiting in freshwater systems whereas N becomes more important in marine systems (Thomann and Mueller, 1987; Sharpley and Rekolainen, 1998). It is more often their absolute quantity or ratio of the two that is the limiting factor to plant growth (Elser *et al.*, 1990): P is accepted as the limiting nutrient when the N:P ratio exceeds 16 (OECD, 1982). N may be the limiting nutrient when the ratio is below this level. Alternatively, McGarrigle (1993) suggests that rivers are at risk from eutrophication when the level of P rises above 47μg P l^{-1}. The EU has proposed to reduce nutrient inputs through the Urban Waste Water Treatment Directive (UWWTD) and defines rivers as eutrophic when they contain a mean reactive P content of 100 μg P l^{-1}, and when there are ecologically sensitive areas downstream. N is not usually considered in eutrophication control because it is seldom the limiting nutrient and nitrogen fixation and atmospheric exchange makes it difficult to control its availability. Therefore most emphasis has focused on P as a nutrient when considering eutrophication (Sharpley and Rekolainen, 1998), and therefore P will be the focus of this project.

P exists in soils in organic and inorganic forms. The inorganic forms are normally associated with aluminium (Al) or iron (Fe) hydroxy phosphates in acidic soils or calcium (Ca) compounds in calcareous soils (Brady, 1990; Sharpley and Rekolainen, 1998). Organic forms are incorporated into plant and animal debris comprising nucleic, humic and fulvic acids, phospholipids and inositols (Sharpley and Rekolainen, 1998). Some forms are fixed and therefore biologically unavailable through strong chemical bonds with ions of Al^{3+}, Fe^{2+} or Ca^{2+} (Holtan *et al.*, 1988). Other forms of P remain available for plant uptake. Over time fixed forms of P will become biologically available when less strongly held P is removed from the soil through harvesting, grazing or leaching (Tiessen *et al.*, 1983 in Sharpley and Rekolainen, 1998). Soil particle size is an important factor in the transport of P. Smaller particles of silt (<50μm >2μm) and clay (<2μm) hold more P than larger particles due to the greater number of binding sites, and are also the most mobile (Sharpley, 1985; Sharpley and Smith, 1990). Once in a river or lake the sediments can settle and re-suspend and alter their chemical bonds through mineralisation and become bioavailable (Viner, 1987; Heathwaite *et al.*, 1996; Haygarth and Jarvis, 1997).

Sewage and industrial effluent is the dominant source of nutrients in and near large conurbations, but have only a minor role in rural areas (Lennox *et al.*, 1998; Withers *et al.*, 2000). Even downstream of small STWs, secondary treatment has exacerbated the problem of biological oxygen demand (BOD). STWs mineralise most P species to phosphate in an attempt to reduce the effects of BOD. However, phosphates are directly available to algae and therefore encourage blooms much more readily than the organic fractions present in effluent prior to treatment (Foy and Withers, 1995).

P exists in different forms (fractions) in the water column of a river system. The flux of P in a river is highly dynamic and is controlled largely by the flow regime (Gibson, 1998). Storms will cause a large amount of particulate matter to enter rivers during which particulate phosphorus (PP) will be the dominant form. During baseflow however, soluble phosphorus (SP) is the most dominant form of P in rivers (House *et al.*, 1998). The chemistry of river-P has not been studied on the scale that lake-P has, but slow moving, lower stretches of river are considered to be similar to lakes (Gibson, 1998). Sediments in the lower stretches of rivers however, do not act as a P-sink in the same way that lake sediments do (Holtan *et al.*, 1988), due to the resuspension caused by scouring. P does not move between water and air in the same way N does (Froelich, 1988), and surface water systems can be considered "closed" in terms of P.

P enters a river from soils primarily as ions of inorganic orthophosphate (HPO_4^{2-} or $H_2PO_4^-$) or associated with organic and inorganic particulates (Holtan *et al.*, 1988; Heathwaite, 1998). The organic forms are most often associated with humic acids and phosphate esters (Enell, 1980). According to Holtan *et al.* (1988) PP exists in the following forms:

- Adsorbed exchangeable P
- Organic P
- Precipitates
- Crystalline minerals and amorphous P

Soluble P forms are orthophosphate, inorganic polyphosphates (includes detergent P) and organic P compounds (Holtan *et al.*, 1988). Once in a river the various forms of P will change as settlement, resuspension and sorption reactions occur (Froelich, 1988). P readily interacts with particulate matter and can be taken up and released through sorption reactions thus moving freely between particulate and soluble forms (Froelich, 1988). Movement of P between the soluble and particulate forms are in continuous state of flux and are partly controlled by pH and geology of the catchment. In acidic rivers P-compounds will be strongly bound to particulates, whereas in basic waters P will form with calcium complexes and precipitate out of the water column (Heathwaite *et al.*, 1996). Organic P can be released from organic matter to inorganic forms through hydrolysis, and inorganic dissolved P can be released through mineralisation (Holtan *et al.*, 1988). Oxygen availability near the sediments controls the rate of decomposition and thus release of inorganic P (Heathwaite *et al*., 1996), but biological activity of microbes (bacteria and fungi), macrophytes and phytoplankton will also remove P temporarily from the water column only to be returned on senescence of the organisms or through excreta from grazers and predators.

1.1.3 Nutrient sources

In the past, the largest proportion of P came from anthropogenic effluent sources, primarily human excreta and detergents (Owens and Wood, 1968; McGarrigle, 1993; Harper, 1992; Harper and Pacini, 1995). Although large reductions of P in effluent have been achieved through reduced detergent-derived polyphosphates (Sharpley *et al*., 1994; Higgs *et al*., 2000), effluent is still the largest supplier of P to surface water in the UK (Withers, 1994). However, effluent input to river systems comes largely from conurbations and industrial areas but eutrophication has increased in the last 50 years even in deeply rural areas (Sharpley and Smith, 1990; McGarrigle, 1993). Stripping of phosphate at sewage treatment works (STWs) is only viable in areas at risk from the effects of eutrophication but the problem still persists (EA, 2000). Increasingly, intensified agriculture is being held to blame (De Willigen *et al*., 1990; Heathwaite *et al*., 1990; Burt and Heathwaite, 1993; Morse *et al*., 1993; Moss *et al*., 1996; Gibson, 1998; Haygarth and Jarvis, 1997; Sharpley *et al*., 2000; Withers *et al*., 2000). Chiaudani and Premazzi (1988 in Heckrath *et al*., 1995) and Withers (1994) indicate that between 35 and 40% of P entering UK surface water comes from agriculture. Subsurface drainage alone has been shown to contain enough P to raise the trophic status of receiving waters above the accepted threshold of 100μg P l^{-1} (Sharpley and Smith, 1990; Heckrath *et al*., 1995; Haygarth *et al*., 1998).

The natural background inputs of P from rivers and wind erosion are minor by comparison with anthropogenic inputs (Newman, 1995; Gibson, 1998; Russell *et al*., 2001), and are outside of human control (Sharpley and Rekolainen, 1998). Large but acute discharges can occur through accidental spillages of agricultural or industrial origin (Haygarth and Jarvis, 1998). All of these factors are minimal nationally and outside direct control and must therefore be seen of incidental interest.

Soil P taken up by crops and livestock is removed by harvesting and needs replenishing on a regular basis to achieve and maintain high modern yields. The application of manures and artificial fertilisers to the land has intensified accordingly over the last forty years. P levels in the soils have approached saturation in many areas in the last decade and phosphorus transport (PT) has increased (Foy and Withers, 1995; Haygarth and Jarvis, 1997; Haygarth *et al*., 1998). Morgan (1998) and Brookes *et al*. (1998) report that P has a low uptake by crops (25% or less) when compared to N or K (up to 80%). Sharpley and Rekolainen (1998) contradict this by suggesting that P uptake is between 56 and 76%. If the former is true it explains why P still needs to be applied even though soil P may be at or near saturation (Preedy *et al.*, 2001). Unfortunately there is also an abundance of anecdotal evidence of poor manure and slurry application practice (Preedy *et al.*, 2001). Farmers have limited storage space for farmyard slurries and manures and suitable weather for spreading is limited. Often a farmer will dispose of the excess on land in sub-optimal conditions and in excessive amounts (Preedy *et al.*, 2001). Additionally, slurries and manures are highly variable in nutrient content and are seldom tested prior to application (Sharpley and Rekolainen, 1997; Heathwaite, 1997). Slurries and manures contain large quantities of soluble P, which is more mobile than PP, and can also seal the soil surface thus increasing the potential for P mobility (Withers *et al.*, 2000). Contrary to that, Withers *et al.*, (2001) have shown that sludge and slurry are more readily adsorbed onto soil particles and can reduce P loss when used in accordance with good practices. In addition to animal waste management, soil tillage regimes and cropping are instrumental in PT. If soils were not repeatedly exposed and worked during adverse weather periods, raindrop detachment and soil surface erosion would be greatly reduced (Young and Wiersma, 1973; Reid *et al.*, 1990; Djodjic *et al.*, 2002). Alternative methods of soil management can reduce erosion and nutrient losses (Reid *et al.*, 1990).

1.1.4 Phosphorus transport

P enters water bodies through diffuse and point sources. Diffuse sources are those that are difficult to pinpoint such as subsurface leaching, or indiscrete surface flow. Point sources are those that form obvious discharges to a channel such as effluent exiting through drainage channels or pipes. Point sources have received more attention in terms of research and regulation because they are so identifiable and often easier to control (Heathwaite, 1998). The more familiar sources are shown below in the two categories:

<u>Diffuse sources</u>

> Leaching, artificial tile drainage surface flow, atmospheric, sprayed fertiliser applications*

<u>Point sources</u>

> Farmyard spillages*, cesspool/cesspit leaks*, accidental road spillages*, effluent outfall, urban surface water runoff

* indicates accidental that cannot be predicted nor easily quantified.

Artificial tile drainage outfalls and concentrated channelled surface flows are identifiable point sources but are multiple and considered to be diffuse. Effluent P is well quantified through discharge licensing and is controllable. It has been reduced in the last thirty years through reductions in detergent P. Further reductions through P stripping are economically unviable except where rivers are very sensitive (Sharpley *et al.*, 1994; EA, 2000). Nutrients from agricultural sources are therefore of major importance and are controllable through management techniques. Various hydrological, biological and physico-chemical mechanisms determine the transport of P from agricultural land to watercourses and these are summarised in Figure 1.1 and 1.2.

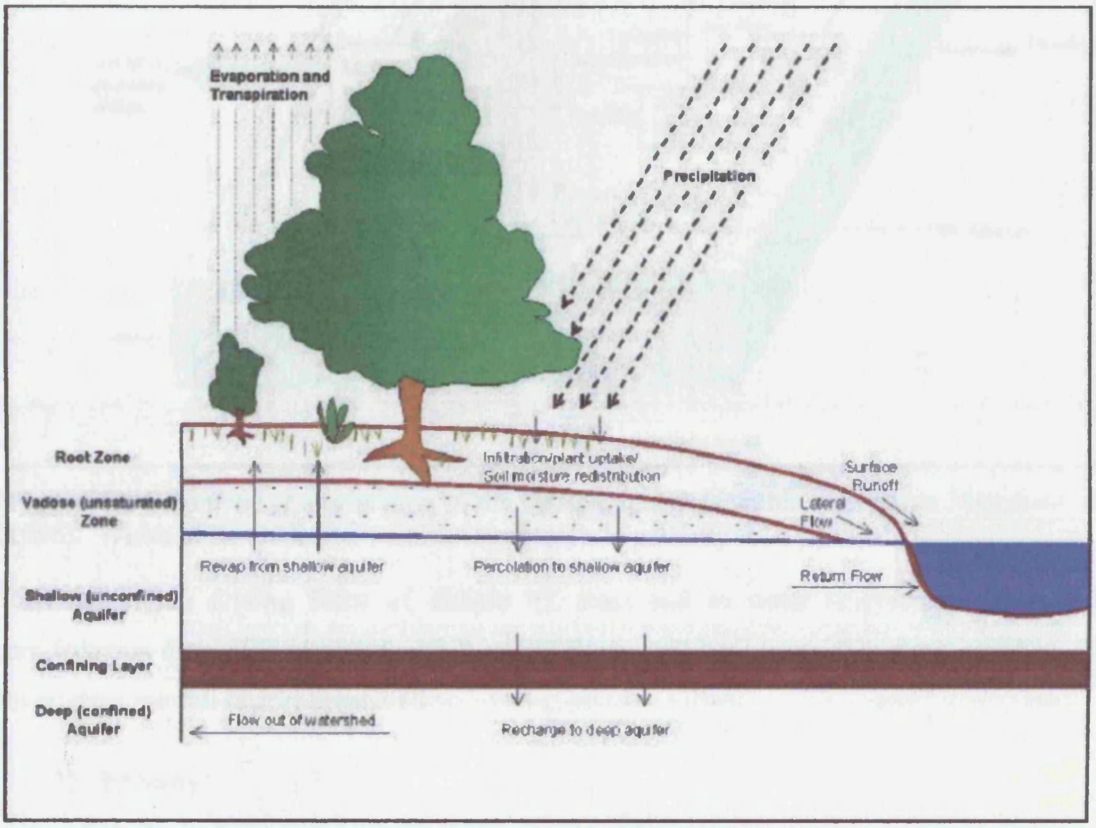

Figure 1.1 Schematic representation of hydrological processes (from Neitsch *et al.*, 2002a)

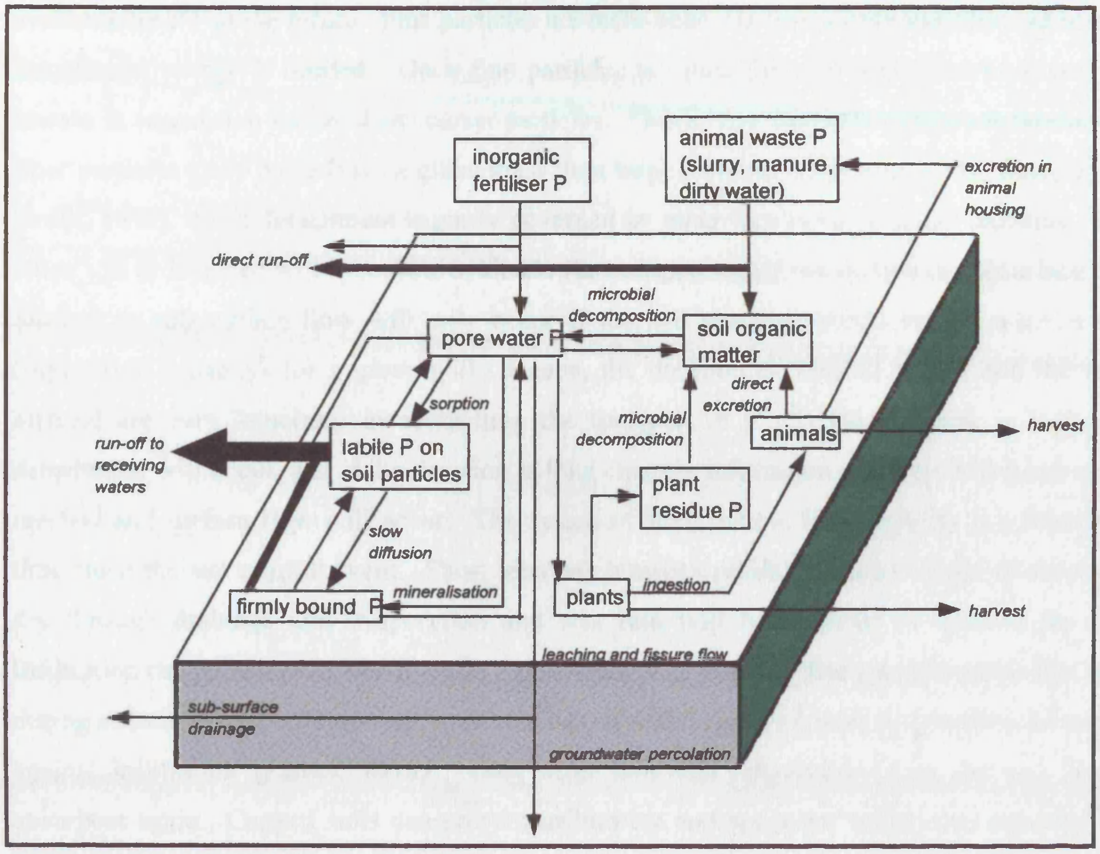

Figure 1.2 Schematic representation of the phosphorus cycle within soils (from Mainstone *et al.*, 1996). Width of line indicates relative importance of pathway.

The underlying driving force of diffuse PT from soil to water is precipitation. Without precipitation even soils saturated with P on hill slopes will not convey P to rivers or lakes. Three overriding rainfall factors govern PT:

1) Intensity

2) Duration

3) The time between rainfall events

These three factors are interrelated and combine to characterise the amount of water moving through the catchment at any one time.

The predominant pathway of diffuse PT is the flow through (preferential) and over the soil during short intense storm events (Sharpley and Smith, 1990; Heathwaite, 1998; Sharpley and Rekolainen 1998; Turner and Haygarth, 2000). Soil particle detachment is dependent on rainfall intensity (Young and Wiersma, 1973). A threshold level of energy is required to detach soil particles from the soil matrix of a given soil and become mobilised. The extreme weather systems that are prophesied in conjunction with global climate change may increase the energy available for PT in the future. Fine particles are more cohesive than larger particles and so more detachment energy is needed. Once fine particles are detached and mobilised however, they remain in suspension longer than coarser particles. This is very important when considering PT; finer particles carry more P for a given mass than large particles (Sharpley, 1985; Sharpley and Smith, 1990). Such detachment is partly governed by other factors such as soil moisture. Only when soil is detached will it become available for transport either via surface or subsurface flow. Surface or sub-surface flow will only occur if the soil moisture levels exceed a given level (infiltration capacity) for a given soil. Hence, the duration or rainfall events and the return interval are very important in controlling the transport of P. If the intensity is high more detachment will occur, and if the duration is long enough, infiltration capacity of the soil will be reached and surface flow will occur. The deficit of water below field capacity is a function of time since the last rainfall event. Short intervals between rainfall events will not allow soils to dry through drainage and evaporation and less rain will be required to saturate the soils. Infiltration can be compromised by soils prone to capping whereby fine particles carried by water during a storm settle on the surface once rain has subsided and are baked, thus sealing the surface against infiltration (Farres, 1978). Only after thorough rehydration does the soil become absorbent again. Capped soils can prevent infiltration and apparent "infiltration capacity" will occur much sooner than if the soil was not capped. Once rain has fallen it will follow one of four possible routes depending primarily on the water content of the soil:

1) Evaporation from the soil surface as a loss to the system. Surface evaporation depends on the soil characteristics, surface texture and air conditions over the soil. Crop cover will influence the air immediately above the soil by affecting airflow, temperature and humidity.

2) Infiltration will occur if the soil is below field capacity in the deeper layers and above field capacity in the upper layers or if flow has been generated within the matrix.

3) Percolation will occur once infiltration has begun and the top layer of soil has reached its own infiltration capacity has.

4) Ground water flow can occur in horizontal or vertical directions. Water can then travel vertically or horizontally through the soil matrix. Given suitable underlying geology it may percolate into subsurface storage reservoirs such as aquifers.

5) Evapotranspiration through uptake via plants and a loss from the system to the air. Only when the soil moisture has reached a certain level - wilting point, will it become available as uptake to plants.

6) Surface flow over the soil if the soil-water reaches field capacity or the soil is capped.

Evaporation, evapotranspiration and subsurface reservoir losses are significant factors that reduce the amount of water in soil. Dingman (1994, in Neitsch *et al.*, 2002) estimated as much as 62% of all precipitation is lost from the land to the air. Thus evaporation is the largest process that influences the point at which field capacity is reached and thus significant flow will occur.

It is accepted that surface flow is more important than subsurface flow for PT (Holtan *et al.*, 1988; Kronvang, 1990; Heathwaite, 1998; Sharpley and Smith, 1990; Sharpley *et al.*, 2000; McDowell *et al.*, 2001; Russell *et al.*, 2001). In the past more emphasis was placed on surface flow than subsurface flow on the perception that P was fixed in the soil and that sediments were not transported through the soil (Cooke, 1976; Dam Kofoed, 1985; Kronvang, 1990). There is growing evidence however, showing that subsurface flow can contribute significantly towards PT (Turner and Haygarth, 2000; Russell *et al.*, 2001). Sharpley and Rekolainen (1998) show that artificial drainage flow will be the dominant pathway where field drains are widely used in a catchment. Conversely, Kronvang (1990), Heckrath *et al.* (1995), Chambers *et al.* (2000), McDowell *et al.* (2001) and Russell *et al.* (2001) show that artificial drainage reduce the interaction time between water and P, and increases the potential for subsurface flow. They also concede that artificial drainage will reduce surface flow and provide a net reduction in PT. Haygarth *et al.* (1998) and Simard *et al.* (2000) found that P was concentrated in the top few centimetres of soil under permanent grassland and did not migrate downwards. Surface or near surface flow would therefore be the predominant pathway for PT under these conditions. Clearly more work is required to assess subsurface flow but it is likely that many factors govern the segregation of subsurface PT and surface PT. Lysimeters are often used to study the export of water borne P. Whilst they remove many of the variables and heterogeneity found at the plot, field or catchment scale, it must be appreciated that they have flaws and extrapolation to larger scales must be done with caution.

P is transported through and over the soil in particulate (PP) and soluble (SP) forms. Therefore physical and chemical forces act on the potential movement of P through the soil (Heathwaite, 1998; Sharpley and Rekolainen, 1998). Soil chemistry will interact with P and define whether it is available for movement or not regardless of the quantity of P (Heathwaite, 1998). Sandy soils have low P retention capabilities and will release P more readily than clay soils. Conversely, clay soils have a high retention capacity but are more prone to surface flow and erosion. The latter can be affected heavily by preferential flow through macropores, worm tunnels and tile drains if present (Turner and Haygarth, 2000; Simard *et al.*, 2001). Most P in short events is transported as particulate P (PP), which as already mentioned, is not necessarily bioavailable but must be considered in terms of the catchment.

In addition to the above controls, much of what has been found is also dependent on the crop grown. Lennox *et al.* (1998) and Sonzongoni *et al.* (1980) found that large variations in PT occurred within crop groups and within soil groups. Arable cropping was found to have higher export rates than low intensity-grassland, and the same crop over sandy soils produced more P export than clay-based soils (Rekolainen, 1989; Lennox *et al.*, 1998). Pasture is present all year round in permanent systems and protects the soil from raindrop erosion and subsequent mobilisation. It is however prone to trampling and poaching adjacent rivers (Heathwaite, 1998) and can be a prime source of nutrients for export. There may be some autocorrelation here however, since the crops grown are often dictated by the soil type. Crop-associated P-loss is more dependent upon when crops are sowed and how the soil is prepared than any other factor (Catt *et al.*, 1998). Minimal cultivation and maintenance of soil structure by inclusion of crop residues will help reduce P-losses. Soil P will be retained under oilseed rape and field beans by the large amount of residue that remains after harvesting. Autumn sown crops such as winter oilseed rape and wheat will help protect the soil surface during the winter and reduce raindrop erosion. Oilseed rape continues to grow leaves over the winter period (see Chapter 4) and offers more protection than wheat sown at the same time. Although Catt *et al.* (1998) recorded highest values of P-loss from under winter wheat for a particularly wet winter compared to barley, potatoes, and fallow. Conversely, spring-sown varieties such as barley will mean land stays fallow for the winter or in some cases exposed tilled soil. Generally, P-losses are higher with root crops than with arable crops (Withers, 1994). Animals consume between 76-94% of the local crop production depending on location (Sharpley and Rekolainen, 1998). Animal production is therefore responsible for the vast majority of all nutrients entering surface water from agricultural land. Crop-dependent fertiliser applications are important but most crops expected in lowland UK receive relatively similar applications of P (FMA, 1998). Winter varieties can be fertilised earlier than spring varieties and possibly avoid the spring storms. Potatoes and grassland are the exceptions with annual averages of 195 and 21 kg P Ha^{-1} compared to between 51 and 68 kg Ha^{-1} for spring barley and winter wheat respectively (FMA, 1999).

When the P finally enters the river it then becomes exposed to the nutrient spiralling and recycling within the river (Holtan *et al.*, 1988; Edwards and Withers 1998; Gibson, 1998). Settlement, resuspension and P transformation from one form to another will occur. Thus the characteristics of P in the river will change from one point to another (McDowell *et al.*, 2001). During any monitoring or modelling of instream PT these factors must be taken into account.

In addition to the instream problems caused by eutrophication, soil erosion and plant nutrient loss must be considered for agricultural economy and sustainability (Chambers *et al.*, 2000).

Boardman *et al.* (1992) showed that soils in the UK have been eroding at an increasing rate since 1970. Compaction and hedgerow removal are partly to blame (Skinner and Chambers, 1996), but the problem is restricted to certain regions, which includes the Midlands (Boardman, 1992). Soil losses have also been shown to reduce long-term soil fertility and reduce crop productivity (Biot and Lu, 1995). Chemical fertilisers are valuable resources that are exhaustible and need to be conserved where possible (Higgs *et al.*, 2000). Soil P is becoming saturated in many areas of lowland UK and excessive additions of P will only result in waste through surface flow and leaching (Foy and Withers, 1995). Likewise, livestock densities have increased over the last century and the amount of manure available as a resource has grown proportionately. Livestock foods can also be a net import of nutrients to an area rather than local self-reliance of fodder crops. Farm slurry and other animal waste is a valuable resource but can be lost from the land if applied at the wrong time e.g. prior to intense rainfall events. The Ministry of Agriculture, Food and Fisheries (now Department of the Environment, Food and Rural Affairs, DEFRA) issued guidelines on the application of fertilizers with the aim of minimizing losses to watercourses (Foy and Withers, 1995; MAFF, 1991; MAFF, 1993).

Remedial actions regarding eutrophication will therefore have positive repercussions on soil erosion and sustainable use of fertilizers. Conversely, the eutrophication problem cannot be considered in isolation of the above factors and a holistic view of a catchment must be covered as in the managerial framework of Integrated Catchment Management (Tané, 1996).

1.1.6 Controls for eutrophication of rivers

Ideally, remediation would stop or reduce the source of nutrients. By reducing the nutrients entering the water bodies further build-up will be limited. Detergent manufacturers have reduced the amount of P (poly-phosphates) in detergents since the 1970s, thus lowering the total amount entering water bodies via STWs (Sharpley *et al.*, 1994; Higgs *et al.*, 2000). But in many river systems sewage effluent is still the largest source of nutrients affecting eutrophication (Withers *et al.*, 2000). The nutrients contained in effluent are a potential resource that could be scavenged through flocculation after dosing with iron salts in the form ferrous ammonium sulphate (Moss, 1988). The flocculate can be incorporated into the sewage sludge and used as fertiliser. However, recovery is not cost effective and P stripping is limited only to areas considered to be highly at risk from the effects of eutrophication (EA, 2000). Similarly diffuse sources are ideally stopped at source. Many soils are near or at saturation capacity of P and removal from the soil is not an option, reductions in the application of further fertiliser must be seen as a remedial option. In order to do this scientists and land managers must first be in a position to know where there are areas of risk or indeed what the mechanics and main factors of nutrient transport are

(Matthews *et al.*, 1985). Land managers routinely sample soils and fertiliser applications can be targeted to only those areas that need nutrients.

Djodjic *et al.* (2002) gave evidence that P incorporated into tillage regimes allow soil particles to adsorb more P than conventional or no-tillage. Tillage breaks up the macropores that increases preferential flow pathways and incorporation of the fertiliser at tillage encourages P uptake by soil particles. This could however reduce infiltration rates and thus increase overland flow. Such practices must be considered for suitability on a case-by-case basis referring to topography, soil and other factors. Some natural and semi-natural riparian systems protect the water body by trapping nutrients so that fewer nutrients reach the water body (Taylor *et al.*, 1971). Thus buffer zones have been used to control nutrient transport (Lowrance *et al.*, 1985).

The catchment must be studied as a single entity to ascertain whether the main impact of P enrichment is from effluent or agriculture. Thereafter the most suitable methods of control can be identified and considered. The act of managing whole catchment areas however, appears prohibitive. Chambers *et al.* (2000) found that the export of P occurs primarily from very small time periods and Pionke *et al.* (1998) and Russell *et al.* (2001) from discrete areas from within the catchment. The latter has given rise to the Critical Source Area concept. If indeed PT can be controlled by focusing on a small portion of the catchment for short periods of the year it would make PT control much more amenable to land-management. The catchment as a system is a complicated and dynamic one. What methods are there to study it whilst taking into account the effluents, domestic use and agricultural impacts?

1.2 Need for catchment-scale modelling

With the ever-increasing performance of computers and software, the possibilities of mathematical simulation of complex systems have likewise increased. Therefore, greater reliance is being placed upon hydrological models to help in collection of information upon which decisions can be made for the management of water resources (Shaw and Falco, 1990; He *et al.*, 1993; Tim and Jolly, 1994; Refsgaard and Abbott, 1996; Tim, 1996b). The rise of geographical information systems (GIS) has helped in the ability of modelling systems to utilise data due to the ability of GIS to store, manage and manipulate data (Deckers and Te Stroet, 1996). Modelling applications are diverse (pesticide movement, hydrograph production), and used by many disciplines for forecasting future trends and scenarios. As well as predictions for management, they offer cheap, repetitive and non-invasive questioning about hypothetical scenarios and can support education and research into physical processes (Oliver *et al.*, 1990; Shaw and Falco, 1990; Refsgaard *et al.*, 1996; Tim, 1996b). Prediction of the movement of rainwater through a catchment has been essential in water resource management, and has been developed more than most other aspects of catchment modelling, such as the transportation of nutrients and pesticides. The growing concern about agricultural nutrients entering water bodies and causing deterioration in water quality has resulted in the development of nutrient transport models. Nutrient transport within a catchment depends almost entirely upon hydrology (Haygarth and Jarvis, 1998). It is not surprising therefore, that many nutrient models have been described as an integral part of a hydrological modelling system (Nearing *et al.*, 1986; Young, *et al.*, 1989; Thorsen *et al.*, 1996). In practice, hydrological modelling has been more successful than nutrient modelling, and although improvements are needed in both, the latter remains to be adequately validated.

Because the nutrients consist partly of a diffuse, chronic component, the overall impact on a river or lake can only be visualised by looking at the whole catchment over a long period of time. The catchment system includes spatial and temporal variables, and is difficult if not impossible to describe without models (Styczen and Nielsen, 1989). Additionally, almost all variables are heterogeneous in both the spatial and temporal dimensions; lowland-UK being a prime example of this. These factors render it very difficult to assess the mixtures of land use, topography, soil types and other environmental considerations that increase the potential of nutrient loss. Indeed, it has been variability in time and space that have given terrestrial modelling its biggest challenge (Jorgensen, 1994).

There are many nutrient transport models available (Donigian and Rao, 1990) but are they all applicable to any catchment and for any scenario? Development of a new model is a complex task but occurs often to utilise specific databases, or be applied to a specific catchment or operation. Consequently, models may be extremely limited in application. For these reasons models are not ubiquitous in application, and each has its own quirks, assumptions and limitations. Unfortunately, many workers see the periodical publications as advertisement for their models and refrain from reporting any negative characteristics. It is therefore very difficult to assess models by published literature only to get a view of how well models have performed (validated).

The choice of model is very important, and is largely influenced by the reasons for using the model. It should first be determined whether modelling is required at all. Boutwell *et al.* (1985) described a flowchart to help in deciding if a model is required and another to assess whether empirically or physically-based modelling is needed as shown in Figures 1.3 and 1.4.

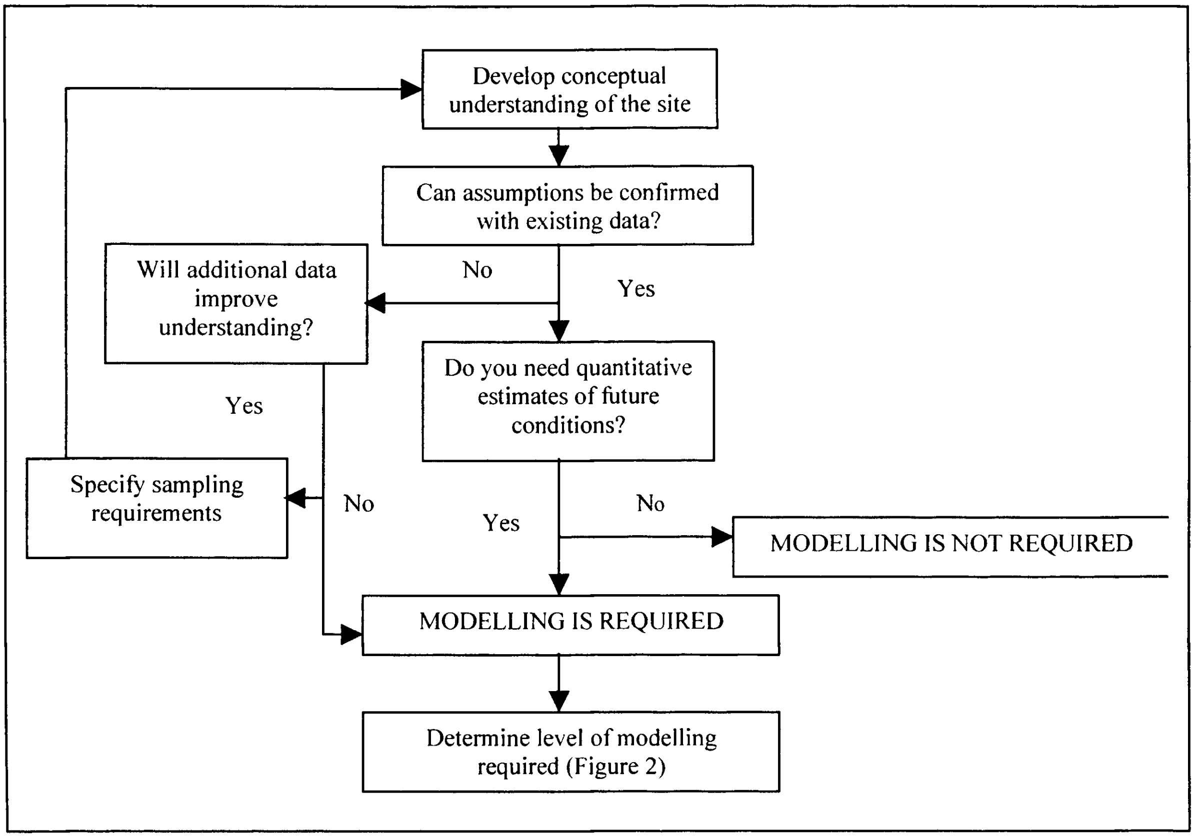

Figure 1.3 Decision flowchart to determine if modelling is required (from Boutwell *et al*, 1985)

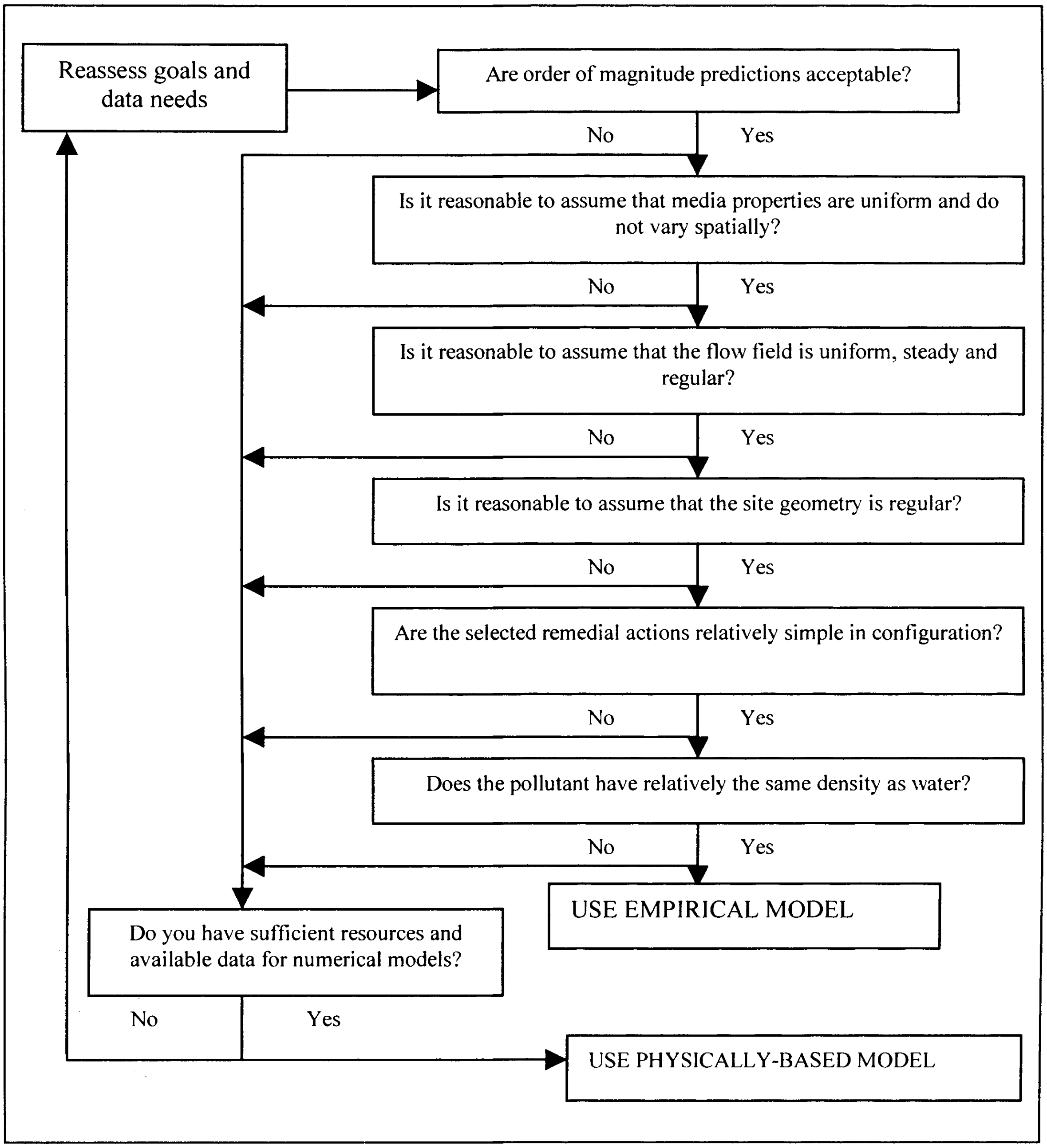

Figure 1.4 Decision flowchart to determine the type of model required (from Boutwell *et al.*, 1985). This flowchart refers specifically to pollutant transport modelling but is also relevant to nutrient transport modelling.

Once it has been established that a model is required and whether it is empirically or physically-based the expected goals of the modelling must be identified. This study is seeking to apply models as catchment management tools, with the following intentions in mind:

1) Apply the model to catchments in lowland England with area greater than 20 km^2

2) Use a model to help in identification of internal processes that affect eutrophication

3) To be based in or linked with GIS

4) To allow parameterisation with remotely sensed data

The above goals together with the catchment characteristics will determine the type of model that is to be employed. This is discussed fully in Chapter 2. The normal procedure for model development and application are as follows:

1) Model conception and production

2) Sensitivity analysis

3) Calibration

4) Validation

The first step is the identification of the components that affect the system to be modelled and the writing of the code. Therefore the hydrological pathways, soil and agronomic processes highlighted in section 1.1.4 above must be represented in mathematical formulae either empirically or physically. Models are tools. For any tool to be used well its mechanisms must be understood and its performance under varying conditions must be assessed. Sensitivity analysis addresses the first of these points whereby the parameters that influence the outcome most from within the model are identified. Normally this is achieved by running many simulations of the model and by adjusting each of the parameters in turn. Some parameters will affect a large change on the model output over small adjustments and are termed the sensitive parameters. Changes in other parameter values will not vary the output at all, even over very large range, and these are the insensitive parameters.

Calibration is a modelling process that has received attention in recent years (Klemes, 1986b; Philip, 1991; Beven and Binley, 1992; Grayson *et al.*, 1992; Beven 1993; Addiscott *et al.*, 1995; Sorooshian and Gupta, 1995; Rykiel, 1996). For certain types of model and for management purposes it is essential to adjust the model output to the measured output. For the physically based models however, calibration may hide certain elements of the model's performance that are useful in the assessment of the model (see review in Chapter 2).

Validation is the continuous application and appraisal of the model. Ideally, the model should be used on several catchments with different data in the course of giving the model credibility (Addiscott *et al.*, 1995; Rykiel, 1995). Some models may perform well under various conditions whereas others may have more specific conditions under which they will work. The issue of scale is highly important here (Jørgensen, 1994). A model that is developed for simulating a field may require information at a sub-metre scale, whereas a catchment scale model may work well with information averaged over the field scale. Data at the sub-metre scale would be too unwieldy to apply across a catchment even if they could be measured accurately. Therefore, models must undergo a period of validation across a range of catchment types, and with varying environmental conditions in order to acquire some idea of the conditions under which they work well (Addiscott *et al.*, 1995).

The first and second stage of the modelling process is more often limited to the scientific disciplines whereas the second is in the realm of the scientists and users. The last process is an ongoing process and therefore a task of the user rather than the scientists.

Catchment-scale modelling is input driven. The quality (accuracy) and quantity (resolution) of that input will affect the model's performance (Klemes, 1986a; van Genuchten *et al.*, 1990; Beven, 1993; Jørgensen, 1994; Tim, 1996a). In the past, point-source measurements have been used for parameterisation of models, even over large geographic areas. Strictly speaking, a model is only as good as its input, but this can be masked as explained towards the end of this section.

1.3 Advantages remote sensing has to offer catchment-scale modelling

Collection of data by point measurements during field survey is limited by resources and does not provide information about the whole area under scrutiny. In addition, interpolative techniques between point measurements can be unreliable. To overcome some of these problems Nearing *et al.* (1989), Young *et al.* (1989) and Arnold *et al.* (1996) suggests that parameter values can be estimated for the Water Erosion Protection Project (WEPP), Agricultural Non-point Source (AGNPS) and Soil and Water Assessment Tool (SWAT) models respectively. Unless very experienced users are involved and know the catchment well, this practice is clearly unsatisfactory. Additionally, some parameters such as soil moisture are so variable in time and space that it is impossible to take point measurements and expect them to apply to the rest of the catchment. Remotely sensed data offers some answers to this predicament in large-scale modelling (Schultz, 1988; de Jong, 1994; Beven, 1996; de Troch *et al.*, 1996; Tim, 1996a). De Jong (1994) highlights the advantages that remote sensing data offer over field survey data:

1) It covers large areas

2) It collects data at regular intervals

3) It has sufficient spatial and temporal resolution

4) It provides data on the required attributes accurately

5) It provides data in a form suitable for further processing and input into GIS and modelling

6) It has cost advantages.

Table 1.1 lists some widely used parameters associated with hydrology that have been successfully extracted from remote sensing data.

Table 1.1 Potential variables measurable with remote sensing data and the sensors used.

Parameter	Platform/Sensor	Method	Key reference
Crop/Land Cover type	AVHRR, ATSR2, CASI	Multi-spectral classification of multi-date data	
Crop/Land Cover type	ERS2 SAR	Maximum Likelihood classification of multi-date data	ERDAS, 1997b
LAI/Ground cover	AVHRR, ATSR2, CASI	Calibration of Vegetation Indices	Elvidge & Chen, 1994
Soil moisture	ERS2 SAR	Integrated Equation Model	Tansey *et al*., 1997
Soil organic matter	CASI		Curran *et al*., 1990
Soil texture*	ERS2 SAR	Integrated Equation Model	Tansey *et al*., 1997
Eroded/non-eroded soil proportions	AVHRR, ATSR2, CASI		Steglik, 1982 and Mather, 1987

*Only possible when fields are bare

Land cover/crop type is the most important of the above for large-scale catchment modelling. It is the vegetation over the soil that determines the amount of energy falling on the soil for particle detachment (Young and Wiersma, 1973), and evapotranspiration. Soil moisture is also important, as it is the level of dryness that determines the probability of surface flow. Soil moisture retrieval by remote sensing however, is limited to bare or lightly vegetated soils (Ulaby *et al*., 1990; van Oevelen and Hoekman, 1999). There is a large proportion of bare soil in the autumn that could be used as a basis for the start of a modelling period or to calibrate a spatial model of soil moisture. The other parameters in Table 1 can be used either as additional input to a model or for secondary investigation to runoff and erosion.

This study could not undertake to measure them all. A set of parameters that would be beneficial to the modelling had to be selected and then the technology applied. Synthetic aperture radar (SAR) from the European Space Agency's (ESA) second Earth Resources Satellite (ERS-2) was seen as being the most flexible source of remote sensing data for the following reasons:

1) Data acquisition is almost independent of weather conditions and solar illuminance

2) Synoptic coverage of relatively large geographical areas

3) That it makes repeat passes using the same track every 35 days

4) It has the potential to detect vegetation and soil parameters relevant to hydrological and nutrient-transport modelling

5) The availability of images under the European Space Agency's 3rd Announcement of Opportunity (AO3) in 1997

To ensure that there are advantages in using remote sensing data, there are two ways in which it can be checked:

1) Comparison between ground surveying and remote sensing data

2) Comparison of predictive modelling output between model parameterised with ground survey data and model parameterised with remote sensing data

Option two is the most appropriate for the PT modelling but the remote sensing data will have to be assessed independently on the chance that the modelling is not successful. Option 1 is essential in case big differences exist between interpolated ground survey data and remote sensing data, but the model may not be sensitive enough for such differences to matter, and the remote sensing data may still be a more cost effective method of collection. Additionally, option 1 may not disclose significant differences between the two data sources from across the whole of the surveyed area, but there may be localised differences that affect the output from the model. This could then provide misinformation about particular management practices within a catchment. Over time and repeated validation exercises, these problems will be revealed. But in the short term, the most appropriate methods should maximise the potential to disclose good or bad practises in order to prioritise the allocation of resources for future research.

1.3.1 Model performance assessment

Confidence intervals surrounding predictions from regression analyses are familiar to most users of statistics, but confidence intervals, or some other estimation of error, are seldom reported for catchment modelling (Klemes, 1986; Beven 1993). In order to assess the reliability of the modelling output and the applicability of the algorithms to the system, some quantitative assessment of modelling error is essential (Beven, 1993). Ideally, error assessment should quantify the error within the data used in parameterisation and the error created by the model algorithms. In this way, better understanding of the theory behind the model can be achieved; models can become useful learning tools as well as predictive ones (Brazier *et al.*, 2000). There are several methods available for assessing predictive uncertainty and model applicability. The simplest are those described by Gupta *et al.* (1999) and quantify the proximity of the predictions to the measured data. Gupta *et al.* (1999) found percent bias (PBIAS) and persistence model efficiency (PME) most useful. Percent bias indicates distance between prediction and measured data. Persistence model efficiency compares the observed output with the predictive output of the next time step i.e. a persistence model using the zeroth order. Whilst these methods do not estimate the error within data they provide values that indicate predictive accuracy and are comparable between simulations.

Gardner *et al.* (1981) and Yeh and Tung (1993) demonstrated that sensitivity analysis on its own is inadequate to identify input uncertainty. Only the most sensitive of parameters, i.e. those that have a large influence on the output from the model, are identified in sensitivity analysis. Insensitive parameters with high uncertainty however, may cause more noise and therefore uncertainty in the model predictions than sensitive parameters with low uncertainty (Melching and Yoon, 1999). Methods such as generalised likelihood uncertainty estimation (GLUE) (Beven, 1993), mollifiers (Keyzer and Sonneveld, 1997) and first order reliability analysis (FORA) (Melching and Yoon, 1996) estimate uncertainty of predictive output, but GLUE and FORA also assess uncertainty in the input. All three methods depend on multiple simulations generated by Monte-Carlo or sensitivity analyses. These methods generate large predictive response surfaces from many hundreds or thousands of simulations produced by incremental adjustments in parameters. The Monte-Carlo method can also be used for sensitivity analyses. Depending on their complexity however, some models may not allow easy execution of Monte Carlo simulation. The biggest drawback with these methods is the high numbers of simulations required.

It is unlikely that adequate resources will be available in this project to apply the sophisticated approaches described by Beven (1993), Keyzer and Sonneveld (1997) or Melching and Yoon (1996), unless the chosen model is very small and uncomplicated. Therefore the methods described by Gupta *et al.* (1999) will be adopted to assess the advantages of remotely sensed data over ground survey.

1.4 Research Objectives

The primary concern of this Ph.D. project is to employ remote sensing in the parameterisation of a phosphorus transport model for a small catchment in lowland UK. Success in this area would allow easier and more thorough investigation into hydrological models and the sources of nutrients that affect eutrophication. Individual objectives were:

1) **To establish and maintain an intense river sampling regime for the whole period of nutrient transport modelling. These data will be the benchmark against which the nutrient transport modelling must be assessed.**

2) **To investigate the extraction of vegetation and soil parameters from ERS-2 SAR that could be used in the nutrient transport model.**

3) **To acquire accurate field boundary maps from aerial photography.**

4) **To extract land cover information from the ERS-2 SAR instrument for use as a land cover map in the nutrient transport model and assess its performance.**

5) **To apply a catchment-scale nutrient transport model to a small catchment in lowland UK. The model must undergo sensitivity analyses and analysis of final output.**

Rather than basic or applied research, this study falls within the area of "operational research" (hard systems methods) as defined by Van Beek *et al.* (1996). The basic and applied categories operate on characteristics of the real world and how different methods can be applied whereas operational research focuses on how applications operate within a scientific context and their technical competence.

1.5 Thesis Structure

This thesis is structured logically through the modelling and data acquisition process. Chapter 1 introduces the subject area with reasons for carrying out the research and the objectives of the project.

Chapter 2 describes the philosophy surrounding modelling and current problems facing hydrological and nutrient transport modelling. The various types of model are described with the relevant advantages and disadvantages. Various models are briefly described that have been developed for hydrology and nutrient transport, and the process used in selecting a suitable model. The model chosen for this project is then described in detail pertaining to the hydrological and nutrient transport processes that were described in Chapter 1. Finally, the method of quantitative analysis of the modelling output suitable for the chosen model and this project is described.

Chapter 3 contains details of the Stonton Brook catchment that was chosen as the site for this project. Overall characteristics of the catchment are given in a general description of the catchment and river and include the historical perspective. The details of several pertinent considerations of hydrology and nutrient transport can be found in several sections that include the biological status of the river, human population, climate, geology and land use. Quantitative details of the climate and river hydrograph are given for background to the modelling.

Chapter 4 contains details of all terrestrial parameters that were measured in the field. The parameters involve land use, vegetation and soils. These parameters were used either as input to the nutrient transport modelling or the remote sensing element of this project. A small literature review is presented and full methodology of data collection, storage and subsequent analyses. Small amounts of data are analysed and presented and experiences with the methodology discussed.

Chapter 5 contains details of the aquatic data that were collected. These data were required for a full comparison with the results of the modelling. This chapter gives a review of sampling protocols and requirements of instream data collection. The methodology is fully described together with details of field equipment. The results are presented in full and problems encountered discussed.

Chapter 6 describes additional data collected from third parties for use in the nutrient transport modelling. These data include soils, weather and additional data from the literature that could not be measured during the study.

Chapter 7 describes the method followed for processing aerial photographs and producing a field boundary map. The product is presented along with a digitised field boundary map derived from the aerial photography.

Chapter 8 focuses on all aspects of the SAR remote sensing. It gives an introduction to the theory of microwave remote sensing together with the interactions between microwave radiation and target surfaces. The various methods of information retrieval from SAR data are reviewed and the methodologies used in this study presented. The methods and results are divided into the land use maps that were created for direct input into the nutrient transport modelling and the investigation into the extraction of data that may serve as indirect input into nutrient transport modelling. All results are presented along with subsequent accuracy analyses. Finally the methods used and results obtained are discussed.

Chapter 9 contains details of the nutrient transport modelling starting with a description of the SWAT/ArcView interface (AVSWAT) and building the databases for the modelling. The methodologies of sensitivity analyses of the hydrology component of AVSWAT are described, as are the methods used in analysis of modelling output. The results are broken down into three sections: hydrological results, sensitivity analyses of hydrological component and P-transport. The final section discusses the relevant merits of the model and the relevance of the data used for parameterisation.

Chapter 10 includes an overall discussion and conclusion of the project. It includes positive and negative details about the systems and methods applied, and relates all results to the original objectives defined in this chapter. The final section contains potential future work to enlarge on this study and where improvements could be achieved.

Chapter 2 Review of Modelling and Model Choice

2.1 Introduction

Hydrological and associated modelling has been through a crisis in recent years (Klemes, 1986a; Beven, 1996). The "hydrological" discipline has been stifled by unquestionable acceptance of modelling and the principles upon which they are based. Unscientific but historically accepted physical processes are perpetuated in hydrological and nutrient transport models through ignorance and poor structure of the discipline. It is therefore appropriate to appraise the current status of what has been termed a pseudo-discipline (Klemes, 1986a).

Karl Popper (1959) established the most accepted scientific framework to date: hypothetical deductive reasoning (HDR) (Peters, 1991; Addiscott *et al.*, 1995). The basic premise of HDR is having an idea and testing it out. Testing must be carried out in a fashion so that the hypothesis under scrutiny can be refuted. If refuted the hypothesis can be cast aside. If it is not refuted then it stands to be tested again. Ultimately, hypotheses that are not rejected after having been repeatedly tested (validated) may become laws of nature. Laws are seldom if ever created in ecology and environmental science (Peters, 1991) because of the complexity and heterogeneity of environmental systems of which hydrology and nutrient transport are part (Plate and Duckstein, 1990; Jørgensen, 1994). Addiscott *et al.* (1995) suggests that forming an idea; forming a hypothesis; proposing a theory; or developing a model are "largely similar". This can be true of simple models such as regression, but the more complex models contain several if not many hypotheses. Testing between the output of the system and output of a model is not suitable to test the hypothesis: *"the processes defined within the model reflect the processes within the system"*. This is however how hydrological models are applied, and is an engineering method rather than scientific (Klemes, 1986a; Beven, 1996). It is difficult to ascertain what hypotheses are supported and what refuted, even if the model appears to perform well when judged by comparing measured output against modelling output. Modelling performance must be scrutinised prior to entrusting it in decision-making. Many of the hypotheses upon which models are based are well supported by evidence from experiments using defined and controlled systems such as homogeneous field systems. They are often found to be irrelevant however, when compared to the highly heterogeneous systems more common in nature (Beven, 1989). Alarmingly, Beven (1993) points out that all current hydrological modelling principles can be invalidated, and accepting the output from models is largely an act of faith based on scientific principles. It is therefore imperative that models are tested thoroughly, not just by comparing outputs but also by assessing at some stage whether individual hypotheses within the model are supported by measured events.

According to Rykiel (1996) the two main questions that must be asked of models are:

1) Is the model acceptable for its intended use?

2) How much confidence can be placed on its reflectance of the system?

The first question concerns the process of validation of the modelling output and can be legitimately outside of the realms of science if used for management purposes. The second is the scientific hypotheses concerning the principles upon which the model is based. Engineers and water quality managers will require accurate predictions from any means, regardless of the modelling principles. They will not need to apply scientific principles and provided that is acknowledged the model details are irrelevant. Klemes (1986a) and Beven object to the application of engineering principles in place of scientific and in the scientific arena the modelling details do matter.

2.1.1 Purposes of models and their limitations

There are three reasons for using models (Klemes, 1986b; Beven, 1989):

1) They predict the behaviour of a system.

2) They investigate assumptions made about the real world. Processes assumed to be relevant and included in the model could be further investigated by using the model across a range of scenarios.

3) They predict the response of a system to perturbations.

The most important role for a model is to predict a system's response (to forecast) within the limits imposed by the development of the model. The second is used to assess the scientific theory behind the modelling mechanisms. In this way it could be used for education and research. Lastly, to investigate a response of a system outside of its developmental "experience" i.e. conditions that were not witnessed or measured during development of the model.

The very definition of a model is a simplified representation of a system, either mathematically or logically. The main problem with model performance however, is that with some tweaking of the parameters (calibration), the predictive ability of a model can be made to look good, and it is near impossible to say whether the mechanics represented by the model are true to the system. Klemes (1986a); Beven (1989), and Wheater *et al.* (1993) stated that models can and do give the "right results for the wrong reasons". Additionally, computer performance has allowed scientists and technicians to run complex model simulations without the means to fully understand the model and its output (Donigian and Rao, 1990). Some detailed examination of modelling output must therefore follow model development.

2.1.2 Model types

Differences of opinion, technical limitations, resource limitations and data availability, has lead to the development of several types of model. The following are the most common types of model in use in hydrology and nutrient transport.

2.1.2.1 Physically-based models

Although all models are conceptual in nature, i.e. an abstraction of a system, some are based upon principles or theories thought to occur within the system. These form some of the most complicated models and are termed physically based or "grey box" models. Physically based models are considered to be the most flexible and powerful (Beven and Jakeman, 1990; Wheater *et al.*, 1993). If the processes upon which they are based are real and most important in the system, then they should perform across systems of the same type, i.e. catchments, and outside of the constraints of data upon which they were built, i.e. catchment or climate change. This has however, been shown to be over optimistic (Brazier *et al.*, 2000). The main drawback with physically based models is that they require measurements of several to many parameters, and therefore are resource intensive (Beven and Jakeman, 1990; Wheater *et al.*, 1993).

2.1.2.2 Conceptual models

Many of the models in use today fall within this category and have also been referred to as "black box models". Some require large amounts of data for parameterisation but all will require data upon which to be calibrated since they do not depict any measurable process. Better calibration will be achieved with increasing amounts of data. The predictive ability is more important than the correct mechanics of the system i.e. generality rather than detail (Wheater *et al.*, 1993; Grimm, 1994). Conceptual models cannot be used outside of the range of data on which the fitting of the model was performed i.e. land use or climate change.

2.1.2.3 Statistical models

Statistical relationships such as those found from regression analyses are models of varying complexity. They range from simple linear regression to generalised additive modelling (Venables and Ripley, 1999). Whilst these serve many purposes they have several limitations: they are limited to the variables upon which they were built and should not be used to extrapolate. If they are, there is great danger that the modelling output will be misleading.

2.1.2.4 Metric models

This most used and successful model in hydrology is the "unit hydrograph". It is a tool that water resource managers have depended on for the last thirty years. Flow is estimated in a river for a given amount of rainfall based on many years of sampling of both rainfall and flow. Therefore each river must be sampled intensively prior to being modelled. It is vulnerable to changes taking place in the catchment and climate and must be treated with caution for long-term simulations (Wheater *et al.*, 1993; Grimm, 1994).

2.1.3 Modelling problems

However good a model is there will always be an element of error. Beven and Jakeman, (1990) lists the error as shown below:

- Properties of the data – this refers to the sampling and measurement error. It includes the quantity of data and the spatial and temporal resolution.
- Model structure identification – is the discrepancy between the principles upon which the model is built and the real world system.
- Parameter estimation method – in execution of the model, parameter values can be extracted from a distribution, which will not always be the appropriate value.
- Algorithm implementation – this is a computerised source of error depending on how the algorithm has been written. Numbers can be rounded for ease of computation and the mathematics may not depict the theory precisely.
- Verification and validation procedure – the amount of data available for the validation procedure can add to the uncertainty of a model's performance. This refers to the future use and validity of a model.
- Future inputs – refers to the inclusion of predicted data in the model. An obvious example would be the results of climate change.

These sources of error are inherent modelling problems that are always going to be present. Hopefully, as our understanding and technology increases some of them will be reduced, but while reliance is placed on models, some attempt to quantify these errors must be made.

Some of the problems already discussed have been partly exacerbated by the practice of model calibration. Under some circumstances, e.g. water management, or types of model, e.g. export coefficient model, this is perfectly legitimate, providing the full assumptions and limitations are acknowledged. But it has been adopted as a standard tool for fitting all models to the measured output. For physically based models it may give a false impression of how well the processes upon which the model is based, apply to the catchment itself (Klemes, 1986a; Beven, 1989). Calibration will also smooth the data and potential information can be lost. If calibration is badly carried out it can lead to the adjustment of parameter values outside of their normal range. Beven (1989) presented several projects that used parameter values outside of their known range. Additionally, it is suggested that all current models are capable of being fitted to measured output through calibration (Wheater *et al.*, 1993). Scientifically this is wrongful practice and a great deal of discussion has taken place in the literature about how this problem can be overcome (Klemes, 1986a; Beven and Jakeman, 1990; Beven, 1993; Wheater *et al.*, 1993; Grimm, 1994; Addiscott *et al.*, 1995; Quinn *et al.*, 1996; Refsgaard and Storm, 1996; Rykiel, 1996)

The above workers agree that the most urgent problem facing hydrological models is overparameterisation. This mainly affects models with high numbers of parameters but certain aspects of this problem can apply to models with only a few parameters also. The net effects of overparameterisation can result in the following:

1) Equifinality

2) Lack of manageability of the data

3) Forces wrongful practices

4) Reduces ability to assess uncertainty

5) Encourages gaps to grow between models and the real world

1) Equifinality

Equifinality is the problem mainly associated with large numbers of parameters but can affect those with low numbers also. The assumption exists whereby each model has an optimum set of parameter values. This optimum set of parameter values can be used to apply the model across catchments. Beven (1993) has shown however, that many models have displayed an optimum set for two different catchments and for different time periods on the same catchment, i.e. the fitting of the model to system output can be achieved with more than one set of parameters. According to Beven (1993) this says very little about the applicability of the mechanics in the model. If the applicability of the model is overestimated due to accurate calibrated output, predictions upon which management decisions are based may be misleading.

2) Lack of manageability of the data

The management resources required to manage a model system will grow with the rise in numbers of parameters. This will impact upon the availability of resources for environmental purposes and possibly lead to an unhealthy dependence on modelling rather than measurements (Philip, 1991). The advent of GIS and better computer performance will however increase our ability to manage high numbers of parameters (Peuquet *et al.*, 1993; Drayton *et al.*, 1992).

3) Forces wrongful practices

Model users will be forced to guess or, at best, estimate many of the parameters, and is suggested as a course of action on the manual for the SWAT model (Arnold *et al.*, 1999). This will of course increase the error associated with the model and increase the need to calibrate. Ultimately the effectiveness of models will be reduced, whether they are bad or good.

4) Reduces ability to assess uncertainty

Models need to be assessed for uncertainty for the act of validation. This will involve either Monte Carlo analysis or some other method involving high numbers of model runs. The more parameters that exist the more onerous the process of uncertainty estimation, and the less likely it is that such methods will be applied on a regular basis. The parameters that affect the modelling output can be identified using sensitivity analyses. Parameters that have a large influence on the output are sensitive and those that have little influence, insensitive. Fixing the values of the insensitive parameters reduces the active parameters and has been termed a "reduction of dimensionality" (Beven and Jakeman, 1990). Out of the 2000 or so parameters found within the SHE model (Refsgaard and Storm, 1996), only 40 or so are sensitive (Beven, 1996)

5) Encourages gaps to grow between models and the real world

Klemes (1986), Philip (1991) and Beven (1993) have outlined the problem that modellers face when they become embroiled in modelling and ignore the real world. If models suffer from the above problems the users will be less inclined to compare the modelling outputs with real world scenarios.

In the recent past hydrologists have included all known information into models (Beven and Jakeman, 1990). Woolhiser *et al.* (1990) suggested that it is the dominant processes that need to be described in a system rather than the micro processes. This will reduce the heterogeneity of some of the more complex models. Thus dimensionality can be reduced and many of the problems associated with it.

2.1.4 Solution to the problems

Firstly, improving the data used for parameterisation can reduce the error. Additionally more research is required to understand hydrological controls and nutrient transport processes. Although there are numerous models available, they should improve over time as knowledge improves.

Advances in technology will achieve better sampling. Remote sensing, automatic sampling and analysis machines will help to collect data more accurately, more often and from more sites. This will improve the quality of data and the quantity. Ultimately it is extrapolation that needs to be reduced and new technology will provide many more measurements and estimations thus reducing our dependency on extrapolation (Peuquet *et al.*, 1993; Drayton *et al.*, 1992).

Although this study is not intending to improve the knowledge of hydrological processes, it will try to improve the data input and the data upon which the model is tested.

All modelling applications need to be assessed for reliability of output and reflection of the system. These methods should become routine so that the output is always questioned. There are several ways of doing this as mentioned in Chapter 1. These methods require large numbers of simulation runs and the means chosen for this study will be discussed later in this chapter.

2.2 Model choice

Current catchment-scale models are far from ideal, but they have a role to play, and only by application and extensive testing will lessons be learned and improvements be made (Beven, 1989). The principal criteria for the model are:

1) Suitable for lowland UK catchments

2) Physically-based

3) Applicable to catchments covering areas of $20km^2$ and greater

4) Distributed output

5) Phosphorus sub-model

6) Cheap to purchase

Using these prerequisites and the information in Table 2.1, a model can be selected for further scrutiny. As already mentioned, all models are conceptual in nature, but the term physically-based will be used here for those models that have been promoted such by their developers. Much of this information has been extracted from Rose *et al.* (1990) and Tim (1996a).

When trying to match the requirements of the study with the above models it becomes apparent that several models will not apply due to scale. There are three models applicable to the field scale and one at the regional scale that can be eliminated. All others have potential at the small scale to which this study is to be applied, but not the large scale. Six remain that are claimed to be physically-based. TOPMODEL was developed for areas with steep gradients and can be eliminated. This leaves only five models; AGNPS, HSPF, SHE, SWAT (US) and WEPP.

Table 2.1 Brief descriptions of some commonly used and documented models potentially suitable for this study.

Model Acronym	**Physical**	**Empirical**	**Lumped**	**Distributed**	**Continuous**	**Event-based**	**Nutrient**	**Scale**
AGNPS Young *et al.*, 1989.	X			X		X	X	Field-catchment
ANSWERS Beasley *et al.*, 1980.		X		X		X		Small catchment
CREAMS Knisel, 1980.		X	X		X		X	Field
GLEAMS Leonard *et al.*, 1987.		X	X		X			Field
HSPF	X			X	X		X	Small to large catchment
IHDM Beven *et al.*, 1987	X			X		X		Hillslope catchments
MINDER		X		X	X		X	Catchment
POPPIE		X		X	X			Regional-national
MIKE SHE Refsgaard and Storm, 1995	X			X	X	X	X	Catchment
Swatcatch Hollis *et al.*, 1995		X		X	X		X	Field
SWAT (USA) Arnold *et al.*, 1996	X			X	X		X	Catchment - catchments
SWRRB Williams *et al.*, 1985.	X			X	X		X	Small catchment – simple catchments
TOPMODEL Beven *et al.*, 1995.	X			X	X	X		Hillslope-catchment
WEPP Lane and Nearing, 1989.	X			X	X			Catchment

Unfortunately, these are quite complicated models and demand large numbers of parameters. During the course of development, the SHE has been diversified into a range of models, of which

MIKE SHE includes a nutrient transport element (Refsgaard and Storm, 1995) but is not public domain and needs to be purchased, the sum of which is outside of this study's budget. The remaining four are public domain and free. WEPP does not contain a nutrient sub-routine and so can be eliminated. AGNPS, HSPF and SWAT are modelling systems that contain nutrient sub-models. AGNPS was developed for simulating the effect of individual events, and is of no use for long simulation runs. Thus HSPF and SWAT remain. The former requires a good understanding of Fortran language and has not been integrated with GIS. The HSPF model is therefore limited in applicability to expert users but is a potential standby should SWAT be unsuitable. SWAT appears to be suitable on first inspection, and unlike HSPF it has existing links to GRASS, ArcINFO and ArcView. It will now be appraised in detail.

2.3 Detailed appraisal of SWAT

A full description of SWAT and its theoretical basis is contained in the User's Manuals (Di Luzio *et al.*, 2002; Neitsch *et al.*, 2002b) and the theoretical document (Neitsch *et al.*, 2002a). SWAT is a logical progression from and amalgamation of other models such as CREAMS, GLEAMS and ROTO developed by the United States Department of Agriculture, Agricultural Research Service (USDA-ARS). It was developed to simulate aspects of land management such as soil erosion and agricultural pollution for large catchments. Dividing the catchment into sub-basins and processing each sub-basin individually limit processing time. Each sub-basin is then individually discretised in a number of ways depending on extent of heterogeneity. Parameter values are stored in database files that are opened as needed and then closed to promote efficient use of computer time. Processes are calculated for homogeneous areas called Hydrological Response Units (HRUs) and then amalgamated through a routing structure. It has a working Graphical User Interface (GUI) and is available for PC, Solaris and IRIX operating systems. To further aid efficient data processing and presentation there is a link programme between SWAT and the GIS systems, ArcINFO, ArcView and GRASS depending on the platform used.

The model looks very suitable and conforms to the basic criteria outlined above. Additionally SWAT has several sub-routines within it for N, pesticides, lake-water quality and crop growth. These are of interest to Water Resource and Land Management. Unfortunately there are 905 parameters used within SWAT (Appendix E). To help overcome the inevitable absence of many measured parameters, SWAT contains many algorithms that estimate values for the user. Solar radiation for example is modelled in SWAT for a given latitude and time of year. Tabular data can be used instead where measured data or estimates are available to the user. Neitsch *et al.* (2002a) suggest that improved reliability and accuracy is achieved when measured data are used. In the following description of the SWAT model, where data are available the corresponding sub-routine for estimating the values will not be described. The description given here is by no means exhaustive but provides an overview of the most pertinent points regarding PT.

2.3.1 Energy

Although gravity is the driving force of hydrological systems, energy in the form of heat and light influence physical, chemical and biological processes such as evaporation, mineralisation and photosynthesis respectively. These processes act as controls on the amount of water flowing through the catchment. Although SWAT contains algorithms to estimate the solar radiation available based on latitude and time of year, it allows direct input of radiation through tables. Solar radiation must be available as MJ m^{-1} and air and soil temperatures in °C.

Water temperature has similar repercussions and if not supplied is estimated using an equation by Stefan and Preud'homme (1993 from Neitsch *et al.*, 2002a):

$$T_{water} = 5.0 + 0.75\overline{T}_{av} \tag{2.1}$$

where T_{water} is the water temperature for the day and T_{av} is the average air temperature on the day. Water temperature is a function of air temperature, solar radiation, water volume and wind speed among others. The SWAT models assumes only the first is significant and acquires it from the maximum and minimum air temperatures that are either input or estimated. Additionally it is assumed in equation 2.1 that lag time is always less than one day.

Wind speed can be input directly (m s^{-1}) and assumes to have been measured 1.7 metres above the ground and without shelter.

2.3.2 Atmospheric water

Precipitation is the driving force and medium of PT through the catchment. Although SWAT contains a rainfall generator it is most important that measured rainfall data be entered (Neitsch *et al.*, 2002a). Other climate data parameters required by SWAT are listed in Table 2.2.

Table 2.2 Climate data used in SWAT

Monthly	Daily	Hourly
Maximum temperature for month	Mean daily rainfall for month	Hourly rainfall
Minimum temperature for month	Average daily radiation for month	
Average wind speed for month	Average relative humidity for month	
No days of precipitation in month	Probability of wet day following a dry day	
Maximum 30 minute storm intensity for month	Probability of wet day following a dry day	

2.3.2.1 Rainfall

Two input options exist for rainfall: daily and hourly. Hourly data are required if the Green and Ampt infiltration model is required.

Maximum half-hour rainfall is calculated from monthly summaries where daily data are used using the following:

$$\alpha_{0.5mon} = adj_{0.5\alpha} \cdot \left[1 - \exp\left(\frac{R_{0.5sm(mon)}}{\mu_{mon} \cdot \ln\left(\frac{0.5}{yrs \cdot days_{wet}} \right)} \right) \right] \quad (2.2)$$

where the extreme monthly values are smoothed ($R_{0.5sm(mon)}$) for a given month using a smoothing equation. Extreme half-hour values for each month are input with the rest of the weather data. If the maximum half-hour rainfall is calculated directly from hourly rainfall data and is a fraction of the maximum hourly data.

2.3.2.2 Water Vapour

Evapotranspiration is estimated using the Penman-Monteith or Priestley-Taylor methods, which require several calculated values e.g. saturation vapour pressure and vapour pressure deficit. These are calculated using standard methods from the values of relative humidity, air temperature entered with the weather parameters. Although SWAT contains a snow component for estimating the water stored in snow-pack, snow is not deemed significant enough in lowland UK to be described here.

2.3.3 Hydrology

Water stored in the soil is represented by the water balance equation:

$$SW_t = SW + \sum_{i=1}^{t} (R_i - Q_i - ET_i - P_i - QR_i) \tag{2.3}$$

where SW is soil water content minus the 15-bar water content, t is time in days and R, Q, ET, P and QR are daily amounts of precipitation, surface flow, evapotranspiration, percolation and return flow all as mm H_2O.

2.3.3.1 Surface runoff

There are two options for estimating surface runoff: SCS curve number and the Green and Ampt method. The SCS curve method was developed for the US and has not been fully developed for the UK although several workers have applied it (MAFF 1999; Morgan, 2001; Swain, 2001; Chaler Navarro, 2002). An extensive collection of graphs for reading SCS curve numbers have been developed in the US for given soil conditions. It is a function of soil permeability, existing soil water conditions and is modified by land use. The Green and Ampt method however uses mostly standard soil parameters and is seen as preferable in this project (A. Parsons, Geography Department, University of Leicester). It is somewhat ironic that the equation used in the SWAT model has been modified and uses the SCS curve number as input. The SCS curve method utilises the following equation:

$$Q_{surf} = \frac{(R_{day} - I_a)^2}{(R_{day} - I_a + S)} \tag{2.4}$$

where Q_{surf} is the rainfall in excess of infiltration (mm H_2O), R_{day} is the rainfall for a given day (mm H_2O), I_a is the initial abstractions and S is a retention parameter. Rainfall is provided by the weather data and I_a is approximated as $0.2S$. The retention parameter S is given by:

$$S = 25.4\left(\frac{1000}{CN} - 10\right) \tag{2.5}$$

where CN is the curve number for the given day.

Alternatively, the Green and Ampt infiltration equation as modified by Mein and Larson (1973 in Neitsch *et al.*, 2002) can be used to estimate surface runoff occurrence and volume. Hourly rainfall data are required for this method.

$$f_{\inf,t} = K_e \cdot \left(1 + \frac{\Psi_{wf} \cdot \Delta\theta_v}{F_{\inf,t}}\right) \tag{2.6}$$

where $f_{\inf}$ is the infiltration rate at time t (mm hr^{-1}), K_e is the effective hydraulic conductivity (mm hr^{-1}) Ψ_{wf} is the wetting front matric potential (mm) $\Delta\theta_v$ is the change in volumetric moisture content across the wetting front (mm mm^{-1}) and F_{inf} is cumulative infiltration at time t (mm H_2O). The time-step is one hour. If the above equation produces a rate that is less than the available rainfall, the cumulative infiltration is calculated using:

$$F_{\inf,t} = F_{\inf,t-1} + R_{\Delta t} \tag{2.7}$$

where $F_{\inf,t}$ is the cumulative infiltration rate for a given time period (mm H_2O), $F_{\inf,t-1}$ is the cumulative infiltration for the previous time period and $R_{\Delta t}$ is the rainfall for the given time period. The effective hydraulic conductivity parameter K_e for equation 2.6 is calculated using a modified approach in the SWAT model as follows:

$$K_e = \frac{56.82 \cdot K_{sat}^{\ 0.286}}{1 + 0.051 \cdot \exp(0.062 \cdot CN)} - 2 \tag{2.8}$$

where K_{sat} is the saturated hydraulic conductivity (mm hr^{-1}) and CN is the SCS curve number. This method is used to incorporate land management practices into the equation. To calculate the wetting front matric potential the following is used:

$$\begin{aligned} \Psi_{wf} &= 10 \cdot \exp[6.5309 - 7.32561 \cdot \phi_{soil} + 0.001583 \cdot m_c^{\ 2} + 3.809479 \\ &\cdot \phi_{soil}^{\ 2} + 0.000344 \cdot m \cdot m_c - 0.049837 \cdot m_s \cdot \phi_{soil} + 0.001608 \cdot m_s^{\ 2} \\ &\cdot \phi_{soil}^{\ 2} + 0.001602 \cdot m_c^{\ 2} \cdot \phi_{soil}^{\ 2} - 0.0000136 \cdot m_s^{\ 2} \cdot m_c - 0.003479 \cdot \\ &m_c^{\ 2} \cdot \phi_{soil} - 0.000799 \cdot m_s^{\ 2} \cdot \phi_{soil}] \end{aligned} \tag{2.9}$$

where ϕ_{soil} refers to the porosity of the soil (mm mm^{-1}), m_c is the percent clay and m_s is the percent sand. These last three values are parameters entered in the soils database.

2.3.3.2 Peak runoff rate

The peak runoff rate is one of the most significant values for PT, since it is during the most intense surface flow events that erosion and thus P is mobilised and transported. SWAT uses a modified rational method:

$$q_{peak} = \frac{\alpha_{tc} \cdot Q_{surf} \cdot Area}{3.6 \cdot t_{conc}} \tag{2.10}$$

where q_{peak} is peak runoff rate (m^3 s^{-1}), *atc* is the fraction of daily rainfall that occurs in the time of concentration, Q_{surf} is the surface runoff (mm H_2O), Area is the sub-basin area (km^2) and t_{conc} is the time of concentration for the sub-basin and 3.6 is a unit conversion factor. The time of concentration is the amount of time it takes for a drop of rainwater to flow from a point furthest from the outlet to the outlet. In addition to calculating the peak runoff rate, it is used to calculate the lag time for surface runoff. It is divided into two fractions: the land component and the channel component. The land component equation is given below:

$$t_{ov} = \frac{L_{slp}^{\ 0.6} \cdot n^{0.6}}{18 \cdot slp^{0.3}} \tag{2.11}$$

where L_{slp} is the slope length (m), n is the Manning's roughness coefficient, *slp* is the average slope and 18 is a unit conversion factor. This is based on a one-metre wide strip down the slope. Values of n are taken from tables given by Engman (1983 in Neitsch *et al.*, 2002) based on the soil management regime. The channel component of time of concentration (t_{ch}) is found using:

$$t_{ch} = \frac{L_c}{3.6 \cdot v_c} \tag{2.12}$$

where L_c is the average flow channel length (km), v_c is the average channel velocity and 3.6 is a conversion factor for a unit. The mean flow length (*Lc*) is found using the total length and the sub-basin centroid.

Flow velocity is found using Manning's equation:

$$v_c = \frac{0.489 \cdot q_{ch}^{\ 0.25} \cdot slp_{ch}^{\ 0.375}}{n^{0.75}} \tag{2.13}$$

where v_c is the average channel velocity (m s^{-1}), q_{ch} is the is average channel flow rate (m^3 s^{-1}) slp_{ch} is the channel slope (m m^{-1}) and n is Manning's roughness coefficient for the channel.

Manning's roughness coefficient is obtained from tables for given channel characteristics. This equation assumes a trapezoidal-shaped cross section of channel with a slope of 2:1 for the sides and 10:1 width-depth ratio for the bottom.

2.3.3.3 Surface runoff lag

For large catchments where the time of concentration is high the lag time will likewise be high. The knock-on effect of a high lag time is that some rainfall entering the system one day will arrive at the channel in subsequent days. Fractions of surface runoff delayed until following days from the rainfall event are taken from plotting the following equation:

$$Q_{surf} = (Q'_{surf} + Q_{stor,i-1}) \cdot \left(1 - \exp\left[\frac{-surlag}{t_{conc}}\right]\right) \tag{2.14}$$

where Q_{surf} is the amount of surface runoff discharged into the main channel (mm H_2O), Q'_{surf} is the amount of surface runoff available for a given day (mm H_2O), $Q_{stor,i-1}$ is the stored runoff from the previous day (mm H_2O), *surlag* is the surface runoff lag coefficient and t_{conc} is the time of concentration for the sub-basin (hrs.).

2.3.4 Evapotranspiration

Evapotranspiration includes all forms of water losses to the atmosphere including evaporation, sublimation (evaporation from snow), plant and standing water surfaces. Evaporation dictates how much water is left stored in the soil and available to rivers. SWAT firstly calculates how much water is potentially available for evaporation and then uses that value to estimate how much actually evaporates. Canopy storage affects potential evaporation as well as infiltration and surface runoff. The amount of water stored on the plant canopy is calculated using:

$$can_{day} = can_{mx} \cdot \frac{LAI}{LAI_{mx}} \tag{2.15}$$

where can_{day} is the maximum amount of water that can be trapped for a given day (mm H_2O), can_{mx} is the maximum amount of water that can be trapped in the canopy when fully developed (mm H_2O), LAI is the leaf area index for a given day, and LAI_{mx} is the maximum leaf area index for the plant. Values of LAI for each species/land cover types are entered into the crop data files.

Potential evaporation is defined as the amount of water that would evaporate from a large area if water supply was unlimited and was not affected by advection or heat storage. Three means of estimating potential evapotranspiration have been incorporated into SWAT:

Penman-Monteith:

$$\lambda E = \frac{\Delta \cdot (H_{net} - G) + \rho_{air} \cdot c_p \cdot [e_z^o - e_z]/r_a}{\Delta + \gamma \cdot (1 + r_c / r_a)} \tag{2.16}$$

where λ is the latent heat flux density (MJ m^{-2} d^{-1}), E is the depth rate evaporation (mm d^{-1}), Δ is the slope of the saturation vapour pressure curve, de/dT (kPa °C^{-1}), H_{net} is the net radiation (MJ m^{-2} d^{-1}), G is the heat flux density to the ground (MJ m^{-2} d^{-1}), ρ_{air} is air density (kg m^{-3}), c_p is the specific heat at constant pressure (MJ kg^{-1} °C^{-1}), e_z^o is the saturation vapour pressure of air at height z (kPa), e_z is the water vapour pressure of air at height z (kPa), γ is the psychrometric constant (kPa °C^{-1}), r_c is the plant canopy resistance (s m^{-1}) and r_a the diffusion resistance of the air layer (s m^{-1}). Many of the values in equation 2.16 have been estimated by SWAT e.g. the net radiation (H_{net}) based on input values of solar radiation and air temperature, and canopy resistance from LAI.

Priestley-Taylor

$$\lambda E_o = \alpha_{pet} \cdot \frac{\Delta}{\Delta + \gamma} \cdot (H_{net} - G) \tag{2.17}$$

where λ is the latent heat of vaporisation (MJ kg^{-1}), E_o is the potential evapotranspiration (mm d^{-1}), α_{pet} is a coefficient, Δ is the slope of the saturation vapour pressure-temperature curve, de/dT (kPa °C^{-1}), γ is the psychrometric constant (kPa °C^{-1}), H_{net} is the net radiation (MJ m^{-2} d^{-1}) and G is the heat flux density to the ground (MJ m^{-2} d^{-1}). All inputs are estimated by numerous other equations from within SWAT based either on user inputs or further estimations.

Hargreaves:

$$\lambda E_o = 0.0023 \cdot H_0 \cdot (T_{mx} - T_{mn})^{0.5} \cdot (\overline{T}_{av} + 17.8) \tag{2.18}$$

where λ is the latent heat of vaporisation (MJ kg^{-1}), E_o is the potential evapotranspiration (mm d^{-1}), H_0 is the extraterrestrial radiation (MJ m^{-2} d^{-1}), T_{mx} is the maximum air temperature for a given day (°C), T_{mn} is the minimum air temperature for a given day (°C) and $\overline{T}_{av}$ is the mean air temperature for a given day (°C).

The actual evapotranspiration is then calculated from the figures of potential evapotranspiration using the following components:

1. Intercepted rainfall

2. Transpiration

3. Sublimation and evaporation from the soil

Two equations exist in SWAT for intercepted rainfall depending on whether potential evapotranspiration is less than or greater than the amount of free water in the canopy. If evapotranspiration is less than the free water in the canopy the following is used:

$$R_{INT(f)} = R_{INT(i)} - E_{can} \tag{2.19}$$

where E_{can} is the evaporation from free water in the canopy (mm H_2O), $R_{INT(i)}$ is the initial free water amount held in the canopy (mm H_2O), and $R_{INT(f)}$ is the final amount of free water in the canopy (mm H_2O). If however the evapotranspiration is more than the free water in the canopy the following is used:

$$E_{can} = R_{INT(i)} \tag{2.20}$$

where the definitions are the same as for equations 2.19.

Transpiration is calculated using equation 2.16 when the Penman-Monteith method is used, but for the other two methods the following applies:

Where $0 \leq LAI \leq 3.0$

$$E_t = \frac{E_o^{'} \cdot LAI}{3.0} \tag{2.21}$$

where E_t is the maximum transpiration on a given day (mm H_2O), $E_o^{'}$ is the potential evapotranspiration after being adjusted for free water in canopy (mm H_2O) and LAI is leaf area index.

Where LAI > 3.0

$$E_t = E_o^{'} \tag{2.22}$$

Definitions are the same as in equation 2.21.

Losses from snow surfaces to the atmosphere (sublimation) are estimated first by calculating the maximum evaporation. Actual sublimation is then calculated using one of two equations depending on whether the water content of the snow pack is greater or less than the maximum sublimation respectively:

$$SNO_{(f)} = SNO_{(i)} - E_s^{'} \tag{2.23}$$

$$E_s^{''} = E_s^{'} - E_{sub} \tag{2.24}$$

where $SNO_{(f)}$ is the amount of water in the snow pack for a given day after adjustment for sublimation (mm H_2O), $SNO_{(i)}$ is the amount of water in the snow pack before adjusting for sublimation (mm H_2O), $E_s^{'}$ is the maximum sublimation and or evaporation adjusted for plant-water use for a given day (mm H_2O) and $E_s^{''}$ is the maximum soil water evaporation for a given day (mm H_2O). Estimated values of actual soil water evaporation are then calculated by partitioning the losses between soil layers. Various fixed coefficients are used in the equations but are chosen to ensure that 50% of evaporation occurs from the top 10mm of soil and 95% from the top 100mm of soil. Evaporation from each soil layer is then defined by:

$$E_{soil,ly} = E_{soil,zl} - E_{soil,zu} \tag{2.25}$$

where $E_{soil,ly}$ is the evaporative demand for layer $_{ly}$ (mm H_2O), $E_{soil,zl}$ is the evaporative demand at the lower boundary of the soil layer (mm H_2O) and $E_{soil,zu}$ is the evaporative demand at the upper boundary (mm H_2O). Evaporative demands are read from graphs recording maximum evaporative demand against soil depth. The user can adjust these values to allow more evaporation from deeper in the soil profile.

2.3.5 Soil water

SWAT allows water to move from or within the soil profile by evapotranspiration, percolation and lateral movement. SWAT mechanics ensure that most of the water in the soil leaves by evapotranspiration. Saturated sub-surface flow is simulated directly by estimating the water content of the various layers. Unsaturated flow is indirectly represented by the depth distribution of soil evaporation and plant water uptake. This is based on the assumption that all water is distributed evenly throughout each soil layer. All water is assumed frozen when the soil temperature is below 0°C, and no water movement occurs. Soil structure is a large influence on water flow through the soil and is therefore described next.

2.3.5.1 Soil structure

Many standard soil characteristics such as porosity, bulk density and hydraulic conductivity are used by SWAT. Bulk and particle densities are used to estimate the pore space within soils and the default value of 2.65 Mg m^{-3} is assumed for particle density for all soils. Hydraulic conductivity is assumed to provide further information on pore transport.

SWAT utilises three stages of soil water content: saturation, field capacity (*FC*), and permanent wilting point (*WP*). The soil is at saturation when the soil water content is at maximum and no water can infiltrate without further drainage. Field capacity is deemed to occur after two days of drainage following saturation. Wilting point is defined as the water content of soil at which a plant would fail to recover after rehydration of the soil. SWAT has defined the two latter points in terms of hydraulic tension as 0.033 and 1.5 MPa respectively. Available plant water content (*AWC*) is defined by:

$$AWC = FC - WP \tag{2.26}$$

where WP is estimated using:

$$WP_{ly} = 0.4 \cdot \frac{m_c \cdot \rho_b}{100} \tag{2.27}$$

where WP_{ly} is the permanent wilting point of a given layer, M_c is the clay content of the layer (%) and ρ_b is the bulk density of the soil layer as input by the user in the soils database.

2.3.5.2 Percolation

Percolation is the vertical movement of water in the soil profile and is simulated in SWAT by estimating the water content of each layer. The field capacity of each layer is the control level of percolation. If soil water exceeds field capacity then percolation will occur, and if below field capacity it will not. The amount of water available for percolation when soil water (SW_{ly}) for a given layer is greater than field capacity (FC_{ly}) is calculated using:

$$SW_{ly,excess} = SW_{ly} - FC_{ly} \tag{2.28}$$

where $SW_{ly,excess}$ is the amount of water available for percolation from a given layer (mm H_2O). If however, the soil water content is less than the field capacity:

$$SW_{ly,excess} = 0 \tag{2.29}$$

The amount of water moving from one soil layer to another is given by:

$$w_{perc,ly} = SW_{ly,excess} \cdot \left(1 - \exp\left[\frac{-\Delta t}{TT_{perc}}\right]\right) \tag{2.30}$$

where $w_{perc,ly}$ is the amount of water percolating to the next soil layer (mm H_2O), $SW_{ly,excess}$ is the drainable volume of water in the soil layer for a given day (mm H_2O), Δt is the time step (hrs) and TT_{perc} is the travel time for the percolation (hrs) calculated by:

$$TT_{perc} = \frac{SAT_{ly} - FC_{ly}}{K_{sat}} \tag{2.31}$$

where TT_{perc} is the travel time for percolation (hrs), SAT_{ly} is the soil water content at saturation (mm H_2O), FC_{ly} is the field capacity of the soil layer (mm H_2O) and K_{sat} is the saturated hydraulic conductivity of the soil layer (mm· h^{-1}). This latter value is entered into the soils database for each soil type.

2.3.5.3 Lateral flow

Lateral flow occurs most easily above an impermeable layer of underlying geology, especially if the porosity of the overlying soil is high. The percolating water travels first vertically until it reaches the impermeable layer and then will flow along the horizontal hydraulic gradient. SWAT models this component using a kinematic storage model developed by Sloan *et al.* (1983 in Neitsch *et al.*, 2002). This model is based on hillslope length, slope and depth of porous layer. The quantity of water at the hillslope outlet (Q_{lat}) is given by:

$$Q_{lat} = 0.024 \cdot \left(\frac{2 \cdot SW_{ly,excess} \cdot K_{sat} \cdot slp}{\phi_d \cdot L_{hill}}\right) \tag{2.32}$$

where 0.024 is a conversion factor for hours and metres, $SW_{ly,excess}$ is the drainable volume of water stored in the saturated zone of the hillslope per unit area (mm H_2O), K_{sat} is the saturated hydraulic conductivity of the soil layer (mm· h^{-1}), slp is the slope of the hillside given by $\tan(\alpha_{hill})$, ϕ_d is the drainable porosity of the soil layer and L_{hill} is the hillslope length (m). Lateral flow is split between the day it is generated and the following day in a similar way to surface runoff lag.

The lag time of the water flowing laterally through the soil is affected by tile drainage systems and SWAT version 2000 incorporates a routine for tile drainage. Where tile drainage is present the lateral flow travel time is:

$$TT_{lag} = \frac{tile_{lag}}{24} \tag{2.33}$$

where TT_{lag} is the lateral travel flow time (days), $tile_{lag}$ is the drain lag time (hrs), and 24 converts the answer to days. In areas without tile drainage the lateral flow travel time is given by:

$$TT_{lag} = 10.4 \cdot \frac{L_{hill}}{K_{sat,mx}} \tag{2.34}$$

where L_{hill} is the hillslope length (m) and $K_{sat,mx}$ is the highest layer saturated hydraulic conductivity in the slope profile (mm hr^{-1}). The actual amount of water reaching the channel on any one day is calculated as a fraction of the total lateral flow based on the value of TT_{lag}.

2.3.5.4 Groundwater

Groundwater is defined as water stored in the soil under greater pressure than atmospheric pressure. This water is below that of the vadose zone. Only shallow unconfined and deep confined aquifers are modelled by SWAT. Shallow aquifers are assumed to contribute only to the stream flow within the sub-basin whereas deep aquifers are a net loss of water to the system. A water balance equation is used to define the shallow aquifer as follows:

$$aq_{sh,i} = aq_{sh,i-1} + w_{rchrg} - Q_{gw} - w_{revap} - w_{deep} - w_{pump,sh} \tag{2.35}$$

where $aq_{sh,i}$ is the amount of water stored in the shallow aquifer on day i (mm H_2O), $aq_{sh,i-1}$ is the amount of water stored in the aquifer on day $i-1$ (mm H_2O), wr_{chrg} is the amount of recharge entering the aquifer on day i (mm H_2O), Q_{gw} is the groundwater flow, into the channel on day i (mm H_2O), w_{revap} is the amount of water moving into the soil zone replacing deficiencies on day i (mm H_2O), w_{deep} is water percolating from the shallow aquifer to the deep aquifer on day i (mm H_2O) and $w_{pump,sh}$ is the amount of extraction from the shallow aquifer on day i (mm H_2O). Recharge is calculated using drainage time of the overlying geology and the amount of water exiting the bottom soil layer. User input is required to specify a threshold value (threshold water level in mm H_2O) for stored water above which groundwater flow into the channel can occur.

2.3.6 Phosphorus cycling

The complete cycle of P is shown in Figure 1.2 and the various pools considered by SWAT shown in Figure 2.1. Users may set the levels of P in the various pools for the initial conditions. If no revisions are made however, the soluble P defaults at five mg kg^{-1} for deep layers and under unmanaged vegetation and 25 mg kg^{-1} for the plough layer under cropland. From these figures, levels of active P are initialised using standardised fractions.

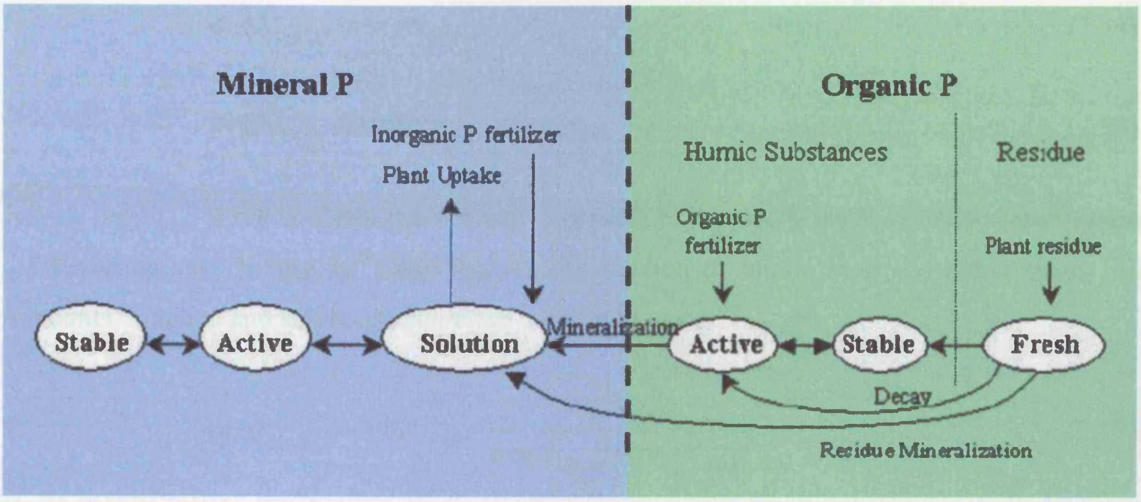

Figure 2.1 Phosphorus processes and pools as simulated by SWAT (from Neitsch *et al*., 2000)

2.3.6.1 Mineralisation and decomposition

SWAT models the breakdown of organic P (decomposition), the conversion of organic P compounds into inorganic plant available P (mineralisation) and the conversion of plant available P into unavailable organic P (immobilisation). Mineralisation and decomposition are microbial processes that slow down at lower soil temperatures and stop when at or below 0°C. Additionally, these two processes are deemed to occur only in the topsoil layer. Firstly the amount of active and stable organic P is calculated using the ratio of humus active organic N to stable organic N. Thereafter the mineralisation from the active organic P in the humus is calculated using:

$$P_{\min a,ly} = 1.4 \cdot \beta_{\min} \cdot \left(\gamma_{tmp,ly} \cdot \gamma_{sw,ly}\right)^{1/2} \cdot orgP_{act,ly} \tag{2.36}$$

where $P_{mina,ly}$ is the P mineralised from the humus active organic P pool (kg P ha^{-1}), β_{min} is the rate coefficient for mineralisation of the humus active organic nutrients, $\gamma_{tmp,ly}$ is the nutrient cycling temperature factor for layer ly, $\gamma_{sw,ly}$ is the nutrient cycling water factor for layer ly and $orgP_{act,ly}$ is the amount of P in the active organic pool (kg P ha^{-1}). The estimated mineralised P then becomes available to the solution P pool.

Decomposition of organic P and its subsequent mineralisation is dependent on temperature and water availability. Both these factors are calculated before partitioning of P into the active and stable organic fractions. The ratio of humus active N to stable organic N is used as the model for the amounts of active and stable organic P. The values of stable and active N are obtained from the following in the nitrogen-cycle component of SWAT:

$$orgN_{act,ly} = orgN_{hum,ly} \cdot fr_{actN} \tag{2.37}$$

$$orgN_{sta,ly} = orgN_{hum,ly} \cdot (1 - fr_{actN}) \tag{2.38}$$

where $orgN_{act,ly}$ is the concentration of active organic N (mg kg^{-1}), $orgN_{sta,ly}$ is the concentration of stable organic N (mg kg^{-1}) and fr_{actN} is the fraction of humic N in the active pool. The amounts of active and stable organic P are calculated using:

$$orgP_{act,ly} = orgP_{hum,ly} \cdot \frac{orgN_{act,ly}}{orgN_{act,ly} + orgN_{sta,ly}} \tag{2.39}$$

$$orgP_{sta,ly} = orgP_{hum,ly} \cdot \frac{orgN_{sta,ly}}{orgN_{act,ly} + orgN_{sta,ly}} \tag{2.40}$$

where $orgP_{act,ly}$ is the amount of organic active P (kg P ha^{-1}), $orgP_{sta,ly}$ is the amount of stable organic P (kg P ha^{-1}), $orgP_{hum,ly}$ is the amount of humic organic P (kg P ha^{-1}), $orgN_{act,ly}$ is the amount of active organic N (kg P ha^{-1}) and $orgN_{sta,ly}$ is the amount of stable organic N (kg P ha^{-1}) all within a given layer. Mineralisation from the humus active organic pool is obtained from:

$$P_{\min a,ly} = 1.4 \cdot \beta_{\min} \cdot (\gamma_{tmp,ly} \cdot \gamma_{sw,ly})^{1/2} \cdot orgP_{act,ly} \tag{2.41}$$

where $P_{mina,ly}$ is the amount of P mineralised from the humus active organic pool (kg P ha^{-1}), β_{min} is the rate coefficient for mineralisation of the humus active organic nutrients, $\gamma_{tmp,ly}$ is the nutrient cycling temperature, $\gamma_{sw,ly}$ is the nutrient cycling water factor and $orgP_{act,ly}$ is the amount of P in the active organic pool (kg P ha^{-1}). Processes of decomposition and mineralisation of the fresh organic P pool is modelled only in the top soil layer and is controlled by a decay-rate constant. The decay-rate constant is a function of the C:N and C:P ratios of the residue, temperature and soil water as calculated by:

$$\varepsilon_{C:N} = \frac{0.58 \cdot rsd_{ly}}{orgN_{frsh,ly} + NO3_{ly}} \tag{2.42}$$

where $\varepsilon_{C:N}$ is the C:N ratio of the residue, rsd_{ly} is the residue in layer ly (kg ha^{-1}), 0.58 is the C fraction in the residue, $orgN_{frsh,ly}$ is the fresh organic N (kg N ha^{-1}) and $NO3_{ly}$ is the amount of nitrate in the layer (kg N ha^{-1}). The C:P ratio is:

$$\varepsilon_{C:P} = \frac{0.58 \cdot rsd_{ly}}{orgP_{frsh,ly} + P_{solution,ly}} \tag{2.43}$$

where $\varepsilon_{C:P}$ is the C:P ratio of the residue, rsd_{ly} is the residue in layer ly (kg ha^{-1}), 0.58 is the C fraction in the residue, $orgP_{frsh,ly}$ is the fresh organic P (kg P ha^{-1}) and $P_{solution,ly}$ is the amount of P in solution in the layer (kg P ha^{-1}). The fraction of residue that is decomposed is defined using the decay-rate constant:

$$\delta_{ntr,ly} = \beta_{rsd} \cdot \gamma_{ntr,ly} \cdot \left(\lambda_{tmp,ly} \cdot \gamma_{sw,ly}\right)^{1/2} \tag{2.44}$$

where $\delta_{ntr,ly}$ is the residue decay-rate constant, β_{rsd} is the rate coefficient for mineralisation of the residue fresh organic nutrients, $\gamma_{ntr,ly}$ is the nutrient cycling residue composition factor for layer ly, $\gamma_{ntmp,ly}$ is the nutrient cycling temperature factor and $\gamma_{sw,ly}$ is the nutrient cycling water factor. Thereafter the nutrient cycling residue composition factor is calculated using:

$$\gamma_{ntr,ly} = \min\left\{\begin{matrix} \exp\left[-0.693 \cdot \frac{(\varepsilon_{C:N} - 25)}{25}\right] \\ \exp\left[-0.693 \cdot \frac{\varepsilon_{C:P} - 200}{200}\right] \\ 1.0 \end{matrix}\right\} \tag{2.45}$$

where $\gamma_{ntr,ly}$ is the nutrient cycling residue composition factor, $\varepsilon_{C:N}$ is the C:N ratio of the residue and $\varepsilon_{C:P}$ is the C:P ratio of the residue. Mineralisation is then calculated using:

$$P_{\min f,ly} = 0.8 \cdot \delta_{ntr,ly} \cdot orgP_{frsh,ly} \tag{2.46}$$

where $P_{minf,ly}$ is the mineralised fresh organic P (kg P ha^{-1}), $\delta_{ntr,ly}$ is the residue decay-rate constant, and $orgP_{frsh,ly}$ is the amount of fresh organic P (kg P ha^{-1}). Decomposition of P from the fresh organic P pool ($P_{dec,ly}$) is given using:

$$P_{dec,ly} = 0.2 \cdot \delta_{ntr,ly} \cdot orgP_{frsh,ly} \tag{2.47}$$

where $\delta_{ntr,ly}$ is the residue decay-rate constant and $orgP_{frsh,ly}$ is the total P in the fresh organic P pool (kg P ha^{-1}). The decomposed P from this calculation is then added to the humus organic P pool.

2.3.6.2 Inorganic P sorption

SWAT models the sorption of P using equations taken from Jones *et al.* (1984 in Neitsch *et al.*, 2002). These equations assume the rapid decrease in soluble P after applications of soluble P fertiliser. The P availability index (*pai*) governs the equilibrium between the active and soluble fractions, and the following equation for *pai* has been created based on experiment:

$$pai = \frac{P_{solution,f} - P_{solution,i}}{fert_{\min P}} \tag{2.48}$$

where $P_{solution,f}$ is the amount of P in solution after fertilisation and incubation, $P_{solution,i}$ is the amount of P in solution before fertilisation and $fert_{minP}$ is the amount of soluble P applied. It is assumed that the P is in constant and slow equilibrium between the soluble and active mineral pools. The stable mineral P pool is four times greater than the active mineral pool when it is in equilibrium. P movement between soluble and active pools is given by:

$$P_{sol\backslash act,ly} = P_{solution,ly} - \min P_{act,ly} \cdot \left(\frac{pai}{1-pai}\right)$$

$$\text{if } P_{solution,ly} > \min P_{act,ly} \cdot \left(\frac{pai}{1-pai}\right) \tag{2.49}$$

$$P_{sol\backslash act,ly} = 0.1 \cdot \left(P_{solution,ly} - \min P_{act,ly} \cdot \left(\frac{pai}{1-pai}\right)\right)$$

$$\text{if } P_{solution,ly} < \min P_{act,ly} \cdot \left(\frac{pai}{1-pai}\right) \tag{2.50}$$

where $P_{sol\,act,ly}$ is the amount of P transferred between the soluble and active mineral pools (kg P ha^{-1}), $P_{solution,ly}$ is the amount of soluble P (kg P ha^{-1}), min$P_{act,ly}$ is the amount of P in the active mineral pool (kg P ha^{-1}) and *pai* is the P availability index. P is transferred from the active mineral pool to solution when $P_{sol\,act,ly}$ is negative, and when positive the opposite is occurring. The model also includes P transfer when not in equilibrium but there is no information to suggest when this occurs in preference to the above.

2.3.6.3 Leaching

Leaching of P occurs only between the top 10mm of soil and the top soil layer. The leaching occurs through a gradient of P concentration primarily through crop root removal and does not include leaching through to tile drainage or lower soil layers.

2.3.7 Erosion

Erosion is modelled using the Modified Universal Soil Loss Equation (MUSLE) as developed by Williams (1975) based on the Universal Soil Loss Equation (USLE) by Wischmeier and Smith (1965). The principle difference is the replacement of the rainfall energy factor with a runoff factor and is represented in the following MUSLE equation:

$$sed = 11.8 \cdot \left(Q_{surf} \cdot q_{peak} \cdot area_{hru}\right)^{0.56} \cdot K_{USLE} \cdot C_{USLE} \cdot P_{USLE} \cdot LS_{USLE} \cdot CFRG \qquad (2.51)$$

where *sed* is the sediment yield for a given day (tonnes), Q_{surf} is the surface runoff volume (mm H_2O ha^{-1}), q_{peak} is the peak runoff rate (m^3 s^{-1}), $area_{hru}$ is the area of the HRU (ha), K_{usle} is the USLE soil erodibility factor (0.013 tonne m^2 hr/(m^3 –tonne cm^{-1})), C_{USLE} is the USLE cover and management factor, P_{USLE} is the USLE support practice factor, LS_{USLE} is the USLE topographic factor and *CFRG* is the coarse fragment factor. All the USLE factors are derived from experimental observation and relate to specific conditions, but the observed results have been replaced by equations that involve an extensive series of parameters. For instance, the following equation is used to calculate the erodibility factor used in equation 2.51:

$$K_{USLE} = \frac{0.00021 \cdot M^{1.14} \cdot (12 - OM) + 3.25 \cdot (c_{soilstr} - 2) + 2.5 \cdot (c_{perm} - 3)}{100} \qquad (2.52)$$

where M is the particle size parameter, OM is the organic matter content (%), $c_{soilstr}$ is the soil structure code used in soil classification and c_{perm} is the profile permeability class. The value of M is defined by the silt, very fine sand and clay contents. There are four values of $c_{soilstr}$ depending on the shape and structure of its peds: platy, prism like, block like and spheroidal. The support practice factor introduces erosion control measures into the equation and is read from tables. The factor c_{perm} is based on the lowest saturated hydraulic conductivity of the soil profile and is defined by one of six classes ranging from "rapid" to "very slow". In addition to the above, SWAT also includes the effects of snow cover and accounts for time lag of sediments in runoff.

2.3.8 Phosphorus movement

SWAT only models P movement in conjunction with surface runoff. It partitions the eroded P into solution and particulate forms. The amount of solute P transported in runoff is equated using:

$$P_{surf} = \frac{P_{solution,surf} \cdot Q_{surf}}{\rho_b \cdot depth_{surf} \cdot k_{d,surf}} \tag{2.53}$$

where P_{surf} is the amount of soluble P in surface runoff (kg P ha^{-1}), $P_{solution,surf}$ is the amount of soluble P in the top 10mm of soil (kg P ha^{-1}), Q_{surf} is the amount of runoff for a given day (mm H_2O), ρ_b is the bulk density of the top 10 mm of soil (Mg m^2), $depth_{surf}$ is the depth of the surface layer (10 mm) and $k_{d,surf}$ is the P partitioning coefficient (m^3 Mg^{-1}). The P partitioning coefficient is the ratio of the soluble P in the top 10 mm of soil to the soluble P in the surface runoff.

The amount of PP transported in surface runoff is calculated using the following from McElroy *et al.* (1976 in Neitsch *et al.*, 2002):

$$sedP_{surf} = 0.001 \cdot conc_{sedP} \cdot \frac{sed}{area_{hru}} \cdot \varepsilon_{P:sed} \tag{2.54}$$

where $sedP_{surf}$ is the amount of PP transported to the main channel (kg P ha^{-1}), $conc_{sedP}$ is the concentration of PP in the top 10 mm (g P tonne-1), sed is the sediment yield on a given day (tonne), $area_{hru}$ is the area of the HRU (ha) and $\varepsilon_{P:sed}$ is the P enrichment ratio. The concentration of PP ($conc_{sedP}$) in the surface layer of the soil is calculated using:

$$conc_{sedP} = 100 \cdot \frac{\left(\min P_{act,surf} + \min P_{sta,surf} + orgP_{hum,surf} + orgP_{frsh,surf}\right)}{\rho_b \cdot depth_{surf}} \tag{2.55}$$

where $\min P_{act,surf}$ is the P in the stable mineral pool in the top 10 mm (kg P ha^{-1}), $orgP_{hum,surf}$ is the amount of humic P in the top 10 mm (kg P ha^{-1}), $orgP_{frsh,surf}$ is the amount of P in the fresh organic pool of the top 10 mm (kg P ha^{-1}), ρ_b is the bulk density of the top 10 mm of soil (Mg m^2), and $depth_{surf}$ is the depth of the top surface layer (10 mm). The P enrichment ratio in equation 2.54 above is found using:

$$\varepsilon_{P:sed} = 0.78 \cdot \left(conc_{sed,surq}\right)^{-0.2468} \tag{2.56}$$

where $\varepsilon_{P:sed}$ is the P enrichment ratio for a given storm event and $conc_{sed,surq}$ is the sediment concentration in surface runoff (Mg sed m^2 H_2O). Once these values have been calculated for each HRU, SWAT estimates the quantities of SP and PP getting to the channel via runoff using the nutrient lag:

$$P_{surf} = \left(P'_{surf} + P_{stor,i-1}\right) \cdot \left(1 - \exp\left[\frac{-surlag}{t_{conc}}\right]\right) \tag{2.57}$$

$$sedP_{surf} = \left(sedP'_{surf} + sedP_{stor,i-1}\right) \cdot \left(1 - \exp\left[\frac{-surlag}{t_{conc}}\right]\right) \tag{2.58}$$

where P_{surf} is the SP transported to the channel in surface runoff on a given day (kg P ha^{-1}), P'_{surf} is the SP produced in a given HRU for a given day (kg P ha^{-1}), $P_{stor,i-1}$ is the lagged SP from the previous day (kg P ha^{-1}), *surlag* is the surface runoff lag coefficient, t_{conc} is the time of concentration for the HRU (hrs), $sedP_{surf}$ is the amount of PP discharged to the channel for a given day (kg P ha^{-1}), $sedP'_{surf}$ is the amount of PP produced in an HRU for a given day (kg P ha^{-1}) and $sedP_{stor,i-1}$ is the PP stored from the previous day's runoff (kg P ha^{-1}).

2.3.9 Crop growth

Crop growth cycle simulation is important in determining quantities of evaporation, transpiration and raindrop erosion among others. Potential plant growth is first modelled and is defined as the growth that would occur if environmental conditions were optimal. Solar radiation and LAI is used to define the potential amount of biomass produced on a given day. SWAT then utilises heat units as the basis for its plant growth model (Barnard, 1948 in Neitsch *et al.*, 2002). Parameters used within the heat unit model include plant temperature range (maximum, minimum and optimum), planting date and time to maturity. These values are input by the user when building the land cover database. The number of heat units is then accumulated for each crop type according to the relevant base temperature and the air temperature, until the plants have matured. Dormancy is included in the growth model and is a function of day length and temperature. The potential plant growth is then adjusted to account for controls such as extremes in temperature and deficiencies in water and nutrients.

LAI is used to estimate the amount of solar energy intercepted by the plant, which in turn is used to estimate biomass production. Solar radiation interception is calculated using Beer's law (from Monsi and Saeki, 1953 in Neitsch *et al.*, 2002):

$$H_{phosyn} = 0.5 \cdot H_{day} \cdot \left(1 - \exp\left[k_{\square} \cdot LAI\right]\right) \tag{2.59}$$

where H_{phosyn} is the intercepted photosynthetically-active solar radiation (MJ m^{-2}), H_{day} is the incident total solar radiation (MJ m^{-2}), $k_{\square}$ is the light extinction coefficient and LAI is leaf area index. The light extinction coefficient is -0.65 for all plants in SWAT, and photosynthetically active radiation is assumed to be 50% of the total solar radiation.

2.3.9.1 Potential crop growth

Potential biomass production for a given crop type is found using:

$$bio = \sum_{i=1}^{d} \Delta bio_i \tag{2.60}$$

where bio is the total plant biomass produced on a given day (kg ha^{-1}) and Δbio_i is the increase in total plant biomass for a given day (kg ha^{-1}). Values of Δbio_i are found using the radiation use efficiency for a given species of crop and can be adjusted for increases in atmospheric CO_2. Plant development including canopy height and LAI are governed using optimal leaf area development curves from the following equation:

$$fr_{LAI,mx} = \frac{fr_{PHU}}{fr_{PHU} + \exp(\square_1 - \square_2 \cdot fr_{PHU})} \tag{2.61}$$

where $fr_{LAI,mx}$ is the fraction of the total LAI relative to the total potential heat units for the plant, fr_{PHU} is the fraction of potential heat units accumulated on a given day and $\square_1$ and $\square_2$ are shape coefficients based on the optimal leaf area development curves. In addition to LAI canopy height is also estimated using:

$$h_c = h_{c,mx} \cdot \sqrt{fr_{LAI,mx}} \tag{2.62}$$

where hc is the canopy height on a particular day (m), $h_{c,mx}$ is the plant's maximum canopy height (m) and $fr_{LAI,mx}$ is specified in equation 2.61. Potential root growth is modelled using the values of above-ground biomass. SWAT assumes the roots system is 40% of the growth at emergence and 20% at maturity with a sliding scale between based on:

$$fr_{root} = 0.4 - 0.2 \cdot fr_{PHU} \tag{2.63}$$

where fr_{root} is the fraction of total biomass given to the root system for a given day, and fr_{PHU} is the fraction of potential heat units accumulated for a given day. Root development and depth is modelled but limited by the rooting depth of the soil profile according to the soil data. Water uptake by plants is calculated by SWAT to specify water loss through the soil profile:

$$w_{up,z} = \frac{E_t}{[1-\exp(-\beta_w)]} \cdot \left[1-\exp\left(\beta_w \cdot \frac{z}{z_{root}}\right)\right] \tag{2.64}$$

where $w_{up,z}$ is the is the potential water uptake from a specified depth of soil (mm H_2O), E_t is the maximum plant transpiration for a given day (mm H_2O), β_w is the water-use distribution parameter, z is the depth of water uptake from the soil (mm), and z_{root} is the depth to which roots occur in the soil (mm). It is assumed that most of the water uptake by plants occurs in the upper layers of soil since it is here that root mass is concentrated.

Nutrient uptake is also modelled to ascertain the removal of N and P from the soil and subsequent storage. The algorithms for P uptake in plants take account of the demands based on the potential biomass production. SWAT plots the P uptake using the particular stages of the growing cycle in a similar fashion to the estimation of potential increases in leaf area index (equation 2.61). Differences in P removal from each soil layer are also considered. Once the crop is mature, removal through harvesting is estimated as a portion of the total biomass as specified in the following equations:

$$yld = bio_{ag} \cdot HI \qquad \text{when HI} \leq 1.00 \tag{2.65}$$

$$yld = bio \cdot \left(1 - \frac{1}{1+HI}\right) \qquad \text{when HI} > 1.00 \tag{2.66}$$

where yld is the crop yield (kg ha^{-1}), bio_{ag} is the biomass above the ground for a given day (kg ha^{-1}), HI is the harvest index for a given crop on the day of harvest, and bio is the total biomass on the day of harvest (kg ha^{-1}). The harvest index ranges from 0.0-1.0 for most stem crops but can exceed 1.0 for root crops since it involves more than the above ground biomass.

2.3.9.2 Actual plant growth

Potential plant growth is altered as a function of water, temperature and nutrient stress to estimate actual plant growth. Water stress is calculated using:

$$wstrs = 1 - \frac{E_{t,act}}{E_t} = 1 - \frac{w_{actualup}}{E_t} \tag{2.67}$$

where $wstrs$ is the water stress, $E_{t,act}$ is the actual amount of transpiration (mm H_2O), Et is the maximum plant transpiration for a given day (mm H_2O), and $w_{actualup}$ is the total plant water uptake for a day (mm H_2O). The actual plant growth is a fraction of the potential plant growth according to curves for a species of plant (see Figure 2.2 below) where the air temperature is below the optimal but above the minimal.

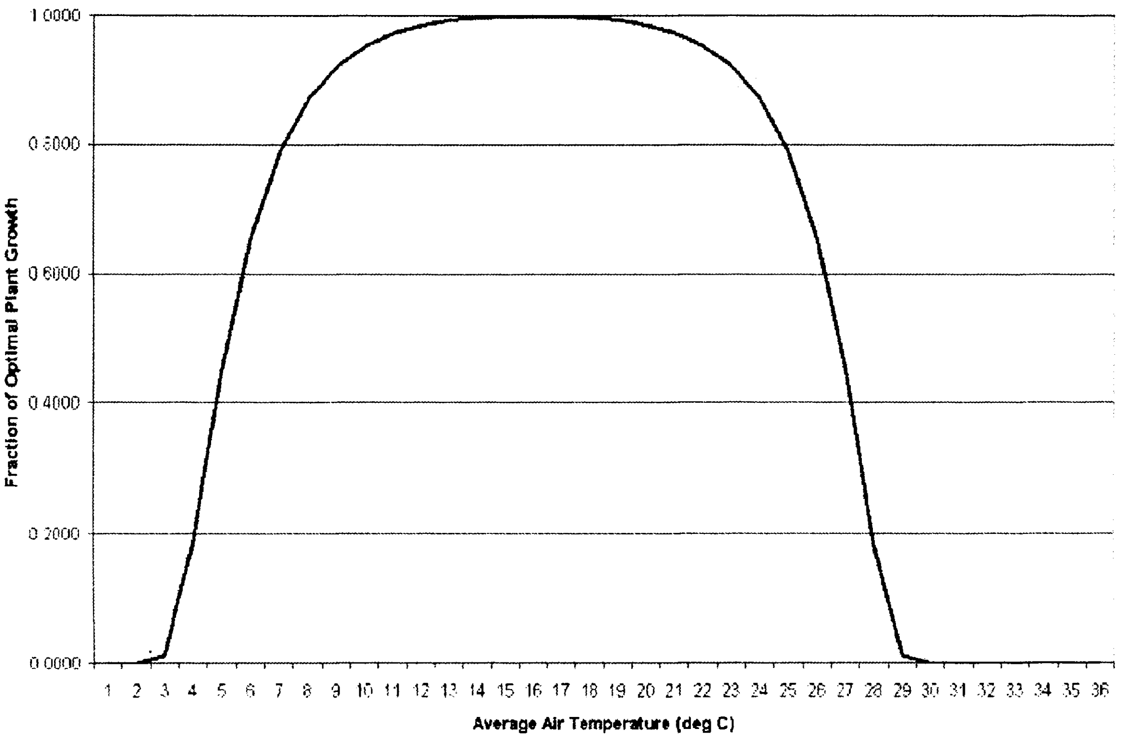

Figure 2.2 Temperature-growth curves for plant with base temperature of 0°C and optimal temperature of 15°C (taken from Neitsch *et al.*, 2002).

On estimation of all the above factors the actual increase in plant biomass is calculated according to:

$$\gamma_{reg} = 1 - \max(wstrs, tstrs, nstrs, pstrs) \tag{2.68}$$

where γ_{reg} is the plant growth factor (0.0-1.0), *wstrs* is the water stress, *tstrs* is the temperature stress, *nstrs* is the nitrogen stress, and *pstrs* is the P stress for a given day. Using the above value of γ_{reg} the result from equation 2.60 above is adjusted with:

$$\Delta bio_{act} = \Delta bio \cdot \gamma_{reg} \tag{2.69}$$

where Δbio_{act} is the actual increase in plant biomass for a given day (kg ha^{-1}), and Δbio is the potential increase in plant biomass for a given day (kg ha^{-1}).

2.3.10 Land management

The management section of SWAT includes the crop planting, harvesting, grazing, and soil management. Input is flexible so that non-standard agricultural procedures can be utilised. In particular the SCS curve number can be varied in time to take account of the changing state of the crop cover. Planting times are needed in order to indicate to the model the beginning of the growth cycle, otherwise the model will assume perennial crops. Kill operations are needed to prevent a crop from regrowing after harvesting. Percentages of the crop biomass removed in harvest can be altered for particular scenarios but is set at the seed fraction plus a typical fraction removed during hay production. The simultaneous biomass removal and subsequent manure application is simulated by grazing details. Dates for the start and end of grazing are required by SWAT and trampling is an option that can be specified by the user. Tillage practice dictates the redistribution of residues and nutrients in the soil profile. Timing of tillage and the particular form of tillage are inputs that can be adjusted by the user, whilst the SCS curve number can also be changed to coincide with changes in the soil characteristics.

2.3.10.1 Fertiliser application

The user can define all fertiliser operations or allow SWAT to specify the operations. This includes the type of fertiliser, the time of application and the amount that has been applied to the soil surface. Once SWAT has simulated the application of fertiliser the various nutrient pools are topped up accordingly. These have already been mentioned in sections 2.3.6 and 2.3.8 above. Additionally, bacterial content is taken into account.

For automated fertiliser applications the user must specify certain conditions such as maximum quantities applied trough the year and application efficiency. SWAT forecasts the N losses due to yield removal at the end of the growing season to estimate the amount of fertiliser applied in the automated procedure. It is only N that is used for this process.

In the most recent version of SWAT the user can define filter or buffer strips along the edge of watercourses to trap nutrients before they enter surface water.

2.3.11 Water management

This section includes irrigation, water transfer, extraction, point source loadings and impounded water. In addition, SWAT 2000 now facilitates tile drainage. To take advantage of tile drainage the user must specify the depth of drains, the lag time of water in the drainage system and the amount of time to drain the soil to field capacity. Field capacity is the threshold at which drainage through the drains are deemed to occur. The amount of water entering tile drainage from the soil layer in which it is laid is calculated using:

$$tile_{wtr} = \left(SW_{ly} - FC_{ly}\right) \cdot \left(1 - \exp\left[\frac{-24}{t_{drain}}\right]\right) \tag{2.70}$$

where $tile_{wtr}$ is the amount of water entering the tile drains (mm H_2O), SW_{ly} is the amount of water in the soil layer in which the tile drains are laid (mm H_2O), FC_{ly} is the field capacity of the layer (mm H_2O) and t_{drain} is the time needed to drain the soil to field capacity (hrs). Water within the tile drains is treated in the same way as lateral flow reviewed in section 2.3.5.3.

2.3.12 Urban areas

Urban areas have more impervious surfaces than rural areas and convey the precipitation through more direct and swift routes to watercourses. The net effect of increased urban areas is reduced lag times and larger peak volumes within river systems, thus altering the instream nutrient transport dynamics. SWAT uses the SCS curve and Green and Ampt methods for runoff in urban areas. Two versions of the SCS curve are used depending on whether the impervious surfaces are directly connected to the channel or indirectly connected. Loadings of sediments in urban runoff are estimated using either a system of linear regression curves based on urban runoff observations or a build up/wash off method based on the Storm Water Management Model (SWMM) (Huber and Dickinson, 1988). The regression equation is:

$$Y = \frac{\beta_0 \cdot (R_{day}/25.4)^{\beta_1} \cdot (DA/2.59)^{\beta_2} \cdot (imp_{tot} \cdot 100 + 1)^{\beta_3} \cdot \beta_4}{2.205} \tag{2.71}$$

where Y is the total constituent load (kg), R_{day} is the precipitation for a given day (mm H_2O), DA is the drainage area of the HRU (km^2), imp_{tot} is the fraction of the total area that is impervious, and the β variables are regression coefficients. All three numerical values shown in this equation are conversion factors from imperial units to metric.

The build up/wash off option simulates the accumulation of particulate matter on hard surfaces during dry periods and its subsequent wash off. Urban areas are divided into impervious and pervious areas. The pervious areas are treated in the same way as agricultural land is treated (section 2.3.7). Build up on impervious areas is quantified using the Michaelis-Menton equation:

$$SED = \frac{SED_{mx} \cdot td}{(t_{half} + td)} \tag{2.72}$$

where SED is the particulate build up (kg curb km^{-1}) td days after the last wash off event, SED_{mx} is the maximum amount of accumulation for the land type (kg curb km^{-1}), and t_{half} is the length of time needed for solid build up to increase for zero to half the maximum for the given urban land type (days). Days are considered dry where surface runoff is less than 0.1 mm. Wash off is then calculated using an exponential relationship:

$$Y_{sed} = SED_0 \cdot \left(1 - e^{-kk \cdot t}\right) \tag{2.73}$$

where Y_{sed} is the particulate matter washed off at time t (kg curb km^{-1}), SED_0 is the amount of solids present at the beginning of the rainfall event (kg curb km^{-1}), and kk is a coefficient. Once estimated all calculated solids are routed to the nearest channel.

2.3.13 Main channel processes

Flow velocity is calculated using Manning's equation and channel characteristics as specified by the user. Channel geometry is assumed to be trapezoidal based on user input of width, depth, length and slope. SWAT assumes a gradient of the bank sides of 0.5. SWAT will then use these values to calculate cross sectional area and wetted perimeter. The Muskingum river routing method and variable storage routing method are used within SWAT to model the channel network and both are based on a kinematic wave model (Chow *et al.*, 1988, in Neitsch *et al.*, 2002).

2.3.13.1 Flow geometry

Volume is then calculated using:

$$V_{ch} = 1000 \cdot L_{ch} \cdot A_{ch} \tag{2.74}$$

where V_{ch} is the volume of water stored in the channel reach (m^3), L_{ch} is the length of the channel (km), and A_{ch} is the cross sectional area of the water flowing in the channel (m^2). When the flow exceeds the capacity of the river cross-section water is modelled to spread into the flood plain.

2.3.13.2 Flow rate and velocity

Flow rate and velocity of water in the channel is based on Manning's equation using the following two equations:

$$q_{ch} = \frac{A_{ch} \cdot R_{ch}^{2/3} \cdot slp_{ch}^{1/2}}{n} \tag{2.75}$$

$$v_c = \frac{R_{ch}^{2/3} \cdot slp_{ch}^{1/2}}{n} \tag{2.76}$$

where q_{ch} is the rate of flow in the channel (m^3 s^{-1}), A_{ch} is the cross-sectional area of water flowing in the channel (m^2), R_{ch} is the hydraulic radius for a given depth of flow (m), slp_{ch} is the slope of the channel (m m^{-1}), n is Manning's "n" coefficient for the channel and v_c is the flow velocity (m s^{-1}). SWAT models the flow on a daily time step and therefore recalculates the overall daily flow once the above has been solved. Manning's n value has been criticised in several papers for it's irrelevance to hydrological and instream drainage (Klemes, 1986; Wheater *et al.*, 1993). It is however, still used in several of the models assessed at the beginning of this project, including the SWAT model.

2.3.13.3 Flow routing

Once flow rate and velocity has been calculated the movement of water through the channel network is modelled using either the variable storage routing method (Williams, 1969) or the Muskingum routing method. Using the former the storage routing is based on:

$$V_{in} - V_{out} = \Delta V_{stored} \tag{2.77}$$

where V_{in} is the water coming into the channel reach during the time step (m^3 H_2O), V_{out} is the water flowing out of the reach for the time step (m^3 H_2O), and ΔV_{stored} is the change in volume of storage in the time step (m^3 H_2O). Travel time within the reach is calculated using:

$$TT = \frac{V_{stored}}{q_{out}} = \frac{V_{stored,1}}{q_{out,1}} = \frac{V_{stored,2}}{q_{out,2}} \tag{2.78}$$

where TT is the travel time (s), V_{stored} is the storage volume (m^3 H_2O), and q_{out} is the discharge rate (m^3 s^{-1}).

The Muskingum routing method estimates movement using wedge and prism storage shapes. A wedge of stored water is produced in the reach with the greatest depth upstream when inflow exceeds outflow. Conversely, when outflow exceeds inflow a negative wedge is produced where the deepest part of the wedge is downstream. The baseflow component is modelled as a prism of storage with constant cross-sectional area along the length of the reach. Total storage is found using:

$$V_{stored} = K \cdot q_{out} + K \cdot X \cdot (q_{in} - q_{out}) \tag{2.79}$$

where V_{stored} is the volume of water stored in the channel reach (m^3 H_2O), q_{in} is the water flowing into the reach (m^3 s^{-1}), q_{out} is the volume flowing out of the reach (m^3 s^{-1}), K is the storage time constant for the reach (s), and X is a weighting factor. The weighting factor can be adjusted by the user but has a lower limit of 0.0 and an upper limit of 0.5. The value will fall between 0.0 and 0.3 for rivers depending on the degree of wedge. The storage time constant is analogous to the travel time in 2.78 above and is found using:

$$K = coef_1 \cdot K_{bnkfull} + coef_2 \cdot K_{0.1bnkfull} \tag{2.80}$$

where $coef_1$ and $coef_2$ are weighting coefficients input by the user, $K_{bnkfull}$ is the storage time constant when the river cross section is full (s), and $K_{0.1bnkfull}$ is the storage time constant for the reach when the river cross section is one-tenth full. The final two values are found with several equations that incorporate Manning's "n" and celerity that is defined as the change in velocity along a channel reach.

2.3.13.4 Instream losses

There are several losses from the stream defined in SWAT; transmission, evaporation and bank storage. Water can be lost from the channel by transmission through the bottom and sides. This is especially so in the case of ephemeral streams. Losses can occur when no groundwater is being fed into the channel and are estimated using:

$$tloss = K_{ch} \cdot TT \cdot P_{ch} \cdot L_{ch} \tag{2.81}$$

where $tloss$ is the channel losses (m^3 H_2O), K_{ch} is the effective hydraulic conductivity of the channel alluvium (mm hr^{-1}), TT is the travel flow time (hr), P_{ch} is the wetted perimeter (m), and L_{ch} is the channel reach length (km).

Evaporation losses are calculated using:

$$E_{ch} = coef_{ev} \cdot E_o \cdot L_{ch} \cdot W \cdot fr_{\Delta t} \tag{2.82}$$

where E_{ch} is the evaporation losses (m^3 H_2O), $coef_{ev}$ is an evaporation coefficient, E_o is the potential evaporation (mm H_2O), L_{ch} is the channel length (km), W is the channel width at water level (m), and $fr_{\Delta t}$ is the fraction of the time step. The evaporation coefficient is a calibration tool for the user.

The amount of water lost to bank storage is found using:

$$bnk_{in} = tloss \cdot (1 - fr_{trns}) \tag{2.83}$$

where bnk_{in} is the volume of water lost to bank storage (m^3 H_2O), t_{loss} is the channel transmission losses (m^3 H_2O), and fr_{trns} is the fraction of transmission losses lost to the deep aquifer. Conversely water enters the channel from bank storage using:

$$V_{bnk} = bnk \cdot (1 - \alpha_{bnk}) \tag{2.84}$$

where V_{bnk} is the water gained by the channel from bank storage (m^3 H_2O), bnk is the total amount of water stored in the bank (m^3 H_2O), and α_{bnk} is the bank flow recession constant. Water can also be drawn back into the soil via demand for evapotranspiration.

2.3.14 Sediment routing

Deposition and degradation are modelled simultaneously in the channel reach. The same channel geometry is used for this as was used for channel flow. For this element SWAT uses the peak channel velocity and models the maximum amount of sediment that can be entrained. Channel velocity is found using:

$$v_{ch,pk} = \frac{q_{ch,pk}}{A_{ch}} \tag{2.85}$$

where $v_{ch,pk}$ is the peak channel velocity (m s^{-1}), $q_{ch,pk}$ is the peak flow rate (m^3 s^{-1}), and A_{ch} is the cross sectional area of flow (m^2). Peak flow rate is defined using:

$$q_{ch,pk} = prf \cdot q_{ch} \tag{2.86}$$

where prf is the peak rate adjustment factor, and q_{ch} is the mean rate of flow (m^3 s^{-1}). The maximum amount of sediment that can be carried from a reach is estimated with:

$$conc_{sed,ch,mx} = c_{sp} \cdot v_{ch,pk}^{\;sp\exp} \tag{2.87}$$

where $conc_{sed,ch,mx}$ is the maximum amount of that can be transported by the water (kg l^{-1}), c_{sp} is a coefficient defined by the user, $v_{ch,pk}$ is the peak channel velocity (m s^{-1}), and $spexp$ is an exponent defined by the user (between 1.0 and 2.0). If this value is lower than the amount of sediment in the reach at the beginning of the time step deposition will occur. Deposition is the difference of the two multiplied by the velocity and its units are kg l^{-1}. Degradation however is dominant and is found using:

$$sed_{\deg} = \left(conc_{sed,ch,mx} - conc_{sed,ch,i}\right) \cdot V_{ch} \cdot K_{CH} \cdot C_{CH} \tag{2.88}$$

where $sed_{\deg}$ is the amount of re-entrainment in the channel (tonnes), $conc_{sed,ch,mx}$ is the maximum amount of sediment that can be carried by the water flow (kg l^{-1}), $conc_{sed,ch,i}$ is the amount of sediment in the channel at the beginning of the time step (kg l^{-1}), V_{ch} is the volume of water (m^3 H_2O), K_{CH} is the channel erodibility factor (cm/hr/Pa) and C_{CH} is the channel cover factor. Finally, the amount of sediment in the reach is found using:

$$sed_{ch} = sed_{ch,i} - sed_{dep} + sed_{\deg} \tag{2.89}$$

where sed_{ch} is the amount of sediment in the channel reach (tonnes), $sed_{ch,i}$ is the amount of suspended sediment at the beginning of the time period (tonnes), sed_{dep} is the amount of sediment deposited from the reach (tonnes) and $sed_{\deg}$ is the amount re-entrained (tonnes). The amount of sediment leaving the channel reach is found using:

$$sed_{out} = sed_{ch} \cdot \frac{V_{out}}{V_{ch}} \tag{2.90}$$

where sed_{out} is the amount of sediment leaving the channel reach (tonnes), sed_{ch} is the amount of suspended sediment in the channel reach (tonnes), V_{out} is the volume of water leaving the reach (m^3 H_2O), and V_{ch} is the volume of water in the channel reach (m^3 H_2O). Erosion of the channel sides is also included in SWAT using an erodibility factor based on submerged water jet observations. The channel cover factor is a ratio between a channel with a specified vegetation cover and a channel with no vegetation cover. Vegetation reduces the channel velocity and hence erosion.

2.3.15 Instream nutrient processes

Consideration of P transformations within instream water is an option for the user. When requested, SWAT models the transformations of P through algal death, mineralisation and subsequent algal uptake. P can also be removed from the water column through deposition. Change in the amount of instream organic P is calculated:

$$\Delta orgP_{str} = \left(\alpha_2 \cdot \rho_a \cdot a\lg ae - \beta_{P,4} \cdot orgP_{str} - \sigma_5 \cdot orgP_{str}\right) \cdot TT \tag{2.91}$$

where $\Delta orgP_{str}$ is the change in organic P in the channel water (mg P l^{-1}), α_2 is the fraction of algal biomass that is P (mg P/mg algal biomass), ρ_a is the death rate of algal biomass (day^{-1}), $\beta_{P,4}$ is the rate constant for mineralisation of organic P (mg alg l^{-1}), $orgP_{str}$ is the organic P concentration for the beginning of the time step (mg alg l^{-1}), σ_5 is the rate coefficient for organic P settling (day-1), and TT is the flow travel time in the reach (day). The user defines the algal biomass portion of P and the rate constant for mineralisation. The latter of which is adjusted thereafter according to water temperature along with settling rate. The inorganic and soluble fractions of P in the water column are increased by mineralisation of the organic pool and diffusion from the sediments. The change in inorganic P for a given channel reach is found using:

$$\Delta solP_{str} = \left(\beta_{P,4} \cdot orgP_{str} + \frac{\sigma_2}{(1000 \cdot depth)} - \alpha_2 \cdot \mu_a \cdot a\lg ae \right) \cdot TT \qquad (2.92)$$

where $\Delta solP_{str}$ is the change in inorganic P in the channel water (mg P l^{-1}), $\beta_{P,4}$ is the rate constant for mineralisation of organic P (mg alg l^{-1}), $orgP_{str}$ is the organic P concentration for the beginning of the time step (mg alg l^{-1}), σ_2 is the benthic source rate for inorganic P (mg P m^2 day^{-1}), *depth* is the depth of water in the channel (m), α_2 is the fraction of algal biomass that is P (mg P/mg algal biomass), μ_a is the growth rate of algal biomass (day^{-1}), algae is the algal biomass concentration at the beginning of the day (mg alg l^{-1}), and *TT* is the flow travel time in the reach (day). The growth rate of algae is calculated using a multiplicative method based on light, nitrogen, P availability and photosynthetic enzyme controls. The benthic source rate is adjusted according to water temperature.

2.3.16 SWAT summary

All of the above processes are controlled and processed by SWAT on a modular basis for efficiency of computation. Databases that are needed are accessed and closed prior to the next being used. Processes are modelled on a daily time step and follow a natural procedure through the catchment, from precipitation to water flow and nutrient loading at the outlet. Values from preceding equations are entered into subsequent ones and the model is therefore an integrated modelling system. Three versions of SWAT are supported by the USDA, of which SWAT 2000 is the latest and is used in this project. Some work was done using SWAT 99 but SWAT 2000 has certain advantages such as the Green and Ampt infiltration model and therefore the latter is used primarily for this work. An interface with ArcView is available for SWAT 2000 (AVSWAT) and makes the management of data more efficient and allows integration with remote sensing. The interface does reduce the efficiency of automated calibration and parameterisation. Automated parameterisation is required for large numbers of simulations as required by the mollifier and GLUE methods of error estimation. Manual adjustment of parameter values will therefore be necessary thus reducing the number of modelling runs possible. For this reason the FORA method will be used in assessment of modelling output.

2.4 Conclusion

The Soil and Water Assessment Tool (SWAT) was chosen as the nutrient transport model for this project. In the US, SWAT has been applied to two catchments for validation at Riesel, Texas of 17.7 km^2, and the Lower Colorado River of 8,927.00 km^2 (Arnold *et al.*, 1990). The former was validated against measured water and sediment yields and the latter was validated against water yields only. Bingner (1996) also used SWAT to simulate water yield on the

Goodwin Creek catchment (21.31 km2). The latter study discretised the catchment into sub-basins that were assumed to be homogeneous. No information has been found regarding its predictive performance of PT. There are 905 parameters used in the SWAT model (listed in Appendix E) and approximately a third of those relevant have been defined in this chapter. Additionally, there are in excess of 50 constants or coefficients, many of which are adjustable for calibration purposes. Many of these are not explained in the SWAT documentation at all. Many parameters can be adjusted by the user but are also available as defaults in SWAT. Ultimately it is left to the expertise and knowledge base of the user to set or adjust accordingly. Such a large set of parameters however makes the task of parameterisation a very onerous one.

Notwithstanding the technical and theoretical problems associated with the high parameterisation, there are also the resource requirements for collection of data. Many of the parameters used in SWAT are available from existing databases relevant to the US but not the UK, e.g. SCS curve numbers. Digitised soil maps are available, and there are some data available from MAFF through the Agricultural Consensus, and from the Fertiliser Society. Most of the data however, will have to be derived and adjusted in some way by hand. Remote sensing data can be processed in a form suitable for use in ArcView GIS, which should then be available to SWAT. It is inevitable that some data will have to be estimated, but the detrimental effects of this can be reduced by identification through sensitivity analysis of the parameters that are not very influential to the hydrology and PT components of SWAT. More emphasis can then be placed on those parameters that are sensitive in the SWAT model.

Chapter 3 Study Catchment: the Stonton Brook

3.1 Introduction

The Stonton Brook catchment lies to the north of Market Harborough in the county of Leicestershire and covers an area approximately 43km^2. It is one of the western tributaries of the larger River Welland (Figure 3.1) the outlet of which lies at the Wash at Tabbs Head some 80km to the east. The catchment has low-lying topography towards the lower stretches and gently undulating hilly headwaters where the gradient rises from the edge of the brook. Below Stonton Wyville the valley has flat a bottom of 1-200m wide. Gradients throughout the catchment do not exceed 13% and average 2.2%. Elevation above ordnance datum ranges from 66.4mOD at the outlet and 210mOD near Skeffington at the headwater (see Figure 6.4).

The Environment Agency (1997) and Harper and Evans (1998) have identified the Stonton Brook as having elevated nutrient levels with TP averaging around 110 μg P. l^{-1} for the first half of 1998. Algal mats showing evidence for this were extensive along much of the brook during the course of this study (Plate 3.4). The Welland is an economically important river for the whole of the east Midlands due to the extraction of water for domestic use, for storage in Rutland Water (Plate 3.5). Krowkowski (1998) showed that the Rivers Welland and Nene supply more than 80% of the phosphorus found in Rutland Water. In 1989 the first serious toxic cyanobacterial bloom occurred in Rutland Water resulting in widespread ecological, economical and recreational damage. Expensive remedial action was necessary in Rutland Water in the form of iron sulphide dosing (Krokowski, 1998). The Stonton Brook catchment is therefore a good choice for the study of nutrient transport. In addition to the economic and ecological importance of studying the Stonton Brook there are further advantages:

1) Low sewerage loading

2) Small losses of water and P to groundwater recharge

3) Existing and operable weir still present near the outlet

The Stonton Brook does not have a large sewage loading owing to the small human population present. This was important because it would have been difficult to study diffuse inputs if they were dwarfed by a high sewage input. The extensive use of septic tanks for domestic sewage storage could compromise a study into nutrient behaviour due to potential but hidden leakages of nutrients from the tanks. Septic tanks are supposed to be secure, but they do leak if poorly maintained.

The underlying Lias clay closed routes to standing groundwater and aquifers and simplified the transport of water through the soil. In this way invisible underground losses of water and phosphorus as confounding variables to the study have been minimised.

The National Rivers Authority and Anglian Region Water Authority monitored the Stonton Brook up until 1985. A disused weir remains upstream to the confluence of the Stonton Brook with the River Welland (Plate 3.7). Although the mechanisms had been removed the concrete crump-profile weir was still operable and could be used to calibrate an automatic depth logger. Some data were still available from the monitoring programme held by the Environment Agency. Details of the characteristics of the Stonton Brook pertaining to nutrient transport such as human population, climate, and geology will now be discussed.

3.2 Human population

The human population occurring in or around the Stonton Brook was 1626 in 1999 (Leicestershire County Council, 2003) concentrated in several small villages and hamlets as shown in Figure 3.2. The parish boundaries do not adhere specifically to the catchment boundary and the population is therefore overestimated by an unknown amount. Most of the parish areas fall within the catchment area as shown on the Ordnance Survey map (Pathfinder series 916) and this overestimation is therefore likely to be small. There were two STWs on the Stonton Brook, only one of which was operational. Thorpe Langton STW was closed whilst the STW at Tugby served the population from Tugby and Skeffington. There were 499 people living in these two villages (Leicestershire County Council, 2003), but the STW served 137 person equivalents according to the records from the Environment Agency, Peterborough. Thorpe Langton was catered for by the STW that drains to the Langton Brook, another tributary of the River Welland. All other accommodation as well as Shangton rehabilitation village for psychological patients was served by septic tanks.

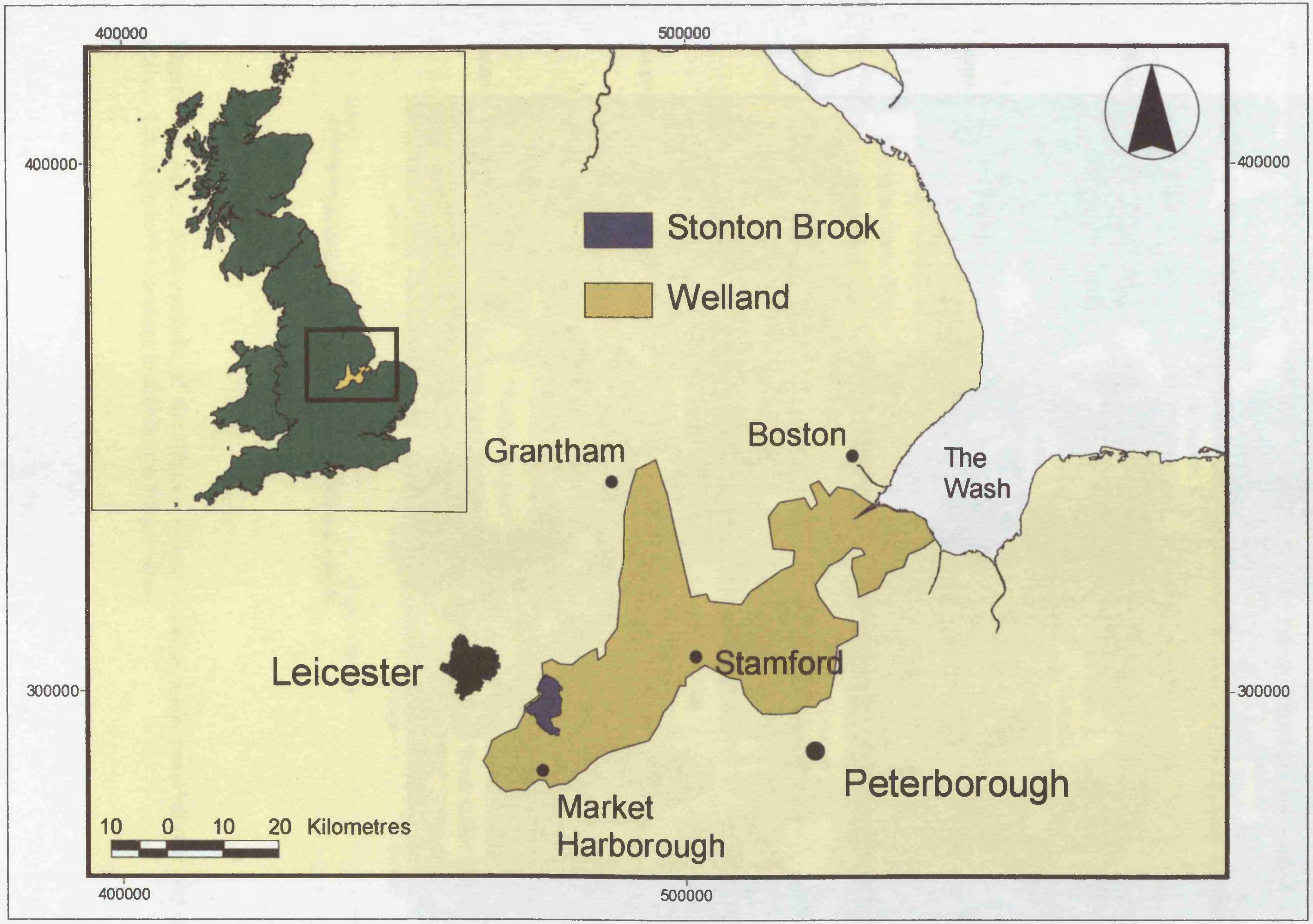

Figure 3.1 Location of the River Welland and Stonton Brook catchments.

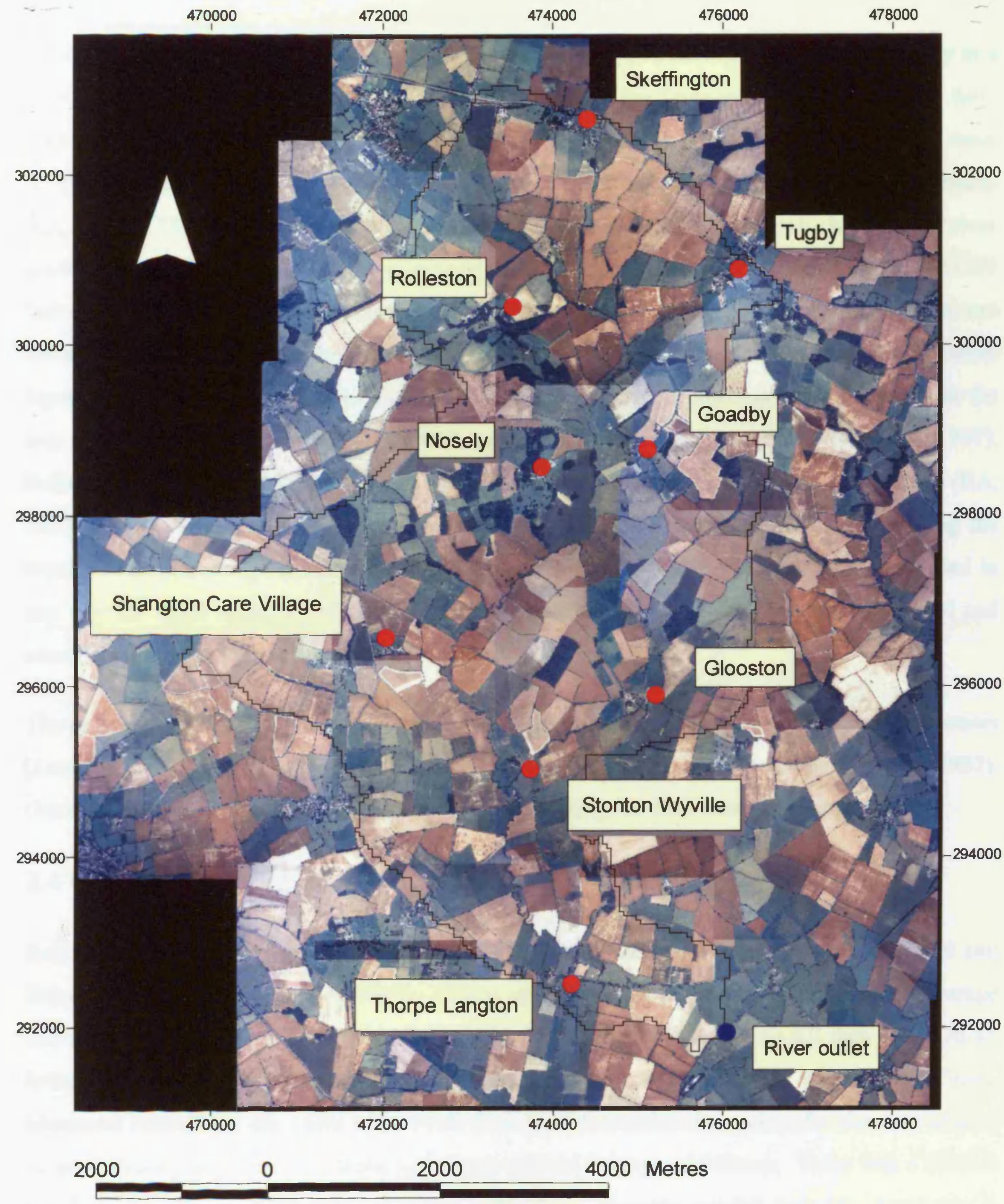

Figure 3.2 Aerial photo-mosaic of the Stonton Brook showing main conurbations and river outlet. The catchment boundary is shown as a black outline.

3.3 River habitat quality

Habitat and biological diversity in and along the brook dropped during the twentieth century as a consequence of intensified productivity. River quality of the Stonton Brook has not been fully documented but the adjacent River Chater which is similar in land use and geology has been designated "good" in terms of chemical water quality and "very good" for biological quality (EA, 1997). This may be more indicative of insufficient standards against which water and river quality are measured since the Environment Agency also declare that the rivers in the area are "adversely affected by eutrophication" (EA, 1997). Another concern for the area is low flow and extraction demand downstream is greater than river volume (EA, 1997). The Environment Agency and Wildlife Trusts have encouraged practices to reduce nutrients entering rivers in the area to counteract problems associated with eutrophication (Colston and Balbi, 1995; EA, 1997). Buffer strips and reduction of wastes are promoted amongst the agricultural community (EA, 1997). At the time of this project there were few signs of such initiatives in place along the brook. The Stonton Brook is not adversely affected by flooding and has not been modified in any way for flood defence. The Stonton Brook has been dredged but seldom straightened and meanders dominate the river system (EA, 1997).

The only notable riparian or aquatic species recorded for the Stonton Brook were European otters (*Lutra lutra*) and possibly white-clawed crayfish (*Austropotamobius pallipes*) (EA, 1997). Otters were seen in the brook on several occasions during the field sampling campaign.

3.4 Climate

Rainfall in the area is typical of the east Midlands with a reported average of between 650 and 760mm (Ragg *et al.*, 1984; EA, 1997). This is approximately two thirds of the national average and makes the area one of the driest in the UK (NRA, 1994). Yearly rainfall data for 1970-85 from Market Harborough ranged between 493.8mm and 767.7mm and averaged 627.5mm. Measured rainfall for the years 1996-1999 from four data collection points for the area around Stonton Brook ranged from 440mm to 799mm with an average of 640mm. There was a distinct trend of increasing yearly rainfall between 1996-1999. Monthly rainfall from the above data is shown in Figure 3.3. Most rainfall occurs in the autumn and summer months with averages of 189 and 176 mm respectively, whilst winter and spring has 155 and 140 mm. Intense storms occur most regularly in August with October and June also having regular intense events. Intense rainfall events occurred in one year only in January, April, May, July, September and December. No intense storms above 15mm in 24 hours were recorded in the other months. More wet days occurred during the winter and autumn months with averages of 16.9 and 15.3 days per month respectively. Spring has the least number of wet days with 13.75, and summer has 14.8 days. It can be seen that intense rainfall events characterise the area with approximately 21% of all precipitation occurring in rainfall events exceeding 15mm in 24 hours.

Temperatures in the east midlands reflect the distance from the sea. Typically temperatures are lower in the winter and higher in the summer than the rest of England at the same latitude (Ragg *et al.*, 1984). All other climate parameters are typical of the UK. Data for these parameters are made available through the British Atmospheric Data Centre (refer Chapter 6).

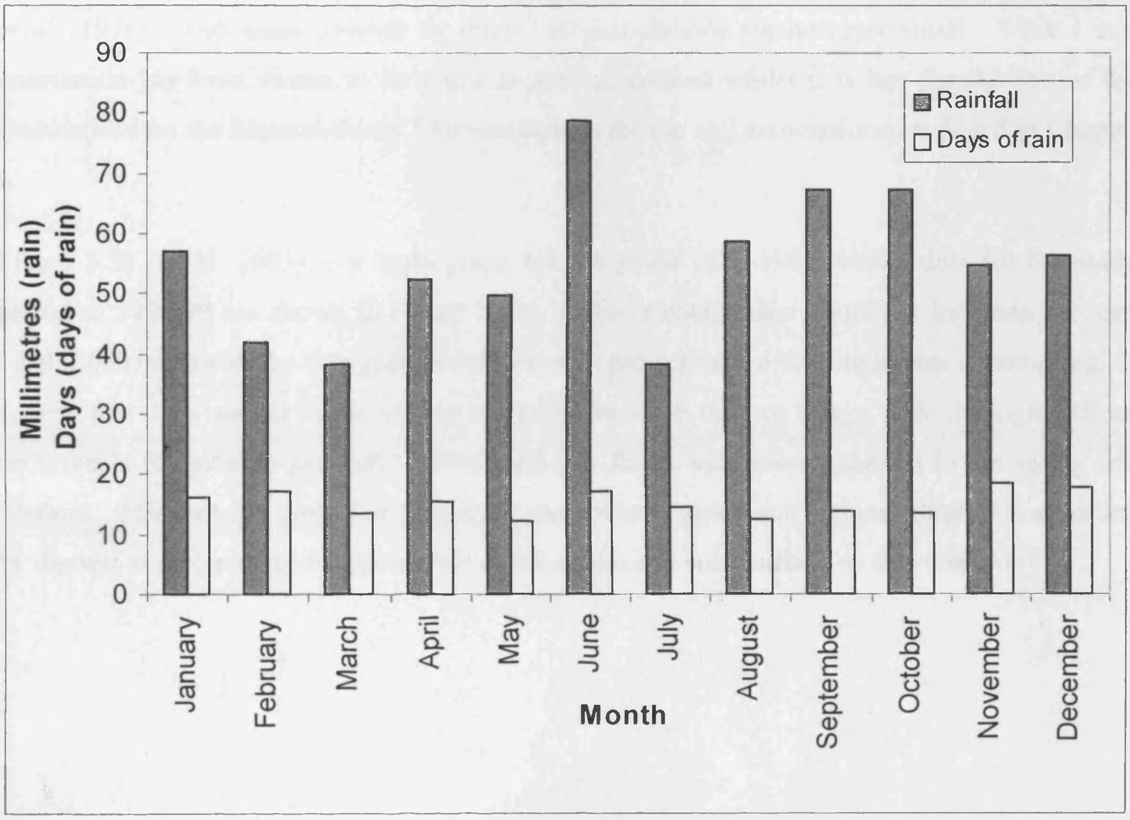

Figure 3.3 Distribution of rainfall and days of rain through the year in Market Harborough for the years 1996-1999 (BADC, 2002)

3.5 Geology and hydrology

The underlying geology of the Stonton Brook consists predominantly of Lias clays from the Lower Lias in the west of the catchment and the Middle Lias in the centre and east (Ragg *et al.*, 1984). The northern area of the catchment has some Upper Lias clay with Boulder clay on the higher ground. The Boulder clay is present due to glacial drift from the Anglian Glaciation *c* 270,000yBP. The soil associations found in the catchment are not homogeneous and discussed more fully in Chapter 4. On the valley flanks the soils are dominated by a variety of stagnogley soils that are all slowly permeable with varying amounts of stone, silt and loam (Curtis *et al.*, 1976; Ragg *et al.*, 1984). The only alluvial soils found within the catchment are from the Fladbury association and these are found under or within a few metres of the brook and towards the confluence with the River Welland (Ragg *et al*., 1984). It is possible that some glaciofluvial deposits exist within the catchment under the Wick 1 association (Ragg *et al*., 1984), but the scale and resolution of the information found was not precise enough to be sure. The one general characteristic of soils on the Stonton Brook is their impermeability. All records show that the soils are at least slowly permeable but the Ragdale is said to be impermeable below 600mm (Curtis *et al*., 1976; Avery, 1990). The two exceptions to this may be the soils of the Banbury and Wick associations, which have been shown to drain well and can be droughty to crops (Ragg *et al*., 1976). The areas covered by these two associations are however small. Wick 1 soil association has been shown to be prone to surface erosion whilst it is low for the rest of the associations on the Stonton Brook. Further details for the soil associations are found in Chapter 6.

Figure 3.5a (CEH, 2003) is a hydrograph for the years 1970-1985, whilst data for the study period of 1998/99 are shown in Figure 3.5b. A direct comparison could not be made between CEH (2003) data and the data gathered during this project due to the single year of sampling. It is clear that the seasonal trends are not dissimilar between the two sets of data: the higher flows occurred in the autumn and early winter, and low flows were more apparent in the spring and summer. This trend is typical of temperate areas where spring and summer rainfall is absorbed by the soil to replenish soil water deficit and does not add substantially to the river flow.

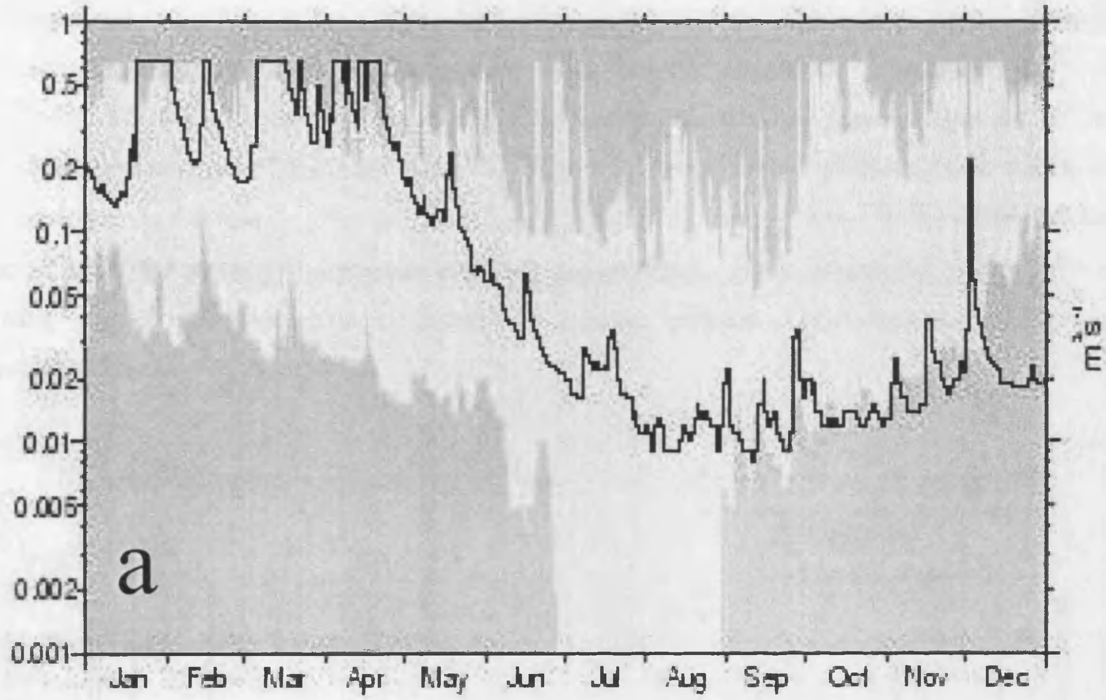

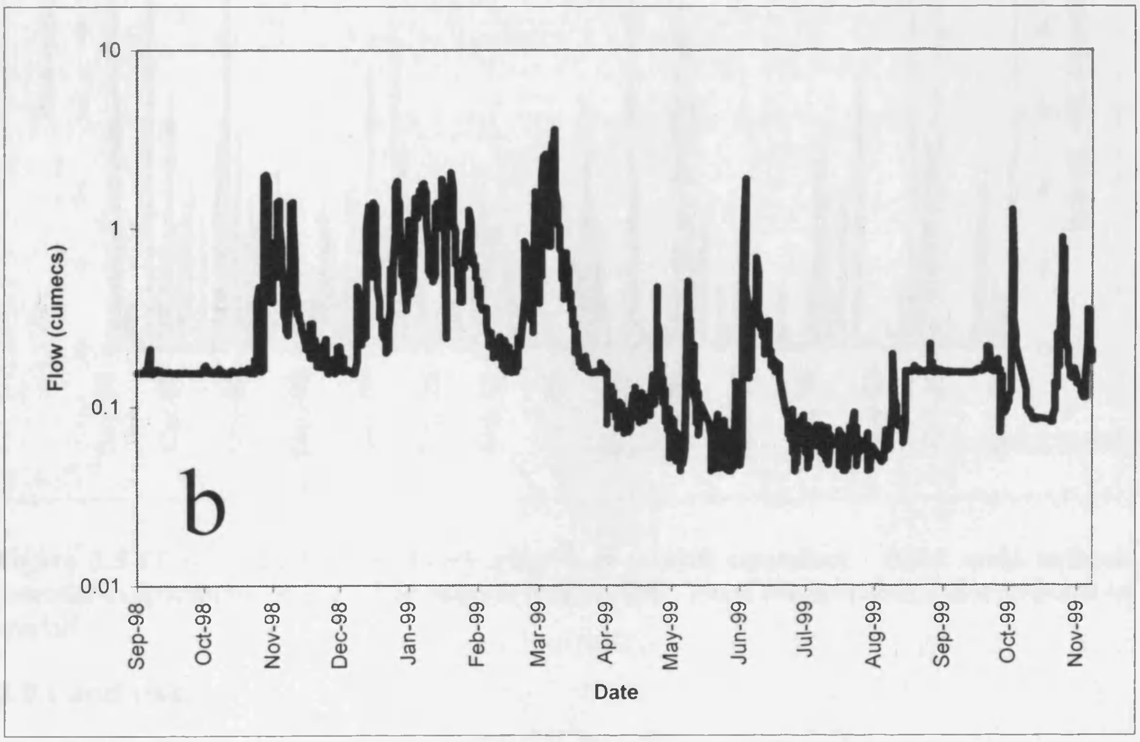

Figure 3.4 Hydrographs of the Stonton Brook, a) from EA records from years 1970-85 with minimum and maximum for each day, and featured year (1975) shown with dark line (taken from CEH, 2003), and b) from data collected during project in years 1998-99. Both graphs have logged y-axes.

Flow in the earlier data was lower overall with a mean flow of 0.13 cumecs, but these data do not include events over 0.65 cumecs due to the limitations of the weir. The average flow in the later period of data collection was 0.283 cumecs, which included all events. The latter value was calculated for the data collected directly from the Stonton Brook rather than the aggregate of the simulated and measured data (see Chapter 6). Figure 3.5 contains flow plotted against rainfall to demonstrate the dominance of evaporation and transpiration. During winter flow and rainfall are almost equal but from April onwards evaporation dominates. Flow volume for March 1999 is greater rainfall and demonstrates potential discrepancy between rainfall records and Stonton Brook catchment (see Chapter 6).

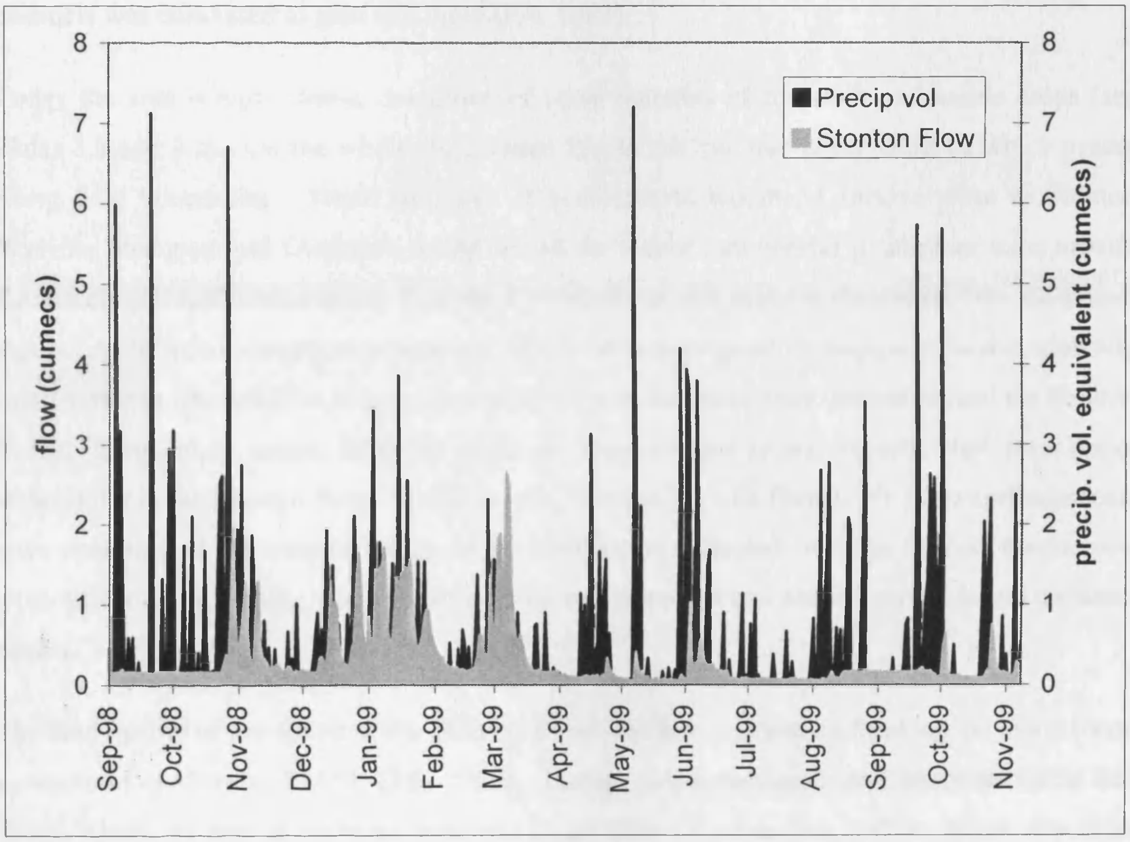

Figure 3.5 Flow in the Stonton Brook plotted on rainfall equivalent. Black areas indicate potential evaporation volume. Note data for March 1999. Flood event in river is not reflected in rainfall.

3.6 Land use

The River Welland and Stonton Brook have been under agricultural management from Roman times and has been in evidence since the deforestation of the UK after the last glaciation (Millward, 1985). There is an important roman road (Gartree Road) cutting across the Stonton Brook from east to west as shown on Ordnance Survey map Pathfinder 916, and a few Neolithic sites have been found in the area (Millward, 1985). Ridge and furrow systems from peasant land

and plough sharing in the 15th and 16th centuries are still preserved and clearly visible in much of the pasture surrounding the villages (see Plate 3.1).

During the 1939-1944 war a large proportion of the male agricultural workers were replaced with female workers but practices remained similar. A small increase in private cropping was witnessed around the villages due to shortages in most foods (Millward, 1985). Livestock farming was much more prevalent in the past but government subsidies in the 1960's and 1970's for artificial land drainage (Plate 3.3) have encouraged farmers to drain the land and convert to arable production (EA, 1997). Many trees and hedgerows were removed to increase productive area but on a much smaller scale than in the fens for example. Additionally, land closer to channels was cultivated to gain still more (EA, 1997).

Today the area is agricultural, consisting of equal amounts of livestock and arable crops (see Plates 3.1 and 3.2). On the whole the Stonton Brook has low tree cover, most of which occurs along field boundaries. Small remnants of semi-natural woodland survive close to Stonton Wyville, Shangton and Glooston, whilst mixed deciduous and conifer plantations exist around the Nosely and Rolleston estates. One small horticultural site exists in the south of the catchment that occupies approximately two hectares. The fields are irregular in shape and remain relatively small between 0.6 and 85ha in size. A number of farm business types operate around the Stonton Brook, from small tenant farms to large privately owned farms; Nosely Hall is a major stakeholder in the Stonton Brook (J. Sanderson, Stonton Wyville Farm). No large agribusinesses were operating in the area according to the information collected from the farmers themselves. Diversification in farming was evident only by two tearooms and several partridge and pheasant shoots.

The land quality of the whole of the Stonton Brook catchment is graded three - good to moderate agricultural quality, by MAFF (EA, 1997). Pasture is the dominant land cover for cattle and sheep, which are held at moderate densities (Agricultural Census data, 1997). North American bison of around 15 head were observed near Nosely. There were no records of swine or poultry farming during the period of study (Agricultural Census data, 1997). Wheat, barley, and oil-seed rape are the main arable crops, with small areas of field beans, linseed, maize and hemp. Some areas are laid up for set-a-side and these are generally left fallow rather than cultivated. Farming practices are typical to those recorded elsewhere, including those not encouraged by MAFF (Preedy *et al.*, 2001). A farmyard waste heap was positioned 30 metres from the river as shown in Plate 3.6. This waste heap was added to over the course of the year and used in the autumn as fertilizer on pasture in the surrounding fields. Such practices increase the potential of nutrient enrichment substantially.

Farmers obtain yields that approach theoretical maximum through high levels of external inputs and intensive crop management (applications of pesticides and fertilisers were observed). There were no yield reductions due to pests or diseases (EA, 1997). Irrigation is not applied, and all cultivation is rain-fed. On the whole water stress is relatively small (EA, 1997), but anecdotal evidence from two of the farmers working within the catchment indicated that water availability is declining. Their opinion was that rainfall had dropped in recent years resulting in reduced yields of grass. Subsequently sheep densities were reduced. This may however be a small temporal phenomenon as the climate data gathered for this area show that rainfall almost doubled between 1996 and 1999. Conversely, it may be that increasing temperatures may induce increases in evapotranspiration.

Plate 3.1 Typical landscape of the Stonton Brook looking northwest from Stonton Wyville. Note the variability in land cover types, low slopes and clearly visible remnants of ridge and furrow system the middle of the picture.

Plate 3.2 Landscape looking south from Skeffington at head of catchment.

Plate 3.3 Land drain outfall in the Stonton Brook. A well-established tile drainage system is in place throughout the Stonton Brook. Location is near head of river where slopes are steeper and grade from the channel.

Plate 3.4 *Cladophora* sp. mats indicating nutrient enrichment in small pond approximately 230 m from main channel of Stonton Brook.

Plate 3.5 Pumping station on the River Welland at Tinwell for Rutland Water reservoir. Green water sampler can be seen behind rails on other side of river. Note extensive algal growth on surface of water. This photograph was taken in July at height of growth season.

Plate 3.6 Farmyard waste heap near outlet of Stonton Brook catchment. Nutrient rich water in foreground was found to have TP levels in excess of 3.5 mg P l^{-1}. To left of heap is an overgrown drainage ditch leading to the river.

Plate 3.7 Crump-profile weir near Welham Road Bridge. Weir was closed in 1985 but still operable for this study. The mechanism housing can be seen to the right of the weir.

Chapter 4 Terrestrial Field Survey and Laboratory Methodology

4.1 Introduction

Field measurements were required for this study for the following reasons:

1) To build a land cover map of the Stonton Brook

2) Direct input to the nutrient transport model

3) For the parameterisation of remote sensing models

4) For the validation of remote sensing

The SWAT model requires a land cover map in the form of a shape-file in ArcView (Di Luzio *et al.*, 2002). Information about the land cover in each field or land-parcel was needed to do this. In addition, SWAT requires many soil and land cover parameters as direct input or through databases. The databases that are supplied with the SWAT model contain most of the crop data but apply to the US and not to the UK. Some of these parameters have been measured and are available in the literature but others have not. It is therefore prudent to measure them in the UK where possible. Certain crops are also not grown in the US and data are needed in order to avoid extrapolating from a different crop. Fortunately, most of these values are needed by the remote sensing element and are therefore not additional data concerns.

Extraction of information from remotely sensed data requires a certain amount of parameter input. Classification of the images for land cover categories requires *a priori* information of the land cover classes and their distribution in the catchment. Simple regression models can be used to estimate values from un-sampled areas of the image, but first requires measured data to parameterise and calibrate the models (Taconet *et al.*, 1996). Information can be extracted from remotely sensed images relating directly to the parameters measured on the ground e.g. soil moisture levels, or using models simulating the behaviour of the radiation measured by a particular sensor, e.g. backscatter with radiation transfer models (see Chapter 8).

Error of sampling comes in many forms (Congalton and Green, 1999; Dungan, 2001) and includes the accuracy of measurement, subsequent data transcription and management, and representativeness of the sample to the population, i.e. how many samples are needed in order to accurately estimate the population parameters (Zar, 1984). Additionally, the method of data collection must be considered to ensure the full range of population values are encountered. Data that are distributed (spatial) in nature have two further considerations of error: positional accuracy, and scale or resolution (Dungan, 2001). The term used to define representativeness of spatial data is "support" (Atkinson, 2001; Dungan, 2001). Support of spatial data depends on the range of values likely to be encountered and across what area. In terms of remotely sensed data, the support concerns the representativeness that an individual pixel value or group of values can give to the population sampled across the area on the ground representative of the pixel (Dungan, 2001). Sampling of spatial parameters must therefore provide adequate support to ensure reliability of the research or monitoring outcomes. Sampling is a compromise between what is ideally required and what is feasible in terms of resources. The number of parameters needing collection for this project is high and will therefore need careful planning.

In addition to data for supervised classification or parameterisation of a model, ground data can be used for the validation and accuracy assessment of the remotely sensed imagery (Stehman, 1996; Congalton and Green, 1999; Nishii and Tanaka, 1999). Remote sensing is prone to error in just the same ways that any other form of sampling are (Congalton and Green, 1999). Resultant images must not be accepted without prior assessment of the accuracy (Stehman, 1996; Congalton and Green, 1999; Nishii and Tanaka, 1999; Foody, 2002). Data extracted from the images must be validated against data measured on the ground. These issues are discussed more fully in Chapter 8.

Soil moisture content is one of the more important factors controlling the flow of phosphorus from the land to surface water (Nearing *et al.*, 1986; Young *et al.*, 1989; Jackson, 1993; Dubois *et al.*, 1995; Loumagne *et al.*, 2001). It is therefore highly desirable to facilitate soil moisture content in nutrient transport models. A soil moisture map would be very useful to define the initial levels, with subsequent maps at intervals to recalibrate the model. Neither has been incorporated into the SWAT model but is being considered (J. Arnold, USDA, ARS). The soil moisture aspect of this exercise is therefore used to assess whether extraction of soil moisture from SAR data is feasible for future modelling practices in the UK.

Soil moisture over the catchment-scale is highly variable in time and space (Loumagne *et al.*, 2001). Field sampling of soil moisture would be prohibitively expensive at the catchment scale, but radar remote sensing has proved successful across large geographic areas (Benalleague *et al.*, 1994; Dubois *et al.*, 1995; Tansey *et al.*, 1997; van Oevelen and Hoekman, 1999). This method could therefore offer the best means for supplying initial status of a catchment prior to the modelling period. Subsequent images could then be used to update the soil moisture contents during the study. However, to assess the potential of such methods, information on the ground must be collected about the parameters we wish to estimate via RS. The subject of support for the ground sampling and remote sensing is discussed in Chapter 8.

The roughness of a surface is one of the important factors that influence radar backscatter (see Chapter 8). Therefore, it is necessary to quantify the roughness properties of the target soil surface prior to estimating the moisture content. There are two statistical parameters important in radar studies, the standard deviation of surface height, also known as root mean square (RMS) height and the correlation length (van Oevelen and Hoekman, 1999). There are several ways to estimate these two variables (Huang and Bradford, 1990), but the simplest is the soil surface profilometer (Plate 4.1). The RMS of a surface indicates to what degree discrete measurements of the height of a surface vary about an arbitrary plane (Cox, 1983). It is estimated using the profilometer by taking the height of every pin above an arbitrary plane and calculating the standard deviation.

The relationship between the height of one point above an arbitrary plane located at point *a* and the height of another point *a'* distant from *a* can be expressed statistically as an autocorrelation coefficient. The variation in the value of the autocorrelation coefficient as the distance between the two points increases is referred to as the autocorrelation function. The correlation length *(l)* is the displacement from the original point, a, when there exists no statistical relationship between the two points. The normalised autocorrelation function, $\rho(a')$ in the discrete case, is given by Cox (1983).

In practice, two sets of measurements from two adjacent profilometer photographs are aligned so that the last measurement from the first image and the first measurement of the next are adjacent each other. A correlation coefficient is then calculated for these two points. The two sets of data are then shunted measurement-by measurement so that two data points are overlapping from each data set then three *etc*., and a correlation coefficient calculated at each step. In theory the correlation length is the distance between the first point of overlap (using one pin measurement from each board) and the overlap when a correlation no longer exists. The correlation length will increase as the surface roughness decreases. Thus, on a smooth surface a correlation will be obtained along the entire length of overlap and an infinite correlation length will exist. On rougher surfaces the correlation will fail over decreasing distances. Although Oh and Kay (1998) and Baghdadi *et al*. (2002b) indicate the flaws of calculating the soil correlation length and indicate that a profile board in the order of 200 multiplied by the soil correlation length is needed for this purpose, it was the only feasible method available for this project. Baghdadi *et al.* (2002b) adopted an alternative approach for measuring soil surface roughness using wave numbers and rms height but the method was adapted after this ground campaign had been completed.

This chapter is divided into sections according to the type of data collected. Because of the routine methods used in this study, discussion will be limited to measurement techniques that are contentious.

4.2 Methodology of data collection

A map of land cover was required as direct input to the nutrient transport model and to assess the accuracy of the land cover map derived from remote sensing. Two land cover surveys were conducted during the simulation period to record the crop type for every land parcel within the Stonton Brook catchment. A parcel of land is defined as an area of land with a dominant land cover type. For the most part, a parcel of land is a field with a well-defined boundary. However many fields had two or more discrete land cover types and each was considered separately. The survey was conducted by vehicle and foot and occurred in the months of January and May 1999. Two surveys were conducted to verify whether the crops were planted as winter or spring varieties and to confirm the crop type by examination of the fruit in May. Pasture was recorded as either pasture or rough pasture depending on whether the grass had been cultivated. This could be identified based on the unevenness of the ground. General categories were used for woodland stands rather than specific tree species. Often large areas of weed species were growing within a crop but for the purpose of this project were ignored due to the difficulties of mapping. Such areas were avoided for the intensive survey efforts as outlined in the next section. Land cover for each parcel was noted on an Ordnance Survey map. This information was then transferred to a digital map in GIS at a later date.

4.2.1 Site selection for collection of detailed parameters

Because of the diversity of land cover types in the Stonton Brook the number of sample sites needed to be high. The sampling sites needed to be easily accessible to aid efficiency and were therefore chosen close to roads and near field gates. The Stonton Brook has a varied topography, and care had to be taken to ensure the sites were suitable for the remote sensing studied. Sites were selected for their land cover type and low slope to avoid excessive effects of incidence angle on the backscatter (ERDAS, 1997b). For replication purposes two sites within each field were sampled, generally 60 m apart. Another important consideration for each site involved the phenomenon of radar speckle (see Chapter 8). The sampling locations within each field were a minimum of 40 m away from any boundary (hedges, roads or trees) to avoid speckle interfering with the efficiency of the land cover classification. Figure 4.1 shows the location and field cover type of each sample point. This level of sampling was not considered to be ideal but was limited by the resources available to this project. Data for input to SWAT were collected each month from October 1998 to October 1999 but only data from the May and July overflights were used for the remote sensing exercise. Sampling was spread over three days due to the amount of data to be sampled. Soil samples were collected on the day the satellite was overhead due to the highly dynamic nature of soil moisture. Vegetation and soil surface roughness were sampled either one day before or one day after.

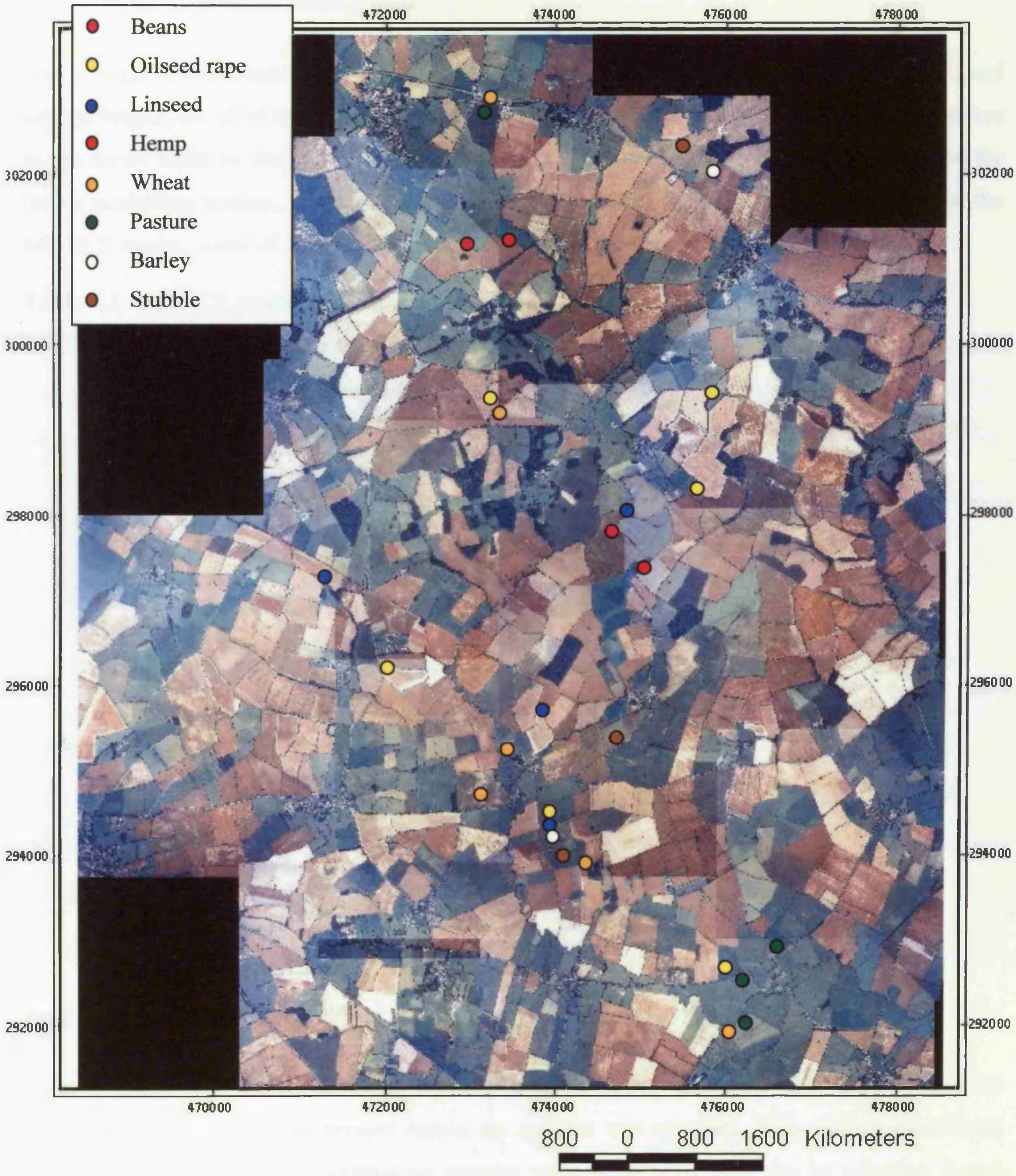

Figure 4.1 Map showing field locations. Background image formed from georectified photo-mosaic (see Chapter 7). Crop cover in image does not correspond with crop covers in Table 4.1 because photographs were taken from 1997. Two sampling sites occur within each field.

4.2.2 Vegetation measurements

There are two reasons for the collection of vegetation parameters:

1) For direct input to SWAT model

2) Input to radiative transfer models

Item 1 refers to the detailed vegetation parameters required for the SWAT model such as LAI and canopy height, not all of which are available in existing databases or literature. The second refers to the direct input to the MIMICS model to assess whether similar technology can be used for future modelling studies. Table 4.1 contains vegetation characteristics that are required for the MIMICS model, some of which are also needed in the SWAT model's vegetation database.

Table 4.1. MIMICS parameters (adapted from Ulaby *et al*, 1990).

Plant density (m^{-2})
Trunk height (m)
Trunk diameter (m)
Trunk moisture (gravimetric)
Branch Density (m^{-3})
Branch Length (m)
Branch Moisture (gravimetric)
Branch Diameter (cm)
Crown thickness (m)
Leaf density (m^{-3})
Leaf moisture (gravimetric)
Leaf Area Index (single sided – cm^2)
Trunk dielectric constant*
Leaf dielectric constant*
Branch dielectric constant*

*indicates parameters derived from vegetation measurements.

Plant densities were estimated using a $0.25m^2$ quadrat thrown randomly over the crop and the number of individual stalks present within the quadrat was counted. This was repeated three times per sample site. Five vegetation samples were taken from each site by selecting shoots randomly. Vegetation samples were collected either one day before or one day after the overflight, whilst soil, and the changeable nature of soil moisture, was seen as a priority for the day of overflight. Whole plants were cut off at the shoot base and stored in black plastic bags.

Prior to analyses they were stored at 4°C. The only land cover types analysed for the remote sensing (MIMICS) modelling were wheat and oilseed rape. These two crops are very common and have very different plant architecture. All other crops were sampled and analysed for the parameters used in the SWAT model, i.e. LAI and canopy height.

To obtain the wet weight of the plants they were weighed after removing the roots to green stem. All other parameters for the MIMICS model were then measured. Leaves fruit and stems were separated and weighed as a total for each part. Leaves were laid flat and put through a LAI metre to get total leaf area per plant. All plant parts were then dried overnight at 60°C, and weighed for their dry weight. All data were entered into MS Excel spreadsheet for calculation of the parameters listed in Table 4.1 and described below.

4.2.2.1 Dielectric Behaviour of the canopy constituents

The dielectric behaviour describes the relationships of the dielectric constants of the various canopy constituents to their respective moisture contents. The same dielectric model is used for all vegetation material, including leaves, trunks and branches. The gravimetric moisture content (mg) and the bulk density define the volumetric moisture content (m_v) and together govern the dielectric behaviour ρ. The dielectric constants are assumed to have the form:

$$\epsilon = \epsilon' - j\epsilon'' \tag{4.1}$$

The dielectric constant of the vegetation material, including leaves, trunks and branches, can be modelled using the Debye-Cole dual dispersion model (Ulaby and El-Rays 1987). This model consists of a free water component that accounts for the volume of the vegetation occupied by water in free form and a bound water component that accounts for the volume of the vegetation occupied by water molecules bound to bulk vegetation molecules. The dielectric constant for vegetation is given as follows:

$$\varepsilon = A + B\left(4.9 + \frac{\varepsilon_s - \varepsilon}{1 + j\dfrac{f(Hz)}{f_o}} - j\frac{22.74}{f(GHz)}\right) + C\left(2.9 + \frac{55}{1 + \sqrt{j\dfrac{f(GHz)}{0.18}}}\right) \tag{4.2}$$

where f(Hz) is frequency in Hz, f(GHz) is frequency in GHz, and

$$\epsilon_\infty = 4.9 \tag{4.3}$$

$$\epsilon_s = 88.045 - 0.1417T + (6.295 \times 10^{-4}T^2) + 1.075 \times 10^{-5}T^3 \tag{4.4}$$

$$f_o = (2\pi\tau)^{-1} \quad (4.5)$$

$$(2\pi\tau) = 1.1109 \times 10^{-10} - 3.824 \times 10^{-12}T + 6.938 \times 10^{-14}T2 - 5.096 \times 10^{-16}T^3 \quad (4.6)$$

where T is temperature in °C and (4.5) gives f_o in Hz. Given the gravimetric moisture content m_g and the dry density of the dry vegetation material ρ, the volumetric water content m_v of the vegetation material can be found from:

$$m_v = \frac{m_g \rho}{1 - m_g(1-\rho)} \quad (4.7)$$

The constants A, B and C are calculated as follows:

$$A = 1.7 + 3.2m_v + 6.5m_v^{\,2} \quad (4.8)$$

$$B = mv(0.82mv + 0.166) \quad (4.9)$$

$$C = \frac{31.4m^2}{59.5m \; +1} \quad (4.10)$$

For leaves, A, B and C in (4.2) are calculated from the gravimetric fraction:

$$A = 1.7 - 0.74m_g + 6.16m_g^{\,2} \quad (4.11)$$

$$B = m_g(0.55m_g - 0.076) \quad (4.12)$$

$$C = \frac{4.64m_g^{\,2}}{7.36m_g^{\,2} + 1} \quad (4.13)$$

The dielectric model given in (4.1) has been found by Ulaby *et al.* (1990) to give good agreement with experimental data.

4.2.3 Additional vegetation parameters

The following parameters were calculated with respect to the vegetation:

1) Trunk height and diameter

2) Moisture content (gravimetric, for trunk, leaf and branch) is defined by Ulaby *et al.* (1990) as:

$$M_g = \frac{M_W}{M_W + M_d} \tag{4.14}$$

where M_w is the mass of the water in the trunk and M_d is the dry mass.

3) Crown thickness is the average height of the plant, since wheat plants have no discernible crown, the height of the plant will be considered as the crown thickness, as measured in the field.

4) Leaf density is defined as:

$$L_d = \frac{numberofleaves}{m^2} \times \frac{1}{plantheight} \tag{4.15}$$

7) LAI is defined by Hunt, (1990) as:

number of leaves/m^2 x LA m^{-2} (4.16)

where LA is leaf area.

Dry density of leaf and trunk material is defined as:

$$D_d = \frac{M_d}{V_p} \tag{4.17}$$

where M_d is the dry mass of the leaf and V_p is the dry volume.

4.2.4 Soil measurements methodology

Three samples were collected from each sampling point over a wide area using a knife and stored in polyethylene sampling jars with sealed tops. The soil samples were taken from the top 50mm of the soil surface. The samples were stored at 4°C until analyses in the laboratory at Leicester University. Only soils were sampled on the day of the satellite overflight because soil moisture is the most changeable parameter of those sampled. Soil surface profiles were collected either one day prior to the overflight or one day after.

4.2.4.1 Soil moisture content and soil organic matter content

The soil moisture content and organic moisture content (loss on ignition) were measured using the method found in Allen *et al.* (1974). The protocol shown in Appendix C2 was applied to the soil samples. The percentage moisture loss was then calculated from loss in weight:

$$Moisture = \frac{wt.loss(g)}{wt.sample(g)} \times 100 \tag{4.18}$$

The organic matter content is taken as the portion of soil combusted during four hours of heating at 450°C. This is calculated from:

$$Organic\ moisture\ content = \frac{E-F}{C} \times 100 \tag{4.19}$$

Where C is the weight of the dry soil (after 17 hrs at 105°C), E is the weight of the soil after all water had been forced out (further 16 hrs at 220°C) and F is the non-combustible portion (further four hrs at 450°C).

For many of the radiative transfer models, volumetric soil moisture content is required which is defined as the volume of water for a given volume of soil, and is calculated using:

$$Sv = S_M / V_M \tag{4.20}$$

where S_M is the percentage soil moisture and V_M average amount of water volume of the samples. To obtain this value the bulk density must be measured. A disk of soil of specific volume was sampled using a steel soil corer with a plastic insert. It was hammered into the soil using a mallet until full. The corer was then extracted from the soil, excess soil trimmed from the plastic insert and then placed in a plastic bag and sealed for analysis in the lab. The inside measurements of the plastic insert was 64mm diameter by 25.4mm deep. The bulk density of the soil core was then calculated from:

$$Soil\ density\ (g/m^3) = \frac{soilweight}{(\pi 0.032^2) \times 0.0254} \tag{4.21}$$

4.2.4.2 Soil texture analysis, % silt sand and clay

The proportions of sand, silt and clay for the soils of each site were found following the procedure in BS 1377: 1975. Soil samples were first air dried by spreading over a baking tray and left overnight in a drying cabinet set to 50°C. The air-dry material was passed through a two mm mesh to remove all stones and gravel. The soil was lightly crushed during sieving to break up aggregates using a pestle and mortar. A 75g sample of sieved soil was placed in a mechanical stirrer for five minutes along with 100 ml of dispersing agent, (sodium hexametaphosphate) and 300 ml of distilled water. The solution was then placed in a measuring cylinder and made up to 1000 ml. The suspension was mixed thoroughly with a plunger and hydrometer readings (g/l) were taken 0.5 minutes, one minute, three minutes, ten minutes and 16 hours after mixing.

Hydrometer readings were then converted into a sedimentation parameter θ and applied to the following formula to give particle size:

$$Particle\ size = \frac{\theta}{\sqrt{t(\min s)}} \tag{4.22}$$

All measured hydrometer readings were then plotted on a graph of particle size (logarithmic scale) against percentage. Soil % sand, silt, clay could then be read from the graph.

4.2.4.3 Soil surface roughness, RMS height and correlation length

The profilometer was 0.5 m in length and contained 96 pins of equal length and spacing that slid within a frame with an attached spirit level. The profilometer was held horizontally above the soil and pins released to let fall to the surface. The upper location of the ends of the pins relative to the frame provides a profile of the surface roughness. The frame was then secured and a board with horizontal lines at 10mm spacing held behind the pins. Photographs were then taken for analysis within a computer. The profilometer must be orientated in the right direction to ensure the surface roughness sampled is the one visible by the microwaves. Tansey (1999) used the profilometer perpendicularly to the direction of the incidental waves. Since the ERS-2 travels on a course approximately 190° and is side looking, the board was placed on the same plane using a magnetic compass. Two profile images were taken at each sampling point.

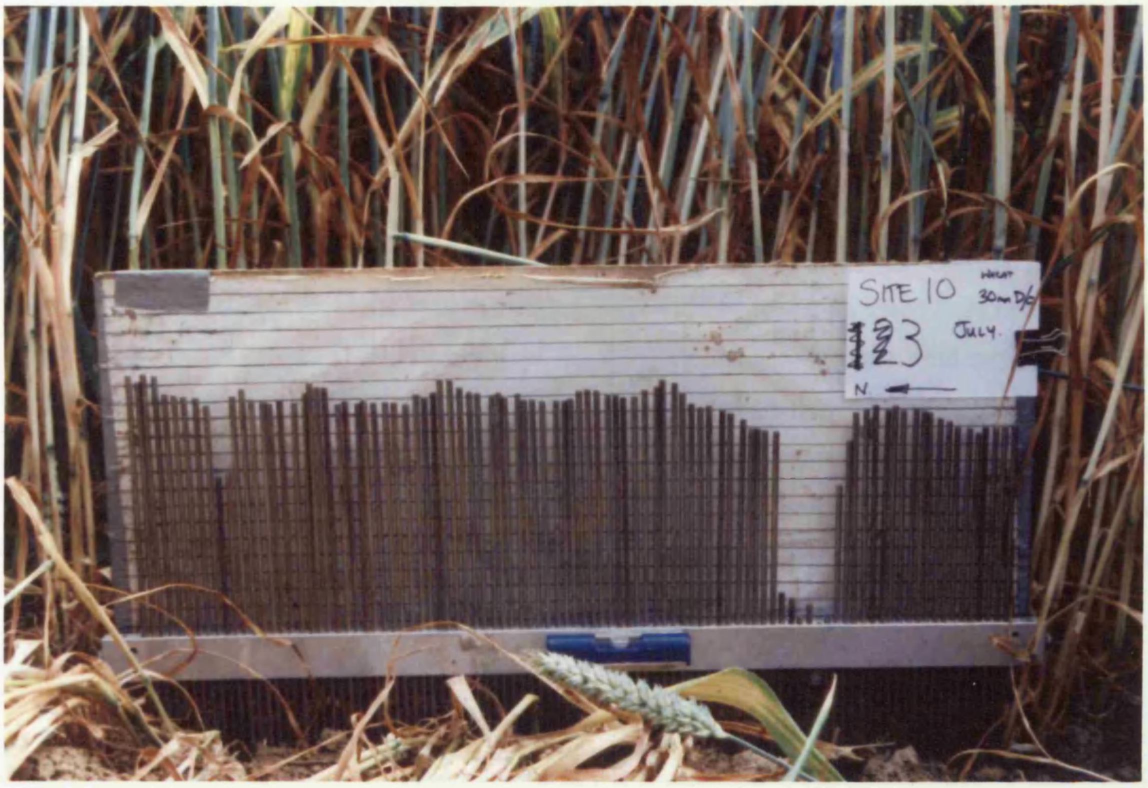

Plate 4.1 Soil profilometer

All photographs or negatives of the profilometer were scanned into a PC, and the images imported to the program "Scion Image" (Scion, 1998). Each image was calibrated in the vertical plane to allow measurement of the pin heights. The lengths of the pins were measured from a baseline within the image and transferred to MS Excel. RMS was calculated as the mean of the two standard deviations from each site.

The two sets of pin measurements for each sample were then standardised against a common datum, in this case the heights of the final pin of the first profilometer image and the first pin of the second image. A macro was written in Excel to enable automatic calculation of correlation coefficients for each consecutive step. The correlation length was taken as the length of the overlap between the two sets of pin measurements whereby a correlation ceased to exist.

4.3 Results

Data relating to the remote sensing were collected on the day of overflight or one day either side. At the time of the two overflights (10:01 GMT), the temperature at ground level was 12°C and 20°C for May and July respectively. On both days the weather was dry but overcast in May and clear in July. The data from the land use survey were applied to the digitised field boundary map (see Figure 7.2, Chapter 7) as attributes of the polygon shapes for each field and land-parcel. Figure 4.2 shows the results of the land use survey and characteristics of the selected fields are summarised in Table 4.2. It is accepted that some areas defined as urban are small rural hamlets with only a few buildings and dominated mostly by trees and grassed areas. Due to the adverse effect on hydrology of the rooftops and hard paving of reducing lag time between rainfall and entry to rivers, definition of these areas is considered important for this exercise.

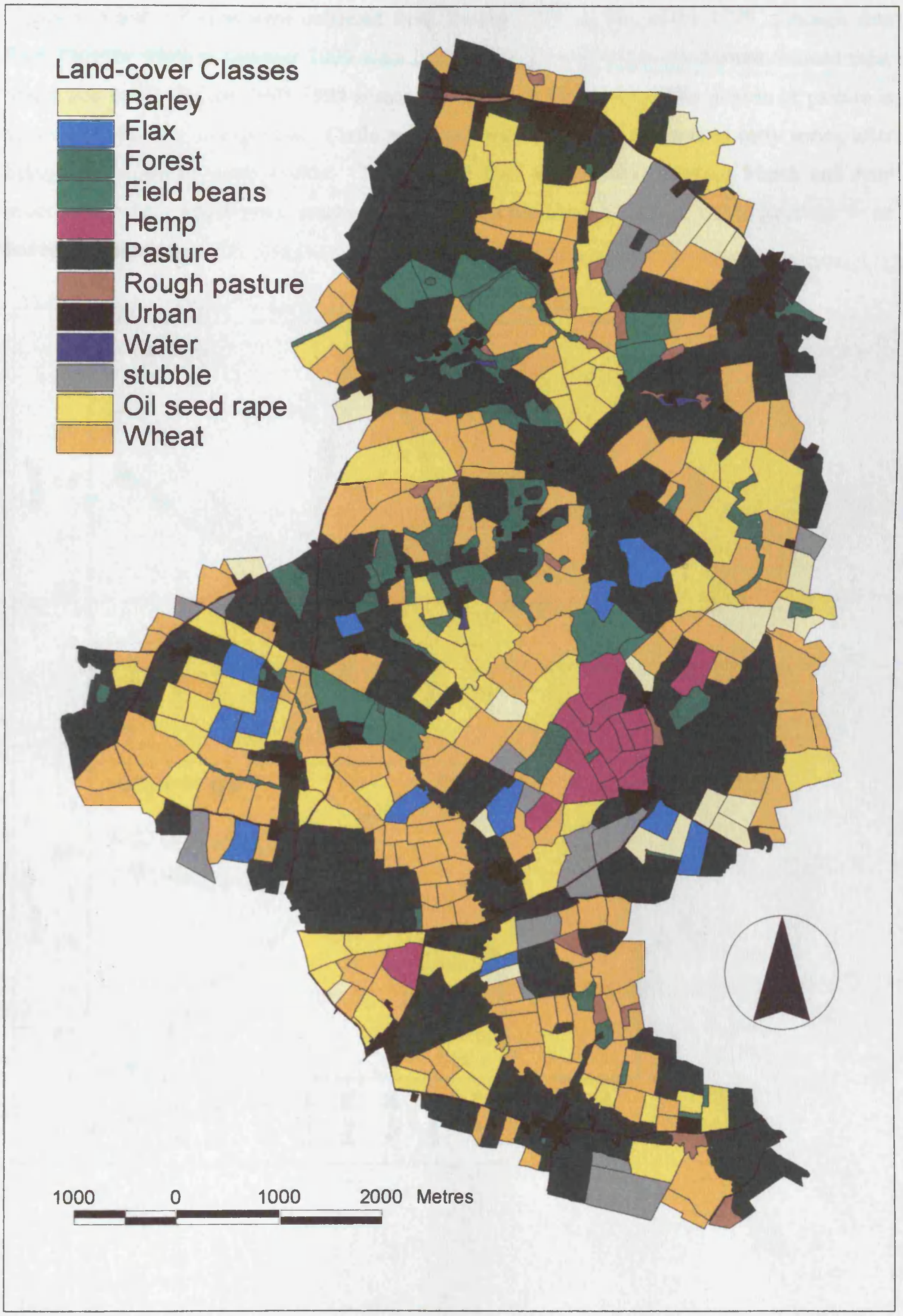

Figure 4.2 Land cover map based on field survey of whole of Stonton Brook for agricultural season 1998-1999. Changes in land cover for late summer and autumn of 1999 are not included.

Vegetation and soil data were collected from January 1998 to November 1999, although data from October 1998 to October 1999 were used. Crop growth charts for pasture, oilseed rape, wheat and barley for the 1998-1999 season are shown in Figure 4.3. The growth of pasture is very erratic but this is expected. Cattle and sheep were placed on the land in early spring after being over wintered under shelter. The drop in LAI and biomass between March and June accounts for this. Sheep were removed in June from the observed fields, which gave rise to an increase in biomass.

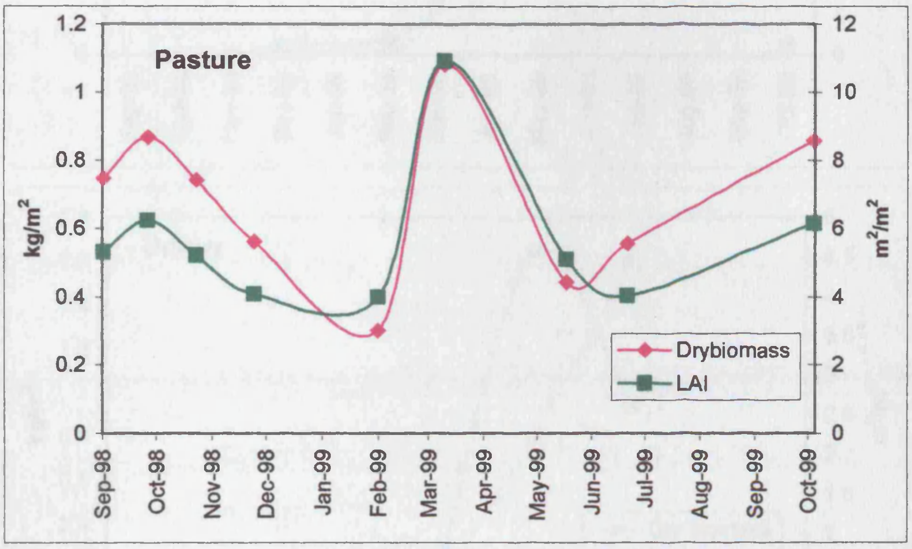

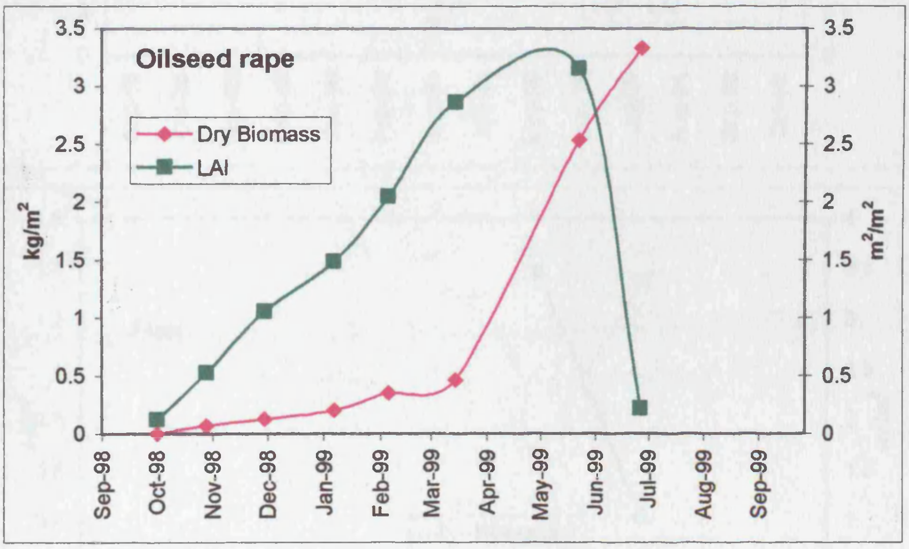

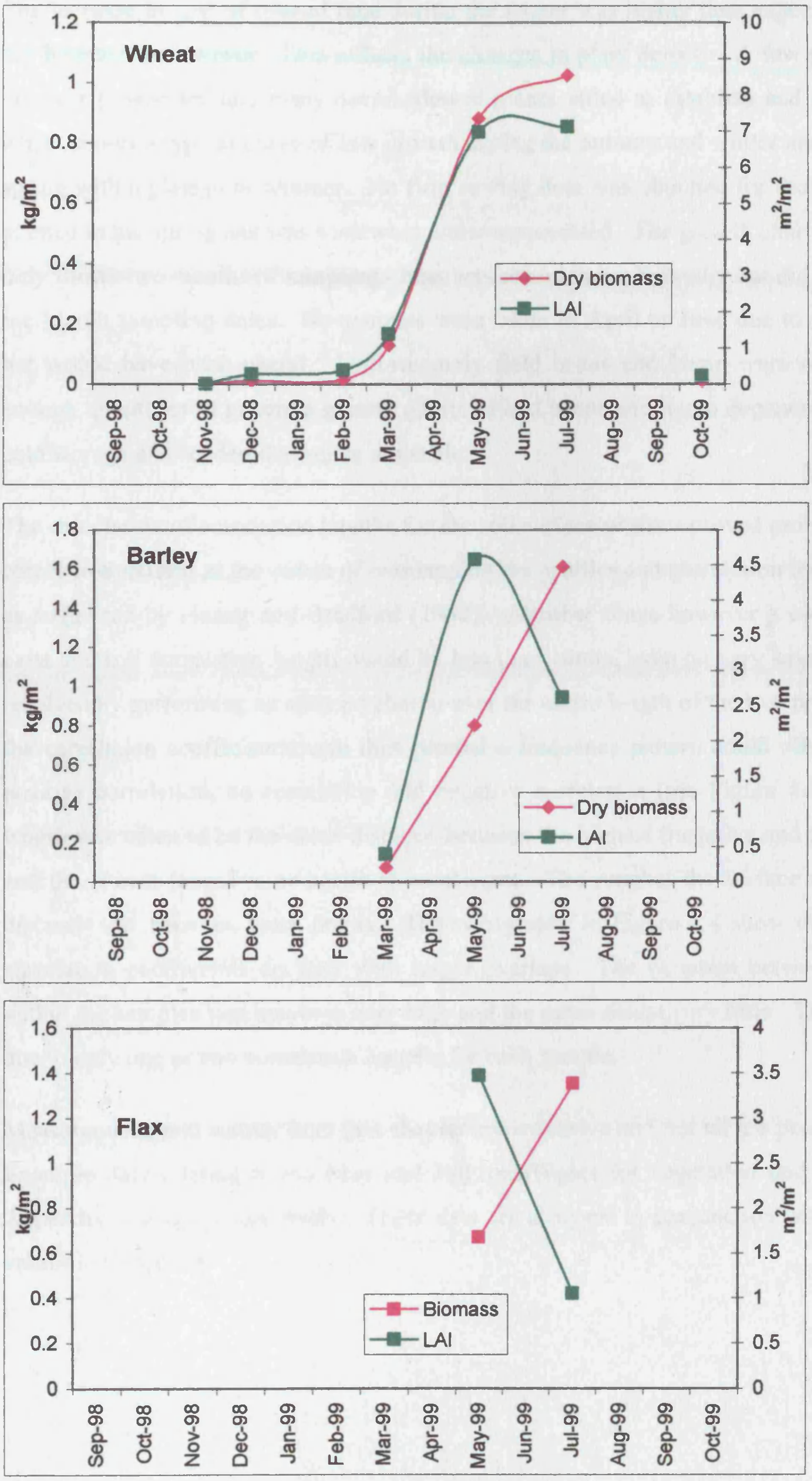

Figure 4.3 Crop growth charts for pasture, oilseed rape, winter wheat, spring barley and flax. Data were averaged from across the catchment. Field beans and hemp are not represented because of incomplete measurements.

The increase in LAI of oilseed rape during the winter was higher than expected but increases in dry biomass were lower. This reflects the changes in plant density. A few plants dominated as the year progressed and many overshadowed plants failed to establish and mature. Growth in wheat shows a typical curve of low growth during the autumn and winter and a sharp rise in the spring with a plateau in summer. No firm sowing date was obtained for the barley. Barley was planted in the spring and was somewhat under represented. The growth chart for flax is poor and only shows two months of sampling. Flax was sowed in the February but did not show until after the March sampling dates. No samples were taken in April or June due to resource limitations but would have been useful. Unfortunately field beans and hemp were not sampled in high enough quantities to generate growth charts. Field beans and hemp degenerated very quickly in cold storage and rendered samples unusable.

The calculation of correlation lengths for the soil surface profiles proved problematic. At times a correlation existed at the outset of overlapping the profiles and correlation lengths were obtained as suggested by Huang and Bradford (1990). At other times however a correlation would not exist and soil correlation length would be less than 10mm, even on very smooth soils. This was resolved by performing an autocorrelation over the entire length of the two profile boards. When the correlation coefficients were then plotted a frequency pattern could often be seen between positive correlation, no correlation and negative correlation (see Figure 4.4). The correlation length was taken to be the mean distance between the highest (negative and positive) coefficient and the lowest (negative or positive) coefficient. The rougher the surface was, the shorter the distance was between these points. The two graphs in Figure 4.4 show that the potential for correlation coefficients declines with larger overlaps. The variation between the samples and within the samples was however very high and the mean meant very little. This was exacerbated due to only one or two correlation lengths for each sample.

Measurements and results from this chapter are extensive and not all are presented in the thesis. Example data relating to the May and July overflights for vegetation and soils are shown in Appendix A and B respectively. These data are analysed in conjunction with radar backscatter values in Chapter 8.

Table 4.2 Sampling locations and characteristics.

Field Code	Ordnance Survey Co-ordinates	Crop cover	Soil association	Sampling dates (crop/soil)
1	475800, 291800	Wheat	Fladbury	Nov 98, Feb99/May, July, Aug 99
2	475820, 291850	Wheat	Fladbury	Nov 98, Feb99/May, July, Aug 99
3	475950, 291900	Pasture (sheep)	Fladbury	Nov 98, Feb99/May, July, Aug 99
4	475970, 291920	Pasture (sheep)	Fladbury	Nov 98, Feb99/May, July, Aug 99
5	475850, 292470	Pasture (cattle)	Fladbury	Nov 98, Feb99/May, July, Aug 99
6	475800, 292470	Pasture (cattle)	Fladbury	Nov 98, Feb99/May, July, Aug 99
7	475680, 292550	Oilseed rape	Wickham 2	Nov 98, Feb99/May, July, Aug 99
8	475720, 292550	Oilseed rape	Wickham 2	Nov 98, Feb99/May, July, Aug 99
9	472870, 294550	Wheat	Hanslope	Nov 98, Feb99/May, July, Aug 99
10	472900, 294550	Wheat	Hanslope	Nov 98, Feb99/May, July, Aug 99
11	474260, 293850	Wheat	Beccles	Nov 98, Feb99/May, July, Aug 99
12	474010, 293800	Wheat	Beccles	Nov 98, Feb99/May, July, Aug 99
13	473900, 293850	Stubble	Beccles	Nov 98, Feb99/May, July, Aug 99
14	473760, 294140	Barley	Beccles	Nov 98, Feb99/May, July, Aug 99
15	473520, 294080	Barley	Beccles	Nov 98, Feb99/May, July, Aug 99
16	473750, 294250	Linseed	Beccles	Nov 98, Feb99/May, July, Aug 99
17	473745, 294290	Linseed	Beccles	Nov 98, Feb99/May, July, Aug 99
18	473740, 294460	Oilseed rape	Beccles	Nov 98, Feb99/May, July, Aug 99
19	473740, 294400	Oilseed rape	Hanslope	Nov 98, Feb99/May, July, Aug 99

Table 4.2 (cont.)

Field Code	Ordnance Survey Co-ordinates	Crop cover	Soil association	Sampling dates (crop/soil)
20	473100, 295040	Wheat	Wickham	Nov 98, Feb99/May, July, Aug 99
21	473270, 295050	Wheat	Fladbury	Nov 98, Feb99/May, July, Aug 99
22	473520, 295500	Linseed	Ragdale	Nov 98, Feb99/May, July, Aug 99
23	473600, 295530	Linseed	Ragdale	Nov 98, Feb99/May, July, Aug 99
24	474520, 295180	Stubble	Wickham	Nov 98, Feb99/May, July, Aug 99
25	474510, 295240	Stubble	Wickham	Nov 98, Feb99/May, July, Aug 99
26	475900, 292600	Pasture (sheep)	Wickham	Nov 98, Feb99/May, July, Aug 99
27	475900, 292680	Pasture (sheep)	Wickham	Nov 98, Feb99/May, July, Aug 99
28	474750, 297150	Hemp	Ragdale	Nov 98, Feb99/May, July, Aug 99
29	474580, 297200	Hemp	Ragdale	Nov 98, Feb99/May, July, Aug 99
30	475350, 298100	Oilseed rape	Ragdale	Nov 98, Feb99/May, July, Aug 99
31	475360, 298070	Oilseed rape	Ragdale	Nov 98, Feb99/May, July, Aug 99
32	475500, 299270	Oilseed rape	Banbury	Nov 98, Feb99/May, July, Aug 99
33	475590, 299210	Oilseed rape	Banbury	Nov 98, Feb99/May, July, Aug 99
34	473150, 299010	Wheat	Hanslope	Nov 98, Feb99/May, July, Aug 99
35	473155, 298950	Wheat	Hanslope	Nov 98, Feb99/May, July, Aug 99
36	473150, 299130	Oilseed rape	Hanslope	Nov 98, Feb99/May, July, Aug 99
37	473050, 299120	Oilseed rape	Hanslope	Nov 98, Feb99/May, July, Aug 99
38	471880, 296100	Oilseed rape	Hanslope	Nov 98, Feb99/May, July, Aug 99

Table 4.2 (cont.)

Field Code	Ordnance Survey Co-ordinates	Crop cover	Soil association	Sampling dates (crop/soil)
39	471800, 295930	Oilseed rape	Hanslope	Nov 98, Feb99/May, July, Aug 99
40	471250, 297210	Linseed	Hanslope	Nov 98, Feb99/May, July, Aug 99
41	471180, 297050	Linseed	Hanslope	Nov 98, Feb99/May, July, Aug 99
42	472960, 302600	Wheat	Ragdale	Nov 98, Feb99/May, July, Aug 99
43	473000, 302520	Wheat	Ragdale	Nov 98, Feb99/May, July, Aug 99
44	472910, 302500	Pasture (sheep)	Ragdale	Nov 98, Feb99/May, July, Aug 99
45	472880, 302440	Pasture (sheep)	Ragdale	Nov 98, Feb99/May, July, Aug 99
46	474670, 297700	Linseed	Ragdale	Nov 98, Feb99/May, July, Aug 99
47	474730, 297750	Linseed	Ragdale	Nov 98, Feb99/May, July, Aug 99
48	474700, 297380	Field beans	Ragdale	Nov 98, Feb99/May, July, Aug 99
49	474610, 297310	Field beans	Ragdale	Nov 98, Feb99/May, July, Aug 99
50	472710, 300950	Field beans	Wickham 2	Nov 98, Feb99/May, July, Aug 99
51	472690, 301050	Field beans	Ragdale	Nov 98, Feb99/May, July, Aug 99
52	473380, 300780	Field beans	Ragdale	Nov 98, Feb99/May, July, Aug 99
53	473440, 300810	Field beans	Wickham 2	Nov 98, Feb99/May, July, Aug 99
54	475320, 302010	Stubble	Ragdale	Nov 98, Feb99/May, July, Aug 99
55	475240, 302100	Stubble	Ragdale	Nov 98, Feb99/May, July, Aug 99
56	475490, 301810	Barley	Hanslope	Nov 98, Feb99/May, July, Aug 99
57	475550, 301750	Barley	Hanslope	Nov 98, Feb99/May, July, Aug 99

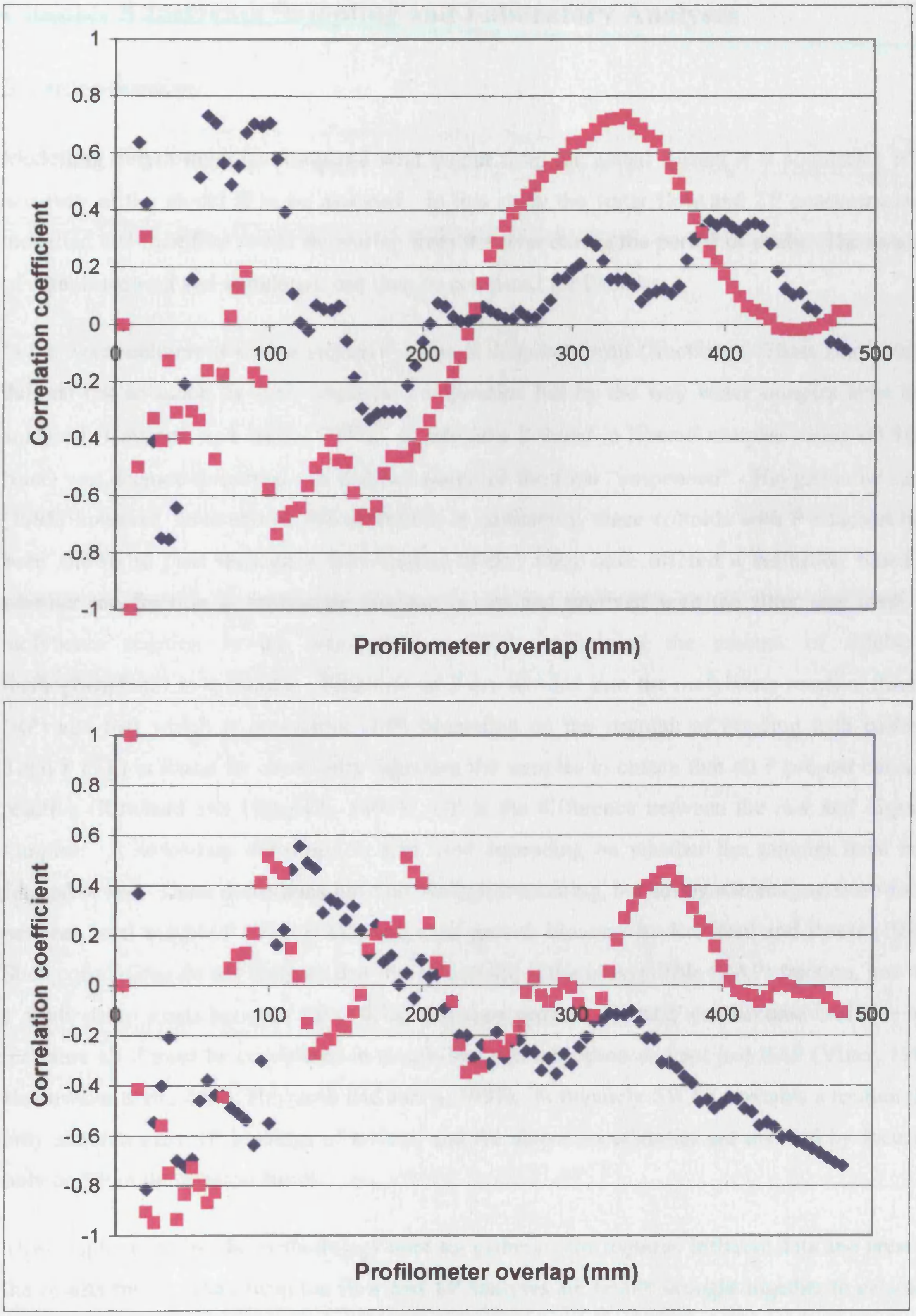

Figure 4.4 Plot of four sets of data from profilometer measurements. The overlapping procedure starts from the left and moves to the right until all values from both sets of data are used in correlation coefficient. Note erratic pattern in correlation coefficients at beginning with clearer pattern to right.

Chapter 5 Instream Sampling and Laboratory Analyses

5.1 Introduction

Modelling output must be compared with output from the actual system it is simulating if the accuracy of the model is to be assessed. In this study the water flow and TP concentration is modelled and therefore needs measuring from the river during the period of study. The two sets of data; measured and simulated, can then be compared for likeness.

In the water column of a river system P exists in different forms (fractions). These fractions are defined not so much by their chemical composition but by the way water samples have been analysed (Haygarth and Jarvis, 1998). At one time P found in filtered samples (using <0.45μm filter) was deemed dissolved and that remaining on the filter "suspended". Haygarth and Jarvis (1998) however, have shown this definition is misleading, since colloids with P attached have been shown to pass through a 0.45-micron filter. They have offered a definition based on whether the fraction is molybdate reactive or not and prefixed with the filter size used. A molybdate reaction is the standard means of determining the amount of soluble P (orthophosphate) in a sample. Fractions of P are divided into the molybdate reactive fraction (RP) and that which is unreactive (UP) depending on the strength of bonding with colloids. Total P (TP) is found by chemically digesting the samples to ensure that all P present becomes reactive (Rowland and Haygarth, 1997). UP is the difference between the raw and digested samples. A secondary definition is also used depending on whether the samples have been filtered or not. These definitions have no biological meaning, but strong correlations were found between total soluble P (TP(<0.45)) and algal growth bioassay by Bradford and Peters (1987). Such correlations do not indicate that the TP (<0.45) is the bioavailable (BAP) fraction, just that a relationship exists between TP (<0.45) and algal growth. Fixed P can become available and therefore all P must be considered in controlling eutrophication and not just BAP (Viner, 1987; Heathwaite *et al.*, 1996; Haygarth and Jarvis, 1997). Fortunately SWAT contains a routine that only simulates the TP loadings of a river, and the above uncertainties are avoided by focusing only on TP in the Stonton Brook.

This chapter explains the methodology used for gathering the required instream data and presents the results found. Data from the flow and TP analyses are finally brought together to calculate TP loadings for the Stonton Brook. The comparisons with simulated flow are given in Chapter 9.

5.2 Methodology for instream data collection

There is a danger that flow and instream chemicals can be underestimated by sub-optimum sampling (OECD, 1982; Burn, 1991). If the sampling regime is inadequate, storm events are likely to be underrepresented and thus flow and P loadings underestimated (OECD, 1982; Burn, 1991). This is especially so with the high dynamics of small rivers and the sudden rise and fall surrounding rainfall events (House and Denison, 1998). Therefore, the sampling frequency needed to be great enough to ensure the dynamics of the river is sampled but few enough to be economically viable. The SWAT model simulates the flow and P loadings on a daily time step. The sampling regime must therefore provide at least daily data for direct comparison. Daily data will be enough to provide a comparison with the simulated output, but they may not be enough to disclose accurate information about the dynamics of TP, and could underestimate the actual P loadings in a river. Burn (1991) highlighted the problem of using a low frequency monitoring scheme to estimate the chemical loading of a river. He suggested a flexible method of sampling at frequencies relative to the flux dynamics in the river. The flux in the river will be greatest just after a rainfall event and until the spate has subsided. The most intense sampling period should therefore be during this period. The sampling frequency can be reduced when no rain has fallen for some time and the change in levels of diffuse chemicals will be minimal. A system such as that suggested by Burn (1991) requires very close monitoring of rainfall events and easy access to the sampling machine to adjust the sampling frequencies. Such flexibility was not available due to other commitments in the Ph.D. A constant high frequency scheme was opted for which sampled throughout the year at the same intensity. Synchronisation between the flow sampling and phosphorus sampling was not a priority but the frequencies were kept similar.

Field characteristics such as soil moisture can change with similar speed to the flow and phosphorus flux in a river. Conversely, changes in other field characteristics such as leaf area or land cover will take longer and require sampling less often. These issues will be dealt with in the relevant chapters.

Due to the lag time between rainfall and water exiting the system, the sampling period was extended for a given time before and after the simulation period. Lag time is a characteristic of each river but is dependent on overall length, soil characteristics, mean slope of land, slope of the main channel and channel geometry. The location and direction of each storm will have a large effect on lag for individual storm events (Viessman and Lewis, 1996) but this cannot be accounted for within the project.

Water samples for TP analysis were collected using an automatic water sampler. The storage of water samples over the period of one week in the field could alter the composition of the P fractions (i.e. SRP and PP) (Haygarth *et al.*, 1995). This would have no effect on the overall TP contained within the sample, but P can be removed from the water by an accumulation of biofilm on the inside of the bottle. If this biofilm is not re-suspended for sub-sample extraction the TP will be underestimated. Acid fixing (Rowland and Haygarth, 1997) was considered using three Molar sulphuric acid placed in the empty bottles prior to placement in the field in order to prevent bioactivity. However, this would have involved elaborate Health and Safety precautions, including a lockable security cage for the sampler. The cage would have attracted attention whereas the sampling unit on its own was sufficiently small to avoid attention, and potential abuse. For these reasons acid fixing was not used, but a comparative test was conducted between raw water samples and water samples fixed with acid.

There are many components of phosphorus contained in the water column of a river (McKelvie *et al.*, 1995). This study is linked to eutrophication and needs to consider those portions of phosphorus that are bioavailable. Phosphorus that is not bioavailable at a given time however, may become so in the river at some later date (Heathewaite *et al.*, 1996; House and Denison, 1998). Additionally, there is much discussion about the definition of the various fractions (McKelvie *et al.*, 1995). The definition of soluble reactive phosphorus (SRP) is the portion passing a 0.45μm sieve that reacts with acidic molybdate to form the phosphomolybdenum blue composite. It has been demonstrated that the fraction passing through the sieve is not just soluble P and that the sieve will retain some of the soluble P as the sample passes through it (McKelvie *et al.*, 1995; Rowland and Haygarth, 1997). Although SWAT can consider particulate P and soluble P (PP and SP respectively), this study only considered total phosphorus (TP) due to the above uncertainties.

5.2.1 Flow measurements

Flow was estimated using a disused weir near the outlet of the Stonton Brook. This weir was only designed and calibrated for flow up to 0.302m (0.65cumecs) above the crest, accounting for just over 90% of the flow records (Plate 5.1). Flow higher than this level would contain a large proportion of the annual phosphorus budget of the brook, and therefore it was important to measure high flow as well (Haygarth *et al.*, 1998). A road bridge existed approximately 15m upstream of the weir that had a concrete base and sidewalls and a uniform cross section. The river was well contained under the bridge and it was therefore suitable as a high-flow weir.

The weir was a suppressed, sharp-crested rectangular weir with a 1.8m wide crest. The standard tables for the weir were obtained from the Environment Agency, and Hugh Laurie (EA, Kettering) helped to ensure the weir flow was still applicable to the table. The weir was excessively overgrown in algae and mosses when first found and had to be cleaned with a wire brush to ensure unrestricted flow. Thereafter it was cleaned on a monthly basis during the growth period. Growth on the weir was vigorous and indicated the elevated nutrient status of the river.

When the river depth was greater than 0.302m on the staff, flow was estimated by measuring velocity below the bridge across the Stonton Brook. The area velocity method was used to estimate the flow at the bridge (Grant and Dawson, 1978). The river cross section was measured during a period of low flow and is shown in Figure 5.1. A Flowmate 2000CM current meter with EM 3000 electromagnetic flow sampler wand was used to measure current velocity. Measurements were taken from a grid across the river of 200mm between the verticals and horizontals and 50mm from the bottom and 100mm from the sides. In addition the 6-tenths method was trialled, which is reported to provide the average velocity for a given cross sectional area of water (Grant and Dawson, 1978). River velocity was then taken as the mean of all measurements. Flow was calculated using the mean velocity multiplied by the cross-sectional area of the river at the depth recorded. Such information was related to the logger data and the gaps infilled using an inverted regression equation.

The flow for the Stonton Brook was indirectly recorded using a data logger and depth transducer. Measurements taken from the data logger were then calibrated using simultaneous readings from the logger and the low and high flow weirs. Readings were taken on every visit made to the brook for data on this relationship. There were few storms during the period of sampling and only five opportunities to measure flow beneath the bridge. A local dog walker informed the author that the river depth reached the underside of the bridge during the extreme storms of February and March 1998, and caused flooding upstream. The maximum flow through this part of the river was therefore approximately six cumecs ($5.7m^2$ x $1m\ sec^{-1}$). This value would have increased if the bridge was breached but would be very difficult to quantify.

Plate 5.1 Stonton Brook weir. Note bridge over river in background that was used as high flow weir.

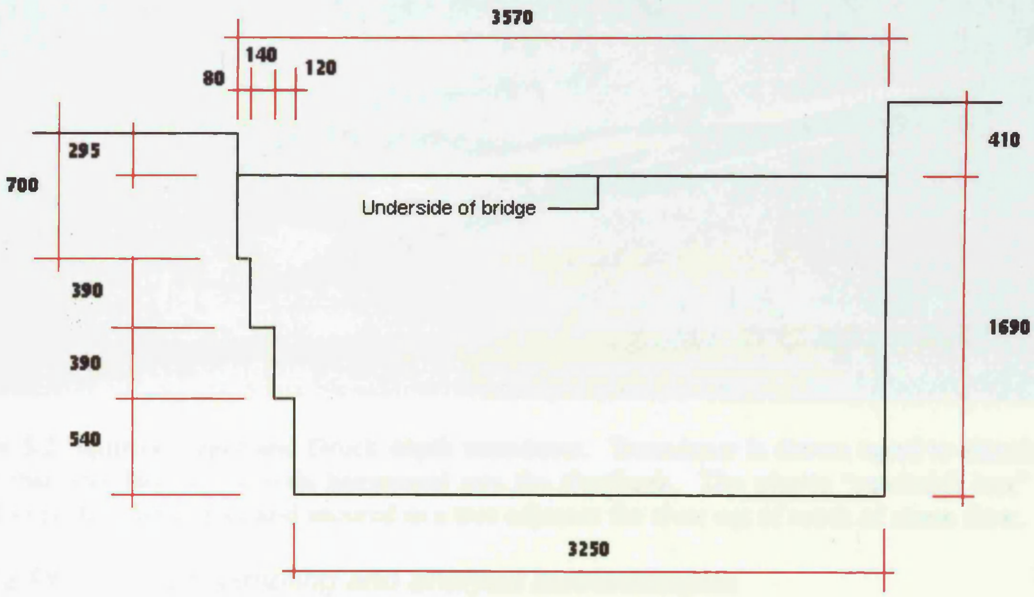

Figure 5.1 Outline sketch of the concrete structure below the bridge over the Stonton Brook at Rowden Lane. On two occasions the brook had swollen to fill the entire area under the bridge.

The depth transducer used was a Druck PTX 530, calibrated for a range of 1.5m depth and resolution of 5mm. This was connected to a Grant Squirrel data logger SQ1001 with 64 KB memory (Plate 5.2). When linked to an external 12V lead acid battery the logger and transducer could collect data on river depth for 2.5 months. The logger and transducer was stationed 25 m upstream from the weir and set to collect a mean depth every thirty minutes based on average readings from ten-minute intervals. Data sets were downloaded to a laptop via serial connection. The data were converted to MS Excel format using the software supplied with the Squirrel logger.

For several intervals during the sampling period the logger or depth transducer didn't work. To fill in these voids data were obtained from Anglian Water Authority for an existing weir on the Welland at Tinwell. A regression was fitted to the data to investigate the relationship, and predict values at Stonton for the missing periods. Although Tinwell was 10 miles from the Stonton Brook it was the nearest suitable location.

Plate 5.2 Squirrel logger and Druck depth transducer. Transducer is shown taped to aluminium pole that was fastened to rods hammered into the riverbank. The plastic "sandwich box" was used to protect the logger and secured in a tree adjacent the river out of reach of storm flow.

5.2.2 Phosphorus sampling and analysis methodologies

Sampling was carried out using a GLI International "Hobo 24" automatic water sampler as shown in Plate 5.3. The unit contained 24 bottles and could be programmed quickly to extract samples as often as one minute. Each bottle could be filled using one sample or four sub-samples. The unit was placed at the outlet of the catchment and set to fill a bottle every seven hours using four sub-samples taken every 1.75 hours. The bottles were collected weekly under this regime. For one period in August 1999 a bottle was filled every 14 hours (sub-samples every 3.5 hours) because the bottles could not be collected for two weeks. The full sample bottles were taken to the laboratory and analysed generally within two days of collection. The laboratory protocol is shown in Appendix C.1 with a photograph of the analysis bottles in Plate 5.4. Cleanliness received the highest of priorities and all equipment was washed by machine with acetic acid rinse and then soaked overnight in 10% v/v nitric acid before three rinses in deionised water and drying. Care was taken to ensure that the bottles were well mixed prior to extraction of an aliquot.

Plate 5.3 Hobo 24 bottle sampler. Control panel is seen to the upper right corner of the box. A single 12V lead acid battery powers the sampler and for cold periods in winter an additional car battery was used in series for reliability.

Plate 5.4 Phosphorus analysis in progress. Note nine control bottles in middle of picture. Colours within the image have been badly affected during the photographic process. Contents of the bottles were all blue.

In an attempt to assess the effects of storage on the TP and potential of acid fixation, eight water samples were taken from the Stonton Brook at a period of slack flow. Four samples received 25ml of three molar sulphuric acid (A) and the other four received 25ml of deionised water (B). The controls (C) were filled with deionised water and 25ml of 3M sulphuric acid. All treatments were stored in identical bottles, sealed and refrigerated at 4°C prior to and between analyses. Two sets of analyses were performed, one within twenty-four hours of collection and another seven days later. This latter period was the same as the interval between the filling of the first and last bottle of the auto-sampler.

The Environment Agency uses the method given in their Laboratory Procedures Manual (NRA, 1991), which is based on the method given by Murphy and Riley (1962) and amended by Eisenreich *et al.* (1975). This method was used at the beginning of the sampling period but a modified method described by Rowland and Haygarth (1997) was more reliable and operationally simpler.

5.3 Results

The sampling period began in January 1998, but because of a weak initial analytical methodology for TP (NRA, 1991) and damage to equipment caused by the floods of February and April 1998, the results were not robust and complete enough until June 1998. The Druck sensor was out of commission between July 1998 and January 1999, and complete data of flow and loadings were not available until the winter of 1999. Data was infilled using relationships between the Stonton Brook and Welland at Tinwell. A continuous data set was produced this way with additional periods for the beginning and end to allow for lag.

5.3.1 Flow results

The instream sampling occurred for a period of 15 months from January 1998 to November 1999. The readings from the depth sensor are shown in Figure 5.2 below. The relative depths were converted to flow by generating a linear, least squares regression equation between the above data and the readings taken at the weir and logger simultaneously. This relationship is shown in Figure 5.3. The graph in Figure 5.3 indicates that a reliable linear relationship existed between the weir readings and the depth logger (n=39). By inverting the regression equation shown in 5.3a, reliable predictions of the depth at the weir were made from readings of the depth transducer to provide predicted weir depths.

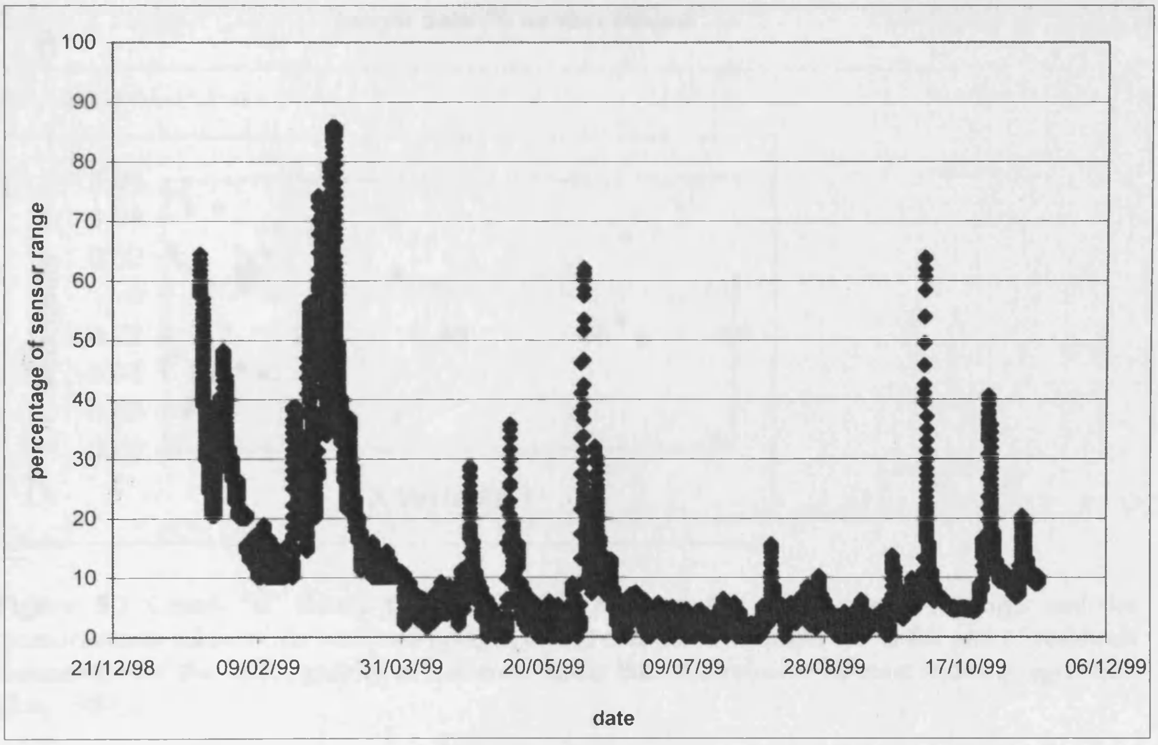

Figure 5.2 Relative river depth as measured by the depth sensor.

Before the flow was estimated the relationship between water depth and flow taken at the bridge was investigated. This is shown in Figure 5.4 and used the data averaged over a seven-hour period to match that of the phosphorus levels. Finally, the depth estimates were converted to flow using the standard table for the weir and the flow estimate from the bridge. The flow data as estimated from the relationships between the depth measurements and the weirs are illustrated in Figure 5.5 (n=155).

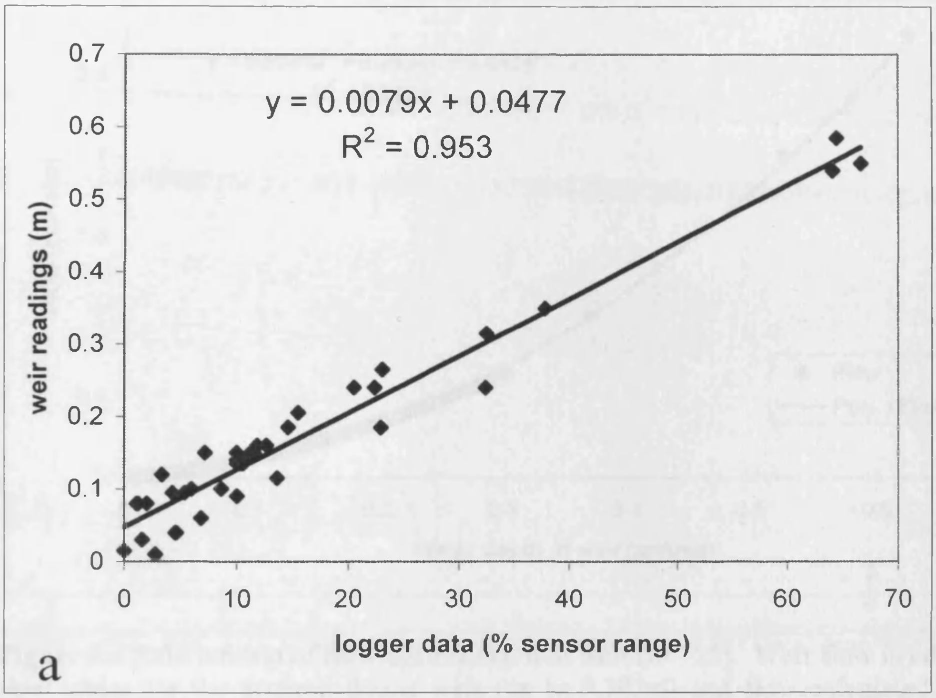

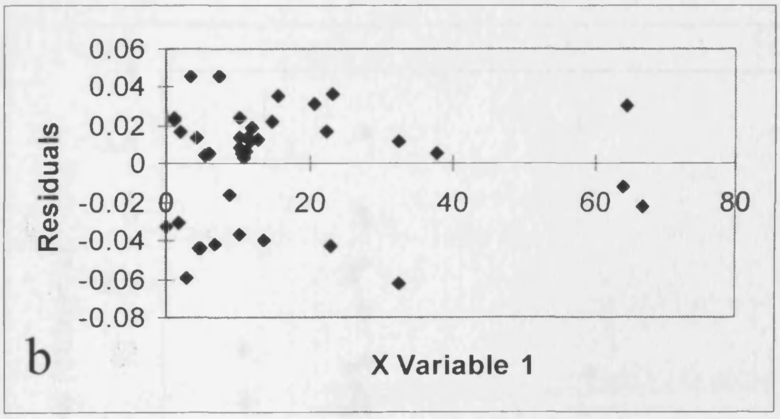

Figure 5.3 Graph "a" shows the relationship between the depth sensor readings and the measurements taken at the weir and bridge (values over 0.3m). Graph "b" is the plot of residuals indicating that the heterogeneity of variance meets the requirements of least squares regression (Zar, 1984).

Gaps in the above data were infilled using a regression equation based on the measurements taken by the Environment Agency from the weir below the extraction point at Tinwell and the measured flow at Stonton Brook. The relationship between these two populations is shown in Figure 5.6. It can clearly be seen that when the flow in the Stonton Brook rises above one cumec the relationship starts to break down. The actual cause of this break down is speculative but is probably due to the influence of storms on other tributaries supplying the river at Tinwell.

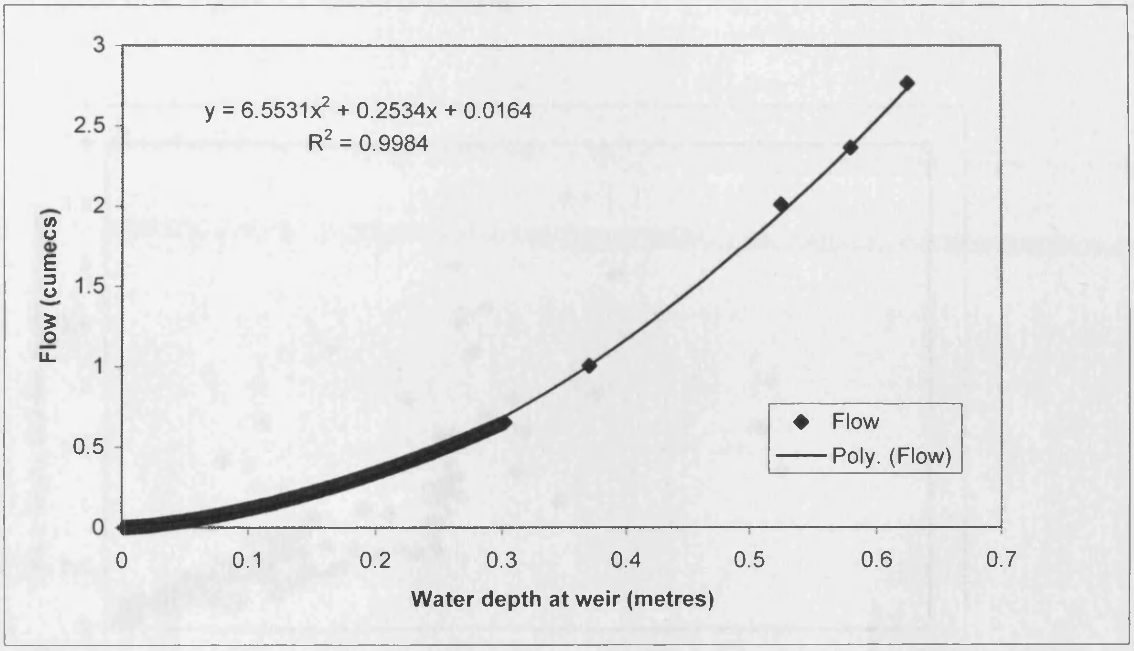

Figure 5.4 Relationship of flow against depth at weir (n=155). Weir flow is taken from standard flow tables for the Stonton Brook weir (up to 0.302m) and flow calculated under the bridge (above 0.302m).

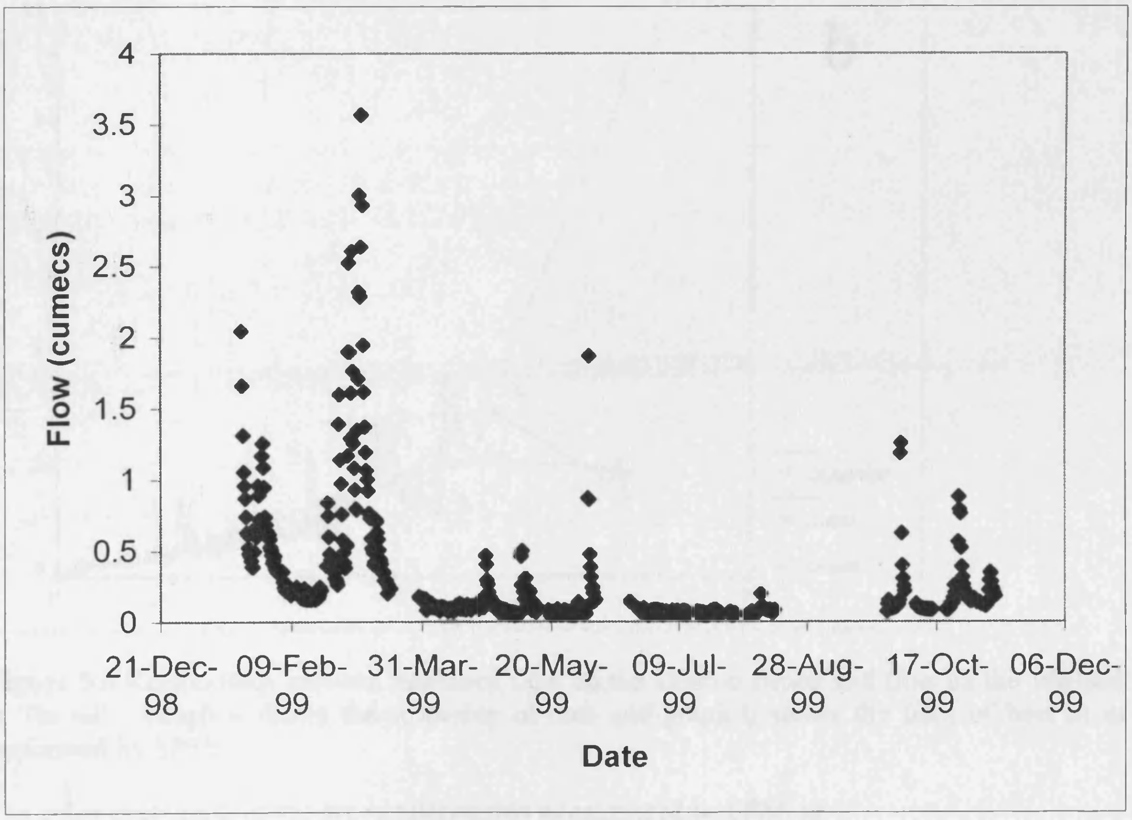

Figure 5.5 Flow data estimates at Stonton Brook between 20 January 1999 and 8th November 1999. The large gaps in data are due to damaged depth measurement equipment. Note fewer data points from Figure 5.2 due to averaging.

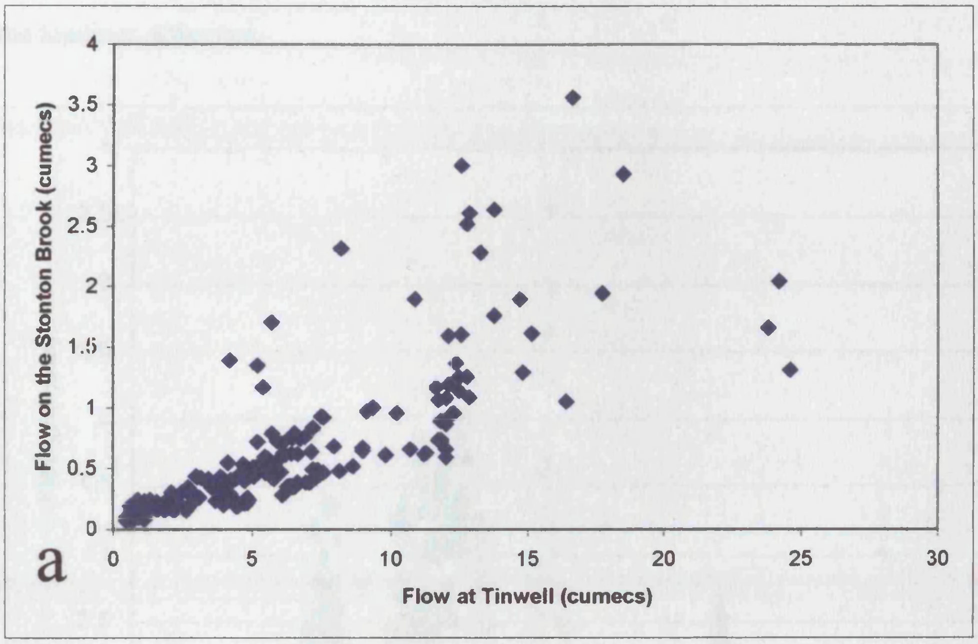

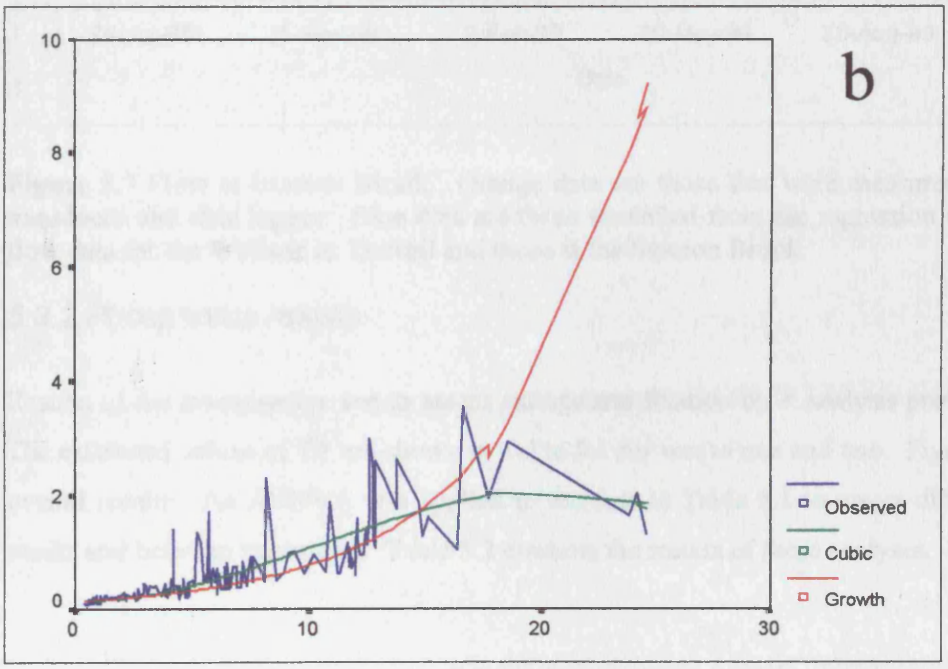

Figure 5.6 Relationship between measured flow on the Stonton Brook and flow on the Welland at Tinwell. Graph a shows the scattering of data and graph b shows the lines of best fit as performed by SPSS.

The cubic expression of the above relationship as calculated by SPSS is:

$$y = 0.1560 - 0.0121x + 0.0153x^2 - 0.0005x^3 \qquad (5.1)$$

This equation is applied to the data from Tinwell to infill missing data for the Stonton Brook. The combined results are shown in Figure 5.7. There is a lower threshold and anomaly in the predicted data due to the regression equation that appears to overestimate the flow during periods of base flow. These data were then amalgamated with the phosphorus data (next section) to form the loadings estimates.

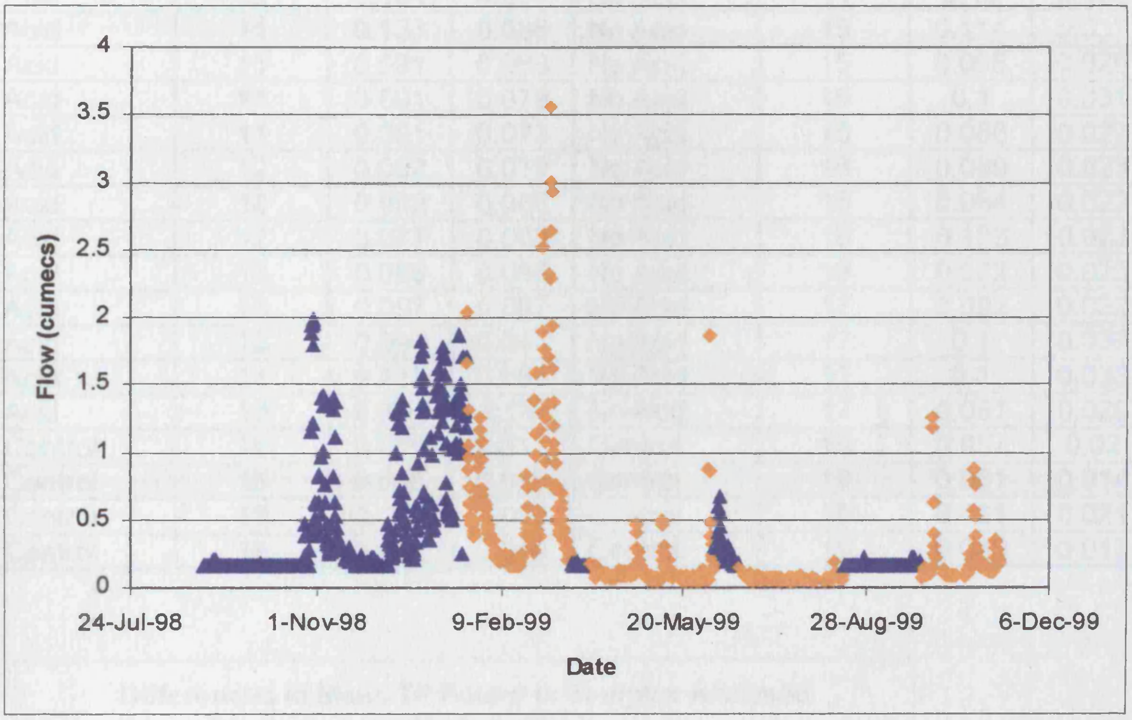

Figure 5.7 Flow at Stonton Brook. Orange data are those that were measured using the depth transducer and data logger. Blue data are those modelled from the regression equation between flow data for the Welland at Tinwell and those at the Stonton Brook.

5.3.2 Phosphorus results

Results of the investigative test to assess storage and fixation on P analysis proved inconclusive. The estimated values of TP are shown in Table 5.1 for weeks one and two. Figure 5.8 shows the overall results. An ANOVA was applied to the data in Table 5.1 to assess differences between weeks and between treatments. Table 5.2 contains the results of these analyses.

Table 5.1 Results from investigative analysis to determine change in TP in stored river water over time. Controls contained deionised water.

Treatment	Sample	TP W1 (μg l^{-1})	TP W2 (μg l^{-1})	Treatment	Sample	TP W1 (μg l^{-1})	TP W2 (μg l^{-1})
Acid	10	0.111	0.093	No Acid	14	0.169	0.093
Acid	10	0.092	0.089	No Acid	14	0.115	0.053
Acid	10	0.089	0.081	No Acid	14	0.114	0.053
Acid	10	0.104	0.077	No Acid	14	0.12	0.038
Acid	11	0.133	0.086	No Acid	15	0.114	0.031
Acid	11	0.091	0.088	No Acid	15	0.098	0.029
Acid	11	0.091	0.079	No Acid	15	0.1	0.031
Acid	11	0.091	0.073	No Acid	15	0.086	0.029
Acid	12	0.092	0.079	No Acid	16	0.089	0.023
Acid	12	0.092	0.086	No Acid	16	0.084	0.022
Acid	12	0.077	0.083	No Acid	16	0.103	0.023
Acid	12	0.088	0.086	No Acid	16	0.072	0.025
Acid	13	0.097	0.097	No Acid	17	0.092	0.032
Acid	13	0.094	0.093	No Acid	17	0.1	0.037
Acid	13	0.113	0.083	No Acid	17	0.1	0.033
Acid	13	0.094	0.08	No Acid	17	0.091	0.029
Control	18	0.055	0.017	Control	19	0.057	0.02
Control	18	0.055	0.015	Control	19	0.061	0.014
Control	18	0.057	0.018	Control	19	0.061	0.021
Control	18	0.063	0.018	Control	19	0.043	0.012

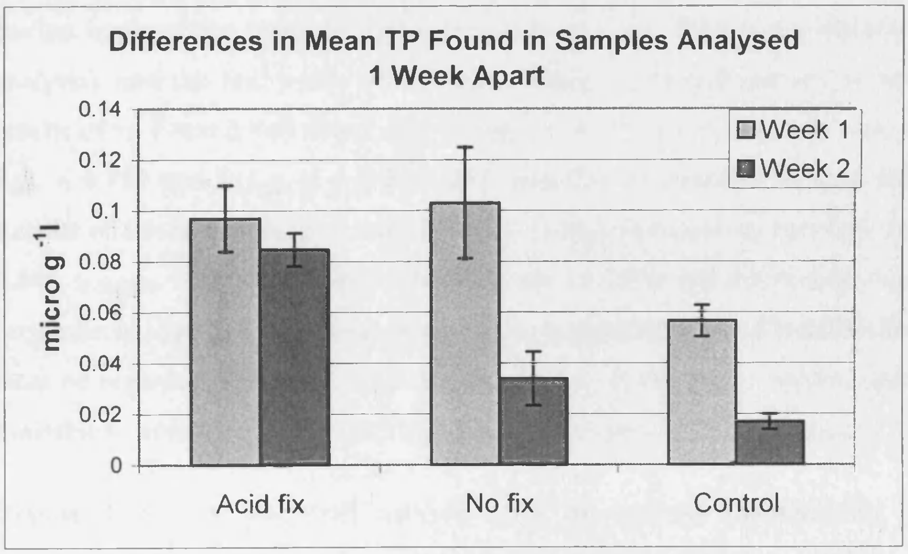

Figure 5.8 Results from analysis carried out on eight samples of river water. Four were treated with acid fix and four without. Error bars indicate standard deviation. Difference between weeks one and two for the control renders the test null.

Table 5.2 Results of the two-way ANOVA to determine differences between treated water and untreated water.

Due To	Sum of Squares	DoF	Mean Square	F-Stat	Significance
Main Effects	0.062	3	0.021	100.251	0.0000
Treatment	0.031	2	0.016	75.331	0.0000
Week	0.031	1	0.031	150.091	0.0000
2-Way Interactions	0.012	2	0.006	28.478	0.0000
Treatment × Week	0.012	2	0.006	28.478	0.0000
Explained	0.074	5	0.015	71.542	0.0000
Error	0.015	74	0.000		
Total	0.090	79	0.001		

Further results using the Student-Newman-Keuls test indicated differences between all treatments and between the weeks for the controls and samples without acid fix. No difference exists between levels of TP in the acid fixed samples. The differences between the control samples rendered the test null and void. The test was repeated but with similar results. Sample analysis would have seen similar effects according to the above test without acid fixation. It could be expected that the first and last bottles would not be comparable due to the drop in TP in the first bottle as indicated above. For this reason adjacent samples from consecutive collections of bottles were assessed for differences to investigate this potential disparity. A t-test was performed on these two sets of data on the basis that there would have been a difference between the last bottle of one collection (after having been in the field for a maximum of 24 hours prior to analysis), and the first bottle of the next collection (a minimum of one week old). From the results of an F-test it was found that the variances of the two data sets were unequal ($P = 0.001$, $F_{calc} = 4.154$ and $F_{0.05(1),\ 21} = 2.084$) and therefore an unequal variance t-test was performed. Results of this test indicate no significant difference between the two data sets ($P = 0.404$, $t_{calc}=-0.846$, $t_{0.05(2),20} = 2.04$). This test indicates there was little effect of storage time on TP. It must be remembered that this was not an experiment purposefully set up to assess the two data sets and must be regarded with some caution. Regardless of the above results, the resources were not available to acid fix and the sampling procedure as described in Appendix C1 was followed.

Results from the analytical method gave an indirect measurement of the compound phosphomolybdenum blue by spectrophotometer absorbance at 880nm. The relationship between the absorbance and TP content is a linear one up to 800μg TP l^{-1} and sensitive down to 14μg TP l^{-1}according to Rowland and Haygarth (1997). Findings from this study indicated that the relationship was linear up to 1200 μg l^{-1}. This relationship can be modelled using simple linear regression and absorbance levels of the standards regressed against the known P content. The resultant regression equation was then inverted to provide concentration of TP from the absorbance of the samples. This was carried out on a weekly basis using nine standards. The relationship was always good, and r^2 values always above 0.899 but generally over 0.99 (see Figure 5.9). Although sampling and analysis was conducted over 22 months, only one year was used due to the excessive work that two years of data would generate.

Table 5.3 Sample collected on 1st March 1999. Graphical results in Figure 5.9 generated from Standards and Abs. columns to far right. Values of TP are calculated from the inverse of the regression equation shown also in Figure 3.7.

Sample No	Date /Time	Abs.	mg TP l^{-1}	Standard	Abs.
1	22/02/99 14:05	0.408	0.320538	0	0.07
2	22/02/99 21:05	0.331	0.246349	0.2	0.298
3	23/02/99 04:05	0.324	0.239604	0.4	0.492
4	23/02/99 11:05	0.367	0.281034	0.8	0.898
5	23/02/99 18:05	0.176	0.097008	1	1.122
6	24/02/99 01:05	0.174	0.095081	0	0.075
7	24/02/99 08:05	0.171	0.092191	0.3	0.383
8	24/02/99 15:05	0.157	0.078702	0.6	0.69
9	24/02/99 20:57	0.157	0.078702	0.9	1.009
10	25/02/99 03:57	0.16	0.081592		
11	25/02/99 10:57	0.149	0.070994		
12	25/02/99 17:57	0.142	0.064249		
13	26/02/99 00:57	0.143	0.065213		
14	26/02/99 07:57	0.143	0.065213		
15	26/02/99 14:57	0.137	0.059432		
16	26/02/99 21:57	0.375	0.288742		
17	27/02/99 04:57	1.156	1.041227		
18	27/02/99 11:57	0.855	0.751217		
19	27/02/99 18:57	0.53	0.438083		
20	28/02/99 01:57	0.371	0.284888		
21	28/02/99 08:57	0.288	0.204919		
22	28/02/99 15:57	0.255	0.173124		
23	28/02/99 22:57	0.218	0.137475		
24	01/03/99 05:57	0.26	0.177941		

Error in regression is calculated from the vertical distances between the points and the line of best fit and strictly speaking the equation should not just be inverted. High r^2 values as found in this system reduced error to an inconsequential level, and inversion was seen as reliable enough to predict unknown x-values from the known values of y.

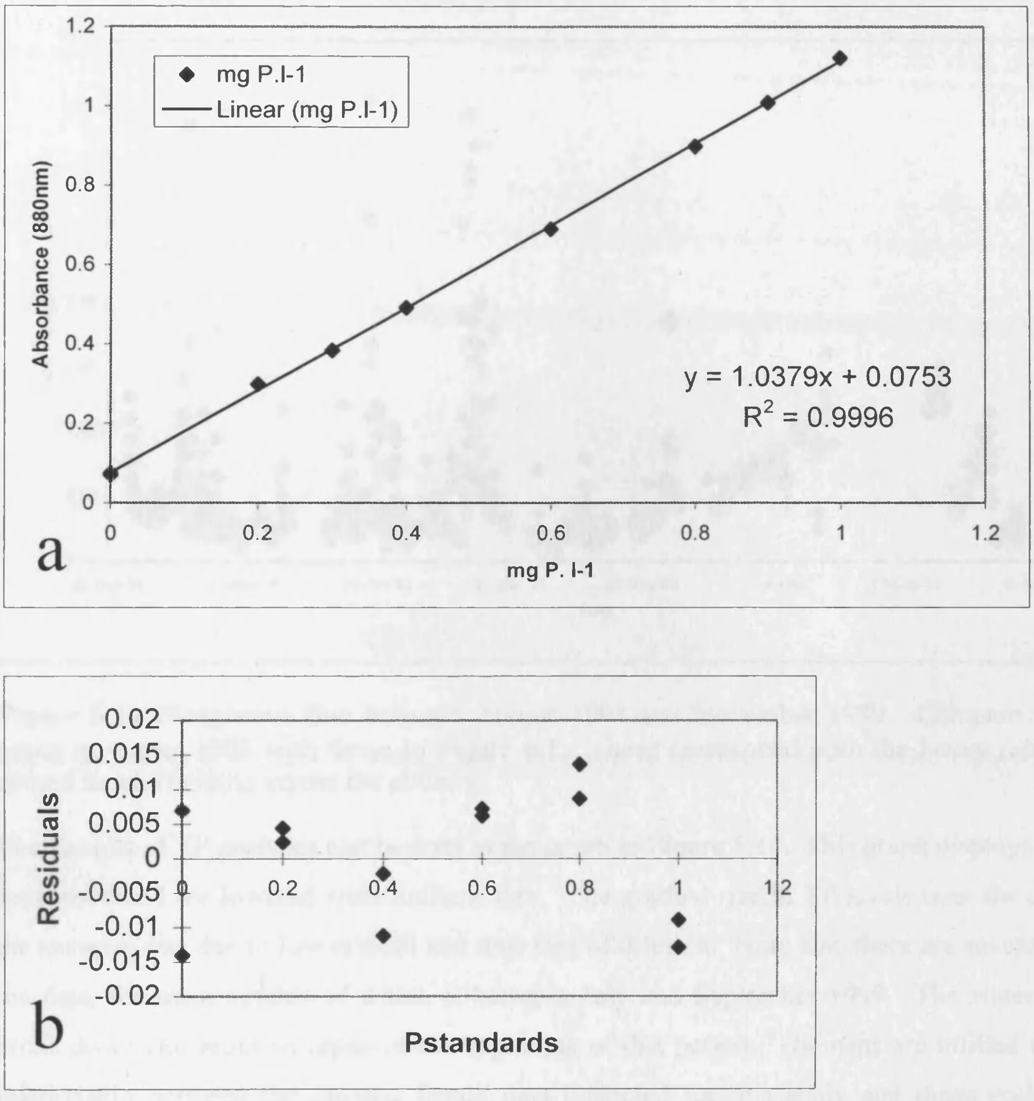

Figure 5.9 Regression graph and equation of phosphorus standards against absorbance. Note high r^2 value. Graph b indicates legitimacy of the test.

Occasionally, the standards failed and provided poor fit to the data. In such instances the analysis was performed again. Over one period of three weeks the filter for the deionised water machine failed and results became very erratic. On replacement of the filter the results returned to their normal high reliability.

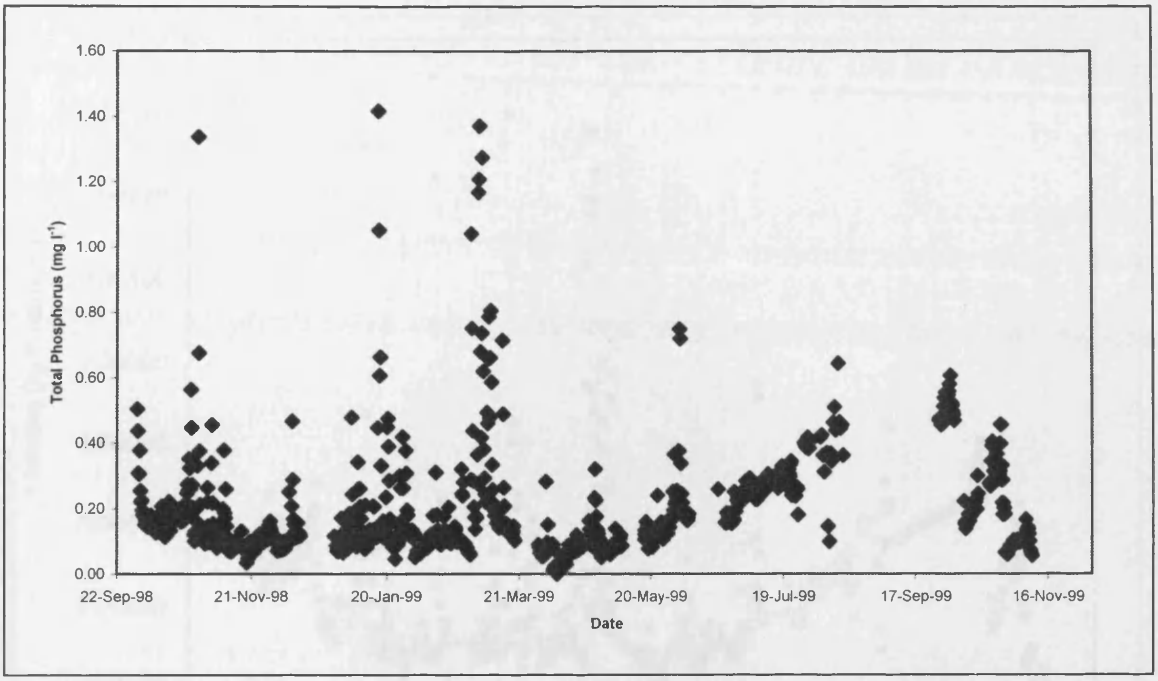

Figure 5.10 Phosphorus flux between August 1998 and November 1999. Compare the large peaks in winter 1999 with those in Figure 6.1. These correspond with the heavy rainfall that caused much flooding across the country.

The Results of TP analyses can be seen in the graph in Figure 5.10. This graph displays a typical seasonal trend for lowland river nutrient flux. The gradual rise in TP levels over the course of the summer was due to low rainfall and thus loss of dilution. Note also there are several gaps in the data, the most notable of which is between July and September 1999. The water sampler broke down and required repair at the beginning of this period. The gaps are infilled using the relationship between the Stonton Brook data collected for this study and those collected by Anglian Water Authority at Tinwell for the River Welland. The TP data were amalgamated with the results from Section 5.3.1 to provide the loadings estimate as discussed in the next section.

5.3.3 Phosphorus Loadings

The results from the previous two sections were combined to provide the TP loadings (kg P cumec^{-1}) for the Stonton Brook. Both datasets were made compatible in time steps to ensure ease of calculation. The flow was estimated via depth measurements for every 30 minutes on the Stonton Brook whereas it was measured every fifteen minutes at Tinwell for the Welland. The P samples were averaged to every seven hours (14 hours for one period in August 99). All data were therefore rounded to 7-hours and converted to loading by multiplying the TP levels (kg P m^{-2}) with the flow (cumecs). Daily and monthly averages of flow and P loading are shown in Figure 5.12.

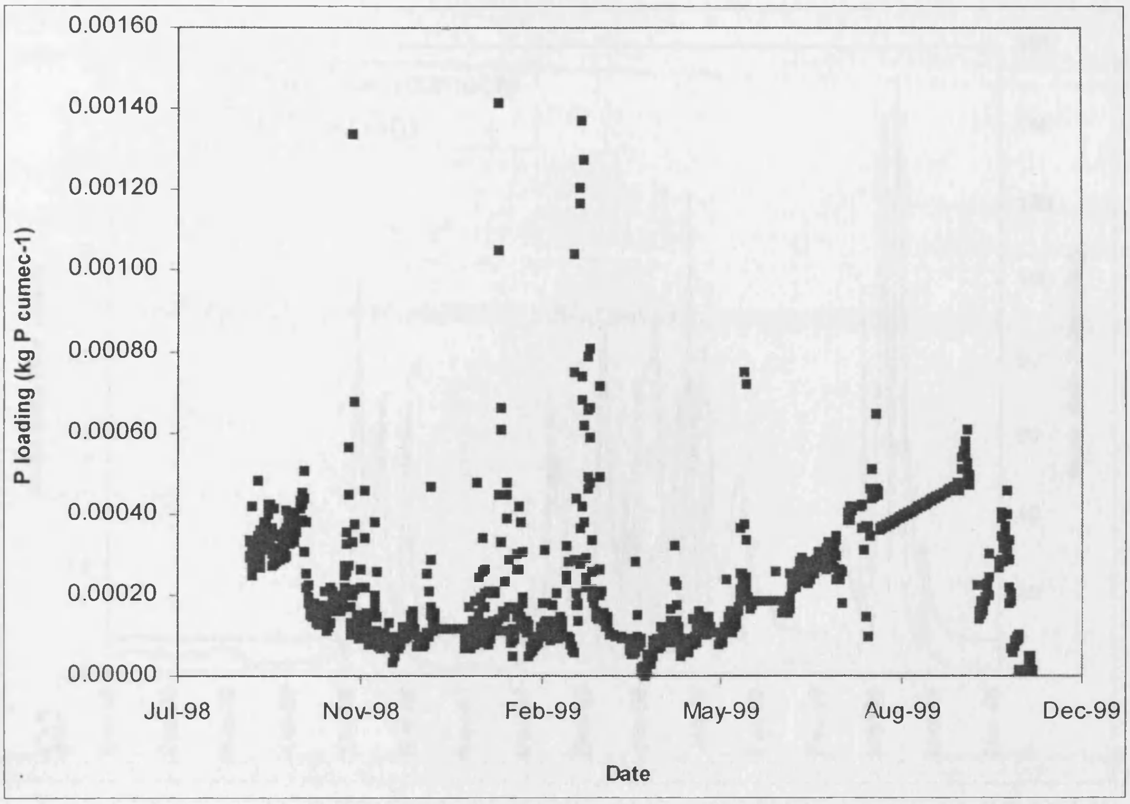

Figure 5.11 Loadings flux graph for the Stonton Brook. Note the gradual rise over the course of the summer.

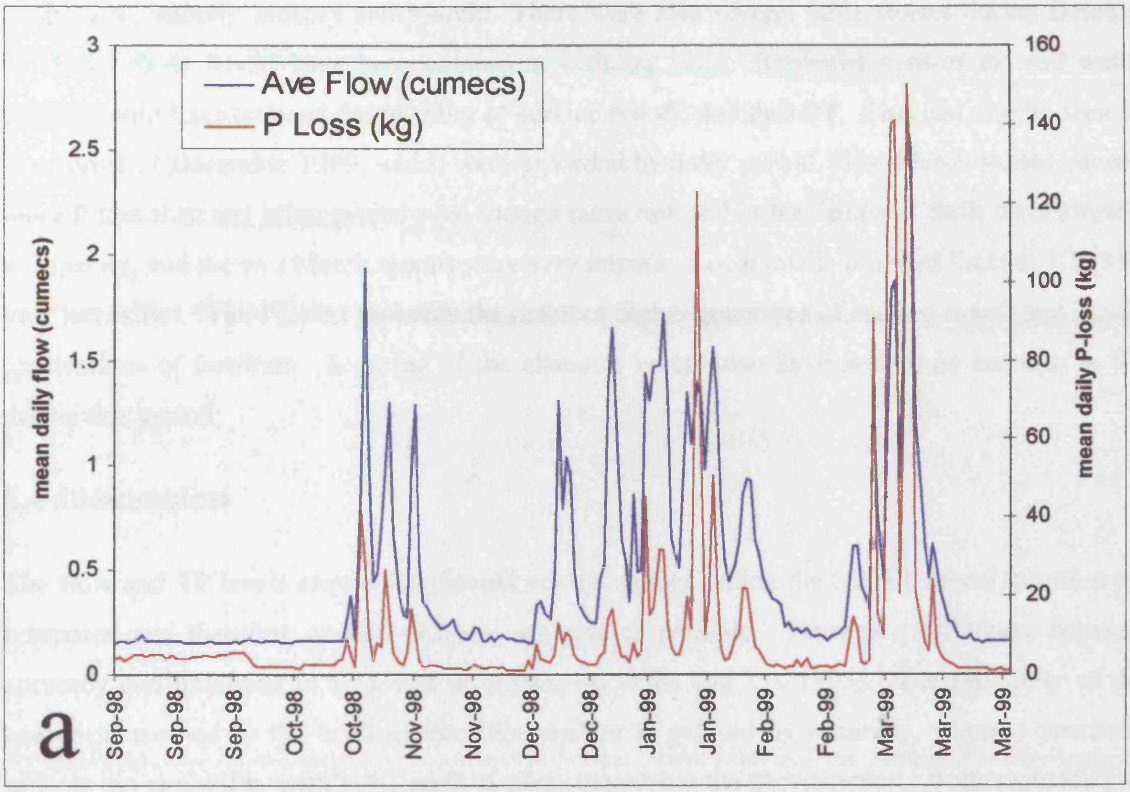

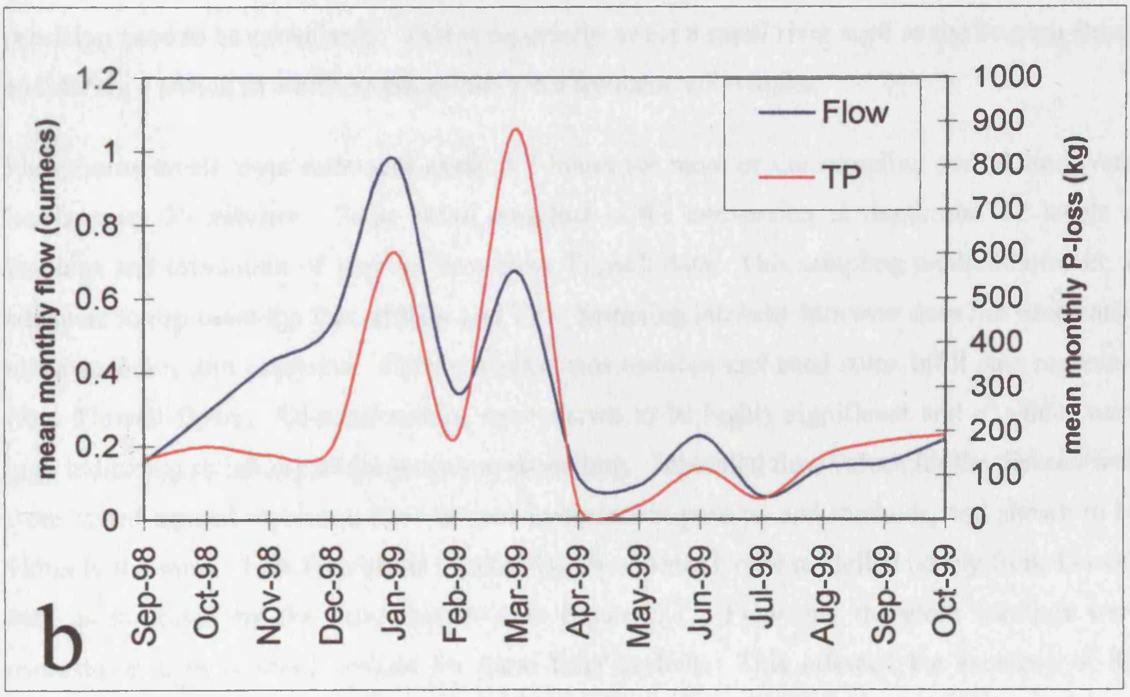

Figure 5.12 Average flow and P-loss for a) daily means and b) monthly means. Daily flow is only shown from September 1998-March 1999 to focus on the main storm events.

The flow and P-loss graphs in Figure 5.12 indicate some interesting characteristics of the hydrology and PT of the Stonton Brook. The most crucial factor demonstrated in Figure 5.12 is the influence storm events have on P-transport. The two large peaks in 5.12b that account for over half of the P-loss during the year are clearly related to the two most intensive storm periods of the year, namely January and March. There were also several large storms during October 1998, but these would have been coincident with dry soils. Replenishment of the soil water deficit would have reduced the quantity of surface runoff, and thus PT. This can also be seen in the storms of December 1999, which were preceded by a dry period. The March storms caused more P-loss than any other period even though more rain fell in the January. Soils were already at capacity, and the two March storms were very intense. Local media reported them as 1-in-150 year intensities. The PT was probably the result of higher quantities of surface runoff and spring applications of fertiliser. Scouring of the channels would also have lead to an increase in PT during this period.

5.4 Discussion

The flow and TP levels are the benchmark results against which the SWAT model output were compared and therefore needed to be as accurate as possible. There is a difference between accuracy and precision in all forms of analyses (Landis and Yu, 1995). The proximity of the analytical method to the level of the phenomenon is defined by accuracy, whereas precision reflects the variability within the method when measuring the phenomenon. Both accuracy and precision need to be considered. This is especially so for a small river such as the Stonton Brook and during a period in which storm events were frequent and extreme.

Phosphorus levels were estimated every 3.5 hours for most of the sampling period, and water levels every 30 minutes. Some detail was lost in the conversion of depth and TP levels to loadings and estimation of Stonton flow from Tinwell data. This sampling method however, is adequate to represent the flux of flow and TP. Sampling intensity however does not necessarily mean accuracy and precision. Flow sampling was tortuous and used some infill data regressed from Tinwell flows. All relationships were shown to be highly significant and r^2 values were high indicating reliability of the inversion modelling. Tabulated flow values for the disused weir were tested against measured flow by two independent persons and methods, and shown to be virtually the same. Low flow at the Stonton Brook appeared to be modelled poorly from Tinwell data as indicated by the false threshold in Figure 5.7. Flow and therefore loadings were overestimated by a small amount for these brief periods. This affected the accuracy of the simulated data during low-flow periods, but can be inspected when comparing the SWAT output with measured data.

High precision of the P analyses was demonstrated by the consistently close fit to a straight line. It is assumed that all the phosphorus in the samples was converted to orthophosphate and then to phosphomolybdenum blue. Underestimation of TP may have occurred however, due to potential P losses during storage. Differences were found between unfixed samples over time but none between acid-fixed samples. Some doubt exists of the validity of this test due to the failed controls, and further analyses between first and last samples of subsequent batches indicated no difference in TP. If this were the result of a purposefully designed experiment, the outcome would indicate that storage of the samples within the sampler had no effect on the TP. This was not the case and so the results must be treated with a small amount of caution. The results described in this chapter are considered overall to be very accurate and precise, and are a good comparison for the modelling output to be judged against.

Chapter 6 Miscellaneous Data Collection

6.1 Introduction

The SWAT model has an extensive list of input parameters, most of which are based on US experiences and standardised datasets (Arnold *et al.*, 1999). Most measurable variables can be altered by direct input or specified datasets. These fall into the categories as listed below:

1) Meteorological data

2) Soils data

3) Vegetation/land cover data

4) Digital terrain model

5) Effluent outfall data

6) Land management information

Many of the required parameters are available through third parties and these will now be addressed more fully under their respective headings. Illustration of all the data included in this study was prohibitive. Data measured in the field or derived from remote sensing are covered in Chapters 4 and 8 respectively. The weather and soils characteristics for the Stonton Brook are summarised in Chapter 3 and only the data used in the SWAT modelling will be described in this chapter.

6.2 Meteorological data

Accurate weather data are very important in the prediction of responses from a catchment (Neitsch *et al.*, 2002a). Weather is the most important single aspect of data and SWAT offers three options:

1) Select from weather gauge datasets based in the USA

2) Utilise a weather simulation routine

3) Include weather databases specific to the study catchment

SWAT can utilise many sets of weather data for a given catchment. Ideally the weather stations should be located within the catchment but this is not essential for the running of SWAT. The

SWAT model requires the weather parameters shown in Table 6.1 for each weather station used in simulations.

Table 6.1 Weather data parameters required by SWAT

Total daily rainfall (hourly if available) (mm)
Maximum daily temperature (°C)
Minimum daily temperature (°C)
Total daily solar radiation (MJ m^{-1} hr^{-1})
Mean daily wind speed (m^{-1})
Mean daily relative humidity
O.5 hr 10 year storm (mm)
6.0 hr 10 year storm (mm)
Number of years data on which storm data are based (yrs)

Most data were collected from the British Atmospheric Data Centre (BADC) on successful application as a NERC student. Many gaps and errors were found in the BADC weather data but were rectified as best as possible. Several datasets were acquired from around the Stonton Brook catchment and integrated into fewer but complete datasets. Infill data for gaps in the other sites datasets were done only after eliminating differences between simultaneous data from the respective sites using regression analyses. There were more rainfall and temperature data than wet bulb temperature (for relative humidity) and solar radiation, resulting in four, three, two and one datasets respectively. These were downloaded from the BADC website (BADC, 2002). The locations were Market Harborough, Stoughton Lodge, Rockingham, Houghton on the Hill, and Hallaton Croft. Some infill data and solar radiation were collected from Cottesmore. Although this latter site was 20 miles from the Stonton Brook the solar radiation was assumed to be very similar to that on the Stonton Brook. Although these sites were outside of the catchment they provided a network of data covering the geographical area of the Stonton Brook. Additional data were also collected from Mr D. Wooldridge of 42 Burnmill Road, Market Harborough. Mr Wooldridge supplied maximum temperature (°C), minimum temperature (°C), and wet-bulb temperature (°C) that were not available through the BADC. All readings were taken at 0900 for the Meteorological Office's records. The weather station was calibrated and checked by the Meteorological Office technicians once every two years. Mr Wooldridge supplied these data as photocopies of a hand written diary. The data were then entered into Excel for management and analyses.

All datasets were collected for the period 1st August 1995 to 30th November 1999. Storm event summaries were obtained from the Hydrological Institute based on Volume 2 of the Flood Estimation Handbook (D. Jakob, Data Centre, Institute of Hydrology). Relative humidity values were calculated from dry and wet-bulb temperatures using the MS Excel macro add-in "WXFun" (http://members.sockets.net/~rhbr/). Weather data are summarised in Figures 6.1 – 6.3.

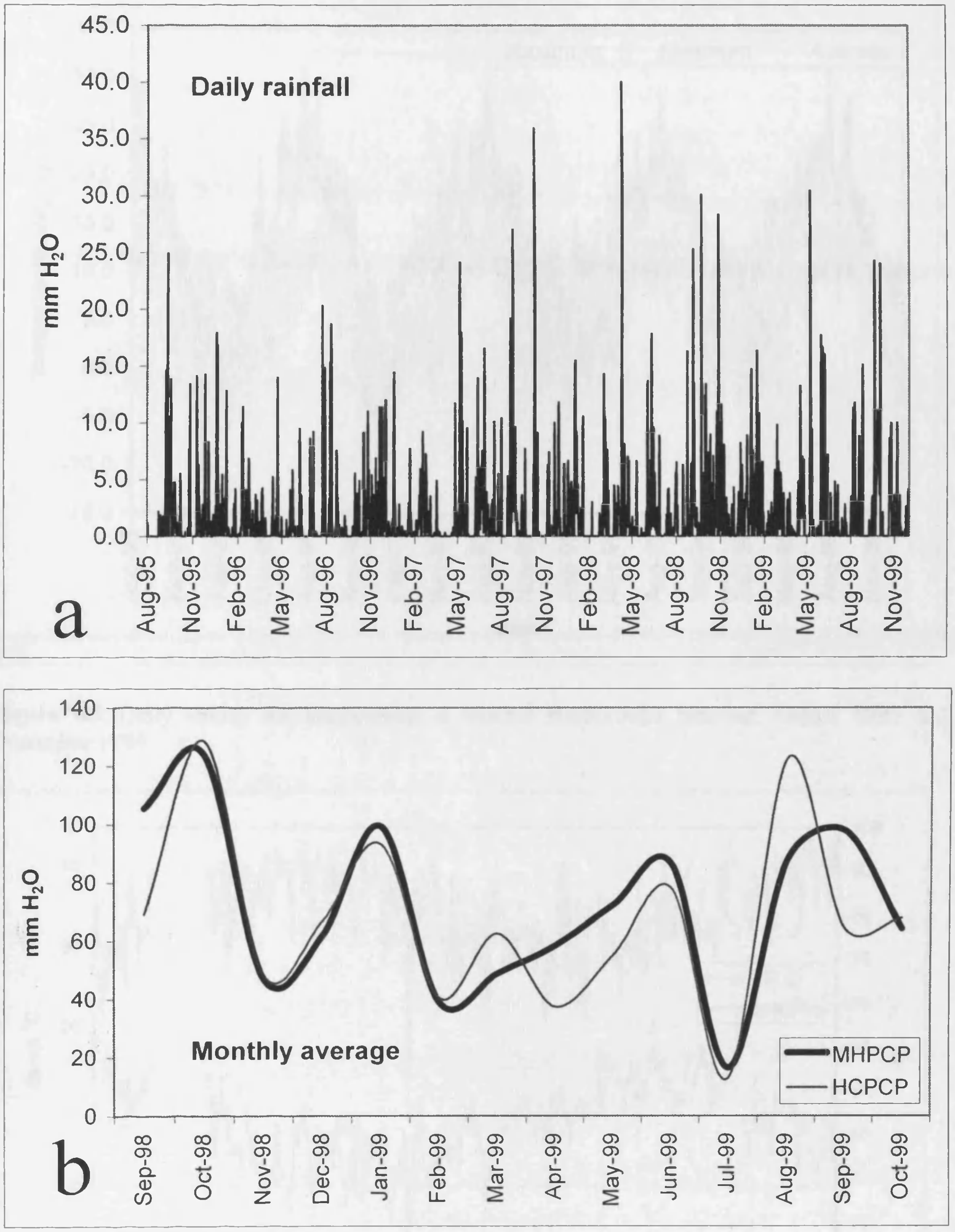

Figure 6.1 Rainfall data for Market Harborough a) daily total, b). Monthly averages for Market Harborough (MHPCP) and Hallaton Croft (HCPCP). Graph is based on daily collections at 0900 hrs. Note the greater amount of rain for 1998 and 1999 in a.

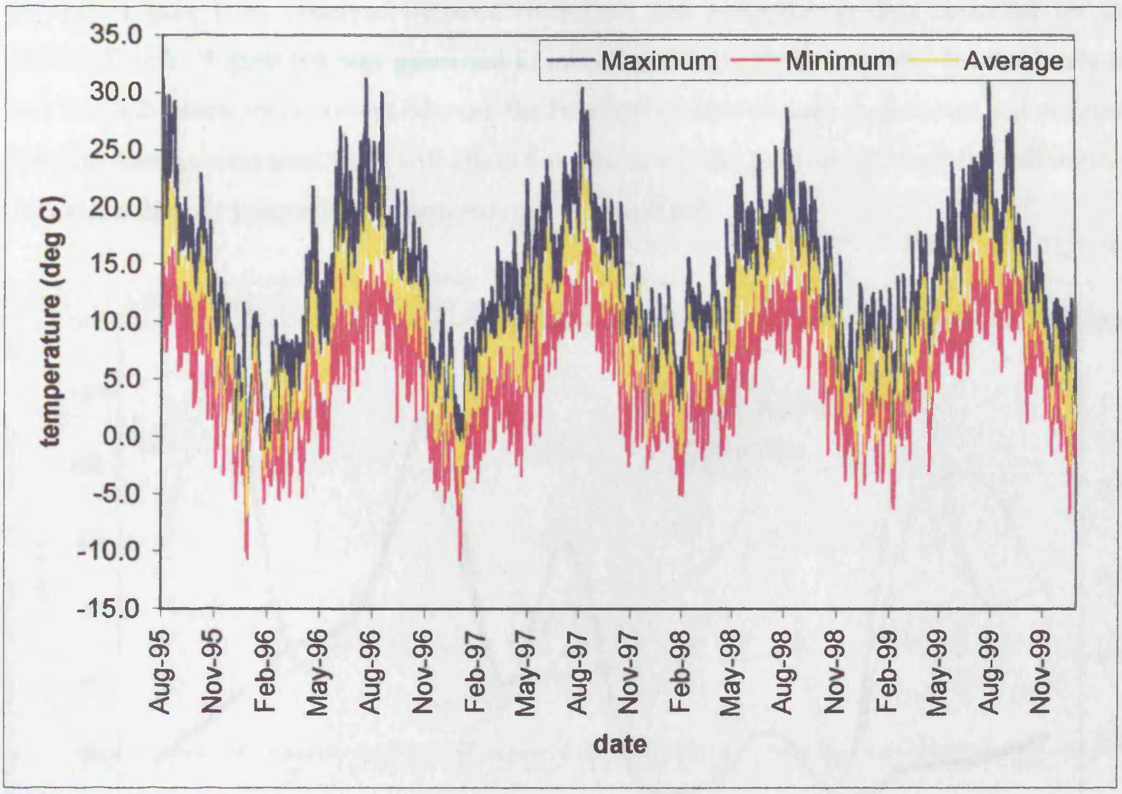

Figure 6.2 Daily values for temperature at Market Harborough between August 1995 and December 1999.

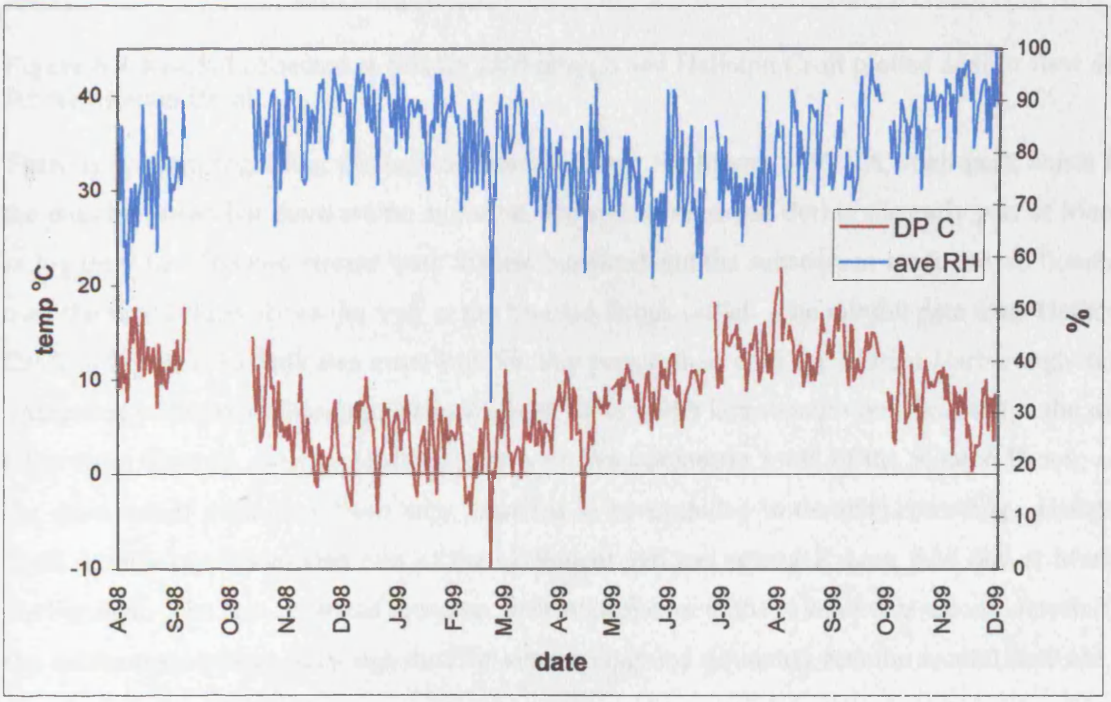

Figure 6.3 Daily values for dew point and relative humidity at Market Harborough between August 1998 and November 1999.

Anomalies have been observed between river flow and precipitation data collected for the Stonton Brook. Figure 6.4 was generated to investigate these disagreements. It can clearly be seen that a discrepancy is present between the flow and rainfall curves. Antecedent soil moisture and land management conditions will affect the volume of water moving through the soil into the river and a directly proportional relationship is not expected.

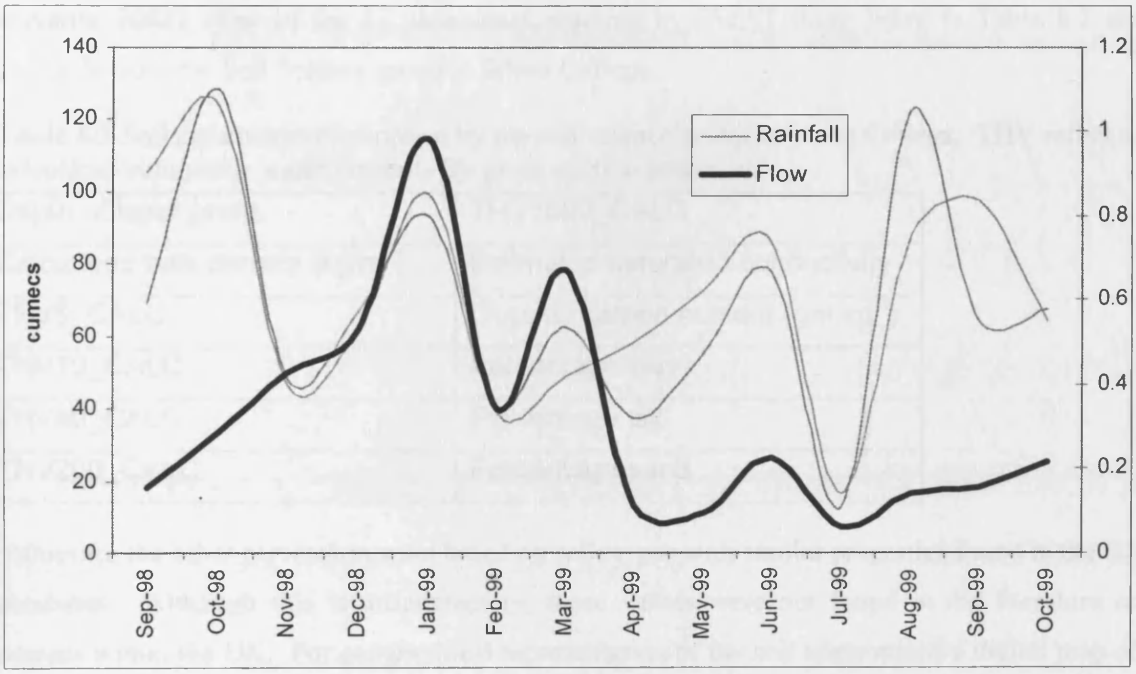

Figure 6.4 Rainfall collected at Market Harborough and Hallaton Croft plotted against flow data for the Stonton Brook.

There is concern regarding the lack of rainfall shown for March 1999. A small peak exists for the monthly mean but there are no major rainfall events recorded during the early part of March in Figure 6.1a. The two storms were intense but short and the subsequent spate caused flooding over the road bridge above the weir at the Stonton Brook outlet. The rainfall data from Hallaton Croft in Figure 6.1b indicates more rain for this period than does the Market Harborough data. There was widespread flooding in the Welland River and a large spate was witnessed in the data taken from Tinwell. Market Harbourgh is only five kilometres south of the Stonton Brook, and the storm event must have been very localised to be excluded in the data recording. Hallaton Croft is only two kilometres east of the catchment and has recorded more than that at Market Harborough. The two autumnal increases in rainfall shown in the rainfall data are not detected in the instream sampling. Although the first autumn contains simulated data the second does not.

6.3 Soils data

Many more soil parameters are required by SWAT than were available in the UK from standard databases. Thirteen parameters are required for each soil layer of each soil association. Three more apply only to the soil association. Two of the parameters are used primarily in the US (USLE-K factor and Hydrological Group), but have been used in the UK (Morgan, 2001; Chaler Novarro, 2002). Out of the 13 parameters required by SWAT those listed in Table 6.2 are available from the Soil Science group at Silsoe College.

Table 6.2 Soil parameters as supplied by the soil science group at Silsoe College. THV refers to calculated volumetric water contents for given suction pressures.

Depth of layer (mm)	THV1500_CALC
Calculated bulk density (kg/m^3)	Estimated saturated conductivity
THV5_CALC	Organic carbon content (gm kg^{-1})
THV10_CALC	Percentage clay
THV40_CALC	Percentage silt
THV200_CALC	Percentage sand

Values for the other parameters were based on soils types with similar properties found in the US databases. Although this is unsatisfactory, these values were not found in the literature or sources within the UK. For geographical representation of the soil associations a digital map of the area was obtained from the Soil Research Institute at Silsoe. This map can be seen in Figure 6.5.

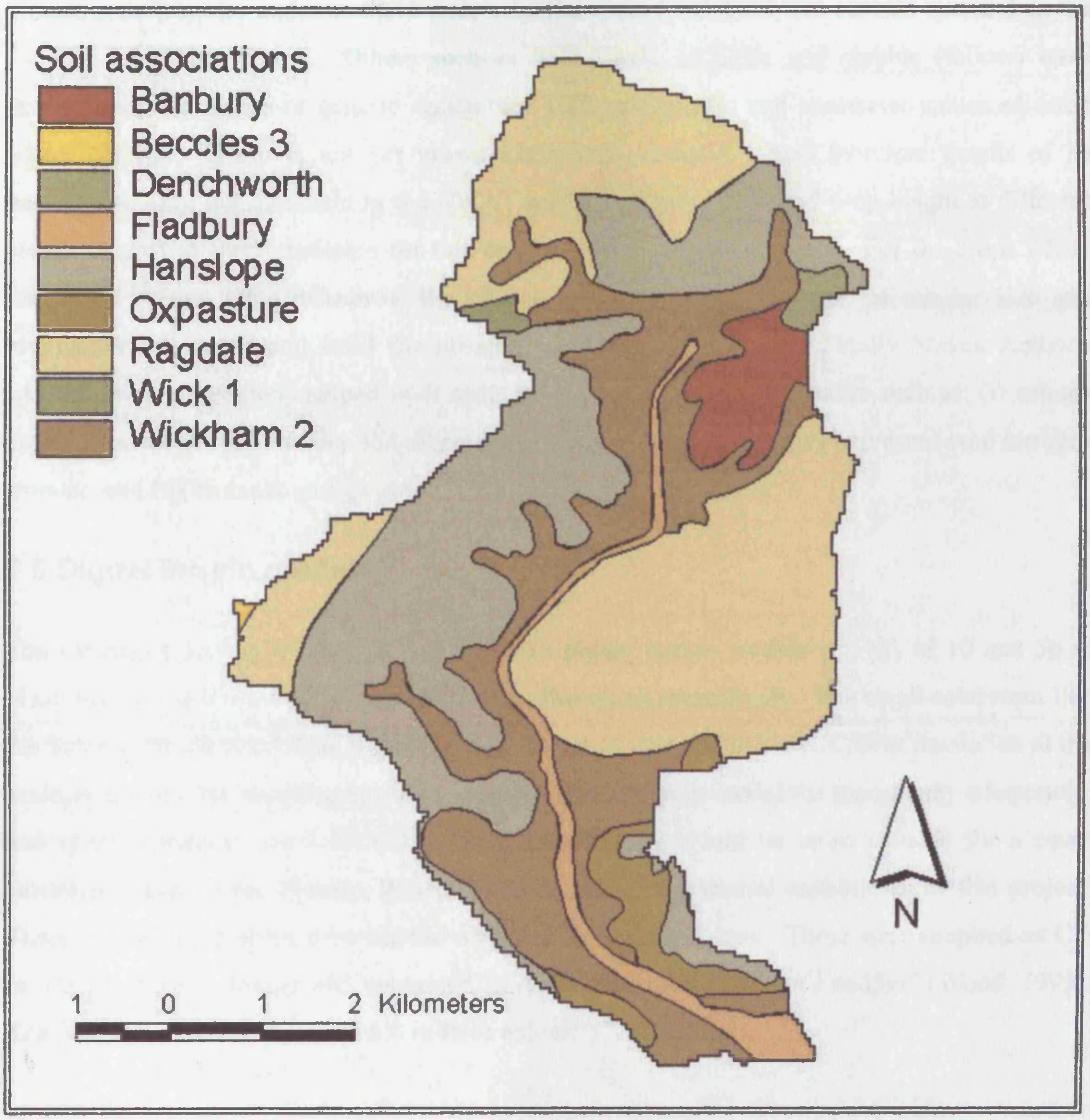

Figure 6.5 Map of soil associations found on the Stonton Brook. Outline follows catchment boundary as defined by SWAT model.

6.4 Vegetation parameters

Vegetation parameters used within SWAT are extensive, and some are not used universally in botanical agronomy e.g. vapour pressure deficit. Some of the vegetation parameters such as crop height and LAI have been measured for most crops found in the Stonton Brook. Many other parameters such as vapour pressure deficit cannot be measured without sophisticated equipment. In place of parameters that have not been measured in the UK, the default values in the standard SWAT databases for similar crop types found have been used.

The SWAT model contains an extensive list of crop species and land cover types with their requisite parameter values. Crops and land cover categories such as barley, wheat, pasture, flax, oilseed rape (canola) and woodland were used the SWAT database, but revised where data for the UK have been found. Others such as field beans, set-aside and stubble (fallow) were designated green beans or generic agricultural land respectively and parameter values adjusted where known. Hemp is not yet grown extensively in the US and therefore details of its parameters were not available in the SWAT model database. LAI and crop height at different stages of growth were available for this crop but many others were not. For the crops where parameter values were unknown, the only option was to select crops of similar size and architecture or genus and infill the missing parameters from them. Finally Steven Anthony (ADAS Wolverhampton) helped with some of the more elusive parameters such as: (i) canopy surface resistance, (ii) wet/dry soil albedos, (iii) crop rooting depths, (iv) harvested crop nitrogen content, and (v) biomass energy ratio.

6.5 Digital terrain model

The Ordnance Survey of the UK supplies two digital terrain models (DTM) of 10 and 50 m resolution, Land-Form Profile and Land-Form Panorama respectively. In a small catchment like the Stonton Brook resolution is an important aspect of data acquisition. Coarse resolution at the scale of say one km would not contain enough information to model the topography adequately, and channel details would be lost. Although the latter would be more suitable for a small catchment such as the Stonton Brook it was beyond the financial capabilities of this project. Three tiles were obtained covering the whole of the Stonton Brook. These were supplied on CD in .ntf file format, joined and converted to Arc Grid raster format in LandSerf (Wood, 1999). The product is shown in Figure 6.6 in false colour.

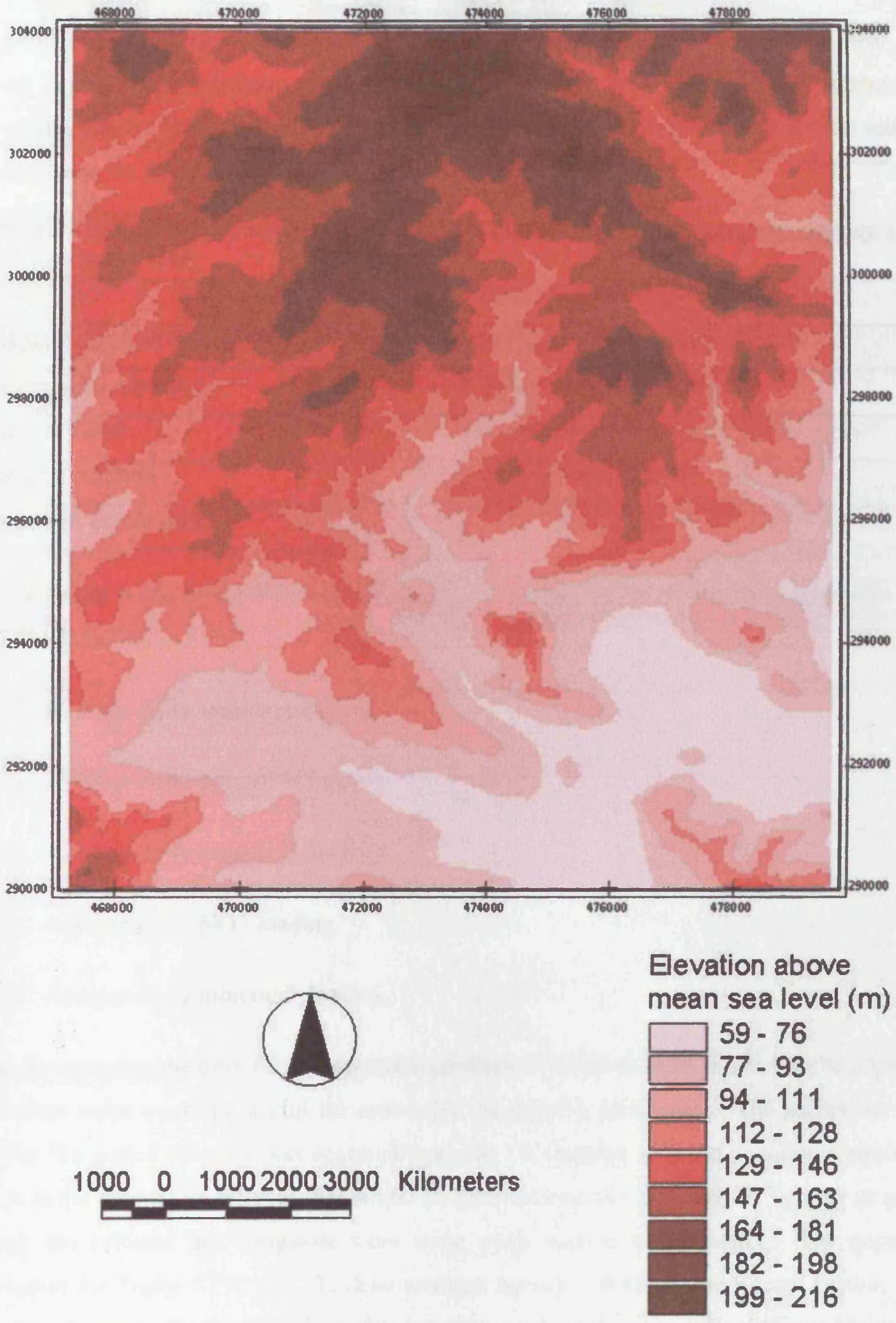

Figure 6.6 False colour image of DEM using OS Land-Form Panorama at 1:50,000 scales. Stonton Brook is seen as low-lying area following north to south direction in centre of image.

6.6 Effluent outfall data

As previously mentioned there was only one operational STW on the Stonton Brook, which served Tugby. The Environment Agency maintains a public database (LIMS) of determinands for instream water quality and effluent discharge. The Environment Agency keeps the following determinands on its LIMS database for Tugby STW:

Table 6.3 Outflow determinands for the Tugby STW held on the Environment Agency's LIMS water quality database.

pH	Chloride
Biological oxygen demand mg l^{-1}	Soluble reactive phosphorus
Ammonia as nitrogen	Total Inorganic nitrogen
Nitrogen Total	Ammonia non-ionised as nitrogen
Particulate solids	Instantaneous flow
Population equivalent	

The following is the list of discharge determinands included in the point source discharge file of the SWAT model:

1) Average daily sediment loading
2) Average daily organic N loading
3) Average daily organic P loading
4) Average daily NO3 loading
5) Average daily mineral P loading

It can be seen that the only fully compatible parameter was particulate solids, but the population equivalent value could be useful for estimating the missing parameters. The particulate solids data for the period of study was acquired from the EA together with the population equivalent, which is the amount of effluent that would be generated by the "equivalent" number of people, though the effluent may originate from some other source, e.g. industry. The population equivalent for Tugby STW was 225 (Environment Agency, LIMS, Public Record Centre, 1999). The default values for the SWAT model cannot be used, as they are quite different between the UK and the USA. Since it is assumed that sewerage loadings per person in the USA are higher than the UK equivalents, the nutrient input to the Stonton Brook from Tugby would have been overestimated if US values used.

Obviously the above information is incomplete when considering the input to SWAT model. The only way that the required information could be acquired was to use the number of people served by Tugby STW and then multiply that value by cited per person values for the SWAT parameters. This information could not be found and these parameters were therefore excluded from the SWAT database on the grounds of incompatibility.

6.7 Discussion

The SWAT model relies upon previous research and databases such as that surrounding the Universal Soil Loss Equation. Parameters used by these equations have not all been measured or estimated for UK conditions. Many parameters were obtained for the SWAT model through field sampling (Chapter 4), public databases (BADC), literature (USLE-K value – Morgan 2001) and personal contacts. Not all were found but hopefully these are the less important parameters. There is however, a large shortfall of measured or validated data. Although the quantity of weather data were adequate it appears from observations in this chapter that either major storm events caused large spates in the catchment but were not recorded by the weather stations or that weather stations recorded major rainfall events that were not recorded as spates in the catchment. The conclusion is that localised storms avoided either the catchment or weather stations and emphasizes the need for multiple weather stations in the catchment. During analyses of the SWAT results these discrepancies in weather and river data will have to be considered.

Chapter 7 Derivation of Field Boundary Map using Airborne Photography

7.1 Introduction

The SWAT model required a digital field boundary map to define discrete land use areas. Field boundaries could be digitised from Ordnance Survey maps but changes on the ground are not reflected in the maps for several years. SAR and LandSAT images are neither detailed nor accurate enough to provide this sort of information. In addition to field boundaries, a digitised river channel was required as an alternative to extrapolation from the DTM. NERC offered airborne photography of the catchment as part of the remote sensing campaign for the project. These photographs proved ideal for digitising field boundaries and identifying the extent of urban land. This chapter describes the photography and the processing methods used.

7.2 Image acquisition and image processing

Lens imperfections and edge effect imparts distortion to photographic images. The former is minimised by high quality lenses (ERDAS, 1997a). Edge effect is due to the change in angle between the plane at the centre of the image to the ground, and the plane at the edge of the image to the ground (ERDAS, 1997a). The area of land captured within a given area on the image is greater at the edge than in the middle, given perfectly flat ground. Edge effect is increased and somewhat random when the land is undulating, but the distortions are minimised when the camera angle is truly vertical. Photographic images therefore required correction, and thereafter georeferencing before use in mapping and GIS (ERDAS, 1997a). Georeferencing is the process of applying a controlled distortion to comply with a geographic grid or map projection. After georectification the photograph is representative of the actual ground layout and is compatible with the projection of the map of reference. Once processed, the photograph can be overlaid or joined with other map data of the same projection.

According to the ERDAS Field Guide (1997b) photographic images require geometric correction using focal lengths of the camera and the image fiducials prior to georeferencing. In practice however a good correction can be achieved without using these characteristics. The process was as follows:

1) Specify the final image projection

2) Identify a grid of 15 – 25 ground control points (GCP's)

3) Adjust the positioning of GCP's to reduce the RMS error to within one pixel.

4) Georectify image by resampling based on GCP's

All georectification was carried out in ERDAS Imagine 8.3.1. Ground control points are used as geographic reference points during standard georectification rather than the fiducials. A minimum of six GCP's are required to calculate the error associated with the correction, but it is advisable to have a minimum of 10 (ERDAS, 1997; J. Wood, Department of Geography, University of Leicester). From experience however, the number of GCP's required for good georectification is between 15 and 25. Ideally they should be well dispersed across the image to ensure resultant correction is as near uniform as possible. The National Grid of the UK was used for the projection and co-ordinates read from a map, in this case the National Grid based on a Pathfinder series (916) Ordnance Survey map at 1:25,000 scale. Fortunately ArcView and the SWAT model accommodate this projection and thus large amounts of conversion from National Grid co-ordinates to longitude and latitude were avoided.

The camera used was a Wild RC-10 survey camera using a 6-inch lens and visible spectrum colour film. Aircraft data recorded on each exposure included altitude and course. The platform was a Piper Navajo Chieftain, flying at the requested altitude of 3300m. Camera angle was vertical. The photography was supplied in the form of large format prints (238x251mm). A single frame covered approximately $18km^2$ and it was necessary to shoot several frames to cover the whole Stonton Brook. Each frame had fiducials (points of reference) at each corner. The batch used in this study had 19 individual photographs with a large amount of overlap between each frame. Four sets of prints were supplied by NERC from the 4th May 1998, 18th May 1998, 24th July 1998 and 5th August 1998. The last set was chosen due to the high occurrence of exposed soil that emphasised the hedgerows and boundaries of fields. An example of the aerial photography is shown in Plate 7.1.

Plate 7.1 Example of airborne high-resolution photography (courtesy of NERC). The road cutting through the centre of the image is the A47. The village to the middle right is Skeffington.

All prints were scanned using a high resolution (9000dpi) A4 flatbed scanner. The scanned image was converted to .tif at 1200dpi, which was then imported into ERDAS Imagine for processing. The scanner was not large enough to include the fiducials from all corners of each frame and so the first image was georectified as if it were a digital image. 20-25 GCP's were then selected based on clearly identifiable features both on the scanned photograph and the Pathfinder map. Six-figure National Grid co-ordinates were read from the map and then entered into Imagine against the relevant GCP. In order to reduce the error associated with each GCP the positions of the GCP's and the map co-ordinates were adjusted little by little. Higher RMS values were targeted first, and lower values next. Each GCP was adjusted in turn until all RMS errors were less than the dimension of one pixel. In most images there were one or two RMS values that could not be lowered without detriment to several others. In such cases the respective GCP's would be removed or changed to the status of checkpoints. The first image was then checked for error using several further identifiable points. After all images were georectified they were joined in a single image to form a photo-mosaic of the Stonton Brook catchment.

7.3 Results

The first image was accurately georectified based on several checkpoints applied post-correction and compared to the Ordnance Survey map. Identifiable features on the corrected image were found to be within five metres of the same feature on the Ordnance Survey map. This is well within the accuracy of obtaining a map reference from a 1:25,000 scale map. Therefore, correction utilising fiducials and focal length prior to georectification was seen as unnecessary. All other images were then georectified in the same manner.

Sixteen of the prints were joined for the mosaic as shown in Figure 7.1. The image was clipped to the catchment outline in ArcView to keep digitising effort to a minimum. The field boundaries were digitised from this image in ArcView 3.2, and then converted to an ArcView shapefile for use in the SWAT model. The final product of this chapter is shown in Figure 7.2 and was used to assign accurate areas to land cover types based on the information outlined in Chapter 4 and the classification of land cover using remotely sensed data (Chapter 8). The final land cover map was then used as input to the SWAT model (Chapter 9).

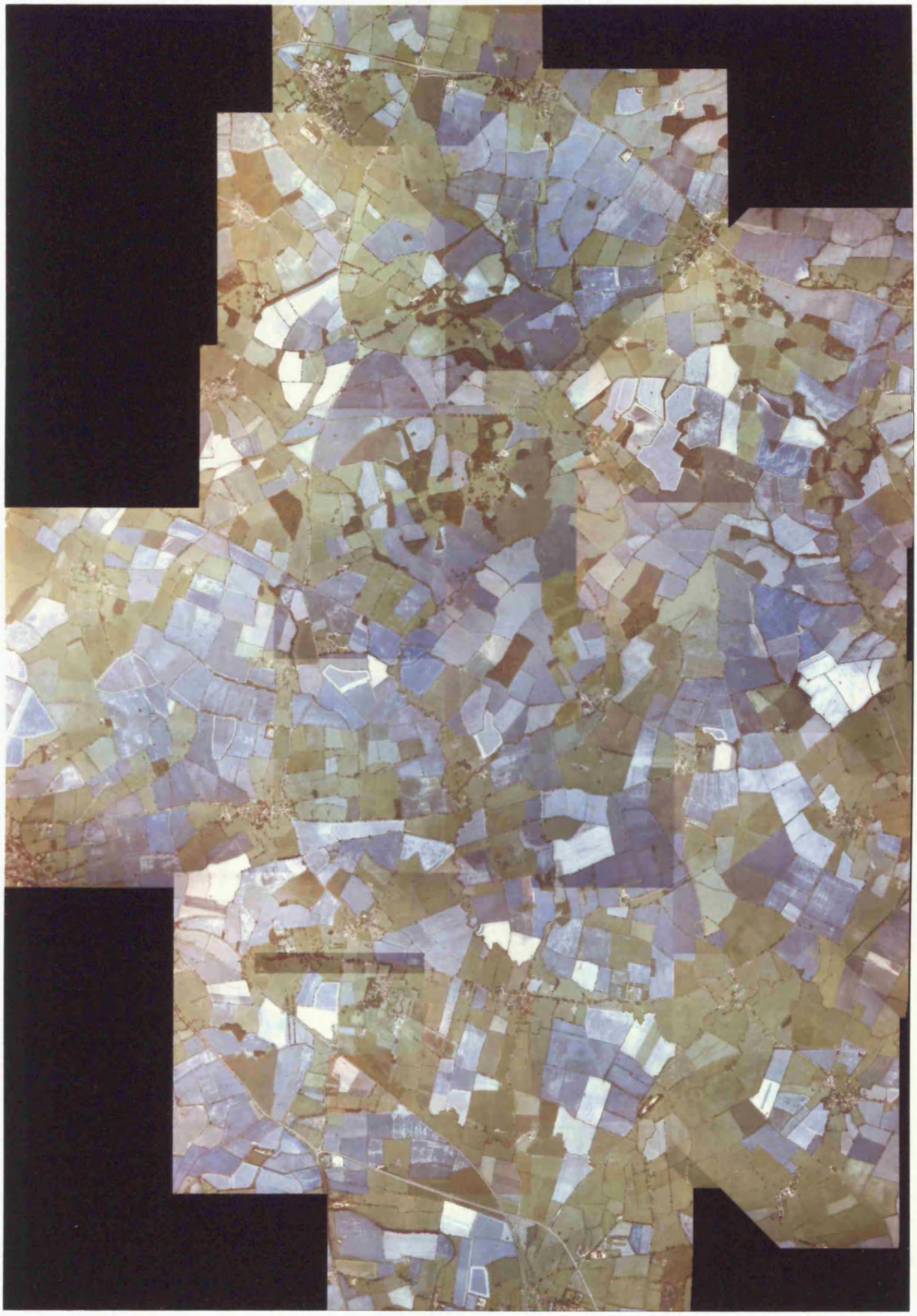

Figure 7.1 Photo-mosaic of the area surrounding the Stonton Brook. Lines of junction between prints can clearly be seen due to colour differences. Close matching of field boundaries and other linear features at junctions indicate good quality georectification. Colour has changed from Plate 7.1 due to the import function in ERDAS Imagine.

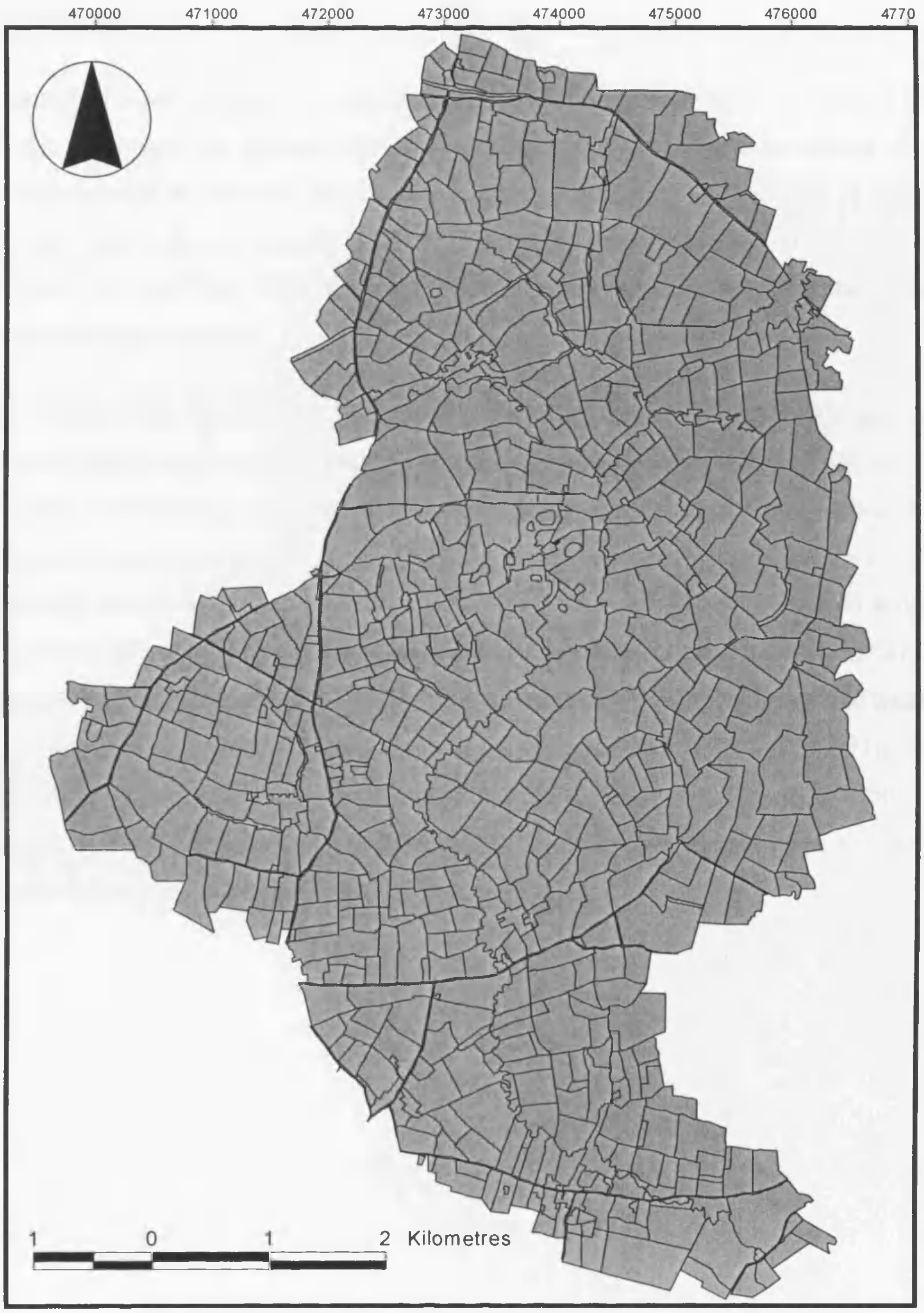

Figure 7.2 Digitised field boundary map of the Stonton Brook catchment based on the photo-mosaic.

7.4 Discussion

It was vitally important to acquire an accurate image of field and land-parcel boundaries for input into SWAT. Although the product of this chapter took a disproportionate amount of time to prepare (4.5 months) it provided an accurate outline of the fields for the year of study. The resultant map was used as a ground survey map and map classified using remote sensing data. The accuracy of the final classified land cover map was also used in the subsequent commission/omission matrices.

Contrary to the advice found in ERDAS (1997a) the correction of the scanned images avoided the use of the focal lengths and fiducials. The photo-mosaic, however, was considered to be the most accurate of all the images georectified during this project. Features were easily identifiable on the photo-mosaic image for the georectification process and therefore six-figure co-ordinates could be easily placed as ground control points. The SAR imagery (next chapter) had a much lower resolution and pinpointing these same features was largely guesswork within an area of approximately two – five pixels (25 – 70m). It has been shown that the fiducials and focal length are not so important for photographic georeferencing as suggested by ERDAS (1997a). The field boundary map was subsequently classified according to field survey data (Chapter 4) and classification of radar remote sensing (next chapter). Classified land cover maps were input into SWAT as ArcView shapefiles as shown in Chapter 9.

Chapter 8 Extraction of Data from SAR Images

8.1 Introduction to the application and principles of active microwave remote sensing

In Chapter 1 the reasons for using SAR data in this research were outlined. These were:

1) Data acquisition is almost independent of weather conditions and solar illuminance
2) Synoptic coverage of relatively large geographical areas
3) Frequent enough repeat passes to capture seasonal changes in vegetation and crop growth
4) The potential to detect vegetation and soil parameters relevant to hydrological and nutrient-transport modelling

SAR has the potential to estimate relevant vegetation and soil parameters throughout the year and could, therefore, be used in several ways:

1) For monitoring land cover classification either by:
    a. Monitoring land cover change and/or
    b. Mapping land cover using multi temporal data
2) For retrieval of soil physical parameters
3) For retrieval of physical vegetation parameters

SWAT can utilise land cover maps directly when combined with ArcView GIS and is therefore compatible with digital maps derived from remotely sensed data. The soil and vegetation parameters that potentially can be derived cannot be used directly, but can serve either to provide parameters in database form e.g. LAI, or in calibrating SWAT outputs e.g. soil moisture. Assigning fields or other parcels of land to particular crops or land cover types can be achieved on a routine basis with multi spectral data such as that acquired by LandSAT TM. However, LandSAT TM suffers from its inability to penetrate cloud (Ulaby and Elachi, 1990) and multi date SAR images are potentially better suited to the temperate and erratic weather of the UK (de Troch *et al.*, 1996; Rignot *et al.*, 1997).

This chapter provides an overview of the principles of remote sensing and the methodology applied, in relevance to this project. Remote sensing applied to environmental management needs to be done on a routine basis and therefore simple methods were sought that could be applied to the extraction of both soil and vegetation parameters. Section 8.1.1 gives a brief introduction into the principles of radar remote sensing and the characteristics of radar sensors that have been used globally to date. A basic description is then given of the ESA's ERS-2 SAR instrument that was used for the acquisition of radar imagery in this study. Section 8.2 reviews the current methods available for deriving land classification, soil and vegetation parameters from SAR images. In Section 8.3 the methodology for pre-processing the images and data extraction will be described in more detail. The results of the data extraction are given in Section 8.4 and the results discussed in Section 8.5.

8.1.1 General characteristics of radar

Remote sensors using active radar operating in the microwave frequencies have the advantage of being independent of background radiation levels and almost independent of weather and atmospheric conditions (Elachi, 1988; Ulaby and Elachi, 1990). In fact, these two references provide comprehensive reviews of the principles of radar remote sensing that readers are referred to. Active sensors generate their own electromagnetic energy in the form of pulses that propagate from the sensor to the ground surface at the speed of light (Elachi, 1988). Depending on the characteristics of the surface the energy is either reflected or attenuated. Some of the reflected energy returns to the sensor where it is recorded as an intensity of backscatter using both the phase and amplitude of the signal. Intensities can then be converted to a ratio of the received/transmitted power, which is termed the backscatter coefficient. The backscatter intensity is a function of the wavelength used, polarization of the outgoing and incoming energy, the incidence angle at the target and the surface characteristics of the target (Elachi, 1988; van Oevelen and Hoekman, 1999). The design of a radar instrument revolves largely around these parameters and the anticipated use of its data.

Microwave energy has wavelengths between 1mm and 100m and the corresponding frequency ranges from 3MHz to 35 GHz. To simplify the instruments of each sensor, the transmitter is engineered so that the transmitted energy falls within a very narrow band or channel. The most frequently used microwave channels are listed in Table 8.1. Sensors may operate with one or several channels depending on the application of the imagery.

Another characteristic of the electromagnetic energy transmitted by the sensors is the orientation of the wavelength energy or polarisation. Transmitters and receivers can be configured for polarised energy. The polarisation can be either in the vertical or the horizontal plane. The abbreviations VV and HH refer to sensors that transmit and receive vertically or horizontally respectively. VH and HV indicate that the sensors are cross polarisation capable, i.e. they transmit in one plane but receive in another.

Table 8.1 Radar frequency bands standardised for satellite radar

Band prefix	Frequency (GHz)	Wavelength (mm)
K-band	10.9 - 36	18
X-band	9.6	31
C-band	5.3	57
S-band	3	200
L-band	1.28	230
P-band	0.44	680

Look angles vary from 10 - 60° and can be fixed or variable for a given sensor and dictates the angle of the incident energy hitting the target (Elachi, 1988). The mean angle of inclination or look angle of the sensor will determine how targets respond to the incident energy. Nadir refers to a vertical look, and sensors that view their targets directly from above have little sensitivity to ground surface parameters other than slope (Elachi, 1988). They are therefore only used for topographical and altitude studies. Increases in look angles from the vertical provide more backscatter from the surface characteristics because more of the incident energy is scattered away from the receiver. A point is reached where the look angle is so large that energy returning to the sensor is negligible.

Single look, single band images provide only one value of backscatter per pixel. It is very difficult to extract useful information from one single band image due to the large numbers of parameters that influence the backscatter coefficient (Elachi, 1988; Tso and Mather, 1999; Dong *et al.*, 2001). For this reason many applications require combinations of SAR images for the extraction of useful data. Ulaby (1998) noted that it is easier to extract biophysical information from multi-channel data from a single image, than it is from single channel data from several images. Ferro-Famil and Pottier (2001) provide details of successful land cover classification from multi frequency polarimetric SAR using NASA AirSAR data. SAR data can be categorised depending on how much data are available either from single sensors or combinations of sensors:

1) Single or multi-date (multi-date)

2) Single or multi-incidence angle

3) Single or multi-channel

4) Single polarisation (VV or HH)

5) Dual polarisation (VV and HH)

6) Fully polarised (VV, HH and HV/VH)

7) Combinations of any or all of the above

Unfortunately multi-channel data are much less common than single channel data but the former can be created using two or more instruments in tandem. Certain parameters can only be acquired through multi-channel data e.g. land cover type, and common approaches are to combine several single-channel images from the same area (multi-date and interferometry).

8.1.2 Microwave sensors and the ESA ERS-2 SAR

The most commonly used radar type for remote sensing purposes is the side looking radar or SLAR. The antenna is oriented to the side of the direction of travel and illuminates a path at an angle to the vertical. There are several design considerations of SLARs that need to be addressed. They generally depend on the application of the final imagery.

SLARs can be divided into the real aperture and synthetic aperture radars (SAR). There are great advantages of the latter over the former. Resolution from real aperture radars is wholly dependent on the length of the antenna that generates the beam of microwave energy, and can be defined thus:

$$X_a = \frac{\lambda h}{L \cos\theta} \tag{8.1}$$

where X_a is the resolution, λ is the wavelength, h is the altitude, L is the length of antenna and θ is the angle of incidence. High spatial resolution of the image demands prohibitively large antennae, and the consequent difficulties of positioning the instrument where it is needed. Therefore, real aperture radar is seldom used where the resolution needs to be less than hundreds or thousands of metres (Elachi, 1988). To overcome the problem of sensor size and achieve a high spatial resolution of tens of metres, SAR was developed. SAR achieves resolutions of <50m and utilises a very small antenna to do so. SAR increases the resolution along the line of travel (azimuth direction) using an array of antennas to observe the ground target and Doppler frequency shift. The ground resolution can be as small as:

$$r_a = L/2 \tag{8.2}$$

where r_a is the resolution and L is the length of the antenna in the azimuth direction. This definition indicates that smaller antennae can achieve higher resolutions, which is one of its real advantages. Ground resolutions are high for SAR and lie between 10 and 35m.

8.1.2.1 Description of the ESA ERS-2

The ESA ERS-2 Synthetic Aperture Radar (SAR) data has been chosen in this study principally for the advantage of being independent of weather and availability. In addition it has an operational return duration of 35 days with a spatial resolution down to 12.5 m. The swath width is 100 km and the swath length is in the order of 102 km. Images can be provided on a regular and reliable basis with relatively high spatial resolution across large areas. Figure 8.1 shows the swath geometry of the ERS-2 SAR instrument whilst the technical specifications are given in Table 8.2. The ERS-2 platform was launched in 1995 following a successful first mission of ERS-1 launched in 1991. Unlike previous radar remote sensing missions the ERS SAR instruments have been shown to be quite stable, which allows confident radiometric and geo-corrections (Grover *et al.*, 1999).

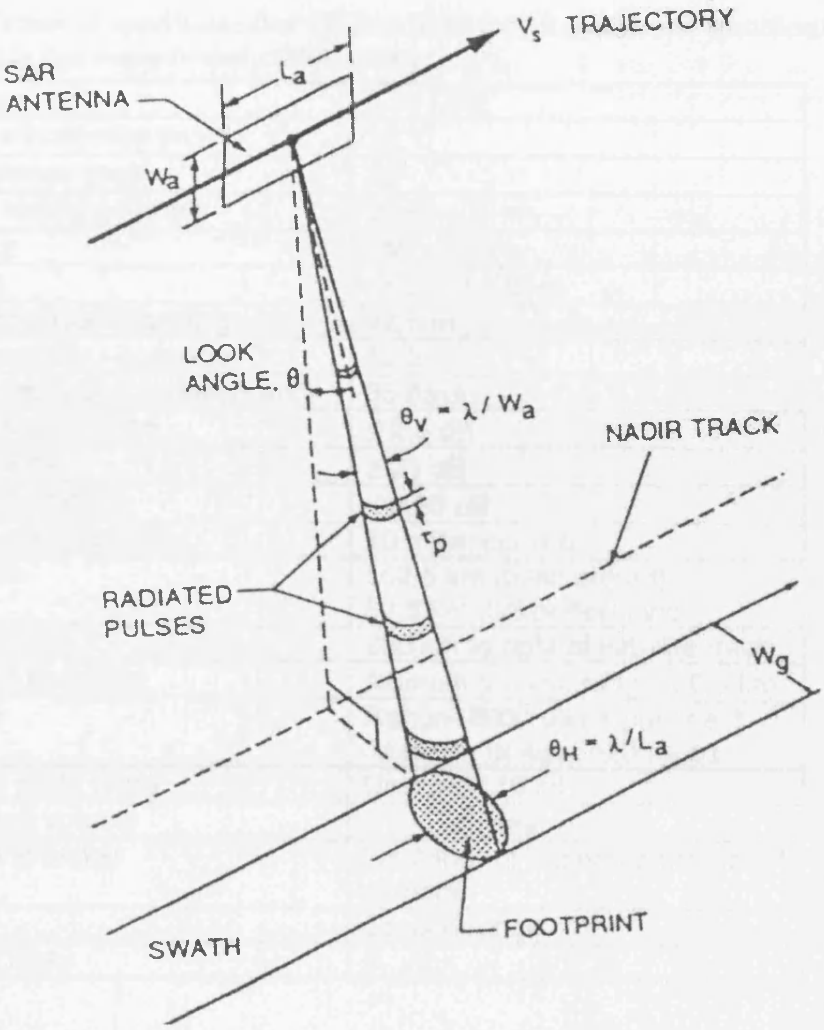

Figure 8.1 ESA ERS-2 SAR geometrical properties (from Ulaby *et al.*, 1996)

Table 8.2 Technical specification of the ESA ERS-2 SAR sensor and specification of the PRI product used in this research study (ESA, 2000).

Frequency	5.34 GHz
Near range incidence angle	20.1°
Mean incidence angle	23°
Far range incidence angle	25.9°
Polarization	VV
Bandwidth	15.55±0.1 MHz
Spatial resolution – northings	12.5 m
Spatial resolution - eastings	12.5 m
Temporal resolution for same track	35 days
Radiometric resolution	≤ 2.5 dB
Dynamic range	≥ 21 dB
Radiometric stability	≤ 0.95 dB
Maximum operation time	10 mins. per orbit
Swath width	102.5 km (telemetered) 82.5 km (full performance)
Swath stand-off	250 km to right of satellite track
Localisation accuracy	Azimuth ≤ 1 km; range ≤ 0.9 km
Scene size	Range- 8000 pixels per line Azimuth- at least 8200 lines
Pixel depth (data type)	Unsigned 16 bit
Total product volume	≈ 131 Mbytes
Annotation in image	Lat./long. of scene centre and 4 corners
Projection	Ground range
Number of looks	3

8.1.3 Interactions between microwave energy and terrestrial surface targets

The dynamic interactions between microwave energy and the soil and vegetation are not fully understood (Elachi, 1988; Ulaby and Elachi, 1990). It is known that microwave energy is scattered or attenuated according to the dielectric properties of the target, or if the target is metallic (Elachi, 1988; Ulaby and Elachi, 1990). The dielectric constant for soil is defined as:

$$\varepsilon = \varepsilon' - j\varepsilon'' \tag{8.3}$$

where ε' is the real part of the dielectric constant and $j\varepsilon''$ is the imaginary part due to losses from the system. The dielectric nature of a material is its ability to reflect or attenuate electromagnetic waves incident to its surface. The dielectric constant of oven-dried soil is ≈ four whereas that of water at 18°C is ≈ 80 at a frequency of 1GHz (Ulaby and Elachi, 1990). It follows that the dielectric response of soil will increase as the soil moisture increases. Saturated soil has a dielectric constant in excess of 24 but is, to an extent, dependent on the textural components of the soil i.e. the proportions of sand, silt and clay (Ulaby and Elachi, 1990). Radar remote sensing can therefore provide an indirect measurement of the moisture content of the target components. In addition to the moisture content of the soil, the three-dimensional distribution of the moisture in the target also has an influence on the response. Rougher surfaces will create more scattering and therefore less energy will return to the sensor (see Figure 8.2). Similarly, on soil covered by vegetation, it is the amount of moisture in the vegetation; the complexity of plant architecture (trunk, branches, leaves and fruit) and the underlying soil moisture that controls the scattering properties (Ulaby *et al.*, 1996).

The target can be divided into various scattering components depending on whether it is a simple or a complex surface (see Figure 8.2). Surface scattering is defined as that occurring from only one interface i.e. air-soil, and is not incident on further structures which might cause further scattering. Volumetric scattering occurs when the energy is scattered from more than one interface i.e. when reflected from the soil, and propagated to vegetation, where it is scattered further (Ulaby and Elachi, 1990; Ulaby *et al.*, 1996). It is the second and third order scattering that is particularly difficult to define in modelling. It leads to a confused return signal, making the separation of backscatter from the various components very difficult (Eom and Fung, 1984; Ulaby *et al.*, 1990).

Water present on the surface of the vegetation caused by dew or precipitation will also affect the backscatter measured by the sensor but in a similar way to the water content of the vegetation. Ice has a dielectric constant of eight compared to 80 for water. Frozen water on target surfaces will therefore affect backscatter by a very different degree to water in the liquid state (Ulaby *et al.*, 1996). Surface wind causes the structure of plants to alter and also affects backscatter of a given vegetative target. Targets in exposed locations may therefore have very different backscatter values than those in sheltered regions even though they are identical (De Troch *et al.*, 1996). This phenomenon is targeted by interferometry whereby two temporally proximal images are acquired from the same area.

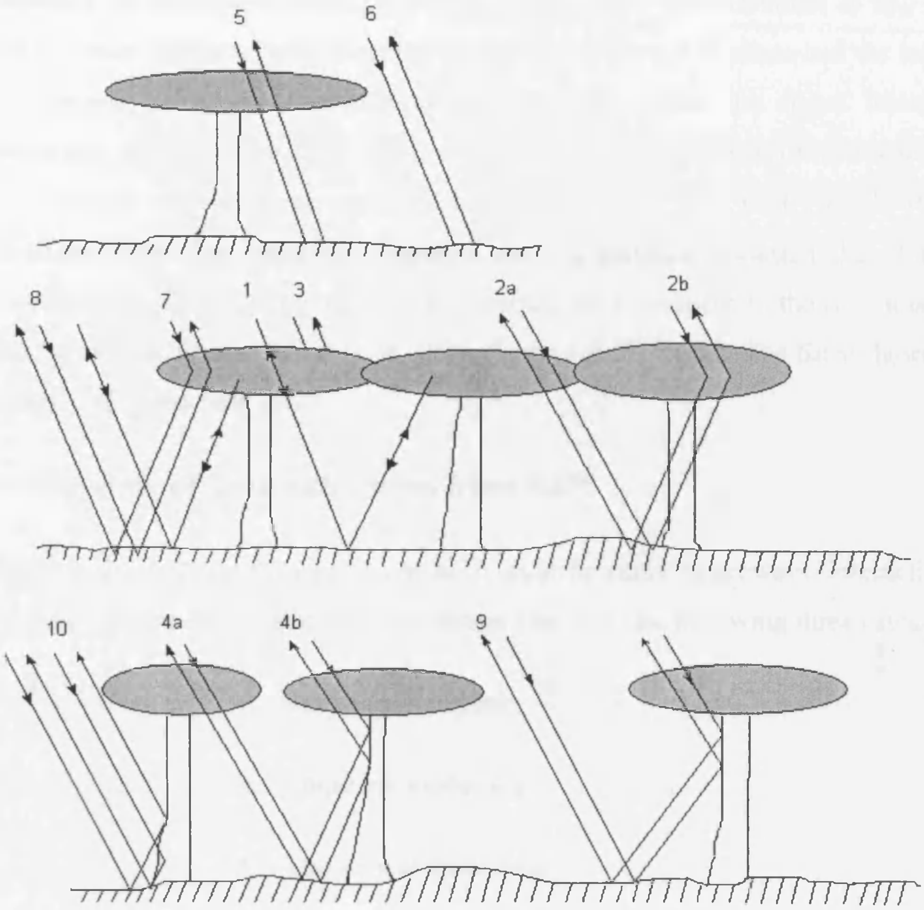

Figure 8.2 Backscattering types (Ulaby *et al.*, 1996). Types three, five and six represent surface scattering, whilst the others describe volumetric scattering.

A significant advantage of using microwave energy for remote sensing is its ability to penetrate cloud and certain surfaces (de Troch *et al.*, 1996; Rignot *et al.*, 1997). Water droplets in clouds are much smaller than the wavelengths of microwave energy and not do interfere with the propagation of energy at these wavelengths. Heavy rainfall will, however, interfere with microwave energy when the density of droplets is high or when the droplets are quite large. Microwave radiation incident on very dry soil surfaces can penetrate to a depth of 0.2-0.25 times the wavelength in free space (λ_0) (Ulaby *et al.*, 1996). Generally, the penetration of the target will increase as the wavelength increases. Conversely, the shorter wavelengths will have greater power to resolve fine detail e.g. surface roughness, but are less able to penetrate the target. Favoured channels for obtaining soil physical properties and the biophysical properties of vegetation are the X-, C-, L- and P-bands (Ulaby *et al.*, 1996).

Negative and positive interference adds noise or speckle to the returning energy and the resultant intensity of each pixel value in a SAR image (Lee, 1986; Durand *et al.*, 1987). Negative interference occurs when two returning waveforms are out of phase and the intensity is reduced. Conversely, when the returning waveforms are in phase the signal intensity is increased. Resultant images can be badly affected by speckle: adjacent pixels of identical characteristics can be rendered with disparate values of backscatter (Lee, 1986; Ulaby *et al.*, 1996). Backscatter from homogeneous areas can therefore have a standard deviation that does not reflect the similarity of surface within each pixel. Speckle can be reduced in the final image by filtering the data with suitable algorithms (Lee, 1986; Durand *et al.*, 1987). The filter algorithm used depends on the use of the final data.

8.2 Review of data extraction from SAR

Several different approaches have been used to study microwave interactions on terrestrial targets. Analytical methods of SAR imagery fall into the following three categories:

1. Statistical analyses
2. Empirical modelling
3. Theoretical modelling

Statistical methods of classification such as maximum likelihood estimation (MLE) can differentiate between land cover types (Durand *et al.*, 1987; Foody *et al.*, 1994; Dobson *et al.*, 1995; Schotten *et al.*, 1995; Grover *et al.*, 1999; Tso and Mather, 1999; Michelson *et al.*, 2000). Classification methods search for patterns within the backscatter data of an image that can be allotted to a particular land cover class (Schotten *et al.*, 1995). These methods are limited to multi-date imagery and are not feasible on single images (Dong *et al.*, 2001).

Empirical approaches include the simplified radiative transfer model used to extract data on vegetation types and model vegetation as a complex water cloud (Attema and Ulaby, 1978). These have been based on multiple regressions and are invertible. One drawback of such models is that they demand large amounts of experimental data for calibration. Wigneron *et al.* (2002) modelled growth parameters of sunflower crops from two radar sensors but with limited success. An empirical approach to extract soil moisture and surface roughness at the field scale was developed by Zribi and Dechambre (2003), but was not available for this project.

Theoretical models have focused on the understanding of the interactions between the targets and incident energy (Fung and Ulaby, 1978; Tsang and Kong, 1981), or the radiative transfer models from Eom and Fung (1984) and Ulaby *et al.* (1990). These are not invertible however, and are computationally demanding (Prevot *et al.*, 1993).

All sampling campaigns aim to acquire data that are representative of the system under scrutiny (Zar, 1984; Atkinson, 2001). In spatial analyses this concept must be taken a step further to include the space within which a sample is representative and is termed the support (Atkinson, 2001; Dungan, 2001). This concept applies to physical samples of for example soil, and to the sampling of backscatter in terms of SAR images. It is therefore vital to balance the support obtained from field sampling with the support from the image acquisition (Atkinson, 2001; Dungan, 2001). Soil samples are taken from a very small region on the ground and then used to define a value that represents the mean for a larger area. In the case of ERS-2 SAR images the larger area is approximately 12.5x12.5m. Support issues therefore affect all the above extraction techniques and must be considered when considering the results. Changes in the target over time are also associated with this concept and therefore frequency of sampling must also be considered. Soil moisture can change very rapidly and many samples per day would be required to characterise it fully. In this case such work is not required and a "snapshot" of the soil moisture at the beginning of the sampling period would be adequate. Characteristics of land cover changes less quickly. Plant biomass can be sampled adequately on a monthly basis to get growth charts whereas individual land cover classes generally exists for no less than a single season. Sampling by remote sensing data must therefore be conducted to ensure the temporal characteristics are represented if required.

8.2.1 Land Cover Classification

One of the most important aspects of catchment-scale nutrient transport modelling is land cover classification, and SAR has been used successfully in this field by Durand *et al.* (1987), Foody *et al.* (1994), Dobson *et al.* (1995), Schotten *et al.* (1995), Grover *et al.* (1999) and Tso and Mather (1999). Michelson *et al.* (2000) found that the extraction of land cover data from multi-temporal SAR provided better signature separation than LandSAT TM. Extraction of land cover from SAR requires a minimum of three images and therefore takes more time to acquire and process than alternative methods e.g. LandSAT TM. LandSAT TM, however, is badly affected by weather conditions where SAR is not.

Classification of images using maximum likelihood estimation is the most common method for categorising land using multi-temporal SAR images (Durand *et al.*, 1987; Dobson *et al.*, 1995; Schotten *et al.*, 1995; Tso and Mather, 1999). Studies that are based on multiple images from single-angle, single-channel and single-polarisation sensors assume that the soil roughness does not change over the period in which the multi-temporal image set was collected. Schotten *et al.*

(1995) found that the earliest point of detection for vegetation classification was May to July, which appears quite late in the growing season. The study by Schotten *et al.* (1995) was based in Flevoland, Netherlands and would have slightly lower temperatures than the UK during the winter and spring and crops would mature slightly later in Flevoland than in the southern UK. Grover *et al.* (1999) adopted a simpler approach to assign land cover to a rainforest area in the Amazon basin. They filtered a multi-date SAR image to reduce speckle, and subsequently calculated backscatter ratios. A threshold image was then generated and two land cover classes applied. Although this method was simple, the two classes of uncleared and cleared rainforest in the Amazon does not compare with the complexity of the agricultural diversity in lowland UK, nor does it consider the diversity of local covers in humid tropical agriculture. For example, differences between barley and wheat, among others, will be much less discernible than uncleared and cleared Amazon rainforest. An alternative statistical approach is discriminant analysis. This was used by Foody *et al.* (1994) on polarimetric C-band data, and therefore is not suited to ERS-2 SAR.

Classification of a multi-date image is performed in one of two ways: using information about the land targeted (supervised training) or without information about the land (unsupervised training) (ERDAS, 1997). Supervised training forces a set of classes onto the image by defining areas with known homogeneous land cover. In order to perform supervised classifications, pixels or areas with known land cover must be selected. These areas are then used to "train" the process to develop signatures for each class. At least one reference point for each land cover type must be used but more points are preferred. All pixels in the image are then assigned a land cover class by a decision rule according to the land cover signature most similar to their own. Reliable and accurate assignation occurs when there is enough separation between the signatures of the classes selected. There are several decision rules that can be applied depending on whether the signatures have non-parametric or parametric distributions. The principle assumption of this method is that all reference points are geographically accurate and the land cover assigned to each reference point is correct on the ground (ERDAS, 1997; Congalton and Green, 1999). Fewer classes produce better results (ERDAS, 1997). Supervised training is the preferred method when ground validation data are available and when distinct homogeneous areas are identifiable in the image.

Unsupervised training detects inherent patterns in the data without using pre-set signatures (ERDAS, 1997). The user is required to specify how many land cover classes are to be found and subsequently assigns land cover types to each of the resultant signatures after the classification of the image. Untrained classification is generally used when no information is available for the ground conditions or when spectral patterns in the data are of interest to the user. The trained method is reported to produce more reliable results and requires *a priori* data from the catchment (ERDAS, 1997). Unsupervised classification can be carried out without using *a priori* information to define class signatures but the assignation of land cover types to each class is performed by the user and is a subjective process. Without some knowledge of the land cover present in an area it would be impossible to assign land covers types to each class.

Once an image has been classified it is necessary to assess the accuracy of the classification (Congalton, 1991; Stehman 1996; Congalton and Green, 1999; Nishii and Tanaka, 1999; Foody, 2002). Historically, areas of individual land cover types were compared between the reference data and the classification. This method ignores potential "mixing" or misclassification of specific land parcels and is now considered inadequate. Congalton and Green (1999) describe error matrices or omission/commission matrices, which do consider the errors of misclassification but are based on the underlying sampling technique (Nasset, 1995; Foody, 2002). The error is divided into: land-survey, positional and classifier. Each must be considered independently for the acquisition of data. It is very important to ensure that sampling prior to image acquisition is adequate in terms of geographical and classification accuracy to cater for error analyses (Foody, 2002). Error matrices estimate the overall accuracy of the image and the accuracies of the individual land cover classes. The accuracy is divided into two parts: producer's accuracy and user's accuracy (Congalton and Green, 1999).

Producer's accuracy is an estimate of the proportion of correctly classified pixels of those known to fall in a given class from ground survey. The producer's error is the proportion of pixels of a known class that are misclassified. Producer's accuracy reflects how well a given land cover type is represented in an image. User's accuracy is an estimate of the proportion of correctly classified pixels assigned to a class on the image. Conversely, the user's error would be the proportion of pixels given a classification that do not have that classification on the ground. The user's accuracy indicates how well an image can predict a given land cover type on the ground and is more important than producer's accuracy in the application under consideration - mapping a catchment for nutrient transport modelling (Congalton and Green, 1999).

The error matrix is also used to compare the classified reference points against a random allocation of classes to the reference pixels and calculate the statistical probability of the difference (Nishii and Tanaka, 1999). As with all statistical and analytical methods the dependability of the system is based on the number of reference sites (Nasset, 1995; Congalton and Green, 1999). Congalton and Green estimate that a minimum of 50 reference pixels for each land cover type is required for reliable error estimation. This can be prohibitive for some land cover types in a small catchment if carried out at the field level but should be possible at the pixel level. Pixels and polygons (fields or land parcels) can be used as reference "points" in error estimation depending on the scale of interest. In terms of remote sensing studies the pixel is the spatial unit of interest. In terms of the nutrient transport modelling it is the field unit that is of interest.

Congalton and Green (1999) do not reflect on the issues arising when land-classes present in the area of interest are not recognised in the classification scheme. If the excluded classes are included in the error matrix the overall accuracy is not affected, but the producer and user accuracies will be by spreading the incorrect reference points across more classes. To include only the recognised classes in the matrix would be misleading. They should be included to estimate the error as accurately as possible. But in so doing they cause an increase in the user's accuracy by removing some commission samples. The producer's accuracies will include the omissions of the recognised classes due to the inclusion of the omitted values. Similarly, the user's accuracies will be correct because the omitted classes do not offer committed values from the omitted classes i.e. misclassified with the land cover types that were not identified in the classification. Although an error matrix can be prepared without the omitted classes it cannot represent a good estimation of error in the image. It is therefore believed that the matrix should be applied in the event of class exclusion.

8.2.2 Extraction of soil characteristics for bare soil from SAR data

Nutrient export models would benefit from a soil moisture map for a starting scenario and receive updates during a simulation run (J. Arnold, USDA, ARS), but the SWAT model does not do so at present. Soil moisture is not a parameter of SWAT but instead is modelled within SWAT using other soil physical properties such as conductivity, and vegetation factors such as transpiration (Neitsch *et al.*, 2002a). The SWAT development team are considering the use of soil moisture maps for future versions of SWAT (J. Arnold, USDA, ARS). The extraction of soil moisture data from SAR was therefore undertaken to assess its potential for future modelling scenarios. The start of the agricultural season in the autumn is the most suitable time for soil moisture investigations whereby large areas of soil are exposed. Autumn weather can also provide variable soil moisture content offering a wide range of sampling conditions.

Ulaby *et al.* (1996) and Tansey (1999) provide reviews of the various methods of extracting soil moisture and surface roughness values using SAR. Paloscia (2002) also provides a useful review of the work investigating SAR carried out by Italian groups. His conclusion is that C-band is more suited to narrow leaf crops and L-band to broad leaf crops and soil conditions. Work carried out to look at microwave – soil interactions (e.g. Fung *et al.*, 1992; Oh *et al.*, 1992; Chen *et al.*, 1995; Altese *et al.*, 1996; Ulaby *et al.*, 1996; Su and Troch, 1996; Tansey, 1999; Van Oevelen and Hoekman, 1999) have centred around the small perturbation model (Shi *et al.*, 1992), the OSU model (Oh *et al*., 1992) and the Integrated Equation Model (IEM) (Fung *et al*., 1992). More recent efforts have used trained neural networks based on measured data and synthetic data created by the IEM (Dawson *et al*., 1997; Baghdadi *et al*., 2002a). Outcomes from the neural network research are potentially applicable across a wide range of soil types when tested on many data sets. In the meantime there may be little gain in accuracy when compared to the use of IEM alone. The inverted model of Oh *et al.* (INVOSU), as described by van Oevelen and Hoekman (1999), works on the ratio between the VV and HH polarization radar cross-section. It is, therefore, strictly applicable only when these data are available. Models such as IEM or MIMICS (Ulaby *et al*., 1990) can output the HH polarised cross-section based on details of the instrument used and an extensive set of ground data. If the results from the IEM or MIMICS model were found to be reliable and accurate output from these models could be used as input to the INVOSU model, which could then be inverted for output into hydrological and nutrient transport modelling.

Inversion modelling has been successfully carried out by Altese *et al.* (1996), Ulaby *et al.* (1996), Van Oevelen and Hoekman (1999) and Baghdadi *et al.* (2002b) using the IEM of Fung *et al.* (1992). Although Tansey (1999) carried out inversion work using the same principles, the inversion was never fully validated due to the time difference between the acquired image dates and the field sampling. In support of this work, the findings of the sensitivity analyses agreed with the other authors. Ulaby *et al.* (1996) noted that the model is valid for soils with a "modest" covering of vegetation with height no more than 100-150mm. Soil moisture levels found in the Stonton Brook catchment during the autumn of 1998 were between 18 and 49% (see Chapter 4). Additionally, up until mid-February the following spring (1999), the vegetation height did not exceed 40-60mm except for some oilseed rape fields. These are within the ranges used by the above workers, indicating that the model should perform well on the proposed data.

Previous research has strongly supported the relationship between the radar backscatter and the dielectric constant of the soil (ε). But van Oevelen and Hoekman (1999) found that the sensitivity of σ^o to the dielectric constant of the soil is reduced as soil moisture increases. This observation was made when using sensitivity analysis and scatterometer trials rather than satellite-based SAR data. Thus the ability to predict soil moisture from these data is limited due to the large amount of error that may be applicable to any predictions. Ulaby *et al.* (1996) states IEM would be able to monitor relative changes in moisture levels providing roughness does not change substantially. Contrarily, Altese *et al.* (1996) found that the effect of root mean square (rms) height on σ^o is small when the rms value is greater than 15mm and when the frequency of the energy is between 4.5 and 7.5GHz. Additionally, sensitivity of the correlation length on σ^o is always less than the rms height but especially so when frequency is less than $\approx$ 6GHz. The work of Dobson *et al.* (1992) and Altese *et al.* (1996) suggests that the ERS-2 SAR with 5.3GHz frequency and 23 mean incidence angle appears most suited to extraction of moisture. It has to be borne in mind that these results are based on synthetic data from IEM. The assumption here is that IEM is a suitable and accurate model for radar cross section.

Taconet *et al.* (1996) describe a simple regression equation from an extensive data set based on bare soil moisture and backscatter values from ERS-1 SAR. The correlation coefficient from regression, R, is reported as 0.96 (r^2 = 0.92), and if repeated in this study will be reliable enough for adequate predictions. Their regression equation is:

$$Wg=44.96+2.54\sigma^{o} \tag{8.4}$$

where Wg is the volumetric moisture content and σ^{o} is the backscatter coefficient. This method was finally chosen to assess potential extraction of soil moisture data from single SAR images.

8.2.3 Vegetation parameter retrieval

Vegetation parameters are much more difficult to model and predict than land cover types or soil variables because of the confusion created by volumetric scattering (Ulaby *et al.*, 1996). It has been possible, however, to retrieve plant biophysical properties such as LAI using SAR (Touré *et al.*, 1994). SWAT utilises vegetation parameters including LAI in the form of a database table rather than a map (see crop growth charts in Chapter 4). Vegetation parameters could therefore benefit from repetitive measurements over the course of the growing season. Crops of the same type but of different growth characteristics could be incorporated into SWAT by giving them different prefixes, e.g. winter wheat one and winter wheat two, and then assigned specific areas. It is not yet known whether SWAT would be sensitive to this sort of detail. Therefore, this aspect of remote sensing will only be assessed for the potential of vegetation parameter extraction using SAR. LAI and biomass values for wheat and oilseed rape will be regressed using against backscatter values extracted from the May and July 1999 SAR images.

8.2.4 Modelling of vegetation

Models such as those described by Touré *et al.* (1994) use empirical relationships between plant properties and radar backscatter. The MIMICS model, however, seeks to describe the backscatter response from a vegetated surface and utilises many soil and plant parameters. The following equation describes the relationship of backscatter to vegetated soil found by Ulaby *et al.* (1996):

$$\sigma^{\circ}=T^{2}\sigma_{S}^{\circ}+\sigma_{dv}^{\circ}+\sigma_{\mathrm{int}}^{\circ} \tag{8.5}$$

Where σ^{o} is the backscatter contribution of bare soil, T^2 is the two-way attenuation of vegetation layer, $\sigma_{dv}°$ is the direct backscatter of vegetation layer and $\sigma_{int}°$ is the multiple scattering from vegetation and soil surfaces.

These governing factors are illustrated in Figure 8.2. It has already been said that the response of vegetation to backscatter is dependent not only on the moisture found within the biomass but also the three-dimensional shape of that water. Measurable variables such as height, density, leaf shape, leaf area index (LAI) and orientation of these components will influence backscatter (Saich *et al.*, 1995). It is therefore easy to see how difficult if not impossible it is to predict any one of these factors from backscatter retrieved from a single SAR image. The problem could be overcome by an extensive ground campaign but an extensive ground campaign is what this study is trying to avoid by using remote sensing data. If the above techniques are successful then it is tempting to use their results as input to the following modelling techniques. Although other Dobson *et al.* (1992) and Altese *et al.* (1996) use this technique it has a considerable risk of error associated with it.

Much of the understanding of backscatter responses of vegetation has come from the development and application of theoretical models such as MIMICS (Ulaby *et al.*, 1990) and RT2 (Saich *et al.*, 1995). MIMICS was developed for closed canopy, temperate forests but has been applied to agricultural crops (Touré *et al.*, 1994). RT2 is based on similar principles but developed specifically for agricultural crops. Work has shown that these models give good correlations between predicted and measured backscatter values but have been limited with certain vegetation types, especially wheat (G. Cookmartin, Department of Physics, University of Sheffield). Modelling outputs from this type of model should ideally be the relative components of backscatter i.e. soil moisture, trunks. This breakdown of information would help to understand the interactions between microwave and the ground targets. Unfortunately they model backscatter values per canopy layer (RT2) or backscatter that has been reflected directly from the vegetation or from the soil or multiple scattering from both. Backscatter values can be extracted from the various components (i.e. leaves) using RT2 (G. Cookmartin, Department of Physics, University of Sheffield) but is a very time consuming process. Again they are not invertible and only offer a tool for research.

Semi-empirical water cloud models, which are simplified radiative transfer models, utilise multiple regression techniques to model backscatter (Attema and Ulaby, 1978; Van Leeuwen, 1996; Rijckenberg, 1997). Regressions are easily inverted and can separate the backscatter into the components of soil and vegetation, of which the latter could be related to biomass. These models must first be based on experimental data and have only been applied successfully where there are several images of different radar configurations e.g. frequency, incidence angles or polarisation (Prevot *et al.*, 1993). Attempts to model backscatter at the field level have failed (Van Leeuwen, 1996; Rijckenberg, 1997) but were more successful at the regional scale (Bouman *et al.*, 1999). This matter is very important to catchment-scale modelling, because detail at the level of the field is required and will largely be lost.

Where the effects of seasons are more apparent such as in temperate zones, multi-temporal and multi-channel images are more desirable (Ferrazzoli *et al.*, 1997; Kurvonen *et al.*, 1999; Pulliainen *et al.*, 1999). Pairs of images (interferometry) also have their uses for biophysical property extraction (Dutra and Huber, 1999), but were not sought for this project.

The purpose of this study is to assess the operational use of SAR with regards to hydrological and nutrient transport modelling. Two methods are discussed above that can be applied depending on the outcome of preliminary analyses. The first method performs Type II regression in a similar fashion to Taconet *et al.* (1996). The measured soil moisture content in the sampling fields will be regressed against the corresponding backscatter coefficients from the overflights between November 1998 and March 1999. This was carried out on approximately half of the sampling sites where both moisture and roughness were known and where vegetation cover does not exceed 20% or 150 mm of growth. Should this method prove accurate, the model could be inverted to provide predictions from the three other images where only the moisture levels are known. Alternatively if the regression fails to disclose any significant relationship there remains little hope that the data can be applied to further simple models.

The second method discussed above will be to apply the soil and vegetation data collected from the Stonton Brook to the MIMICS model. Output from this model will not be suitable for inclusion in the SWAT model but may disclose some information about the behaviour of microwave radiation on the conditions found in the Stonton Brook.

8.3 Methods of image acquisition, pre-processing and data extraction

The images shown in Table 8.3 have been made available for this project under the European Space Agency's 3rd Announcement of Opportunity (AO3). Other images were provided but could not be used for this study. The data were provided in PRI format on CD within one month of each overflight and were imported into ERDAS Imagine for all processing.

8.3.1 Image pre-processing

Reliable extraction of any data from radar imagery depends upon good quality SAR images. Speckle and weather effects (dew, precipitation or wind) will add variation to the backscatter response of the microwave energy and therefore compromise the extraction of reliable data.

Each image must be assessed in turn and accepted or rejected as necessary. The effects of ice and wind on the backscatter coefficient are very difficult to define and were therefore ignored or images avoided if it was felt these effects compromised their interpretability.

Table 8.3 List of ESA ERS-2 SAR PRI images provided by ESA as part of the AO3. UK-PAF and I-PAF indicate whether the images were acquired by the United Kingdom or Italian acquisition facilities.

Date Acquired	Orbit	Frame	Facility
2nd Nov 1998	18485	2547	UK-PAF
15th February 1999	19988	2547	UK-PAF
2nd March 1999	19988	2547	UK-PAF
26th April 1999	20990	2547	UK-PAF
31st May 1999	21491	2547	UK-PAF
5th July 1999	21992	2547	I-PAF
9th August 1999	22493	2547	I-PAF
10th October 1999	23495	2547	I-PAF

In order to reduce the impact of speckle to a minimum, all images were filtered prior to any resampling. Durand *et al.* (1987) compared several filters and found that for agricultural applications of SAR, the Lee filter was preferable. This filter was used against differing numbers of pixels to assess the best method.

All image pixel values were then converted from radar brightness, β^0, to backscatter coefficient, σ^0, using the equations given by Laur *et al.* (1998), as shown below:

$$A_{ij}^{\ 2} = DN_{ij}^{\ 2}\,\frac{1}{K}\frac{\sin\alpha_i}{\sin\alpha_{ref}} \tag{8.6}$$

where A is the amplitude corresponding to the pixel at location (i,j), DN_{ij} is the radar brightness value of pixel at location i,j, 1/K is the factor relating the pixel value to the backscattering coefficient and α_i is the incidence angle of the corresponding pixel. The method was applied using the spatial modelling facility found in Imagine.

Once the data were filtered the images were georectified as discussed in Chapter 7, and a sub-set of the Stonton Brook area taken to reduce the processing time needed for any further work. Images from May, July and August were then overlaid in Imagine and resampled to produce one multi date image with three layers. For visual clarity each layer was coloured either red yellow or blue. This image was then subjected to classification and MLE methods to extract land cover categories.

8.3.2 Extraction of land cover classification using MLE

Supervised and unsupervised training schemes were employed to assess the potential of multi-date SAR images where ground data were available and where they were not. The supervised training and subsequent classification was carried out on the multi-date image based on the MLE method of land cover classification as used by Schotten *et al.* (1995) and Tso and Mather (1999). All methods were applied within ERDAS Imagine 8.3.1. Signatures were created at the sampling points shown in Figure 4.1. Three additional areas of lake and urban, and four of woodland (two deciduous and two coniferous) were also used. Two separate training schemes were applied based on whole fields and individual pixels. The distributions of the signatures in each land cover class were assessed for normality using Shapiro-Wilk or Kolmogorov-Smirnoff depending on the number of data points (Zar, 1984). The outcome of this test would then dictate the decision rule used to classify the image. Three parametric decision rules are available in Imagine: minimum distance, Mahalanobis distance and maximum likelihood, whilst parallelpiped and feature space exist for non-parametric signatures.

Unsupervised classification was carried out on the multi-date image based on 12, 13, 14 and 15 classes. The lower value corresponds to the number of land cover classes found in the catchment and the upper value used to obtain potentially better definition between classes. The signatures were then assigned a land cover class by the distribution of each signature and the most likely land cover class following that pattern.

Because all land cover classes are known for the entire Stonton Brook (Figure 4.2), all fields can be used for accuracy estimation. Error matrices were generated automatically in Imagine for the two classification schemes. Matrices from land cover maps were built in Excel using the database tables generated from the maps in ArcView. Congalton and Green (1999) suggest that a minimum of 50 reference points should be used for each land cover class present in the image. Approximately 270 reference points were used in the matrices from the images due to the laborious nature of the procedure in Imagine. The best outcome from the image classification was then overlaid on the field boundary map and field classes reassigned according to the predominant class present in each field boundary polygon. Further error matrices were generated for the field maps based at the field boundary scale rather than pixel scale after reassigning the land cover from the output of the SAR imagery. All 762 polygons in the land cover map were used for the matrices of the field-based accuracy assessment. Matrices for the field maps were built in Excel using the database tables associated to the field polygon shapefile. Kappa analysis was then applied to each matrix to assess whether the assignation of land cover to pixels through the classification process was significantly different to random assignation. One small error existed in the equations given by Congalton and Green (1999) for the KHAT statistic (J. Norris, Schlumberger). The chance agreement as defined by Congalton and Green (p 49) was:

$$p_c = \sum_{i=1}^{k} p_{i+} p_{+j} \tag{8.7}$$

and should read:

$$p_c = \sum p_{i+} p_{+i} \tag{8.8}$$

The latter of the two equations were used for the manual calculation of the KHAT statistic. Finally, the two error matrices for the classified images were compared against each other to see whether a significant difference existed.

8.3.3 Extraction of soil moisture and soil surface roughness estimates from SAR

Backscatter values from the February 1999 and November 1998 images were extracted for the field sampling sites containing exposed soil. Due to inaccuracies in the processed images, means were extracted from the nine pixels surrounding the approximate position of the field sampling sites. Inaccuracies in the georectification of the SAR images rendered selection by co-ordinates unfeasible. Therefore, the pixels were chosen based on the identifiable features in the proximity of the sampling sites.

All the soil moisture and soil surface roughness models capable of inversion are quite simple and reflect relationships that are capable of analysis with regression. The relationships between the backscatter (dB) and soil moisture content and soil surface roughness were plotted for November 1998 and February 1999. It was hoped that the summer months could also be included for the drier soils, but availability of exposed soil was too limited to represent good support.

The backscatter values from the two images were correlated with the soil moisture values using least-squares linear regression. All statistical analyses were performed in SPSS.

8.3.4 Application of the MIMICS radiative transfer model

The vegetation and soil parameters shown in Tables 8.4 and 8.5 were input to the MIMICS model on a Silicon Graphics Indigo workstation.

In addition to those parameters shown in Tables 8.4 and 8.5, the characteristics of the SAR sensor in Table 8.2 were also required. An example input dataset is provided in Appendix D.

Each sampling site was simulated individually for each month. Backscatter values for HH polarization energy in decibels were amongst the output variables, and these were then correlated against the backscatter values extracted from the relevant SAR images. Data were analysed for normality using the Shapiro–Wilk method and a suitable parametric or non-parametric correlation function used accordingly.

Table 8.4 Vegetation parameters input to MIMICS radiative transfer model.

Canopy density /m sq	2' Branch diameter (cm)
Trunk height (m)	2' Branch density
Trunk diameter (m)	2' Branch dry density (kg/m^3)
Trunk Moisture (gravimetric)	Crown thickness (m)
Trunk dry density (kg/m^3)	Leaf density (/m^3)
Trunk diameter standard deviation	Leaf moisture (gravimetric)
Trunk length standard deviation	LAI (cm sq m^{-1})
Branch density (/m^3)	Leaf thickness (mm)
1' Branch length (m)	Leaf dry density (kg/m^3)
1' Branch moisture (gravimetric)	Fruit density /m^3
1' Branch diameter (cm)	Fruit moisture (gravimetric)
1' Branch dry density (kg/m^3)	Fruit length (cm)
2' Branch length (m)	Fruit density in crown (/m^3)
2' Branch moisture (gravimetric)	Fruit dry density (kg/m^3)
Trunk dielectric constant	2' Branch dielectric constant
Leaf dielectric constant	Fruit dielectric constant
1' Branch dielectric constant	

Table 8.5 Soil parameters input into MIMICS.

Soil root mean square (cm)
Soil correlation length (cm)
Soil volumetric moisture (l/m^3)
% sand
% silt
% clay

8.4 Results

The eight images were filtered using the Lee filter present in Imagine using the coefficient of variation for the whole image. A 7x7 pixel window gave the best visual results based on the clarity of identifiable objects. An example of a processed image is shown in Figures 8.3.

Unlike the aerial photography in Chapter 7 the georectification of the whole PRI scene was inadequate for the degree of accuracy required for this project. Checks were carried out using identifiable features such as road junctions and field boundaries that were different from the GCPs used in georectification. These checks indicated that the positions of features in the centre of the Stonton Brook sub-set were displaced by as much as 500 m. The Orthoradar module of Imagine (ERDAS, 1997c) was also used to see if it produced better results. This method uses positional data from within the SAR PRI header file but the results were also found to be inadequate. To overcome this inaccuracy the Stonton Brook sub-sets were further georectified using GCPs found in and around the Stonton Brook catchment only. On completion the overall accuracy within the catchment had improved markedly and errors were reduced to a maximum observed of around 40 m but normally around 10-15 (one pixel). All these images were then available for the proposed work.

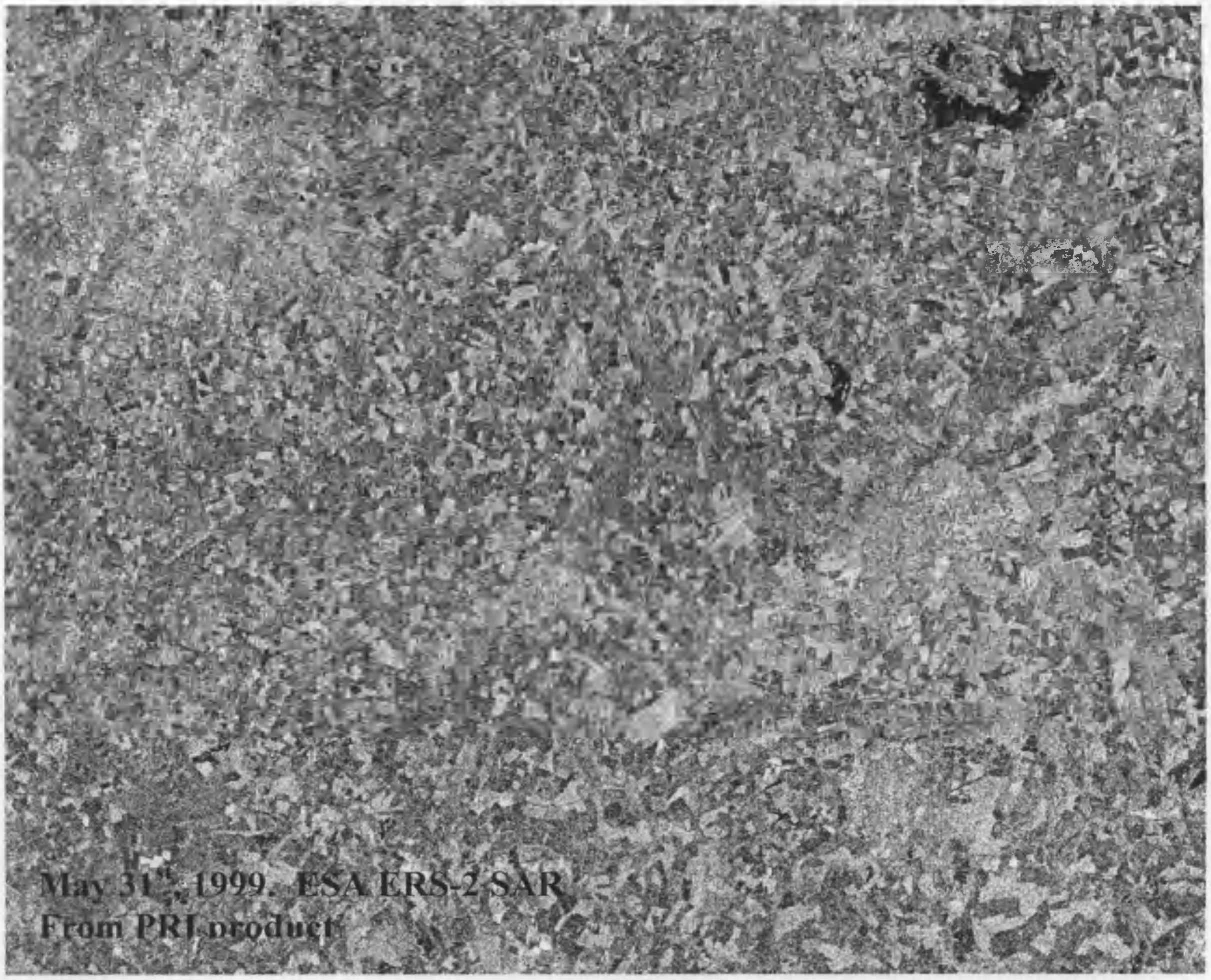

Figure 8.3 ERS-2 SAR PRI image of the Leicestershire region (102x100 km). Image has been filtered and georectified. Rutland Water can be seen as a dark patch in the top right corner and Leicester is a light patch in the top left corner. Georectification accuracy of this image was found to be inadequate and further work was carried out on a sub-set centred on the Stonton Brook area.

After secondary georectification of the Stonton Brook sub-sets the various images from 1999 were overlaid to assess the best combination. The secondary georectification of March proved inadequate and was omitted. Heavy rainfall occurred two days prior to the acquisition of the October image and was possibly detrimental to obtaining a good image. The October image did not show the levels of discrimination between fields that the May, July and August images gave. The best clarity and apparent discrimination of land cover types visually was provided by the combination of the images from May, July and August. The three layers were then loaded to different colour guns and the resultant multi-date (false colour) composite image is shown in Figure 8.4. The problems of geographical inaccuracy are demonstrated in this image where the only area appearing in “focus” is the centre area that has been georectified twice.

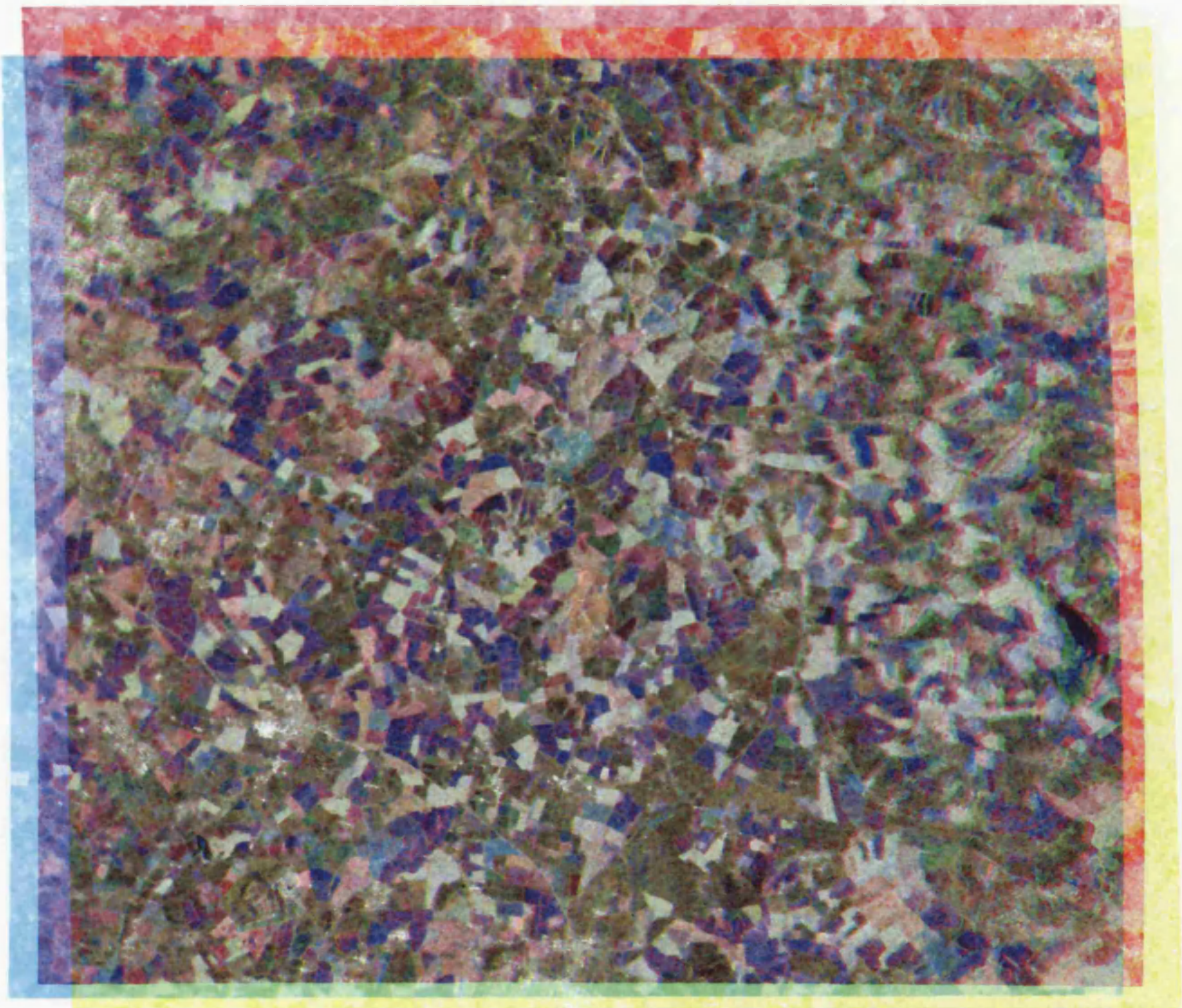

Figure 8.4 Multi-date subset of three SAR images (approximate size 16x18 km). The red image refers to May, yellow to July and blue to August. Note the clarity in the centre of the image where secondary georectification was carried out. The blurred outer edges indicate the variation in georectification of the whole PRI scenes.

8.4.1 Land cover classification

The image shown in Figure 8.4 was subset, and subjected to supervised and unsupervised training. Subsequently MLE classification was performed. All training and classification work was carried out in ERDAS Imagine. An error matrix was created in Imagine for the supervised classification but could not be generated automatically in Imagine for the unsupervised image due to omission of one or more land cover types. This error matrix was created and analysed in Excel.

8.4.1.1 Supervised training

Supervised training was performed on the multi-date image using the 57 field sampling points in Table 4.1. Additionally, five urban areas, three wooded areas and two small lakes were also used within the Stonton Brook as reference points. The resultant classification included all classes but the lake areas were vastly over represented in comparison to the actual areas. SWAT cannot utilise the lake as a land classification in the land cover map but instead lakes and reservoirs are specified through data entry. Additionally, the lakes accounted for less than 1% of the total catchment area and were excluded from further classification. Most pasture fields were empty for a large portion of the year and animals moved frequently from one field to another. Pasture containing cattle was not distinguishable from pasture containing sheep and therefore was not differentiated into cattle and sheep. On first inspection of the initial classifications, the signatures from deciduous and coniferous woodland showed almost complete agreement and no differences were found in the resulting classified image. These two land cover types were therefore combined to provide one woodland class.

The training method was experimented with by sequential selection of: individual pixels, 9x9 windows surrounding the locations, and polygons enclosing homogeneous fields. Variance in the signatures became progressively greater from individual pixels to field polygons, and it was the latter selection method that gave best results in the final classification. The first two methods gave highly confused results, and little homogeneity could be seen in the land cover in any of the identifiable fields. Signatures of the pixels selected for supervised training were assessed for normality and no departure from normality was observed in any of the groups. Some scepticism must be used in this process because hemp had only two replicates, and urban and wooded areas were represented by only three locations. Notwithstanding the homogeneity of variance test, parametric maximum likelihood decision rule was applied. The resultant signatures are shown in Figure 8.5 using only the May and August layers whilst the classified image is shown in Figure 8.6.

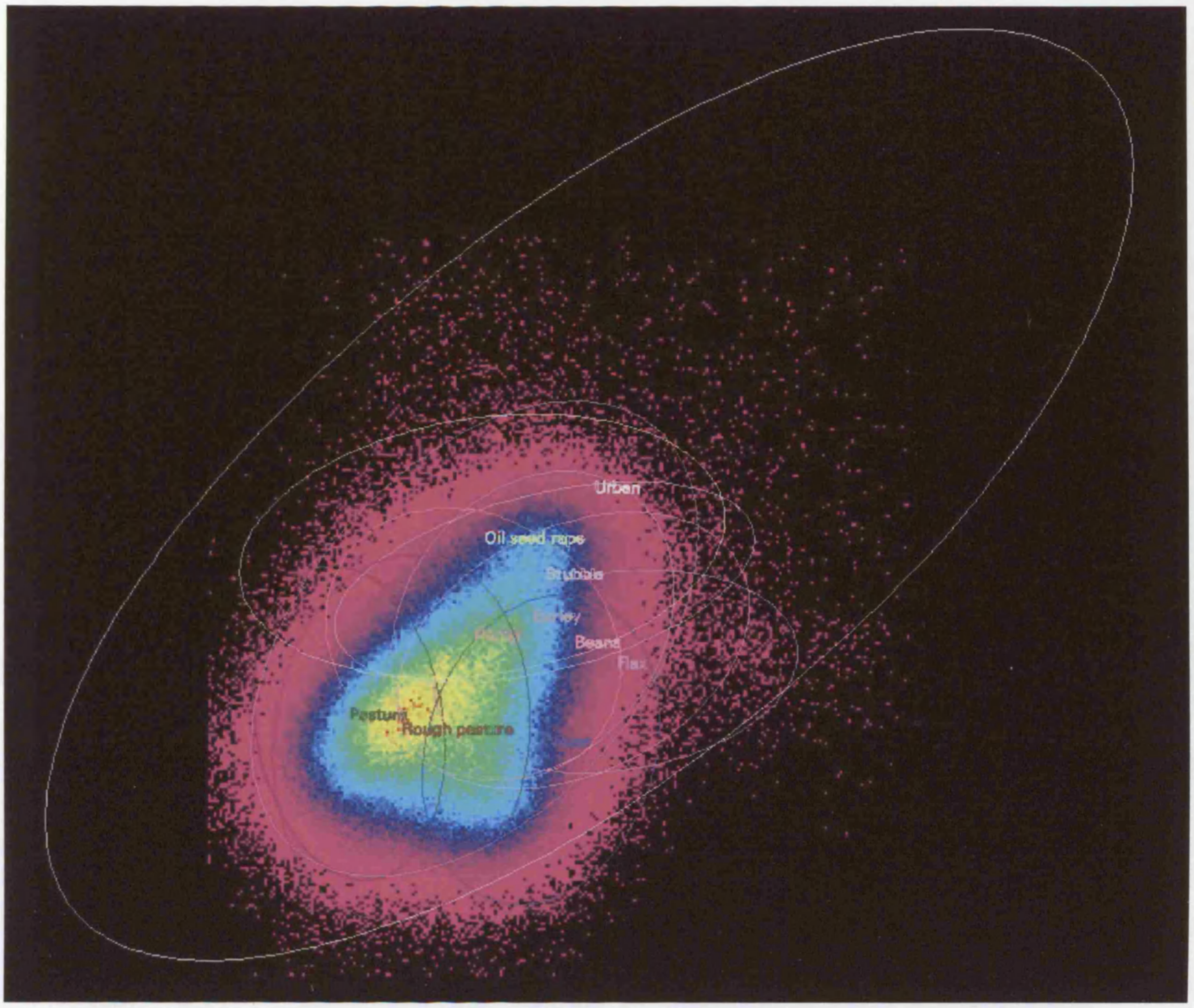

Figure 8.5 Signature plots from training samples used in supervised classification. Labels for land covers are placed in the centre of each ellipse.

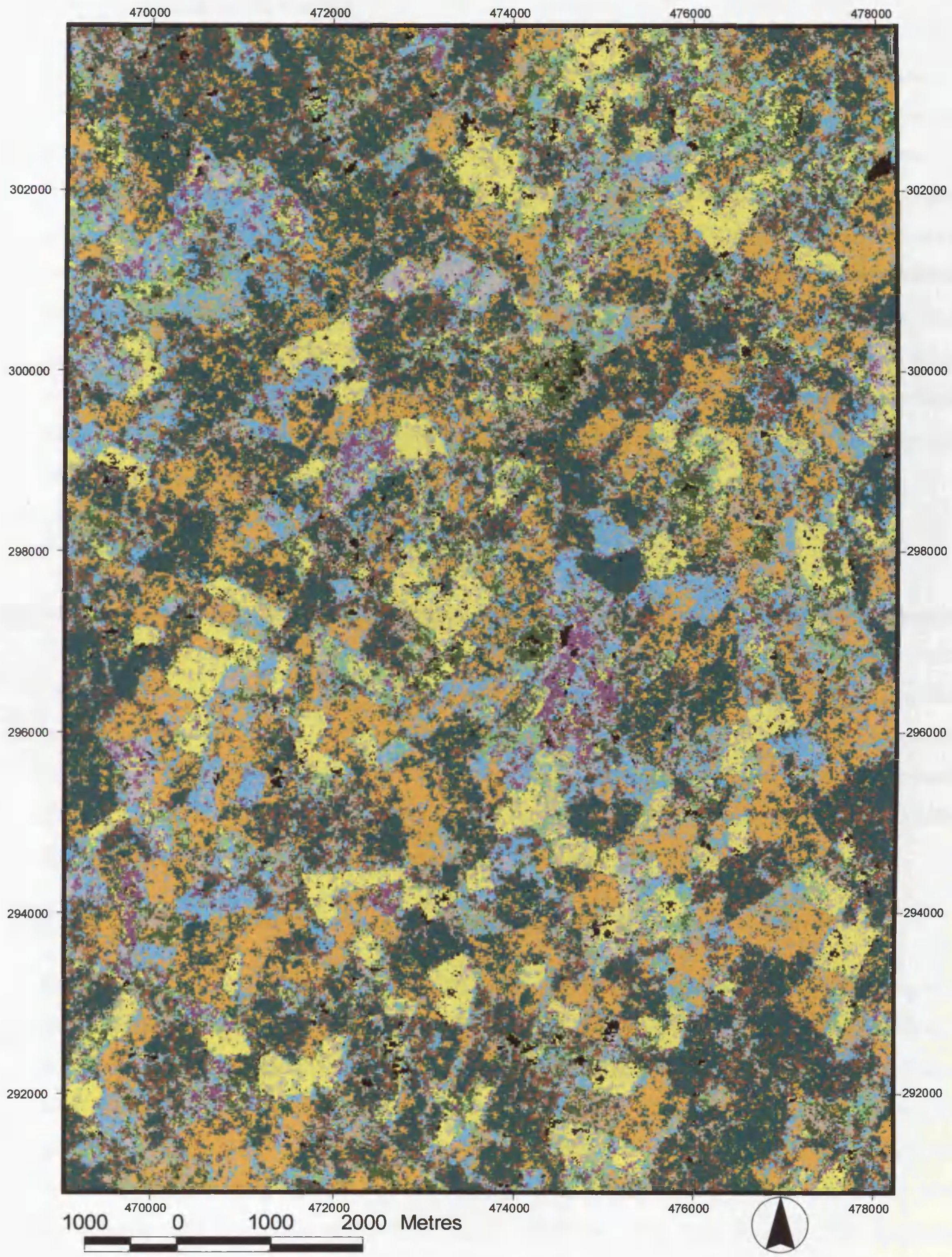

Figure 8.6 Image created using MLE based on multi date image from May, July and August (9.5x14.5 km). Purple is hemp, yellow is oilseed rape, dark green is pasture, mid green is forest, light green is field beans, orange is wheat, black is urban, beige is barley, grey is stubble, red-brown is rough pasture, and light blue represents flax.

8.4.1.2 Unsupervised training

Unsupervised classification was applied to the same composite image using four different sets of land classes (12-15). This was carried out to ensure that the minimum number of categories found in the catchment was included and to allow better differentiation of classes if a particular signature dominated two or more classes. No differences between the four trials were discernible and the image defined with 12 classes was used for the following process. Resultant signatures were allocated land cover classes depending on the dominance of a signature in a recognisable feature such as homogeneous field shape of known type. Only seven land cover classes could be applied confidently out of any of the 12-15 classes applied to the image. Barley, urban, wheat stubble, water and rough pasture were omitted using this method and the resultant image seen in Figure 8.7. Multiple classes from the procedure falling into one identifiable class on the ground were amalgamated into one.

8.4.2 Error matrices at the pixel-scale of resolution

Error matrices were created for the images shown in Figures 8.6 and 8.7 using the information from ground validation (Figure 4.1). They were created using 272 and 273 reference points respectively. The reference points were generated automatically using the stratified random option in ERDAS Imagine. This method is preferred when the land cover classes are unequally represented in the catchment. Therefore the most dominant types will have a proportionately greater number of reference points than those with very little area. The error matrix for the first image is shown in Table 8.6 and for the unsupervised classification in Table 8.7.

8.4.2.1 Error matrix for supervised classification at the pixel-scale of resolution

Overall accuracy for the supervised classification was 46% and included all classes. Barley was the most unreliable land cover classified and was not accurately reproduced in the error matrix although it was present in the classified image. It was confused to a small extent with field beans and flax. In terms of producer's accuracy, stubble, hemp and oilseed rape were reproduced with greatest reliability of 80%, 67%, 62% respectively. Stubble on the ground is therefore predicted as stubble in the image in 80% of the corresponding pixels. Flax, pasture and wheat were represented with moderate accuracies of 50%, 49% and 49% respectively. The remaining categories of urban, field beans, forest and rough pasture were poorly reproduced in the image and had 11%, 10%, 25% and 33% of the corresponding pixels with accurate land cover classes. These classes however cover very small areas in the catchment and the errors cannot therefore be considered very significant.

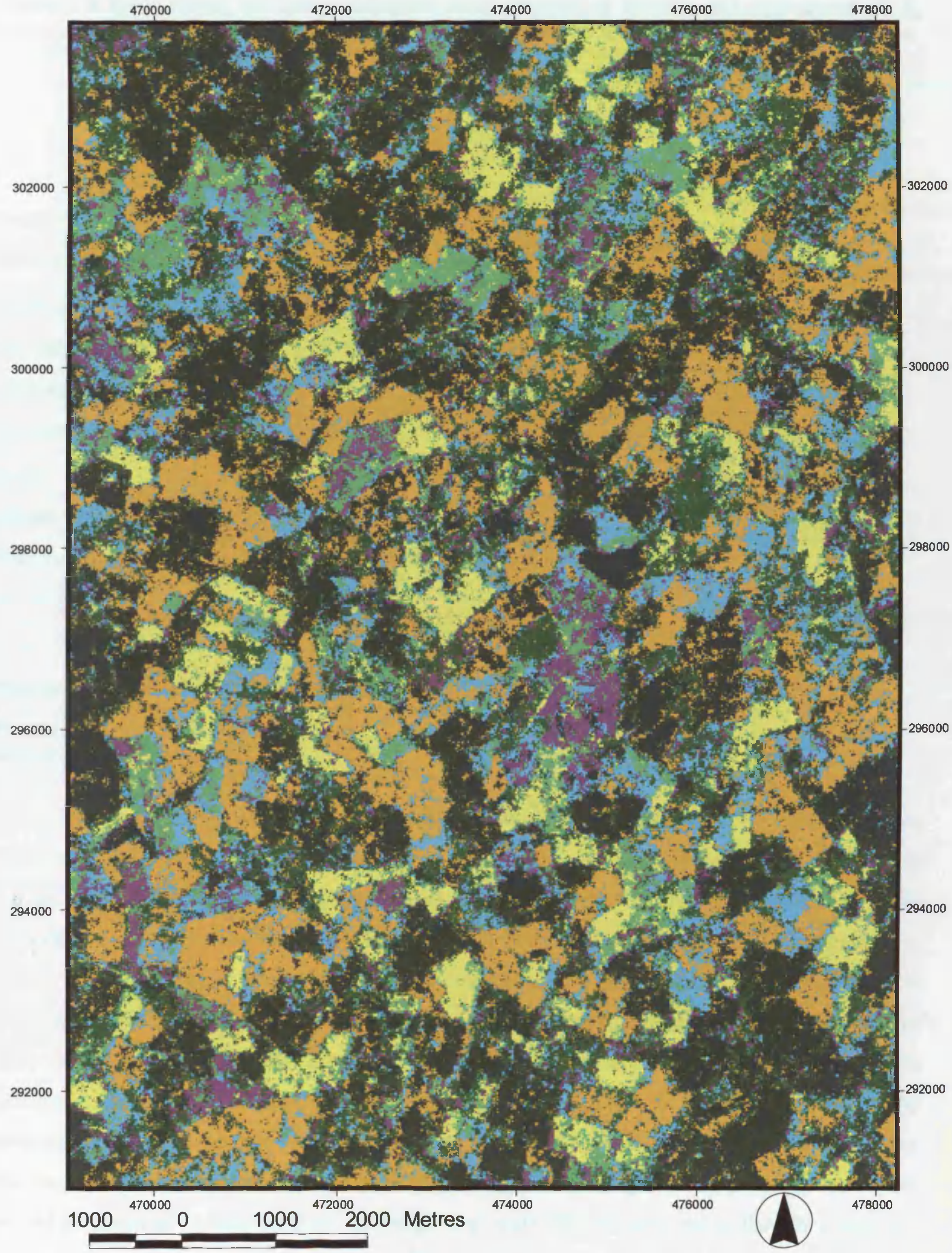

Figure 8.7 Image created through unsupervised training based on multi date image from May, July and August (9.5x14.5 km). Purple is hemp, yellow is oilseed rape, dark green is pasture, mid green is forest, light green is field beans, orange is wheat and light blue represents flax.

Table 8.6 Error matrix for image classified using supervised training and subsequent MLE. Rows relate to the classified data and columns to the reference data. Overall accuracy was 46%.

	pasture	wheat	barley	oilseed rape	urban	stubble	flax	hemp	field beans	forest	rough pasture	Totals	User's Accuracy
PASTURE	**43**	12	0	1	2	0	0	0	0	1	0	**59**	**73**
WHEAT	6	**34**	3	0	0	0	0	0	0	0	0	**43**	**79**
BARLEY	1	2	**0**	2	1	0	1	0	3	0	1	**11**	**0**
OILSEED RAPE	1	2	0	**26**	2	0	0	1	2	3	0	**37**	**70**
URBAN	2	1	0	2	**1**	0	0	0	0	0	0	**6**	**17**
STUBBLE	12	7	1	3	1	**4**	1	0	3	3	1	**36**	**11**
FLAX	4	5	2	2	1	0	**3**	2	1	1	0	**21**	**14**
HEMP	1	0	0	1	0	0	0	**8**	0	0	0	**10**	**80**
FIELD BEANS	4	1	3	0	0	1	0	1	**1**	3	0	**14**	**7**
FOREST	5	3	0	4	1	0	1	0	0	**4**	0	**18**	**22**
ROUGH PASTURE	9	3	2	1	0	0	0	0	0	1	**1**	**17**	**6**
Totals	**88**	**70**	**11**	**42**	**9**	**5**	**6**	**12**	**10**	**16**	**3**	**272**	
Producer's Accuracy	**49**	**49**	**0**	**62**	**11**	**80**	**50**	**67**	**10**	**25**	**33**		

The most reliable group when considering user's accuracy was hemp with 80%. Therefore when predicting ground conditions from the image 80% of the pixels on the image indicating hemp would be hemp on the ground (Congalton and Green, 1999). The user's accuracies are more important when using the image to predict ground conditions from the image (Congalton and Green, 1999). Pasture, wheat and oilseed rape were also good with 73%, 79% and 70% respectively. All other categories would be unreliably predicted from the image with fewer than 22% of all pixels within the classes being incorrectly classified. The poorest of the user's accuracies was barley with 0%, meaning the image fails to predict any barley correctly on the ground according to the error matrix. Although seven of the 12 categories had poor accuracies the majority of land was covered in pasture, wheat or oilseed rape. These land cover classes would be accurately predicted from the image in at least 70% of cases and is therefore seen as a reasonably good product as an input to the SWAT model.

The occurrence of pasture is confused by all other categories in the image i.e. the classification scheme wrongly assigned some pixels as wheat, barley, forest, oilseed rape, when they should have been pasture. Rough pasture, flax and wheat are particularly confusing to the correct prediction of pasture. Stubble and flax are confused by most other categories to some degree.

The Kappa analysis for this matrix provided a $\hat{K}$ value of 0.367 or 37%. This indicates that the allocation of the land cover classes to the reference pixels were only moderately accurate (Landis and Koch, 1977). The variance of Kappa was found to be 0.00114, and the Z-statistic of 10.8447 is greater than standard deviation at 95% (1.96) indicating that the classification is significantly better than random.

8.4.2.2 Error matrix for unsupervised classification at the pixel-scale of resolution

The error matrix for the unsupervised classification gave an overall accuracy of 53% but only included seven of the 12 categories found in the catchment. The spatial distributions of the signatures specified in the image did not reflect the distributions of barley, urban, stubble, water or rough pasture on the ground. These five classes were therefore deemed not to be included in the unsupervised classification when assigning land cover classes to the signatures. The classes omitted, except water, were included in the error matrix. Including the omitted classes in the error matrix would not influence the overall accuracy but would affect the user's accuracy and confusion assessment. Inclusion therefore provides a truer analysis of accuracy.

The producer's accuracy for hemp, field beans, forest and pasture were good with 83%, 78%, 63% and 62% respectively. The producer's accuracy for wheat, flax and oilseed rape is moderate with 59%, 50% and 42% respectively.

The user's accuracy for pasture, wheat and oilseed rape is very good with 83%, 81% and 71%. These three values have been increased by the including the lost classes in the matrix and may therefore be overestimated. These three classes cover the majority of the catchment and so are very important. Field beans, hemp, forest and flax were poor with 32%, 31%, 21% and 9% respectively. The remaining classes: barley, urban, stubble and rough pasture were not represented at all in the image. None of these classes however cover more than 3% of the catchment and therefore cannot, in terms of remote sensing exercise, be considered very significant. Failure to identify these classes in terms of the hydrological impact however, may be very significant due to the disproportionate effect of the class on hydrology or nutrient transport.

Table 8.7 Error matrix for classified image using unsupervised training. Rows relate to the classified data and columns to the reference data. Overall accuracy was 53%.

	pasture	wheat	oilseed rape	field beans	hemp	forest	flax	barley	urban	stubble	rough pasture	Totals	User's Accuracy
PASTURE	**58**	7	0	0	0	0	0	3	0	1	1	**70**	**83**
WHEAT	6	**44**	0	0	0	1	1	1	0	0	1	**54**	**81**
OILSEED RAPE	1	2	**15**	0	0	0	0	0	1	2	0	**21**	**71**
FIELD BEANS	2	2	6	**7**	0	0	2	0	1	2	0	**22**	**32**
HEMP	2	0	1	1	**5**	4	0	0	1	2	0	**16**	**31**
FOREST	18	7	12	1	0	**12**	0	1	4	1	0	**56**	**21**
FLAX	6	12	2	0	1	2	**3**	6	0	1	1	**34**	**9**
BARLEY	0	0	0	0	0	0	0	**0**	0	0	0	**0**	**0**
URBAN	0	0	0	0	0	0	0	0	**0**	0	0	**0**	**0**
STUBBLE	0	0	0	0.	0	0	0	0	0	**0**	0	**0**	**0**
ROUGH PASTURE	0	0	0	0	0	0	0	0	0	0	**0**	**0**	**0**
Totals	**93**	**74**	**36**	**9**	**6**	**19**	**6**	**11**	**7**	**9**	**3**	**273**	
Producer's Accuracy	**62**	**59**	**42**	**78**	**83**	**63**	**50**	**0**	**0**	**0**	**0**		

The omitted classes have the largest influence on the confusion within the matrix. Pixels that relate to barley, urban, stubble or rough pasture on the ground are represented, wrongly, by one of the included classes by default. All of these classes cover only small areas of land however, and cannot be considered very significant in terms of detection accuracy. They may have a disproportionate influence on the hydrology however, and therefore cannot be considered entirely insignificant for this exercise. The allocation of pasture, wheat and oilseed rape to areas within the image is confused by the other categories present, but forest is particularly confused by wheat and oilseed rape. Oilseed rape has a complex botanical "architecture" and can be visualised as miniature trees. Confusion between forest and oilseed rape can therefore be expected. Conversely there is confusion in discriminating wheat from flax.

The Kappa analysis for this matrix gave the $\hat{K}$ statistic of 0.43 (43%), which indicates a moderate agreement between the ground and the image (Landis and Koch, 1977). The variance of Kappa was calculated as 0.0015 and the Z-statistic was 11.063. The latter value is greater than the standard deviation at 95% level (1.96) and shows that the classification is better than random.

8.4.2.3 Comparison of pixel-scale error matrices and field-survey map

Pairwise comparison of the two classification schemes at the pixel level gave a Z-statistic of 1.21. This value is below the 95% confidence level of 1.96 and shows that there is no significant difference between the error matrix analyses. This suggests that there is no significant difference between the two classification schemes used.

Although no significant differences have been found between the two error matrices the two images are substantially different in reflecting the ground conditions in the catchment. The overall accuracies are similar but a more detailed inspection and analysis of the error matrices show that the supervised classification scheme gives a more reliable indication of the land cover than the unsupervised scheme. The former scheme includes all land cover types except water, and the three land cover classes that account for the majority of land receive user accuracies in excess of 70%. The unsupervised classification has higher overall accuracy and the three most common categories have higher user's accuracies than the supervised classification although the reliability of these figures may be compromised by the inclusion of missed classes however small the area they cover. Five land use categories are lost from the unsupervised classification scheme whereas only water is omitted from the supervised method. None of the lost categories cover particularly large areas, but urban areas have specific impacts on the hydrology that, if omitted, could severely affect the accuracy of the nutrient transport modelling.

Table 8.8 Summary of analyses of error matrices based on the pixel unit and 272 and 273 reference for 12 potential categories of land cover.

	MLE	Unsup.
Total Accuracy	46%	53%
$\hat{K}$	0.366821	0.429268
$\hat{\text{var}}(\hat{K})$	0.001144	0.001506
Z-statistic	10.8447	11.06339

8.4.3 Error matrices for images at the field-scale

At the beginning of this research it was envisaged that a single field map of land classification of the Stonton Brook would be created from remote sensing for use in the SWAT model. The results from SWAT based on the field map derived from remote sensing data would then be compared with the results obtained from the actual land cover map to assess whether there were any advantages in using remote sensing data to parameterise catchment-scale nutrient transport modelling. The image offering the best classification would have been chosen to derive a land use map for input to SWAT. The differences between the two classification schemes are inconclusive, however, and both images will subsequently be used to construct separate land use maps. The above classification exercises and error matrices focused on the pixel. For remote sensing interests the pixel level is suitable. Hydrological and PT modelling is affected by the field unit rather than the pixel and therefore error matrices were generated for the two land use maps using field units. These maps were then assessed using error matrices at the field-scale and either rejected or input to the SWAT model. Incorporating both land use maps for separate simulations in the SWAT model would be an interesting investigation into its distributed performance. The field boundary map shown in Figure 4.1 was overlaid on both classified images to give two land use maps as shown in Figures 8.9 and 8.10. These maps were required for inclusion in the SWAT model through ArcView, and were provided as shape files with attributes contained in associated database tables. The percentages of the land cover categories for the ground survey and the two maps classified by the SAR images are shown in Table 8.9 and Figure 8.8. Error matrices were generated for both field maps using all 765 polygons for reference.

Table 8.9 Total numbers of fields and the total areas for the SAR MLE and unsupervised classification results and the field survey. Areas are in hectares.

	Field Survey		MLE		Unsupervised	
Land use	**Area**	**Number**	**Area**	**Number**	**Area**	**Number**
Barley	177.91	20	40.51	12	0	0
Field beans	150.12	11	280.39	31	306.458	34
Flax	117.79	12	288.18	40	427.466	64
Forest	214.88	56	234.95	42	543.435	128
Hemp	132.38	16	143.76	19	260.618	36
Oilseed rape	840.62	76	932.73	103	732.382	86
Pasture	1819.41	297	1506.42	247	1594.058	243
Rough Pasture	51.45	21	59.03	24	0	0
Stubble	177.41	15	291.54	60	0	0
Urban	177.40	75	107.47	27	0	0
Water	4.77	5	0	0	0	0
Wheat	1383.74	161	1362.95	160	1383.448	174

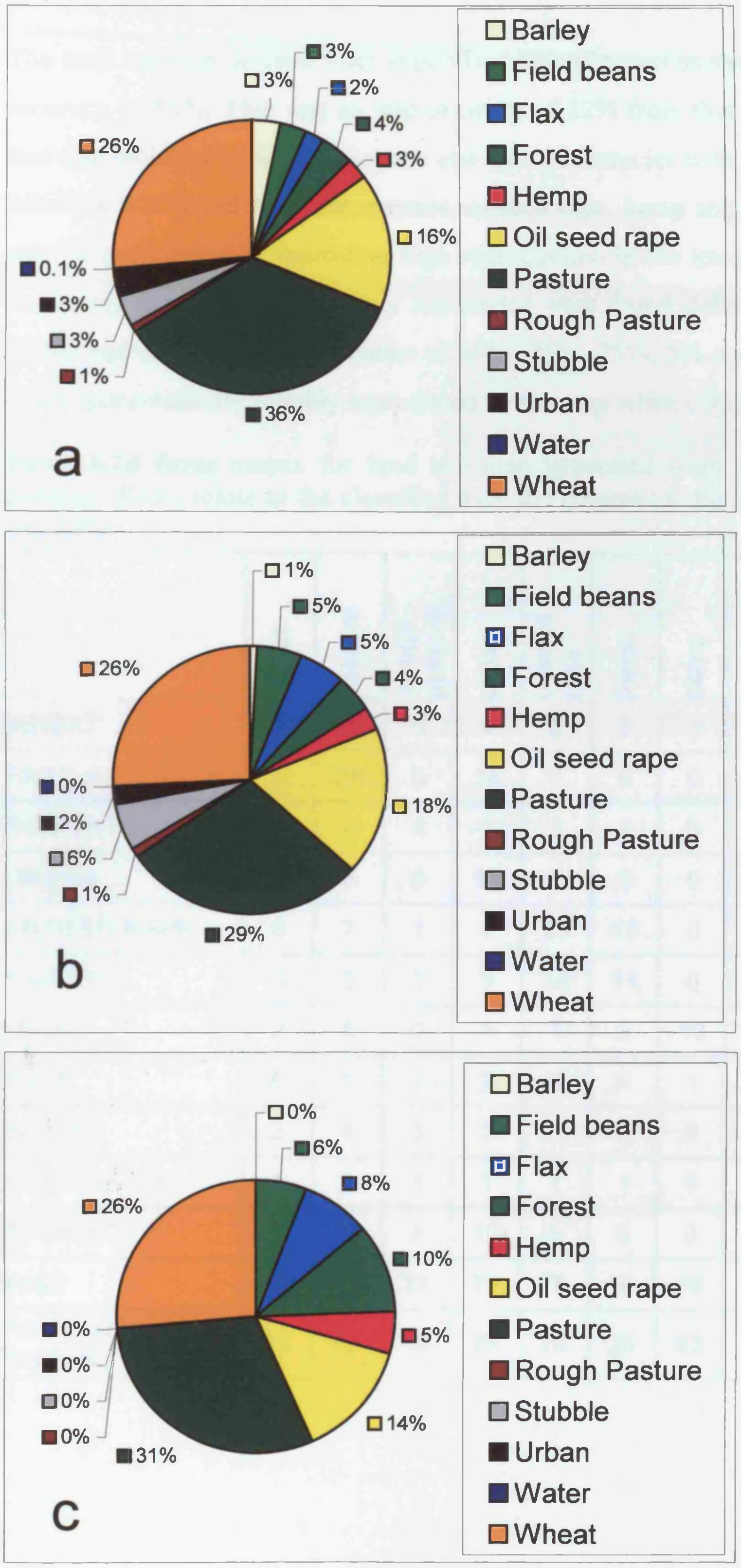

Figure 8.8 Proportions of land cover as found using: a) field survey, b) MLE on multi date SAR image and c) unsupervised classification on multi date SAR image. Note absence of water in the MLE and rough pasture, stubble, urban and barley in unsupervised classification totals. These classes were not distinguishable in the unsupervised classification method.

8.4.3.4 Error matrix for supervised classification at the field-scale of resolution

The land use map derived from supervised classification as shown in Figure 8.9 had an overall accuracy of 58%. This was an improvement of 12% from that found at the pixel level. Barley was also included in both producer's and user's accuracies with 5% and 8%. The best producer's accuracy was found in wheat, pasture, oilseed rape, hemp and flax with 71%, 66%, 78%, 63% and 92% respectively, indicating high reproduction in the image. Field beans were moderately accurately mapped at 55%. Poor accuracies were found defining rough pasture, urban, forest, barley and stubble with accuracies of 19%, 25%, 25%, 5% and 27% respectively. These land cover types were not reliably reproduced on the map when compared to the ground conditions.

Table 8.10 Error matrix for land use map generated from map classified using supervised training. Rows relate to the classified data and columns to the reference data. Overall accuracy was 58%.

	wheat	**pasture**	**rough pasture**	**urban**	**oilseed rape**	**forest**	**hemp**	**flax**	**barley**	**field beans**	**stubble**	**Totals**	**User's Accuracy**
WHEAT	**115**	25	0	4	2	5	1	0	7	0	1	**160**	**72**
PASTURE	12	**200**	6	16	1	9	0	0	1	0	2	**247**	**81**
ROUGH PASTURE	0	14	**4**	4	0	2	0	0	0	0	0	**24**	**17**
URBAN	1	6	0	**19**	1	0	0	0	0	0	0	**27**	**70**
OILSEED RAPE	8	7	1	4	**59**	15	0	1	3	3	2	**103**	**57**
FOREST	3	3	3	9	10	**14**	0	0	0	0	0	**42**	**33**
HEMP	2	1	0	4	1	0	**10**	0	0	0	1	**19**	**53**
FLAX	6	6	2	2	0	4	1	**11**	4	2	2	**40**	**28**
BARLEY	2	4	3	2	0	0	0	0	**1**	0	0	**12**	**8**
FIELD BEANS	4	8	1	1	1	1	4	0	2	**6**	3	**31**	**19**
STUBBLE	8	28	1	10	1	6	0	0	2	0	**4**	**60**	**7**
Total	**161**	**302**	**21**	**75**	**76**	**56**	**16**	**12**	**20**	**11**	**15**	**765**	
Producer's Accuracy	**71**	**66**	**19**	**25**	**78**	**25**	**63**	**92**	**5**	**55**	**27**		

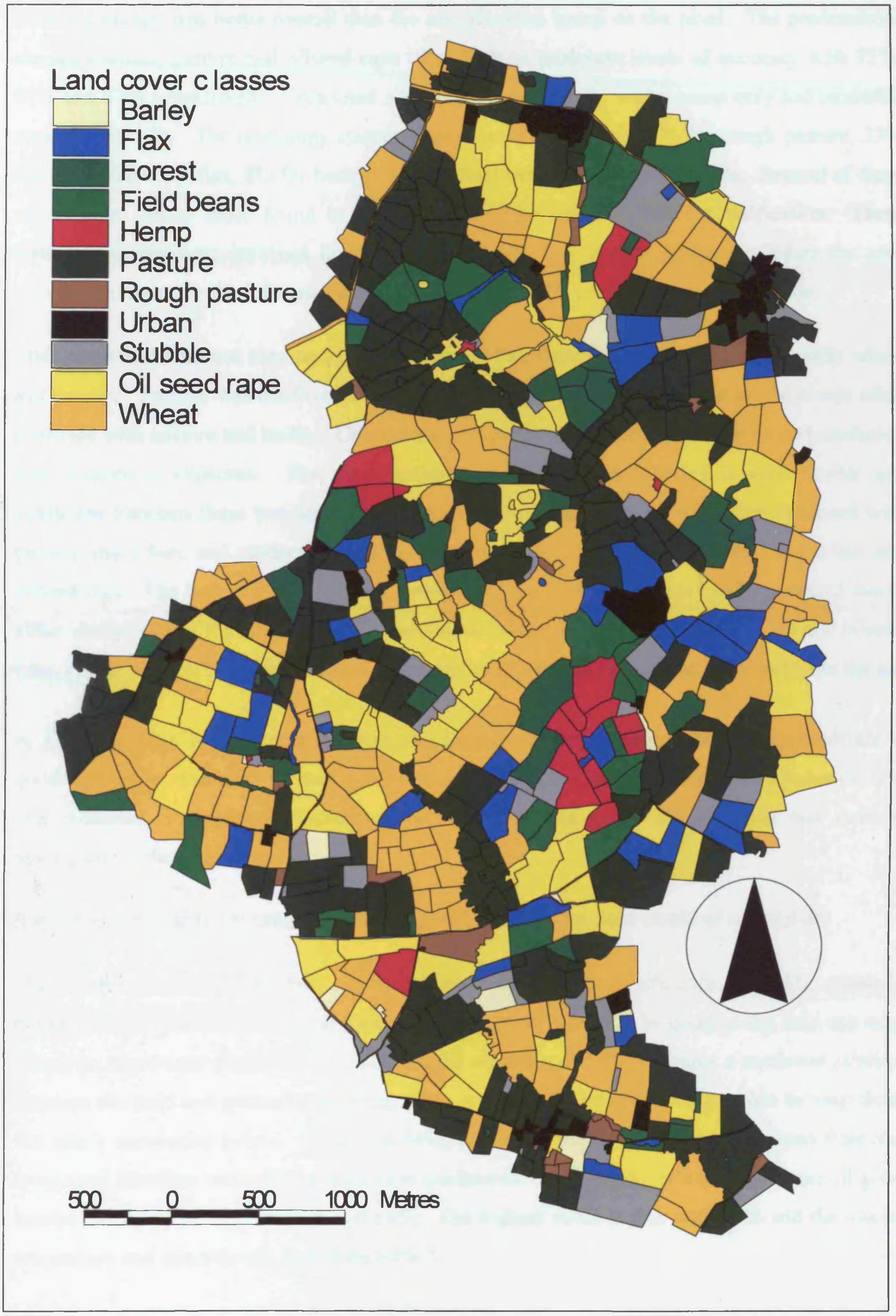

Figure 8.9 Land use map classified by supervised training of multi-date SAR image. Compare this figure with Figure 4.1. Proportions of all land cover categories are shown in Figure 8.8b.

User's accuracy was better overall than the classification based on the pixel. The predominant classes - wheat, pasture and oilseed rape - had high to moderate levels of accuracy with 72%, 81% and 57% respectively. Urban had a high accuracy of 70%, whilst hemp only had moderate accuracy of 53%. The remaining classes were of poor reliability; 17% for rough pasture, 33% for forest, 28% for flax, 8% for barley 19% for field beans and 7% for stubble. Several of these values were below those found in the error matrix for the pixel-based classification. These differences, however, involved land cover types with low overall impact on either the area covered i.e. forest or the influence over hydrological and PT considerations i.e. stubble.

The supervised land use map poorly discriminated flax from the other classes, especially wheat and pasture. Pasture was confused with wheat and urban to a high degree, and wheat was often confused with pasture and barley. Urban areas contain large proportions of garden and confusion with pasture is expected. The plant architecture of wheat and barley is very similar and confusion between these two land covers again is expected. Stubble was often confused with pasture and urban, and moderate levels of confusion was found between forests and urban and oilseed rape. The lack of discrimination between certain land cover types can be expected due to either similarities in the structure of the vegetation i.e. stubble and pasture, and forest and oilseed rape, or that some urban areas contain large number of trees and could portray forest from the air.

A $\hat{K}$ value of 0.476 (48%) was found for this map using Kappa analysis indicating a moderate to good correlation between the map and ground conditions. The Z-statistic gave a value of 22.6 and indicated a significant difference between the land cover classification and random assortment of the field units.

8.4.3.5 Error matrix for unsupervised classification at the field-scale of resolution

The overall accuracy of the land use map from unsupervised classification was 54%, which is higher than the pixel-based classification accuracy of 49% but not as good as the land use map based on supervised classification. The overall accuracy of 54% indicates a moderate relation between the map and ground conditions. This is however very misleading as can be seen from the user's accuracies below. Barley, stubble, urban and rough pasture were omitted from the image and therefore were also omitted from the land use map. Producer's accuracies are all good except forest, which was moderate at 54%. The highest value is flax with 83% and the lowest are pasture and oilseed rape, both with 64%.

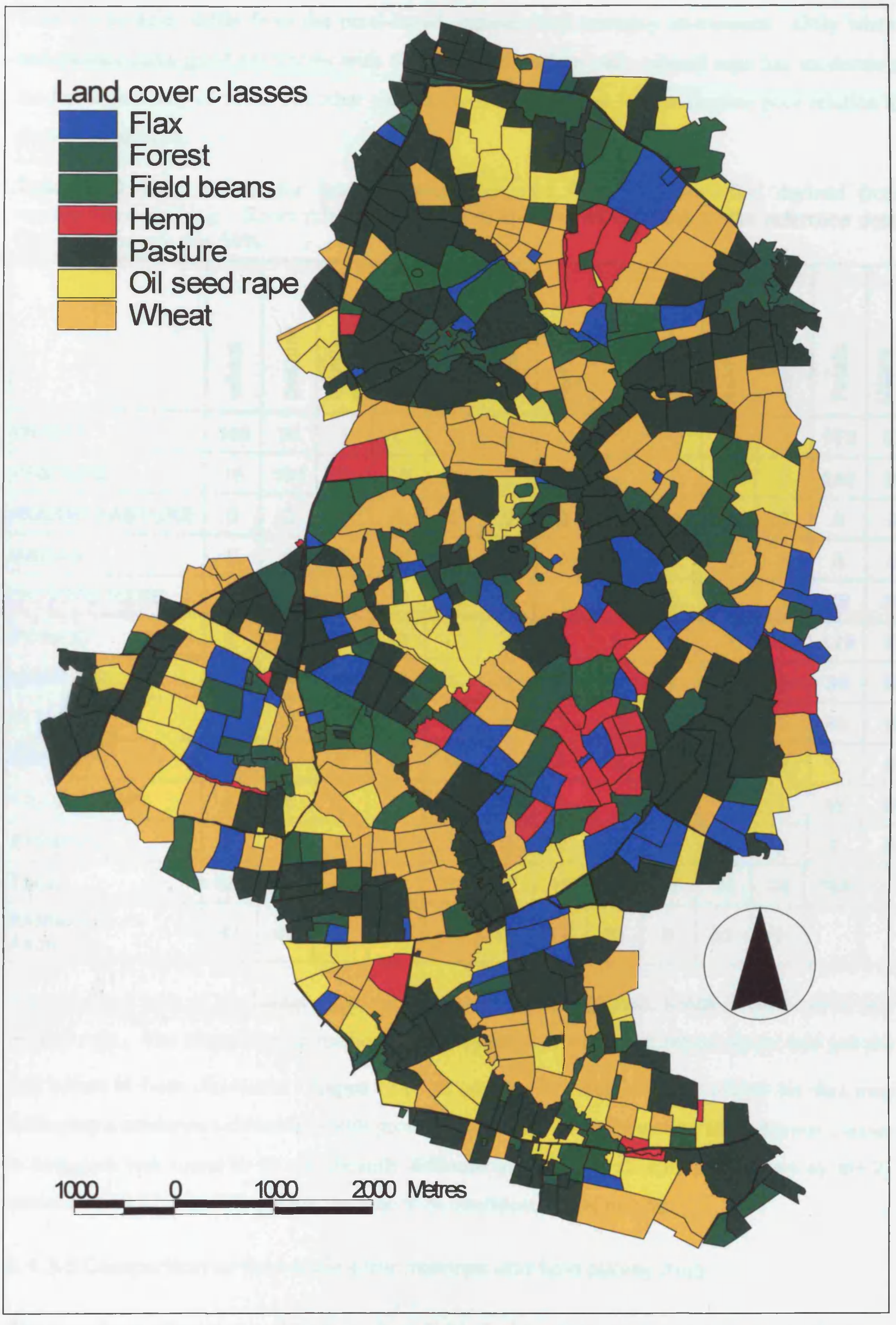

Figure 8.10 Land use map classified by unsupervised training of multi-date SAR image. Proportions of land cover categories are shown by comparison with ground survey data in Figure 8.8c. Only seven categories were represented in this classification process.

User's accuracies differ from the pixel-based unsupervised accuracy assessment. Only wheat and pasture have good accuracies with 63% and 80% whilst only oilseed rape has moderate a moderate accuracy of 56%. All other class accuracies are below 36% indicating poor relation to ground conditions.

Table 8.11 Error matrix for land use map generated from map classified derived from unsupervised training. Rows relate to the classified data and columns to the reference data. Overall accuracy was 54%.

	wheat	pasture	rough pasture	urban	oilseed rape	forest	hemp	flax	barley	field beans	stubble	Totals	Users accuracy
WHEAT	**109**	36	1	6	6	3	1	0	7	0	3	**172**	**63**
PASTURE	16	**191**	5	19	0	6	0	0	1	0	2	**240**	**80**
ROUGH PASTURE	0	0	**0**	0	0	0	0	0	0	0	0	**0**	**0**
URBAN	0	0	0	**0**	0	0	0	0	0	0	0	**0**	**0**
OILSEED RAPE	8	4	2	14	**49**	6	0	1	3	0	1	**88**	**56**
FOREST	6	43	10	24	13	**30**	0	0	2	0	1	**129**	**23**
HEMP	1	6	1	3	4	4	**13**	0	1	2	1	**36**	**36**
FLAX	16	12	2	6	1	5	2	**10**	6	0	5	**65**	**15**
BARLEY	0	0	0	0	0	0	0	0	**0**	0	0	**0**	**0**
FIELD BEANS	6	6	1	3	3	2	1	1	1	**9**	2	**35**	**26**
STUBBLE	0	0	0	0	0	0	0	0	0	0	**0**	**0**	**0**
Total	**162**	**298**	**22**	**75**	**76**	**56**	**17**	**12**	**21**	**11**	**15**	**765**	
Producers Accuracy	**67**	**64**	**0**	**0**	**64**	**54**	**76**	**83**	**0**	**82**	**0**		

The principal area of confusion arose with forest and wheat, pasture, rough pasture, urban and oilseed rape. The classification method also confused flax with most other classes and pasture and wheat in both directions. Kappa analysis gave a $\hat{K}$ value of 0.424 (42%) for this map indicating a moderate relationship with ground conditions. The assignation of land cover classes to polygons was found to be significantly different to a random allocation as shown by the Z-statistic of 20.22, which is greater than the 95% confidence level of 1.96.

8.4.3.6 Comparison of field-scale error matrices and field-survey map

The pairwise analyses using the values from Table 8.12 found no significant difference between the two land use maps through error matrices. A pairwise Z-statistic of 1.7438 was the nearest value to the 95% confidence level of the two pairwise comparisons conducted but still did not indicate a significant difference.

Table 8.12 Summary of matrix analyses using land use maps.

	MLE	Unsup.
Total Accuracy	58%	54%
$\hat{K}$	0.475779	0.423995
$\hat{\text{var}}(\hat{K})$	0.000442	0.00044
Z-statistic	22.62344	20.22398

The confusion found in the error matrices corresponds well with the differences between the summary data of the land-survey map (Figure 4.1) and the summary data of the land covers in Figures 8.8, 8.9 and 8.10 and Table 8.9. Wheat, pasture and oilseed rape are represented in similar proportions in all land use maps, which account for the majority of land area in the catchment. A decrease of 7% occurred in the MLE image from the ground conditions. This is closely reflected in their associated user's accuracy, where pasture has a lower value of 66% compared with 71% and 78% for wheat and oilseed rape. Small increases in accuracy were achieved for field beans, flax and stubble in the land use map derived from MLE classification. These three classes have high user's accuracies in comparison to the remaining categories.

8.4.4 Soil moisture and surface roughness

A feasibility study was carried out to assess soil moisture, soil organic matter content and soil surface roughness data against radar backscatter collected in November 1998 and February 1999. If a good relationship existed between soil moisture, organic matter content and surface roughness and radar backscatter, the IEM developed by Fung *et al.* (1992) could have been trialled on a similar data set. The IEM is invertible and may possibly make more accurate predictions of these soil characteristics than simple regression. The IEM is regression-based and if no relationship exists between the soil characteristics and radar backscatter, it is unlikely that the IEM would apply. Regression equations were calculated from the plots in Figures 8.11 and 8.12 of soil moisture, organic matter and surface roughness against radar backscatter. There were more exposed soil sites available for the November overflight hence the higher number of data points. All the plots show very poor or non-existent relationships but the quantitative analyses were carried out for assurance purposes.

The results of the volumetric moisture content for November indicated no significant correlation (P-value: 0.7789 and F-stat$_{0.05,2,21}$: 0.0808) and a very poor fit to the line of best fit (r^2 = 0.0038). February's data displayed similar results (P-value: 0.7216 and F-stat$_{0.05,2,10}$: 0.1343). In both cases the residual plots indicated slight deviations from homogeneity of variance but this was considered to be within the capabilities of linear regression (Zar, 1984).

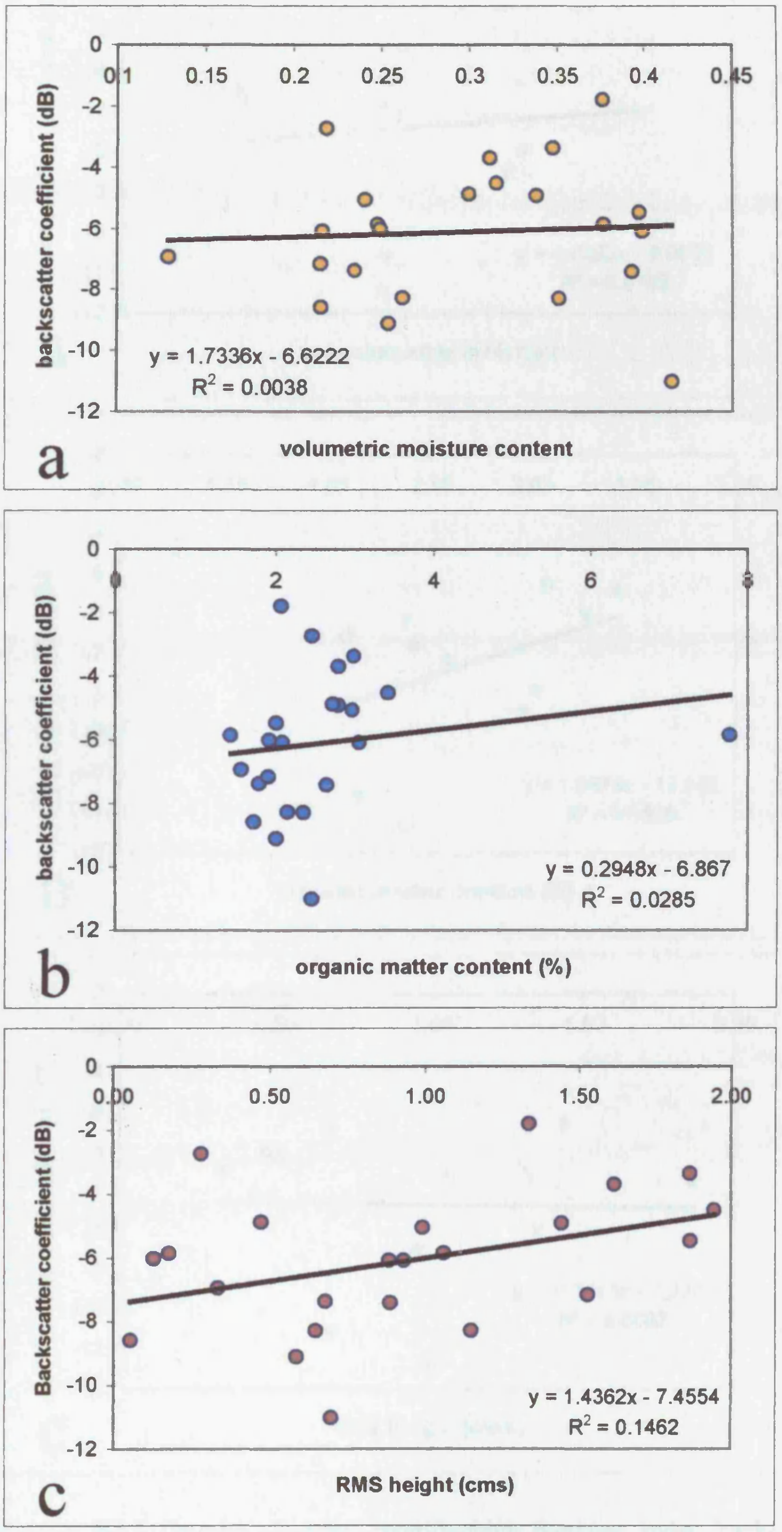

Figure 8.11 Response of backscatter to a) volumetric moisture content, b) organic matter content and c) RMS height for November 1998. When outlier was removed from b) relationship worsened. In all cases n=15.

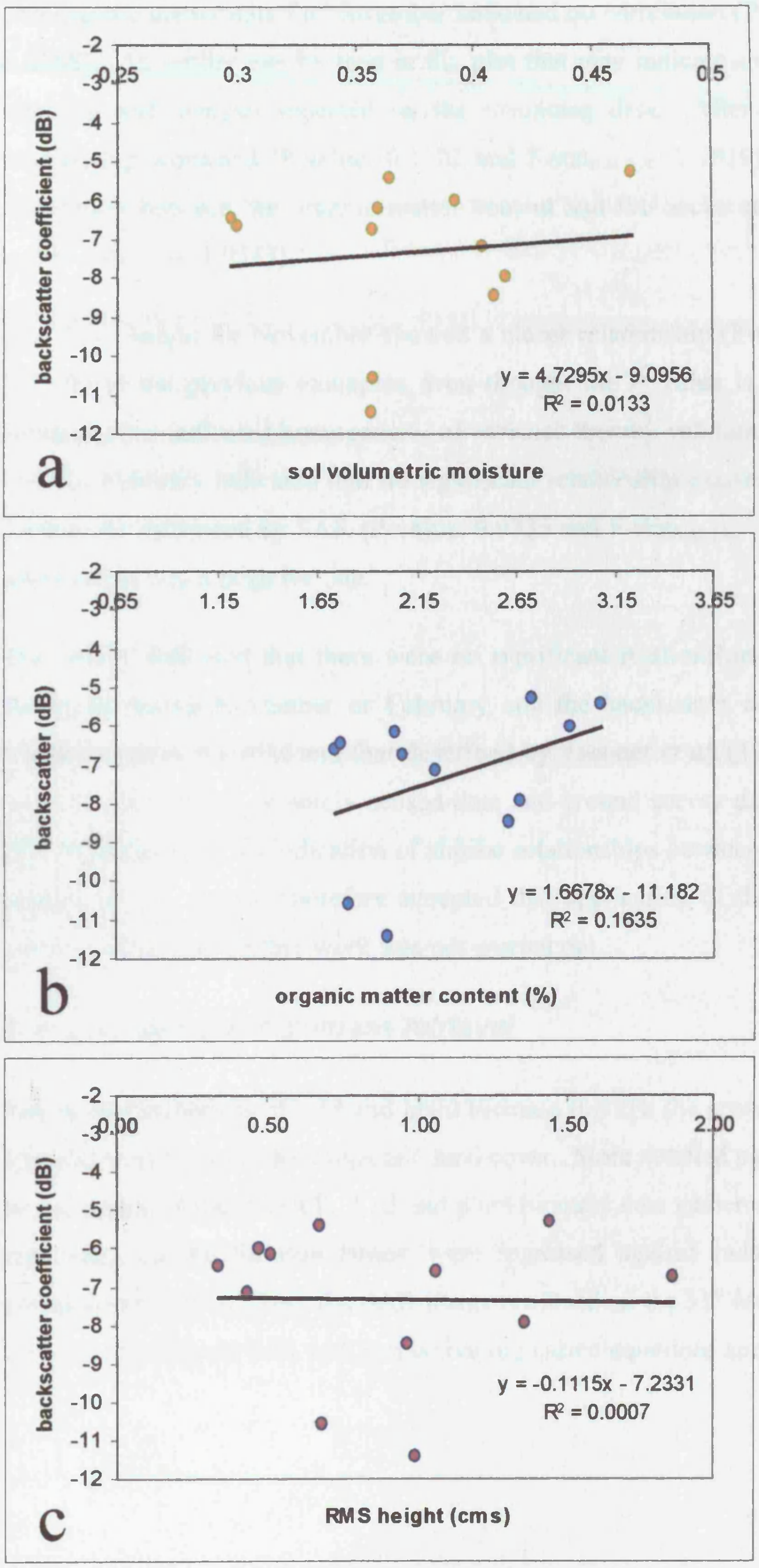

Figure 8.12 Graphs showing relationships between radar backscatter and a) soil volumetric moisture content, b) organic matter content and c) RMS height for February 1999. In all cases n=12.

The organic matter data for November indicated no correlation (P-value: 0.441 and $F\text{-stat}_{0.05,2,21}$: 0.6168). An outlier can be seen in the plot that may indicate an error in measurement so was removed and analysis repeated on the remaining data. After the outlier was removed the relationship worsened (P-value: 0.1103 and $F\text{-stat}_{0.05,2,20}$: 2.7919). February's data showed no correlation between the organic matter content and the backscatter estimates (P-value: 0.1923 and $F\text{-stat}_{0.05,2,10}$: 1.9543).

The RMS height for November showed a closer relationship (P-value: 0.0718 and $F\text{-stat}_{0.05,2,21}$: 3.5951) to the previous examples even thought the r^2 value is not very high (0.1462). The residual plots indicated homogeneity of variance thereby validating the data for regression. The data for February indicated that no significant relationship existed between the RMS height and backscatter estimated by SAR (P-value: 0.9335 and $F\text{-stat}_{0.05,2,10}$: 0.0073) but in this instance the relationship was a negative one.

The results indicated that there were no significant relationships between any of the variables measured during November or February and the backscatter coefficients estimated by SAR. Models such as the IEM and that described by Taconet *et al.* (1996) were simple and based on correlations between remotely sensed data and ground survey data. The data obtained through this campaign gave no indication of similar relationships between backscatter values and ground measurements. It was therefore accepted that application of these models on the data would prove fruitless and further work was not carried out.

8.4.5 LAI and plant biomass retrieval

Repeat measurements of LAI and plant biomass through the growing season would provide site-specific growth curves for crops and land cover. More detailed parameter distribution could then be incorporated into SWAT. LAI and plant biomass data gathered in May 1999 from all oilseed rape sites on the Stonton Brook were regressed against radar backscatter taken from the corresponding pixels from the SAR image retrieved on the 31st May 1999 (Figure 8.3). The data are plotted in Figure 8.13 with respective regression equations and regression coefficients.

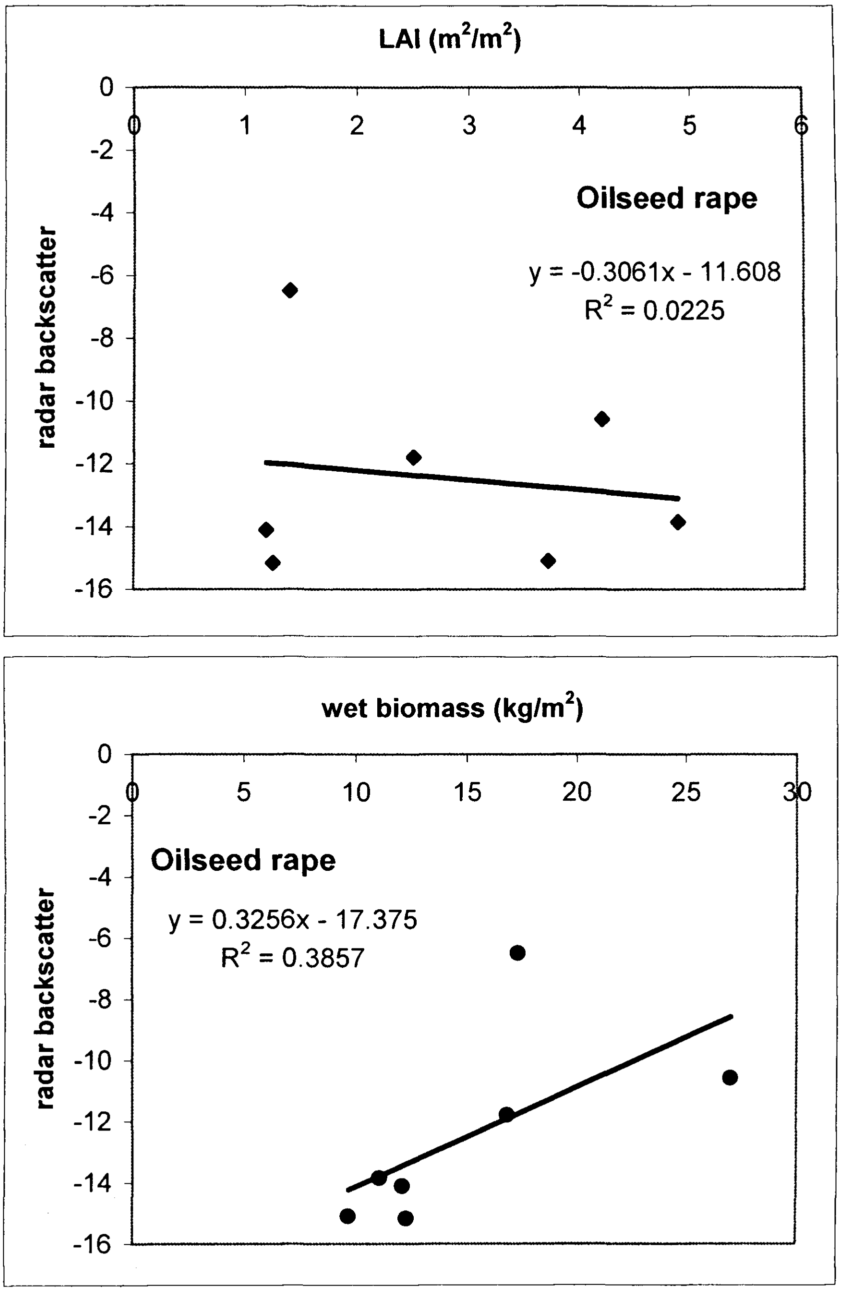

Figure 8.13 Plots of data for a) LAI, and b) wet biomass against radar backscatter for the month of May 1999. In both cases *n*=7.

Neither regressions found significant relationships between LAI or plant biomass of oilseed rape and radar backscatter. The relationship between LAI and backscatter is slightly negative not significant. The regression gave a P-value of 0.748 and an $F\text{-stat}_{0.05,2,6}$ of 0.115. The regression coefficient (R^2) was 0.0225 indicating a very poor fit of the data to a line of best fit. The relationship between biomass and backscatter was better and positive, but still insignificant with a P-value of 0.137 and $F\text{-stat}_{0.05,2,6}$ of 3.139. The fit of the data to the line was better but again not good, as indicated by the low R^2 value of 0.386.

8.4.6 MIMICS radiative transfer modelling

The MIMICS model was applied to wheat data for the months of May and July and oilseed rape data for the month of May. MIMICS is not invertible and cannot make predictions from backscatter values for areas with unknown crop characteristics. It was trialled to see whether such modelling theory could be applicable in the future should inversion techniques be developed.

Data were extracted from the May and July images after applying the Lee filter and primary and secondary georectification. Locations of the pixels corresponding to the sampling sites on the ground were based primarily on co-ordinates but adjusted in some cases by identifiable features such as field margins, buildings and roads. The results from the extraction of backscatter values from each of the wheat and oilseed rape fields sampled in May and July 1998 are listed with their respective simulation results from the MIMICS model in Tables 8.13 and 8.14. The MIMICS model was not invertible and therefore there was no expectation of data input to the SWAT model using this technique. To assess the output of the MIMICS model correlation tests were used. None of the data sets displayed any deviation from normality using the Shapiro-Wilk test (Zar, 1984), and therefore the parametric Pearson's product moment test was used.

Table 8.13 Backscatter values for wheat from SAR image and simulations from MIMICS radiative transfer model.

Site	σ^o (dB)			
	May SAR	May MIMICS	July SAR	July MIMICS
1a	-15.25	-12.95	-12.29	-14.57
1b	-15.17	-13.70	-11.44	-10.21
2a	-11.79	-13.35	-10.55	-15.68
2b	-10.58	-14.14	-9.81	-11.18
3a	-15.10	-14.04	-13.19	-11.00
3b	-13.85	-14.12	-13.56	-15.80
4a	-15.84	-13.95	-11.98	-15.32
4b	-13.26	-13.81	-10.61	-15.32
5a	-14.11	-12.26	-12.67	-14.77
5b	-15.34	-10.28	-12.79	-13.83
6a	-14.76	-11.11	-13.32	-14.94
6b	-14.23	-14.05	-14.57	-14.77

Table 8.14 Backscatter values for May from oilseed rape from SAR image and simulations from MIMICS.

Site	σ° (dB)	
	May SAR	May MIMICS
7	-6.49	-9.25
8	-15.17	-13.70
18	-11.79	-13.35
19	-10.58	-14.14
30	-15.10	-14.04
31	-13.85	-14.12
33	-15.84	-13.95
34	-13.26	-13.81
37	-14.11	-12.26
38	-15.34	-10.28
43	-14.76	-11.11
44	-14.23	-14.05

The values from Tables 8.13 and 8.14 were plotted and are shown in Figure 8.14. The oilseed rape simulation indicated a fairly good correlation but was shown not to be significant according to the Pearson's product moment ($R_{0.05,2,10}$: 0.407 and P-value: 0.189). Wheat had mixed results. Data for May showed no significant correlation ($R_{0.05,2,11}$: -0.181 and P-value:0.573), whereas the July data displayed a significant correlation ($R_{0.05,2,11}$: 0.614 with P-value: 0.034).

Sensitivity analyses were also carried out on the MIMICS model to define which parameters influenced the backscatter coefficients most in the simulation. Values from all input parameters in Table 8.4 were manipulated sequentially and a series of simulations executed. Values were not varied outside the measured range of the parameters. For example, temperature values were adjusted between 0 and 25°C in 1°C increments. In each case the corresponding backscatter value was recorded to establish how sensitive the model was to the change in the parameter value. No single parameter was found to produce a greater change in decibel output than any other using the full ranges found within the data of the parameters collected. In all cases output was varied by a maximum of ± 4dB across the range of values.

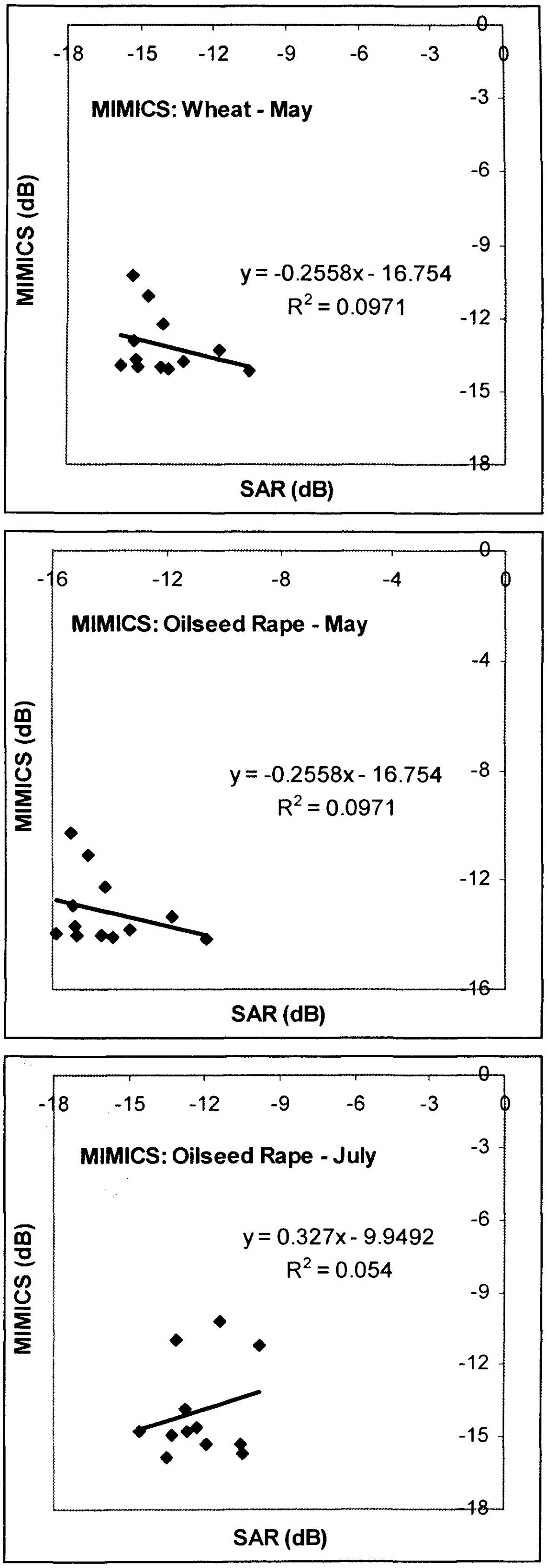

Figure 8.14 Backscatter values extracted from SAR images plotted against predictions from MIMICS for a) oilseed rape and b) wheat for the month of May, 1999 and c) wheat for the month of July 1999.

8.5 Discussion

Extraction of data from the SAR images produced mixed results. The classification procedure was successful in predicting up to 58% of the land cover and provided a land cover map for input into the SWAT model described as moderate by Landis and Koch (1977). Radiative transfer modelling with MIMICS found a significant correlation between model output and backscatter values for wheat in July. Conversely, poor agreement was found between measured backscatter and backscatter output from MIMICS with wheat and oilseed rape in May. Additionally, regressions failed to provide any indication of relationships between backscatter and the estimates of soil moisture and soil surface roughness. The results will now be discussed in more detail for each of the exercises conducted.

8.5.1 Classification

Overall this procedure provided two land use maps for separate inclusion in the SWAT model. Land cover is the single most important aspect of SWAT that lends itself to inputs from remote sensing. Although neither of the classifications successfully recognised surface water in the Stonton Brook, this is not a problem, as SWAT cannot model it as a land cover type; and standing water must be provided in a database format. The small lakes in the Stonton Brook would be affected by edge effect and speckle. Conversely, the large expanse of Rutland Water reservoir would not be affected in the same way and can be identified as previously stated (Figure 8.3), but does not have any bearing on this project.

The most obvious limitation in classification is the failing of unsupervised classification to recognise barley, stubble, urban and rough pasture. Although only small areas are involved in the omitted classes and individually insignificant over the entire catchment, the omitted classes could have a significant bearing on the modelling. This is not clearly seen in the error matrices. Some doubt exists whether the error matrix provides a realistic assessment of accuracy when classes have been omitted in the classification scheme. In this instance the omitted classes were considered subjectively rather than quantitatively. The largest component misclassified in the unsupervised method at the field-scale was the forest. Forestry is not managed to the same degree that agriculture is and fertilisers are almost never applied. The sensitivity of SWAT to small changes like this would be of interest to this project. Although both images will be used in the SWAT model it is firmly accepted that the supervised method provided a classified image of higher quality than the unsupervised method. Pasture is reasonably well identified by both classification methods but is limited by not differentiating between pasture grazed by sheep and pasture grazed by cows or any other livestock. The answer to this problem is to apportion pasture to a particular animal based on some acquired information about the agricultural management i.e. Agricultural Census of the UK.

Another limitation of the use of SAR was in its ability to detect roads in the remote sensing derived land cover maps. This limitation, however, must be anticipated in SAR data due to the small width of such features and the resolution of the images. A large junction can be seen to the top of the images in Figures 8.3 and 8.4 but speckle prevented the classification from differentiating the road metal from the surrounding features. Major motorways were clearly identifiable in the whole scenes and were ideally suited for locating ground control points.

Michelson *et al.* (2000) found that combinations of LandSAT TM and SAR offer the best classifiers for temperate agricultural land, but accuracies found in this project were similar to the best found in the Stonton Brook. The accuracies of the images classified in this project do not meet the generally accepted but arbitrary minimum of 85% (Thomlinson *et al.*, 1999), but most of the main land cover categories do meet the criteria of 70% for individual classes.

Both sets of accuracies could have been improved by including more reference points in the error matrices. Congalton and Green (1999) suggest a minimum of 50 reference samples for each land cover class, which indicates that 272-3 reference samples are too few. This would require a minimum of 550 reference points for each image for pixel-based analyses. All fields were sampled and therefore analysis at this intensity is feasible given more resources. Improvements in the error analyses were obtained after transferring the classification to the field polygons. The reason for this is that many more pixel values were used for each reference sample than in the pixel-level of error assessment, i.e. all those contained in a field. Substantial improvements in accuracy were obtained when applying accuracy assessment at the field-scale rather than at the pixel-scale. This was more pronounced in the supervised classification method when compared to the unsupervised classification method. It is therefore possible that greater accuracies for the pixel level of accuracy assessment for the unsupervised classification were artefacts of using too few reference samples. Limitations are imposed on the error analyses at the field level because of the low numbers of certain land cover types such as hemp, stubble and barley. Weighted sampling is not possible when using all areas and is therefore, unavoidable for a small area like the Stonton Brook.

Georectification was problematic in the initial phase of image analysis in similar ways to those discussed by Bastin *et al.* (2000). Improvements were obtained during secondary georectification. It was clear however, that when assigning land use from the image to field polygons, many areas of the images were offset against the field boundary map. This latter map was digitised from the aerial photography and was considered very accurate when tested against other features identifiable on the image and Ordnance Survey Pathfinder series map. This problem primarily affected small parcels of urban land. Urban land was only identified using supervised classification and therefore improvements in georectification would only be translated to the supervised classification method. Future improvements could be made in georectification using radar targets on the ground for the overflight (Ulaby and Elachi, 1990). The targets show up clearly on the final image as bright spots. Some of the guesswork is then removed in georectification when allocating ground control points to the image.

SWAT will only consider distinct patches of land use, i.e. fields, woods and roads but could utilise hedges and individual trees if characterised in the land use map. Crops were grown within half a metre of field boundaries in the majority of fields. It was however considered more important to describe the extent of the crop growth than describing the hedges and trees on field perimeters. Many large hedges and trees on the boundaries were identified in the supervised and unsupervised images and could have been used but were not due to the time needed to digitise the additional features. These features would however have had some influence on the pixel-based accuracy assessment of both images by influencing the signatures around the perimeters by only considering the crop type in the reference data. Training in supervised classification avoided edge effects by using pixels well away from the edges of fields. The pixel-based error analyses however, generated weighted random reference points that would not have avoided edge effects. These effects are of interest in terms of remote sensing but probably generated errors over and above that necessary for consideration in terms of the SWAT model. The field-based accuracy assessment avoided the edge effect problem by using all pixels falling within individual land use polygons. Further increases in accuracy could have been obtained in the images by categorising the land cover more precisely. For example, there were patches of weeds and different crops within the same field in some cases. Often wheat or oilseed rape was left to reseed from the previous year and had grown within a different crop species. All the land cover types for use in the Stonton Brook were selected because of their hydrological influences or overall area. Most of the confusion came between woodland and oilseed rape. These two categories contain plants, which can have similar architectures during the late growth period of oilseed rape. The vegetation canopy of mature oilseed rape is very irregular and appears much the same as the canopy of woodland. Additionally, many urban areas within the Stonton Brook contain many trees, which could account for its replacement by woodland. A smaller proportion of the urban area was also replaced by pasture probably because of the presence of lawns. If the land parcels had included detail of lawns and individual stands of trees in urban better accuracies may have emerged.

It is clear from the error matrix analyses that maximum likelihood supervised classification gave better results for use in SWAT than unsupervised classification. Land cover maps have been created using both classification methods and can be used with little further effort by the SWAT model. Both maps will now be used to assess how SWAT behaves with different sets of spatial land cover data.

8.5.2 Soil moisture and soil surface roughness

Several workers (Fung *et al.*, 1992; Oh *et al.*, 1992; Shi *et al.*, 1992; Chen *et al.*, 1995; Altese *et al.*, 1996; Ulaby *et al.*, 1996; Su and Troch, 1996; Tansey, 1999; van Oevelen and Hoekman, 1999) have successfully extracted soil moisture and surface roughness from SAR images, but no significant correlations were found in this instance. Most of the work outlined in these projects has taken place in arid areas where soil moisture levels are much lower and less variable over short time periods. Soils sampled in November 1998 and February 1999 were used for this part of the project. The Stonton Brook was wet throughout the winter of 1998/1999 and received more rain than in any of the previous four years (see Chapter 4). On the day of the November overflight 15mm of rain fell, although it was not raining at the time of the overflight (1100hrs). On the two days prior to the February overflight 3mm and 2mm of rain fell respectively. Soil sampling was limited to these periods due to the lack of soil surface exposure during the rest of the year. It may be that the sensitivity of radar backscatter to soil is limited to soils with low moisture content and power to resolve differences between wet and very wet soil is low. This may explain the lack of papers reporting on wet soil moisture retrieval from SAR. C-band data from ERS-2 SAR may not be the ideal type of microwave for the detection of soil moisture. A review of Italian research by Paloscia (2002) revealed that L-band was found to be more appropriate for soil moisture and surface roughness estimation. Additionally, the Italian research found that gross averages over areas and dates markedly improved accuracies of soil moisture roughness. Such general information would be suited to areas with low variability but in the case of temperate UK would prove of little use.

There is some doubt about the orientation of the profile board when sampling the soil surface roughness with the profilometer in relation to the incident radiation. Tansey (1999) suggested that the profilometer should be perpendicular to the incident radiation. This however may be wrong. The incident radiation hits the target at an angle of 24° and therefore is going to be more influenced by the roughness of the soil, parallel to the direction of incident energy. Where the ground is uniform in its surface roughness irrespective of direction this may not prove to be a problem. However, where the ground has differential directional roughness e.g. when ploughed, one direction will appear to be much rougher than another and be influential over backscatter (Zribi *et al.*, 2002). This may be the confounding reason why so little correlation was found in soil moisture and surface roughness. In the case of SAR it is the roughness in the direction of the incident rays that will influence the backscatter most. Soil surface roughness in November was extremely varied between sample sites. Several fields had been recently ploughed and others had been prepared and sown for cropping. Baghdadi *et al.* (2002c) found that the lower incidence angle of ERS-2 SAR (23°) is insufficient for modelling soil surface roughness and that higher incidence angles of 47 degrees were needed for discriminating between roughness of different soils. The varied topography of Stonton Brook may have confounded even these angles unless a DEM was used in the orthorectification of the returning signals.

The results from the soil/SAR interactions may also have been influenced by the relatively low number of samples obtained when compared to the overall variation in moisture and roughness values for the sampling sites (support). The fine resolution of ERS-2 SAR images would be ideal from the perspective of field sampling if speckle were not an issue. Samples were collected from within three metres of each other for both sample locations for each sample site. This was done for accuracy within a given pixel but may have been too optimistic given the effects of speckle. In retrospect better support for the soil sampling would have been provided by taking samples over a much larger area and relating the averages to the values of backscatter across the 7x7 pixels as used.

The most obvious source of potential error is in the geographical accuracy of the images. It is assumed that the sampling locations on the ground correspond accurately to the backscatter values extracted from the images (coregistration). This may not be the case! Geographical accuracy was known to be dubious when performing the classification and was primarily due to problems of locating a particular pixel in the georectification and query of the final image. This is similar to the problem discussed by Bastin *et al.* (2000). Data from the single-date images for the soil and vegetation studies were therefore selected partly by the co-ordinates shown and partly by location with features in the image. Values were averaged across pixels but inaccuracies in selection may have occurred. Improvements in georectification may have an influence on this and further work would have to be carried out either on the existing images or by using positional radar targets.

8.5.3 LAI and plant biomass retrieval from SAR

Only one crop type was used in the regression analyses between LAI and plant biomass. Oilseed rape has a different plant architecture from most crops such as grasses, wheat and flax, and this exercise was therefore limited in its approach to the land cover types of the Stonton Brook. Additionally, the sampling techniques of measuring LAI and biomass are labour intensive and sampling numbers were low. This was affected by the additional parameters required for the

MIMICS model. Conversely pixel values can be affected by speckle and greater sample sizes were needed to compensate for this additional variation.

The regression for LAI did not show any form of correlation and many more samples would be required to attain adequate support to test the hypothesis reliably. The biomass relationship was stronger and more samples may have changed the outcome.

8.5.4 Modelling soil and vegetation cover using MIMICS radiative transfer model

The MIMICS model requires a large number of parameters from soil and vegetation. The collection and subsequent processing of samples for this investigation were limited and therefore so was the ground support for all parameters. Data were collected for months other than May and July but not used due to constraints on resources.

Geographical accuracy of the backscatter corresponding to each sampling site would also affect the outcome of the MIMICS modelling as discussed in the two sections above. Possible improvements may be obtained if the backscatter values were averaged at the field scale rather than pixel scale. This would eliminate some of the problems encountered through geographical inaccuracy and eliminate some of the variance of the backscatter response of the crops. Elements of speckle were reduced through filtration using 7x7 pixels and this would have helped in obtaining a more representative backscatter value for wheat and oilseed rape but it may not have been adequate.

Overall backscatter values retrievable from a SAR image extend from +20 to –28dB, and like the MIMICS output, wheat fields were identified within a similar 5dB, –10 to –15dB range. Unlike MIMICS, however, statistical analysis indicated a significant difference between data from the two overpass dates, with an average backscatter of -14.11 and -12.23dB for May and July respectively. Therefore, within a SAR image a wheat field could be identified theoretically, within a 5dB ‘window’ out of a possible 48dB range. It may therefore be possible to distinguish wheat fields from dissimilar fields such as oilseed rape or pasture, but doubt remains over fields with similar crop structures such as barley. This assumption could only be verified if the entire investigation were carried out again and included these different land cover types. The differences between May and July are possibly due to the differences in moisture content of the plants and lower LAI in July once leaf dieback has begun.

8.5.5 Conclusion

The outcome of the MIMICS modelling provided mixed results. This model was developed to support research into the microwave interaction with forests in the USA and therefore may not be suited to wheat and oilseed rape. The classification signatures of forest and oilseed rape were found to overlap and the error matrices did reveal a large amount of confusion between these two classes. Paloscia (2002) reported that C-band radar data were more suited to wheat than to oilseed rape and L-band to oilseed rape rather than wheat. The results presented in this chapter concur with that to some degree. Modelling of the backscatter from SAR images does not show any potential for aiding hydrological and nutrient transport modelling either through empirical or theoretical modelling. Svoray *et al.* (2001) also found little correlation between vegetation parameters and SAR backscatter but good correlation with green leaf biomass volumetric density. This characteristic of vegetation may therefore be a more suitable unit to compare with backscatter coefficients, but may not relate easily to parameters involved in hydrological modelling. SAR can support hydrological modelling in temperate regions using multi date imagery and maximum likelihood classification techniques. The next chapter applies the two land cover maps produced in this chapter to the SWAT model. Results from those simulations will disclose whether the maps are suitable or not.

Chapter 9 Application of the SWAT model

9.1 Introduction

Three versions of SWAT were used in this project. The first two were SWAT99 and SWAT2000 using links to ArcView GIS (AVSWAT99 and AVSWAT2000 respectively). Differences between the 99 and 2000 versions include correction of some programming errors and modelling additions, most of the code for the hydrological, erosion and nutrient transport processes remained virtually the same (K. Karayanan, Institute of Water and Environment, Cranfield University). The most notable addition to AVSWAT2000 was the Green and Ampt model for simulation of surface runoff as well as the SCS curve. The newer version also includes a facility to check for erroneous data and is considered to be more stable.

The last version used was a revised version of SWAT2000 (RAVSWAT) after several critical programming errors had been identified and resolved by N. Karayanan (Institute of Water and Environment, Cranfield University). RAVSWAT became available in April 2003, which was too late in this project to be thoroughly assessed. Revisions included in RAVSWAT include (K. Karayanan, Institute of Water and Environment, Cranfield University):

1) Correction of harvest code to ensure crops are harvested when specified

2) Correct calculation of baseflow

3) Correction of excessive aeration stress of plants that reduce plant growth

The above problems require additional input from the user in addition to those parameters required by AVSWAT. These parameters were not available during this project but the model was used with existing data to assess improvements obtained. Other problems have been found as listed below but were not incorporated into RAVSWAT in time for inclusion in this project:

4) Maximum rooting depth for all crops is taken as that specified in first crop database – all other specified rooting depths are ignored

5) AVSWAT includes an additional and unparameterised 10 mm soil layer

6) Root growth is inadequately simulated for all crops due to wrongly utilised plant heat units

All of the above problems were present in all versions of SWAT and AVSWAT as programming or exclusion errors. Although SWAT has been tested by Bingner (1996), Manguerra and Engel

(1998), Peterson and Hamlett (1998) and Muttiah and Wurbs (2001) there has been no record of these issues.

The AVSWAT interface, common to all three versions, makes the data and image selection process very straightforward, provided the preparatory work has been done beforehand. Contrary to many specialist programs that use command-line instructions, AVSWAT can be used within a short period of time. There is however, no room for complacency. It is a sophisticated system with many hundreds of parameters (see Appendix E), many of which are not well documented. It is easy to overlook what data the model is using in simulation and careful scrutiny of the output files is essential. The AVSWAT model process is summarised as follows:

1) Data gathering including:
   i. Data table generation (weather, soils and crops)
   ii. Soils map
   iii. Land use map
   iv. River shapefile
2) Project set up specifying all items from 1), delineation and discretisation schemes
3) Detailed parameterisation including:
   i. Additional soil parameters
   ii. Routing parameters
   iii. HRU parameters
   iv. Groundwater parameters
   v. Land-management practices
   vi. Existing soil chemistry
4) Sensitivity analysis
5) Interpretation and reporting

The SWAT model has been described in detail in Chapter 2 and the data collected or derived specifically for the Stonton Brook described in Chapters 4, 6 and 8. This chapter describes the processes that bring the model and data together and the methods of evaluation. Section 9.2 describes the preparation of the AVSWAT project files including the processes of delineation and discretisation. Methods of analyses are also discussed in this section. Section 9.3 contains all results from simulations from all three models used in this project and comparison between model output using field survey map and land use map derived from remote sensing data. Section 9.4 contains the discussion and the conclusions.

9.2 Methodology: AVSWAT project set up, model preparation and output analyses

The AVSWAT model and ArcView interface can be downloaded from the SWAT website (USDA, 2002). It is installed with ease providing ArcView version 3.1 or 3.2 is present on the computer system. The SWAT manual (1999) advises that a separate disk drive or partition is used to store the programs and associated files. Modelling work was carried out on two computers: an AMD Athlon 1.3 GHz with 1Gb RAM and 20Gb hard disk drive, and an AMD Athlon 1.0 GHz with 128Mb RAM and 20Gb hard disk drive. The hard drives were partitioned into two drives to enable the model and data to be held on a separate drive from the system. Selection of land use maps and discretisation schemes took between 40 and 60 minutes depending on the resolution used. Once the project environment was set up the management and detailed databases needed to be completed. This could take anywhere between two and nine hours depending on the number of parameters and factors that needed changing. Thereafter simulations took approximately five minutes. Calibration techniques using the AVSWAT calibration tool used much less time than manual calibration. The calibration tool allows specific values to be adjusted up or down by a given amount or percentage. The adjusted values were then calculated as the data are processed in simulation rather than writing a new set of parameter files. Selection of the detailed parameters and subsequent adjustment took the largest amount of time and would be more suited to a smaller catchment before applying it to a large catchment. This time element was minimised using a coarse discretisation method, which shortens data file generation and allows quicker assessment of output data.

After installation of the AVSWAT program, AVSWAT is available for use as an extension to ArcView. To use AVSWAT, ArcView must be opened and the project selection dialogue box closed. The AVSWAT extension must then be selected from the File – Extensions command. Failure to open AVSWAT in this fashion will generate script errors. The AVSWAT interface is shown in Figure 9.1. AVSWAT requires that the files for the modelling be organised in a specific way in order for it to access them. When a new project file is created (.swat extension) a folder is made by AVSWAT with the same name as the project. All working images and database files must be placed within this folder before they can be used for the modelling process. Database and map files for land use, soils, weather and crops need to be written before the preparation begins. Soil series and crop/land cover types databases are linked to the maps and weather databases built using the AVSWAT interface as shown for soils in Figure 9.2. Several reference files used to instruct AVSWAT to refer to customised databases also need to be written, but can be created from the table facility in ArcView or any other database or spreadsheet program. Similarly the image files need to be prepared and converted to ArcGrid format where necessary. The system is quite sensitive to disturbance and it is necessary to build the weather, soil and crop databases prior to selecting the images. It is also important to save and close the program in the appropriate manner to avoid rendering the project files inaccessible.

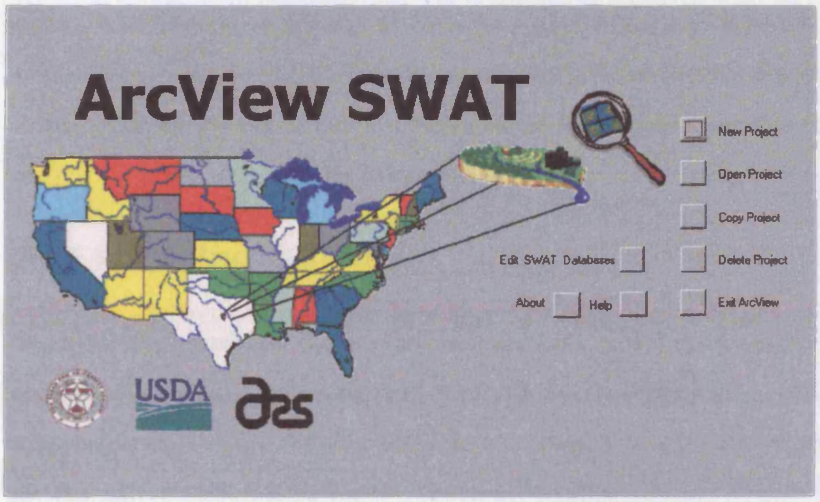

Figure 9.1 Reception interface of SWAT.

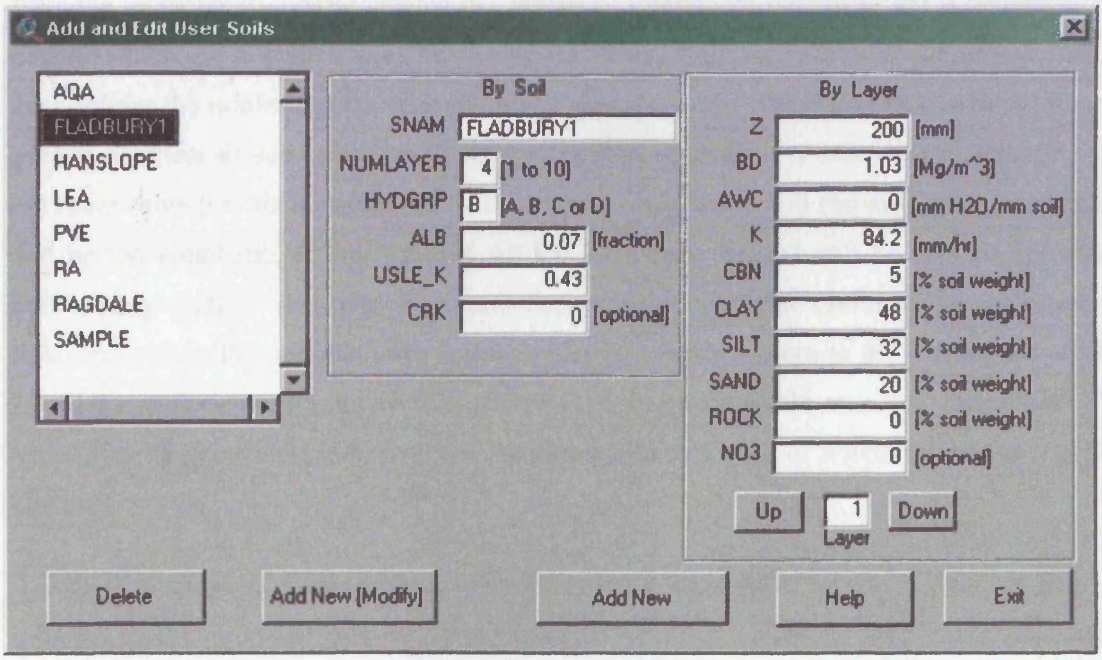

Figure 9.2 Input dialogue window for the soils characteristics. The soil series shown is Fladbury 1 found in the Stonton Brook.

On completing specification of the project environment the catchment was defined and land areas discretised. The catchment is divided into sub-basins, which are further divided into HRUs. The sub-basins define the channel reaches and area of land draining into them. HRUs define homogeneous parcels of land within each sub-basin that have common soil and land use.

Scale is considered in the modelling process by the discretisation methods used. SWAT does this with the HRU. AVSWAT utilises HRU's in order to organise the catchment system and make processing and output simpler. Small HRU's will divide the catchment up into small units in which rare land cover types will be represented. Conversely, if the HRU's are large, the crop type or soil series covering only small areas will be overlooked in favour of the more dominant ones. AVSWAT can specify HRU's on a grid basis, e.g. a raster map or by sub-catchment as described in Section 9.2.1. Discretisation of the former method provides a detailed picture at the sub-field scale for small catchments or detailed studies, whereas the latter would give a coarse resolution better suited to large catchment areas.

9.2.1 Watershed delineation

Once all the database files were built the catchment maps were selected to define the river channel and divide the catchment into sub-basins (delineated). The DEM was the first digital map required. AVSWAT can build its own river system based on the low points in the DEM but an alternative option is to use the "burn-in" method that defines the river system from a digitised line-shapefile of the river. The burn-in option was used based on a digitised river map taken from the aerial photo-mosaic created in Chapter 7. Thereafter, the catchment is divided into sub basins, which are allocated specific river channel sections (reach) into which they drain. The user defines the minimum size of each area "threshold area". Small threshold area values create greater numbers of sub-basins and thus shorter river reaches. For any river system there is an optimum value for this phenomenon: if set too high, large areas will contain few channel sections and be too simplistic, if this value is set too low, each channel will be divided into smaller unnecessary sections and overcomplicate the computation. The optimum threshold area was considered to be the one that gave the most similar channel pattern to the Stonton Brook itself. By trial and error the optimum value for sub-catchment threshold area was found to be 40ha. This value divided the catchment into 53 sub-catchments each of which drained into a single channel.

The final element to the watershed delineation is the location of stream outlets. A point was selected on the river that defined the outlet of the catchment studied. This is then processed to produce the image shown in Figure 9.3.

9.2.2 Land use and soil definition

After delineation the land use and soils were defined using the dialogue box shown in Figure 9.4. For assessment purposes the model was run first with the field survey data map for modelling assessment but later with the two maps derived from remote sensing. The grid files were related to the land use categories in the AVSWAT database as attributes. The categories available were those already specified in the crop database. Most crop types such as wheat and barley were available as standard, though modified to suit UK conditions (see Chapter 4). Others such as hemp needed to be written into the database from new. Once all fields had been allocated a class the data were processed.

The soils map was then selected and a similar procedure followed for assigning specific soils on the map to specific entries in the soils database. Once all were selected the data were processed. This normally takes between a minute and three minutes depending on the resolution of the maps, the threshold areas and the speed of the computer processor. The resultant map is shown in Figure 9.5.

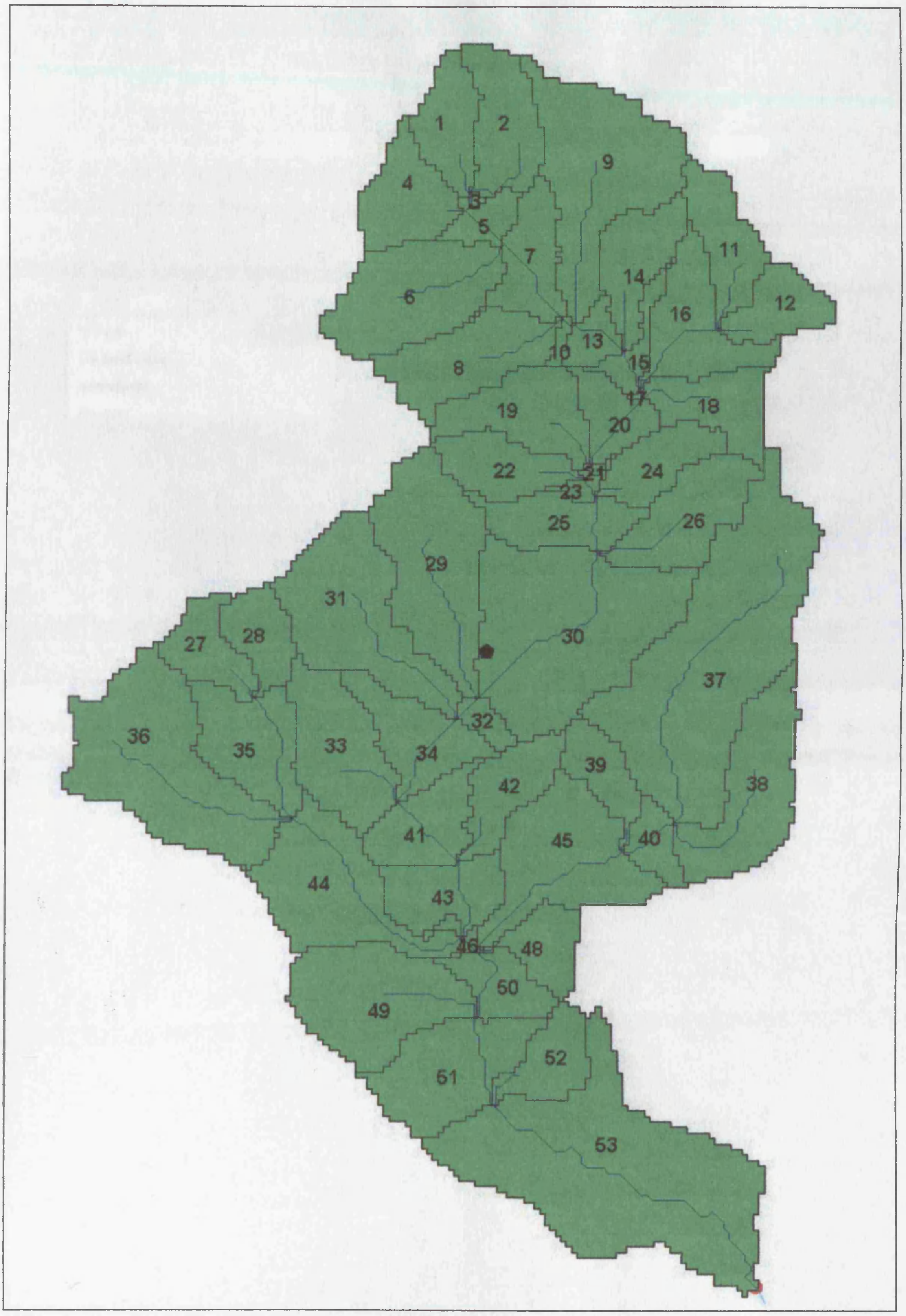

Figure 9.3 Catchment delineation. The blue lines represent the burn-in river channels and the black lines define the sub-basins.

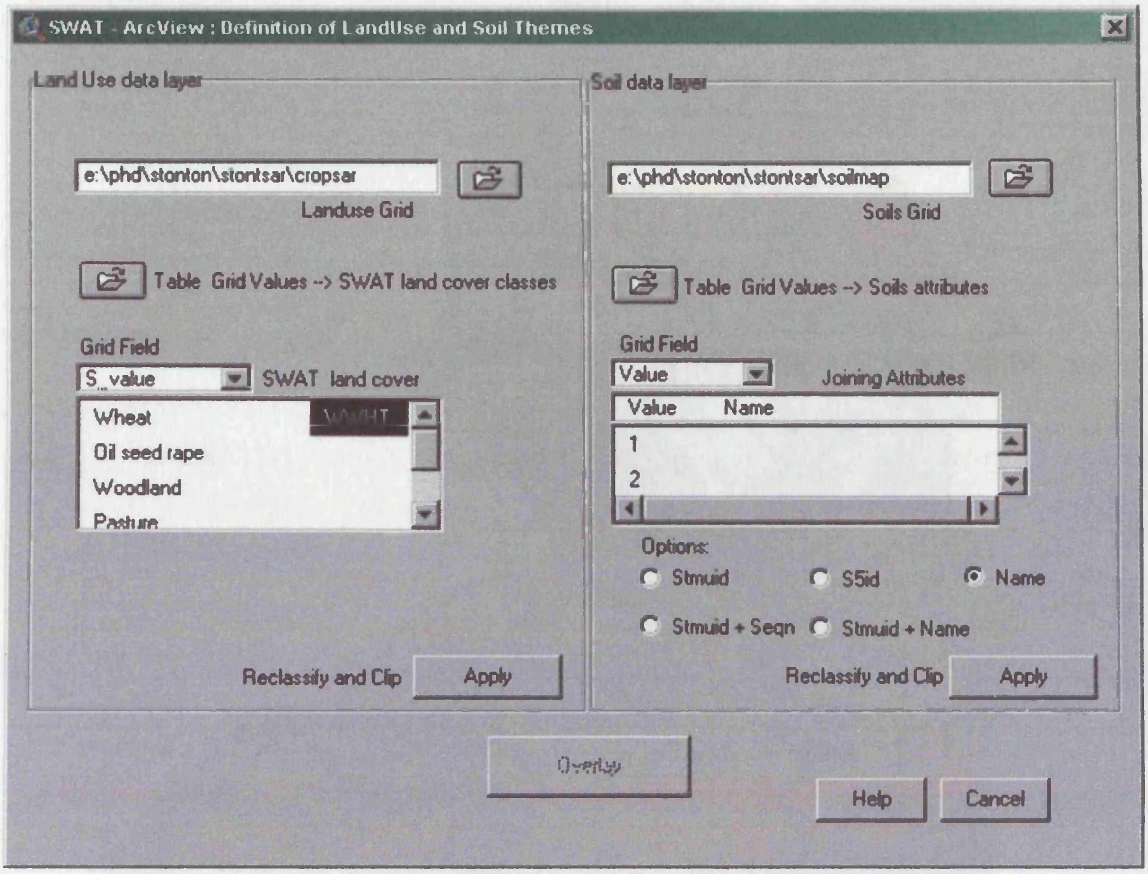

Figure 9.4 Land use and soil definition dialogue box. The Arc grid file must first be selected towards the top of the box and then SWAT land use categories must be allocated by selection in the centre of the box.

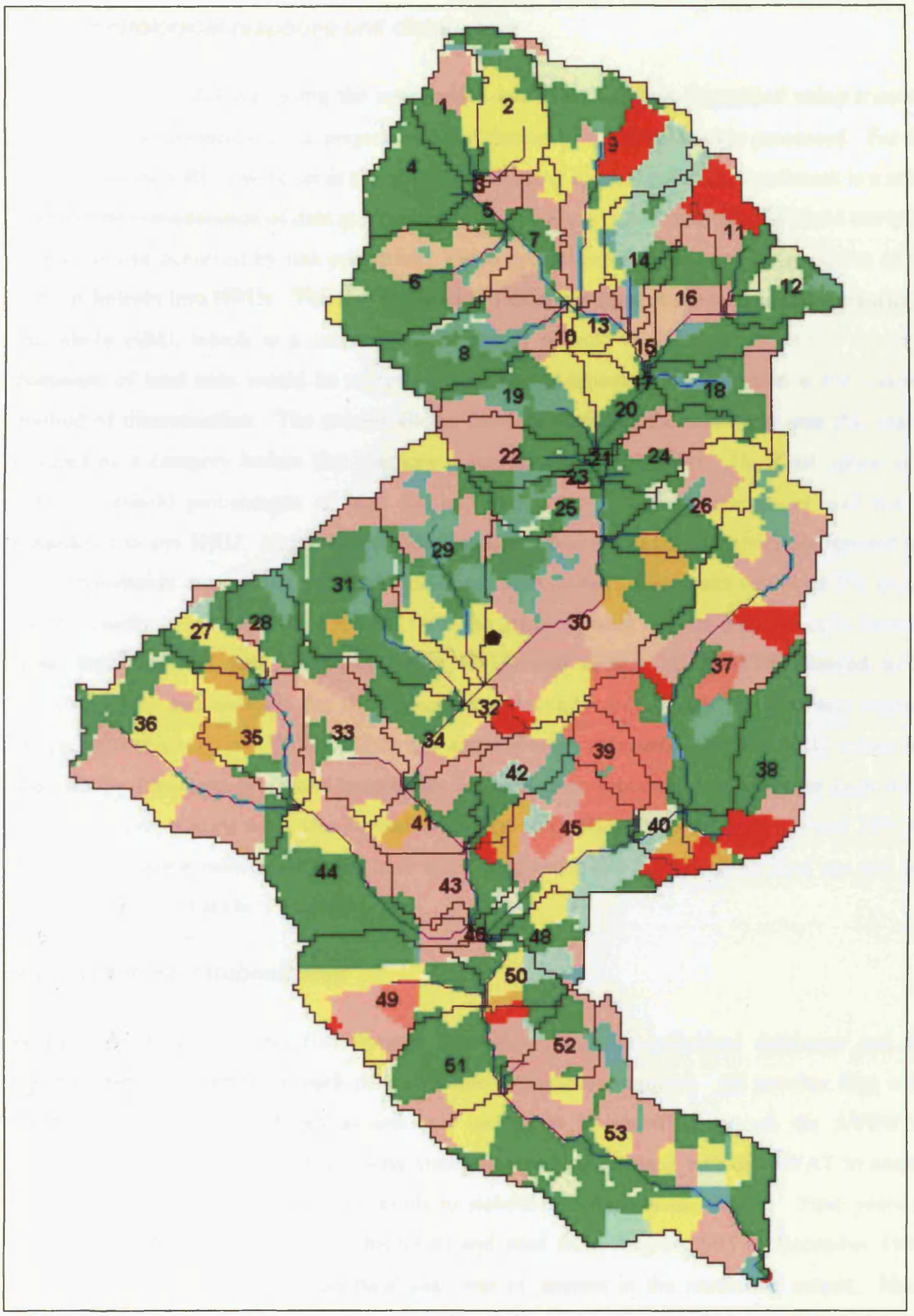

Figure 9.5 Land use map of the Stonton Brook as generated by the AVSWAT model. Note the coarser resolution than the map displayed in Figure 8.6 on which it was based. The resolution applied to this map is the same as the DEM (50 m). Numbered areas define individual sub-catchments. Each colour depicts land cover but HRUs are defined on a further level that combines contiguous areas of common soil types and land cover types in each sub-catchment.

9.2.3 Hydrological response unit distribution

To ensure the model was using the appropriate data it was at first discretised using a coarse resolution. Adjustments to the project files and databases could be quickly processed. For the simulations the HRU's were set at a high resolution using a small grid. The catchment is a small one and the consideration of data at sub-field scale was important. Inclusion of all land use types would only be achieved by fine resolution. Three options are available for discretisation of the sub catchments into HRUs. The first allocates the most common of the land cover categories to the whole HRU, which is a sub-catchment area as defined in 9.2.1 above. Only the most dominant of land uses would be represented in the catchment. This selection is the coarsest method of discretisation. The second allows the user to define the minimum area (%) that is covered by a category before that category is represented in the HRU. The final option is to define threshold percentages of land use and soil below which the categories will not be considered in any HRU. Higher thresholds dictate that less dominant categories are ignored and lower thresholds ensure that more categories are represented. Threshold values of 0% ensure that the catchment is discretised into HRUs at the grid cell level. Where adjacent cells have the same land use and soil categories larger HRUs will exist. AVSWAT99 proved to be temperamental and unstable for this operation and would only accept the first and coarsest option. For this reason AVSWAT2000 was adopted when released. After the HRU values had been set the files were processed to calculate the land cover types and soil series for each HRU. The initial preparatory work was carried out using 157 HRUs (25% for land use and 20% for soils). Simulation results presented here were done using 490 HRUs. Both land use and soil categories were set at the 1% level.

9.2.4 Weather database files

Weather databases are specified through files identifying the individual databases and the weather station locations for each of the weather parameters required. All weather files were created prior to AVSWAT set up and only needed to be specified through the AVSWAT interface. It is recommended that long simulation periods be used with AVSWAT to enable various processes and storage components to stabilise (Neitsch *et al.*, 2000). Four years of weather data were collected (see Chapter 6) and used from August 1995 to December 1999, although only the 1998-99 agricultural year was of interest in the modelling output. Many parameters such as soil moisture content are given initial values and would be poorly simulated if modelled for just one agricultural season.

9.2.5 Detailed parameterisation

AVSWAT will use default parameters for all processes including instream and land management factors. These are however very general and require extensive amendments to ensure appropriate representation in the catchment. The most important of all these files is the management file (.Mgt). Agricultural rotation and practices can be included in terms of plant heat units (PHU) or by dates. Both model plant growth using heat units, but the former specifies fertiliser and tillage operations on appropriate stages in modelled plant growth. The latter accepts specified operations regardless of the stage of growth.

9.2.6 Model simulations

Initial simulations were performed using AVSWAT99 and AVSWAT2000 with the land-survey map described in Chapter 4. The data set that provided the best results in the latter version of AVSWAT were then applied to RAVSWAT when it became available. It was inappropriate to apply the land cover maps to a model that was shown to have inherent coding problems and poor performance and therefore, these maps were only applied to RAVSWAT. The land cover maps derived from remote sensing were applied to RAVSWAT only and comparisons made with results obtained using the land survey map. Model simulations were run from August 1995 to December 1999 to coincide with the available weather data. Only the simulated output for the period September 1998 – October 1999 was of interest. The simulation period before the year of interest was used to stabilise the system processes. The agricultural management parameters collected during the year of field study are simply repeated for each of the years preceding 1998-1999 season. Several model options such as the evapotranspiration model, were tried to see what implications they had upon modelling output.

9.2.7 Model output analyses

Analyses of the results are somewhat compromised by the possible lack of representation of rainfall data to the Stonton Brook. At all stages of the assessment process, the differences between the rainfall data and response of the Stonton Brook to rainfall events will be taken into account. There are various methods for assessing model output as described briefly in Chapter 1. Thorough examination of simulation output is the first stage in assessing the model performance. AVSWAT generates three main results files documenting the system processes (.sbs), the sub-basin output (.bsb) and the instream output (.rch). The system processes document the simulations generated within the catchment such as plant growth and water storage. The sub-basin file records all data produced by each sub-basin such as runoff volume and evapotranspiration. The reach output file records all values simulated within the stream, the most important being flow and phosphorus concentrations. These files are in .dbf format and can be imported to Excel to generate graphs. If the processes are found to be logical and simulate the system well, further analyses can be performed. Sensitivity analyses are useful for determining which parameters are most influential in the following assessment at the process level

Several key parameters suggested by Di Luzio *et al.* (2002), and listed in Table 9.1, were used in sensitivity analysis. Additionally, soil saturated conductivity, which is not a suggested calibration parameter, was also included. Proportionality between the values distributed across the catchment was maintained by adjusting all values up or down in 10% increments (K. Beven, Dept. of Environmental Science, Lancaster University; Melching and Yoon, 1996). Problems with this method could exist where a value of a distributed parameter is at or near the limit of the range of that parameter. Sensitivity analyses were also useful in obtaining higher simulation replications. If the model was only run with one parameter set (n=1) the outcome could be affected by chance events. Multiple simulations will ensure that AVSWAT conforms to a level of repetition and stability that is required of a scientific model.

Table 9.1 Parameters used in sensitivity analyses in AVSWAT2000.

SWAT code	Parameter	Effect on modelled processes
CN2	Initial SCS curve number for soil condition II	Affects the amount of infiltration and runoff occurring at any one time. It is a function of soil permeability, land use and existing soil water.
GW_REVAP	Groundwater revaporation coefficient	A coefficient controlling the flow of water from a shallow aquifer vertically to the overlying root zone.
SOL_AWC	Available water capacity of the soil water layer (mm H_2O)	Defines the amount of water between plant wilting capacity and field capacity, and therefore affects the stored component of groundwater.
ESCO	Soil evaporation compensation coefficient	A factor allowing the user to adjust the depth of soil from which evaporative demand can be drawn
SOL_K	Soil saturated conductivity	The saturated conductivity of soil and will be applied only to the top layer of soil

Four methods of model output assessment were described by Gupta *et al.* (1999), only two of which were shown to be useful. Simple standard deviation between the measured and simulated flow data and the Nash-Sutcliffe methods were shown to be poor indicators of model performance. All four methods depend on deterministic time series output from the model and use simple statistical mathematics. The percent bias value (PBIAS) provides a negative or positive percentage. Negative values show the model is overestimating and positive values show the model is underestimating and is calculated using:

$$\text{PBIAS} = \frac{\sum_{t=1}^{N}(q_t^{obs} - q_t^{sim})}{\sum_{t=1}^{N} q_t^{obs} \times 100\%} \tag{9.1}$$

Error in the modelling predictions is described by large PBIAS values. The second good indicator of model performance is the persistent model efficiency (PME) and is calculated with:

$$\text{PME} = 1 - \frac{\sum_{t=1}^{N}(q_t^{sim} - q_t^{obs})^2}{\sum_{t=1}^{N}(q_t^{obs} - q_{t-1}^{obs})^2} \tag{9.2}$$

PME is based on a simple persistence model and estimates the relative magnitude of the residual variance in the output against the errors obtained by the simple persistence model. Values fall between zero and one the former of which shows poor performance and the latter of which shows a perfect match between measured and simulated data. Values must be larger than zero to indicate minimally acceptable performance (Gupta *et al.*, 1999).

9.3 Modelling results

All three versions of the AVSWAT model were parameterised with the same data and consequent simulations performed. The oldest version of this model, AVSWAT99 was used very little. It proved to be very unstable and would not perform discretisation tasks as requested. Predicted values of water flow and P-loss were poor but no investigation was made into reasons why it performed so badly. Results are reported nonetheless. Soon after the initial work on AVSWAT99 was carried out, AVSWAT2000 was released and used instead.

Setting the agricultural and land use management files proved particularly difficult to set without disrupting the plant growth and evapotranspiration substantially. Although the AVSWAT manual suggests that any given agricultural practice or routine can be applied this is not the case. For instance, perennial land cover was not managed appropriately by AVSWAT. Long-term pasture and all forestry required a "kill" event at the beginning of the simulation period, which then affected biomass and LAI in any one year. In an attempt to overcome this effect, the crops were given initial biomass to simulate a translocation exercise. Initial biomass was, however, limited to 200 kg Ha^{-1}, and does not match the several tonnes per hectare normally found on pastureland at the beginning of a growing season.

The optimum potential evapotranspiration option was found to be the Hargreaves method. This model gave the best fit of water flow compared to the other options. Several other options highlighted in Chapter 2 that were either chosen or turned off are listed in Table 9.2.

Table 9.2 AVSWAT settings found to best describe the data set acquired for the Stonton Brook.

Option/Method	Setting
Rainfall/runoff/routing	Daily rain/Curve number/Daily
Rainfall distribution	Skewed normal
Potential evapotranspiration method	Hargreaves method
Crack flow	Not active
Channel water routing method	Variable storage
Channel dimensions	Not active
Stream water quality processes	Active
Lake water quality processes	Active

The system simulations (e.g. LAI, plant stresses) and hydrological simulations were assessed and adjusted at first to ensure the P transport medium was performing correctly. However, it is demonstrated in this chapter that the system processes affecting hydrology do not perform well enough to warrant a thorough investigation into the PT component. It has been shown that critical components of the AVSWAT model were badly written at the coding level (K. Karayanan, Institute of Water and Environment, Cranfield University), hence the revised AVSWAT model was used. These errors were resolved too late into this project to be properly assessed, but initial simulations indicate improvements into the hydrology component. It is revealed that the PT element is highly overestimated which may be a combination of poor sediment transport and PT programming. The PT component is however scrutinised and potential reasons for poor performance discussed in the next section.

9.3.1 AVSWAT99 simulations

The AVSWAT99 model simulation was initiated on completion of the preparation and parameterisation. Flow, organic P and mineral P results were extracted from the "Basins.rch" file whilst baseflow and stormflow were converted from extracting GWQ, SURQ and WYLD results from the "Basins.bsb" file. Plots of monthly-simulated flow and P-loss are shown in Figure 9.6 together with the measured plots. AVSWAT99 severely underestimated flow and severely overestimated TP. The coefficient of variation between the measured and simulated flow was 103% for the water flow. The mean difference between the two sets of flow data was 0.3732. This clearly indicates differences between the quantity and pattern of flow between the measured and simulated data. Two flood events appear to be synchronised but the middle simulated flood event does not reflect the same event in the measured data. On inspection of the output files it became apparent that AVSWAT99 was generating weather data instead of reading-in tabulated measured data.

The coefficient of variation in the differences between measured and simulated P-loss is 133% and the mean was 311.1. This indicated a strong disagreement between the simulated and measured data. Additionally, the PBIAS value was 78.96 indicating a large overestimation of flow, and a PME value of –0.274 indicating that flow was unable to provide a prediction superior to a simple persistent model. Simulated P-loss intensity follows similar patterns to simulated high flow and two peaks shown in Figure 9.6a are synchronous. P-loss is however overestimated in the peaks and underestimated during baseflow.

The changes in AVSWAT2000 were bug fixes and process additions rather than code defining the hydrological and nutrient transport processes. Although the processes code remained the same it was hoped AVSWAT2000 would be more stable and reliable. It was therefore decided to change to AVSWAT2000 and no further work was carried out on AVSWAT99.

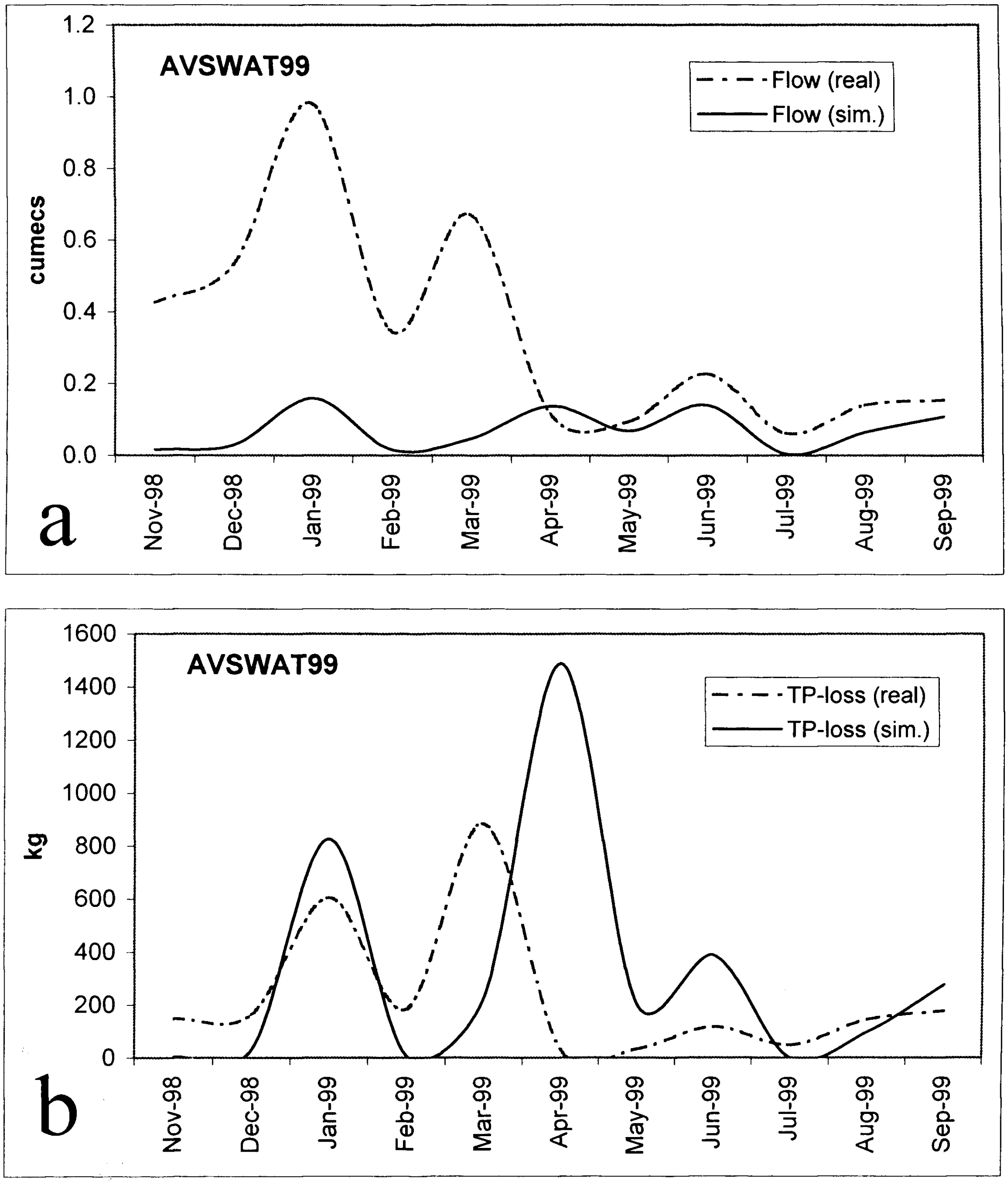

Figure 9.6 Comparison of simulation results with measured values of river flow and total phosphorus loss from the catchment. Negative numbers in TP-loss are artefacts of the smoothing process. All data were based on monthly averages from daily values.

9.3.2 AVSWAT2000 simulation results and analyses

This section was completed prior to the knowledge that key coding problems in AVSWAT had been identified and resolved. Although the results contained in this section are therefore based on an obsolete and flawed model they are presented in support of the findings of Karayanan (Institute of Water and Environment, Cranfteld University). The best simulation for water flow using AVSWAT2000 was better than those from AVSWAT99 as shown in Figure 9.7. Simulated flow is close to measured flow with a coefficient of variation between predicted and measured of 93.16% and a mean of 0.149. The low mean indicates the two data sets are close to each other, but the high coefficient of variation shows the inconsistent differences between predicted and measured flows. Calculation of PBIAS for flow gave –26.88 cumecs indicating AVSWAT2000 has a tendency to overestimate (Gupta *et al.*, 1999). Results of the PME equation gave a value of 0.5 indicating that AVSWAT2000 did perform better than a simple persistence model (PME >0). Timing of spates and intensities follow similar patterns but several differences are present. There is little definition between the predicted spate in January and that in March as displayed in the measured data. Drop-off from a spate does not occur as rapidly in prediction as it does in reality. In addition, the late spring and early summer predictions are higher than measured values, but this is probably due to the rainfall patterns recorded outside of the catchment. Before PT can be reliably modelled the hydrology must be accurate and processes appropriate. The discrepancy in simulated P from measured P therefore, will be ignored for the present until the hydrological component has been investigated.

Although base flow and stormflow were not measured in the river, the simulation of baseflow is overestimated and stormflow underestimated for given periods as shown in Figure 9.7b. This can be deduced by comparing with the peaks and troughs in March of Figure 9.7a. The lowest value in the trough is less than four cumecs, whereas the predicted baseflow is greater than seven. The intense storms of March, exhibited in the flow, were not present in all sets of rainfall data and therefore not accounted for by AVSWAT2000. Likewise the overestimation of stormflow during late spring and early summer are not present in measured flow possibly because these storm events did not fall on the Stonton Brook but were recorded by the weather stations. Inspection of factors such as evaporation, precipitation and percolation in the Basins.sbs indicated what the model is trying to do. March was a dry month punctuated with two-days of intense rainfall activity. A third more rain fell in May than in March and a fifth more in April but during less intensive bouts. Soil water content was high in March (401 mm H_2O) compared to May (378 mm H_2O). Conversely evaporation was low in March (17 mm H_2O) compared with 63 mm H_2O for May. These results are expected and logical but there is a sudden change in proportions of surface water and ground water in May when compare to the previous two months. On inspection of the daily precipitation data this was preceded by a rainfall event of 54 mm in 24 hours. Consequently the ground flow and surface flow ratios change markedly from 53.7/1.1 in March to 24/15.3 in May. Although his is a logical response to the rainfall data it is not representative of the Stonton Brook and must be treated with some caution.

Results affecting hydrology were extracted from the "basin.sbs" output file and plotted in order to assess the system simulations, as shown in Figure 9.8 and 9.9. The former contains simulations of biomass growth, whilst the latter contains LAI of the six most dominant land covers. Additionally, Figure 9.10 and 9.11 contains graphs of temperature and nitrogen stress for the same plants. Plots are made of the whole simulation period to indicate the variation between years.

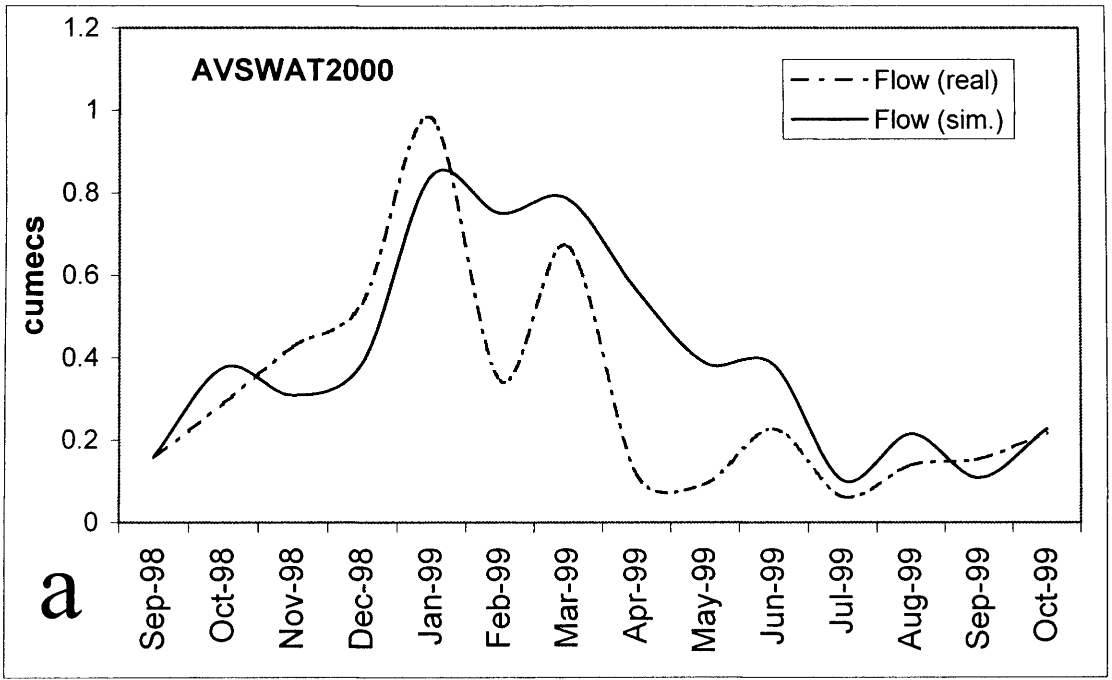

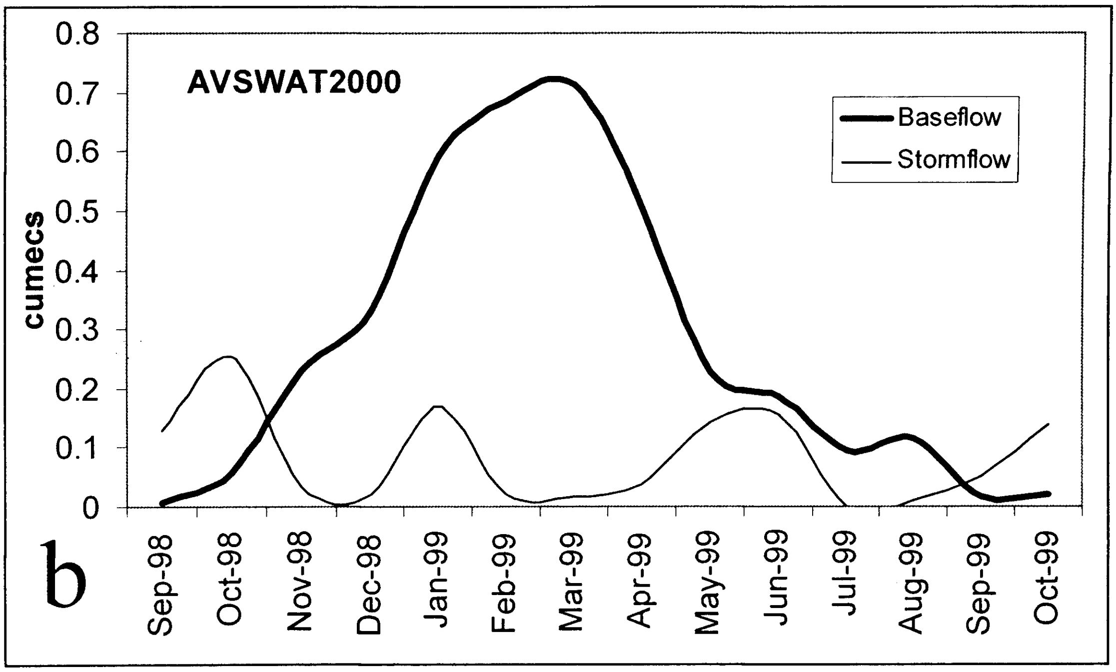

Figure 9.7 Best hydrological results from AVSWAT2000. The model was parameterised with all available data and information. River flow is overestimated but follows the same trend. Breakdown of simulated flow into baseflow and stormflow indicates base flow is overestimated and stormflow underestimated. Differences between totals from graph b and simulation flow in a, define the precipitation falling directly on the river.

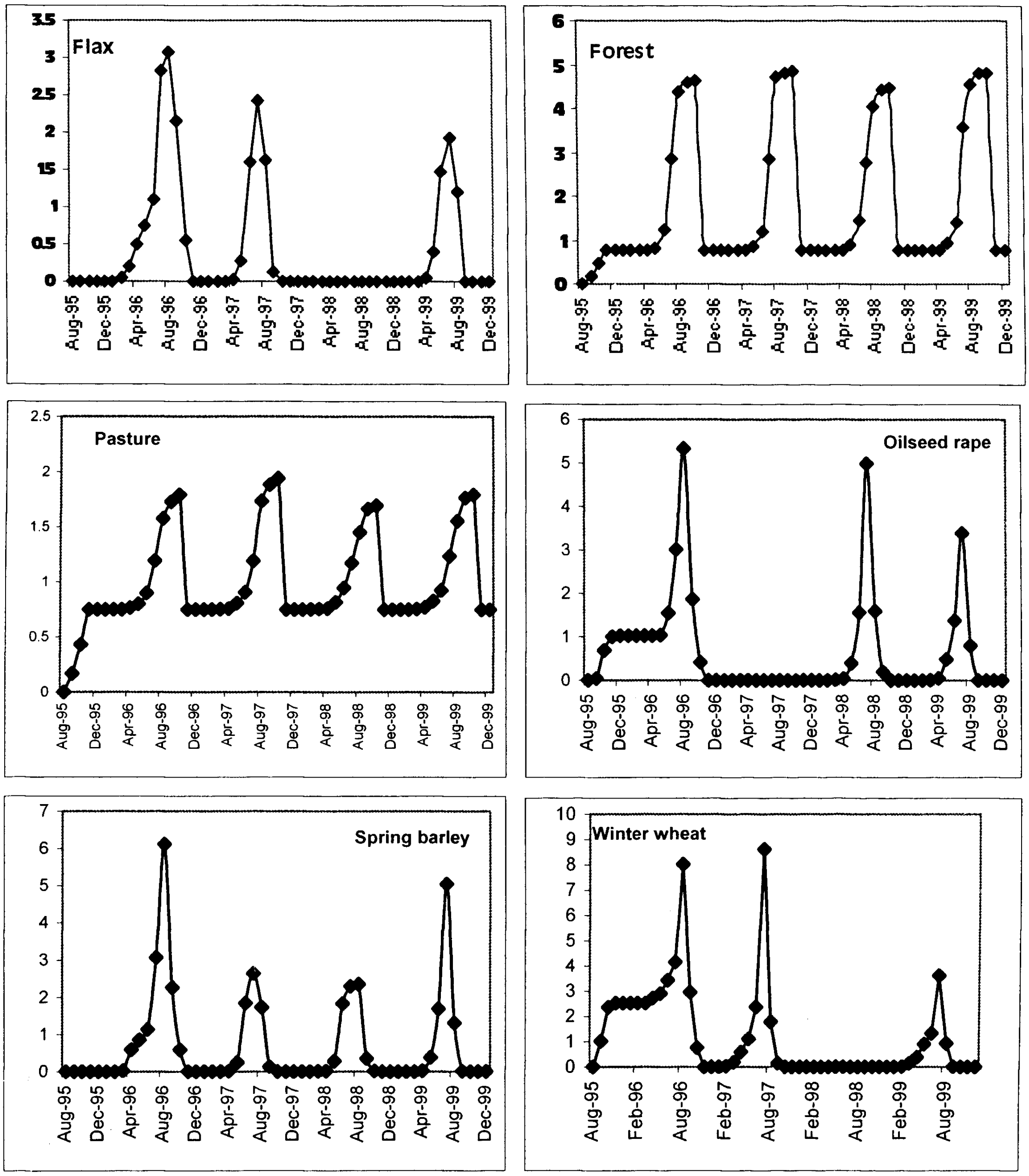

Figure 9.8 AVSWAT2000 LAI simulations for the 4-year modelling period for six land covers. Units are m^2/m^2.

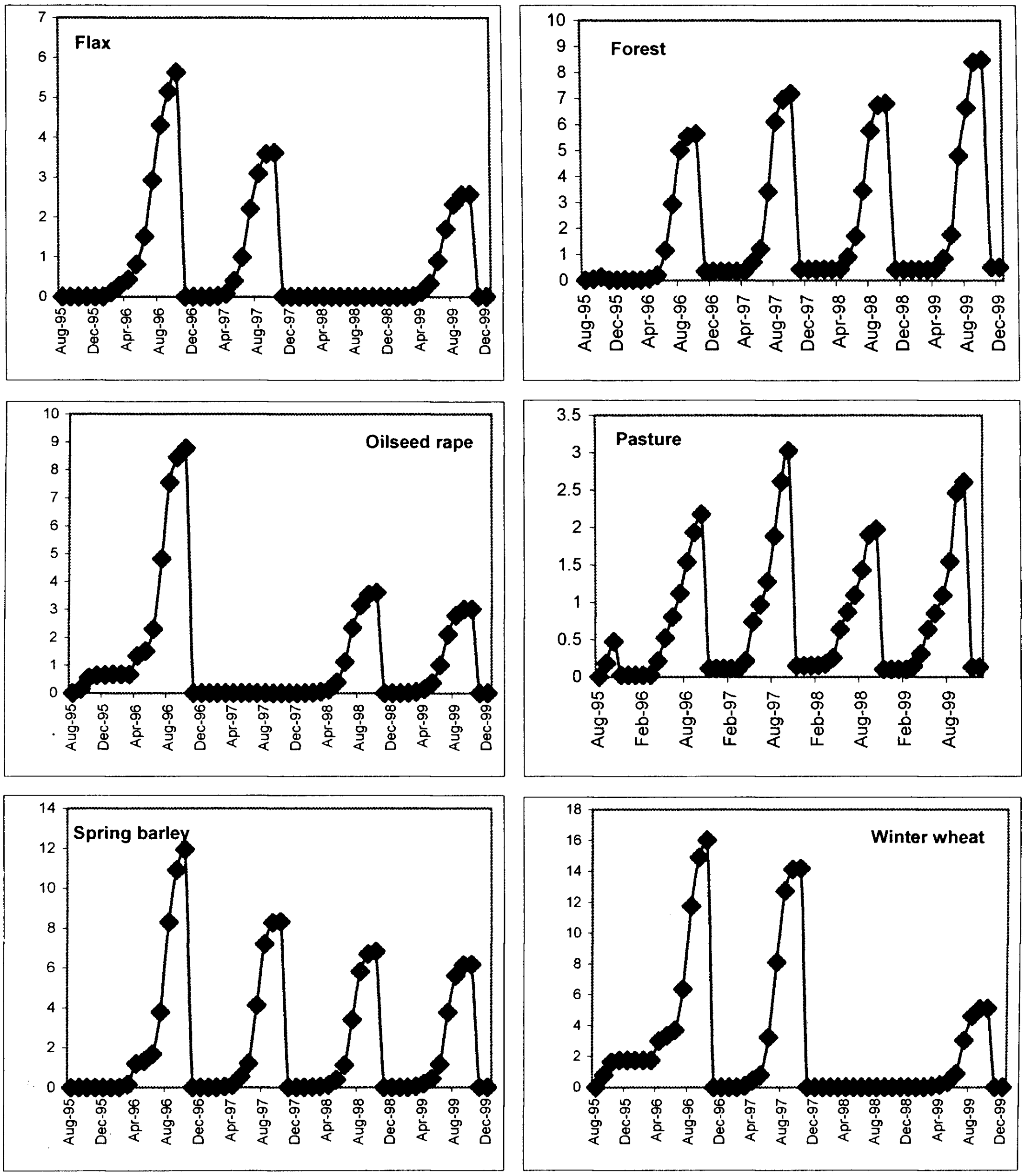

Figure 9.9 Wet biomass simulations using AVSWAT2000 for six land covers. Units are tonnes Ha^{-1}.

Simulated plant growth in the first year is comparable to that measured for wheat barley and oilseed rape. Subsequent years are poorly modelled. The results shown in Figures 9.8 and 9.9 also do not match the land management specified in AVSWAT2000. The model ignored specified harvest and kill operations as indicated by extended plant growth into October and November. Except for barley, each annual crop misses a year of growth. Two of the crops do not grow in the third year and oilseed rape does not grow in the second. Perennial land covers are poorly modelled. Forest and pasture do not achieve their expected growth levels, and grazing events specified over the pasture are ignored. This was partially expected from experience in the initial preparatory simulations. Growth curves for over wintering crops are simulated well in the first year but, presumably, due to the extended autumnal growth are poorly modelled in subsequent years. Some contradiction exists in the barley growth simulation. It is the only annual that grows each year of the simulation, but its management specifications are almost identical to that of flax. Temperature and weather data are not unusual in the third year so there is no apparent reason for this discrepancy. LAI and wet biomass attains similar values to those measured but the duration of growth and absence in year three indicate problems with either the data or model. The vegetation cover during the last year is modelled, and therefore, exposed soil due to poor plant growth modelling does not account for the high levels of predicted sediment export during late spring and summer.

Results of factors affecting plant growth are plotted in Figures 9.10 and 9.11 to try and identify the above problems. Temperature stress appears to be high in certain summer periods and low in winter periods. The one exception to this is oilseed rape. The consistent yearly patterns do not reflect seasonal temperature fluctuations, nor do they reflect anomalies for particular years. There is no temperature stress shown for most land covers in the December of any year. Light would be more limiting than temperature in December in the UK, and therefore temperature stress may be low due to a simultaneous absence of potential growth. It is possible that certain parameters are causing this anomaly but those for oilseed rape are not very different to winter wheat. Oilseed rape however, was observed growing throughout the winter and does not suffer the same temperature stresses.

Nitrogen stress is simulated throughout the period of growth for all land covers except forest where stress is minimal. Nitrogen stress on this scale would not be present in intensive agricultural systems where soil nutrient levels are maintained to reduce or eliminate nutrient stresses. Low levels of nitrogen stress are coincident with the years in which flax and winter wheat do not grow. Conversely, there is a large period of nitrogen stress when oilseed rape does not grow. It is reasonable to expect that if plants are not growing, stresses do not exist and this may have accounted for the low nutrient stress if the contradiction did not exist. Phosphorus stresses were almost non-existent for the entire period of simulation. Typical levels of soil nitrogen and phosphorus were specified for all soils and typical applications of fertiliser were specified for each year. Plant growth is not represented well by AVSWAT2000. The most obvious reasons for this are the lack of control of specified management practices, and poorly modelled plant stresses. The algorithms used in these processes have been widely tested and, therefore they are likely to be coding problems within AVSWAT2000.

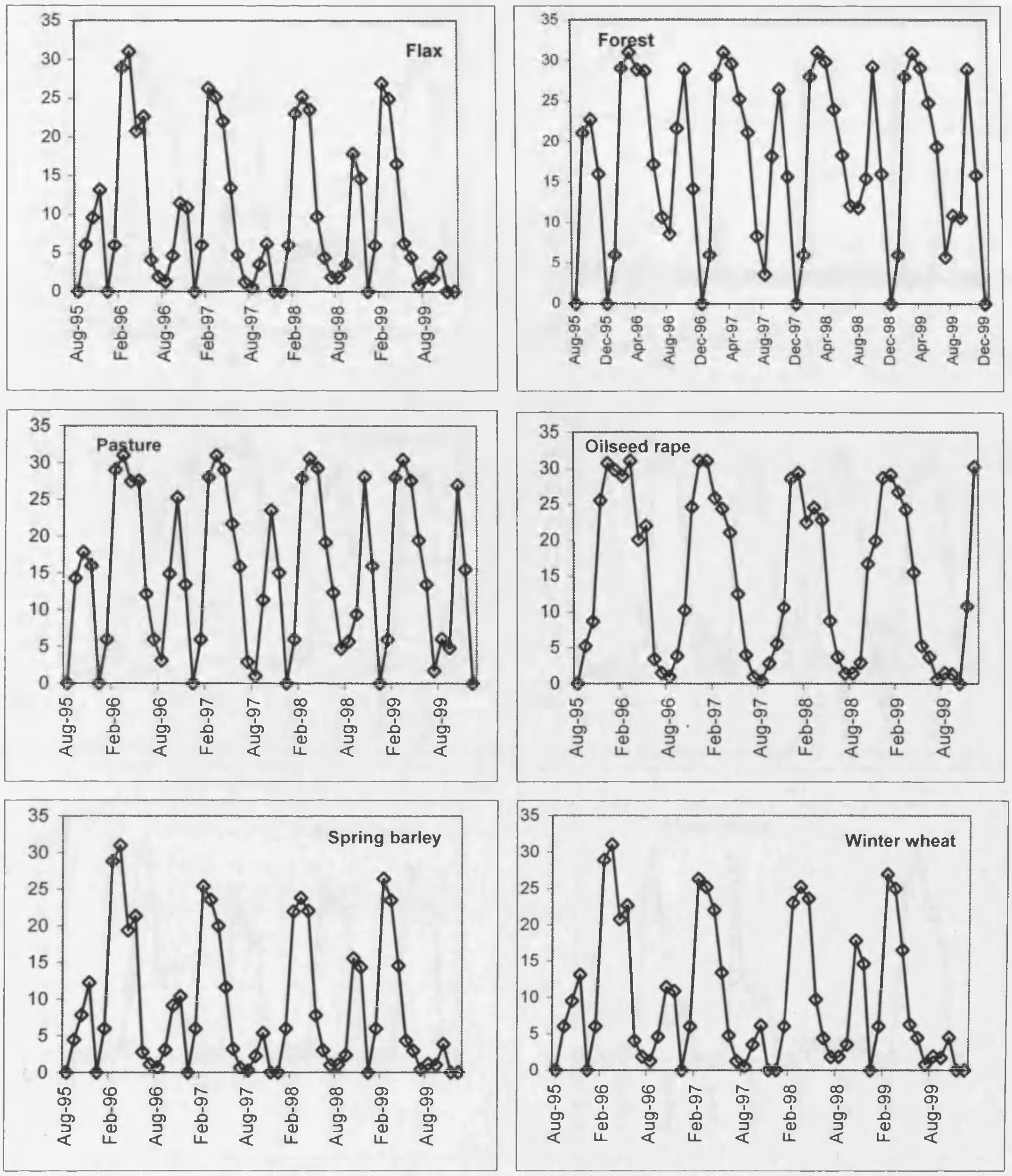

Figure 9.10 Temperature stress simulated in AVSWAT2000 for six land covers. Stress units in days where stress has restricted plant growth.

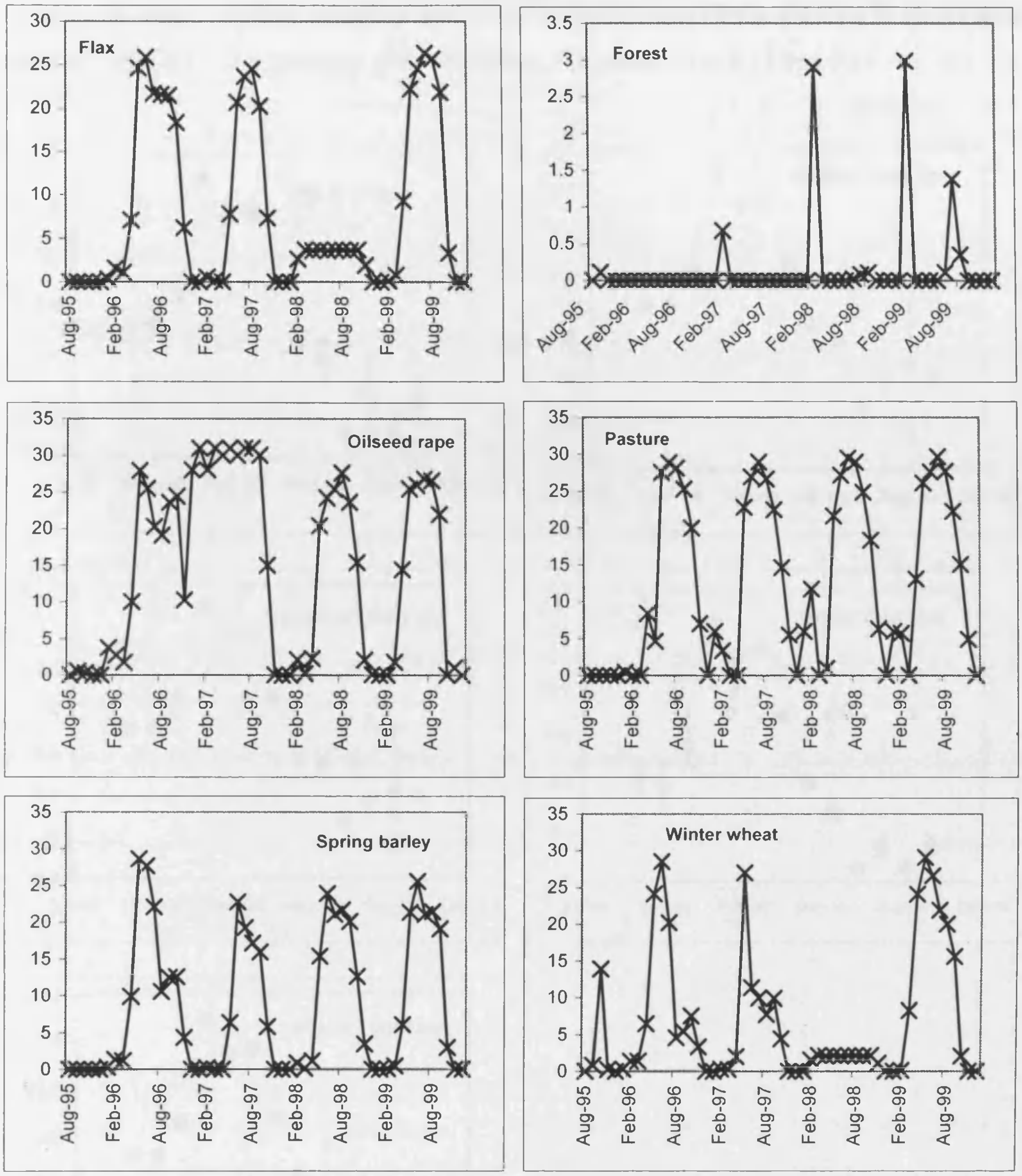

Figure 9.11 Nitrogen stress simulated in AVSWAT2000 for six land covers. Stress units are in days where stress has restricted plant growth.

9.3.2.1 Sensitivity analyses

Some underlying simulations affecting hydrology in AVSWAT2000 have been shown to be unrealistic. Sensitivity analyses may help to disclose reasons for the poor simulations. Parameters that vary in space require a system of adjustment that maintains the proportional relationship between the distributed values of the same parameter (K. Beven, Department of Environmental Science, Lancaster University). This was achieved by adjusting parameter values by incremental percentages. Correlation coefficients were then calculated for each set of parameter values and the respective resultant values for flow, baseflow or stormflow. The variation in output of flow, baseflow and stormflow are plotted for variations in the parameters listed in Table 9.1. The resultant plots are shown in Figures 9.12, 9.13 and 9.14.

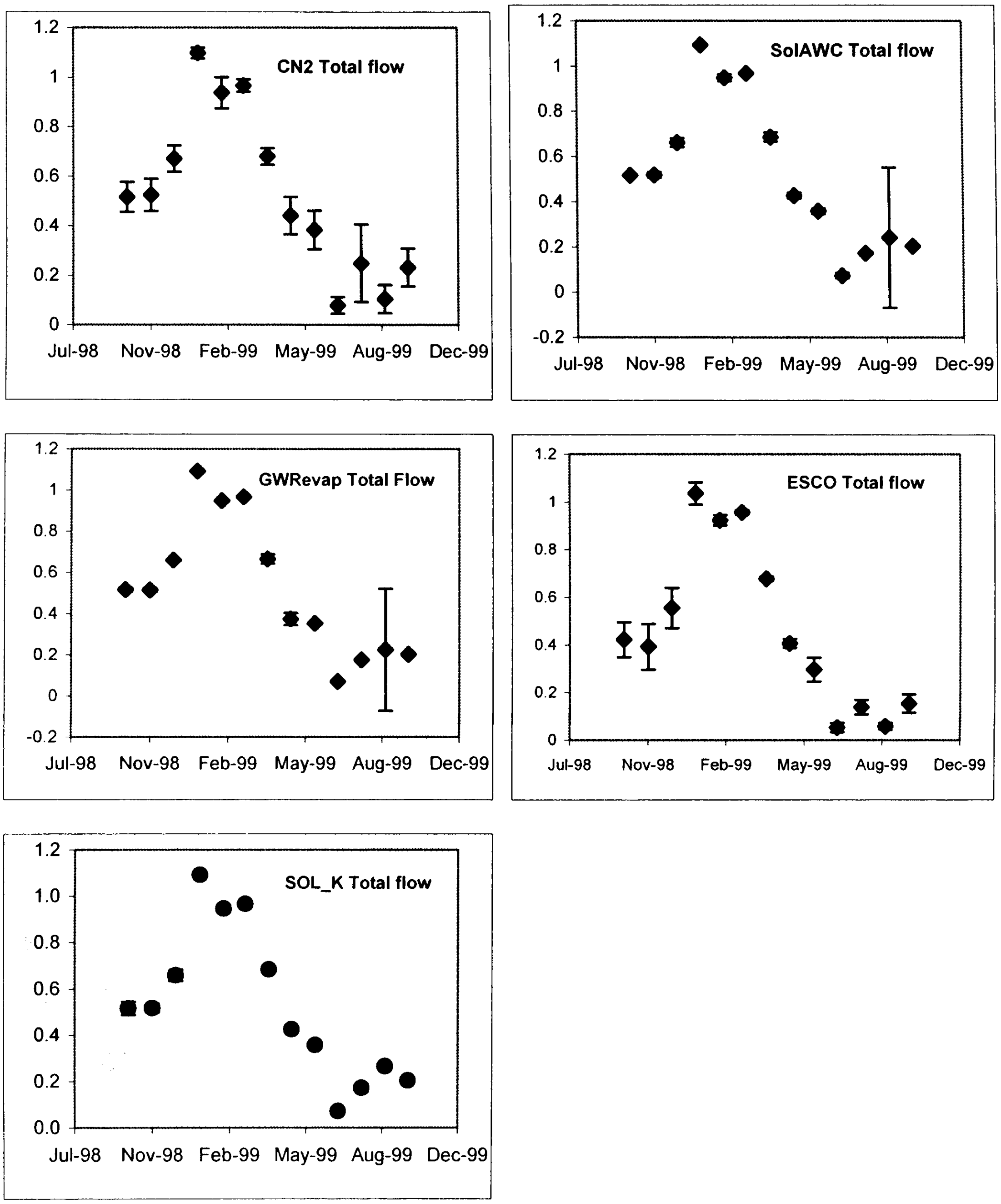

Figure 9.12 Sensitivity plots of monthly flow for the five parameters listed in Table 9.1. Error bars denote one standard deviation and units are cumecs.

There are two anomalies observed in the response of the model with SOL_AWC and GW_REVAP in Figure 9.12. Particular values of these parameters produce a sharp and uncharacteristic rise in the output as shown by the large error bars. Negative and positive values generate this response in SOL_AWC, whilst values either side of the "offending" values do not. A low and high value of GW_REVAP caused the same response. It is interesting that both wayward responses occur in September. If this happened in all incremental steps it could be associated with some seasonal aspect of management or growth. This is not the case and no logical explanation can be offered for it. Correlation results related to the data in Figure 9.12 were calculated for each month in the final year of simulation. They are not presented here due to the extensive list of values and quantity of figures that would be required. Melching and Yoon (1996) suggest that significant correlations indicate parameter importance. All data were tested using Pearson's Product moment and distributions were assumed to be normal.

The set of correlation coefficients for CN2 are all positive and generally highly significant (average $r_{s,0.05,2,3}$: 0.9593). Only June and July did not have significant relationships indicating CN2 is not important during low-flow periods. The range of the response was higher than most other variables. Otherwise for high flow it is a significant parameter. Di Luzio *et al.* (2002) named this parameter for calibration purposes of flow volume, and so the significant correlations were expected. SOL_AWC gave a varied response from the sensitivity analysis. There were significant positive and negative relationships, and months with no significant correlations. There were no apparent patterns to the results. For instance, positive correlations were found in wet and dry periods, and negative correlations were found in wet conditions. Positive correlations were found in periods of low crop growth, but also no significant correlations in data from two winter months. Because most months of simulation have significant correlations in the data, SOL_AWC must be considered an important parameter, but shows a complex or confused response in sensitivity analyses. Simulated results against the adjusted values of the parameter ESCO showed no significant correlations in any month, but all relationships were positive. ESCO cannot therefore be considered important in terms of sensitivity for the data used in parameterisation of the Stonton Brook. Only simulation data from April and May were significantly correlated with variation in the GW_REVAP parameter. Both were negative whilst all other coefficients were positive. The GW_REVAP controls the depth of soil from which water can be taken for evapotranspiration and can be expected to be high at the height of the growing period when soil water stores are low. It will also have a negative effect on flow at this time. The response of simulated flow to adjustments in SOL_K was also mixed, but mostly positive significant relationships. December through to April, July and October (1999) had highly significant negative correlations whereas all other months, including October 1998, except May were significant positive correlations. The negative correlations generally relate to high rainfall periods whereas the positive correlations relate to low rainfall.

The parameters affecting total flow volume the most (sensitive) is the curve number (CN2) and saturated conductivity of the top layer of soil (SOL_K). This latter value is very variable and difficult to measure properly and so is an ideal alternative for calibrating procedure to those listed by Di Luzio *et al.* (2002). (ESCO) also shows some sensitivity across the simulation period but is somewhat confused and follows no apparent pattern of rainfall or plant growth. Simulated flow displays no sensitivity to ESCO and there are limited responses when adjusting SOL_AWC and GW_REVAP.

The same procedure was carried out on the baseflow results as taken from the "Basins.sbs" file. Sensitivity of baseflow to the calibration parameters is shown in Figure 9.13. Unlike total flow there are no obvious anomalies in the results. Visually CN2 and ESCO produce the greatest response in the baseflow output, and can produce a reduction of the peak of baseflow shown in Figure 9.7b. SOL_K has an intermediate response during high flow, whilst SOL_AWC and GW_REVAP produce lower responses still. Small adjustments in flow can be achieved by SOL_K, which is something of a surprise given the controlling effect that saturated conductivity has on groundwater infiltration. Correlation coefficients between the baseflow simulation and variation in parameter values for CN2 are all negative and significantly correlated in all settings except for two months - July and September, which are still negative. Of the significant correlations seven are highly significant. This indicates that as the potential for infiltration increases the flow in the river decreases as would be expected. All correlation coefficients for the SOL_AWC parameter are positive except one – September. All those in the period November to July are highly significantly correlated to baseflow predictions. October 1999 is significantly correlated whereas October 1998 and August 1999 are strongly but not significantly correlated. All ESCO data have positive correlations with simulated baseflow but only one is significant (September). This indicates that the coefficient allowing adjustment of the depth of soil from which evapotranspiration can be drawn is not a sensitive parameter. Only two months of the GW_REVAP data show significant correlations (April and May) and these are both negative. June is also negative but all the rest are positive but insignificant relationships. This reflects the response of total flow on GW_REVAP adjustments and is associated with the high biomass growth during this period. The SOL_K correlations are all highly significant and negative. Although SOL_K is the most sensitive of all parameters tested with baseflow it only illicit a small response in baseflow and is therefore limited for calibration purposes.

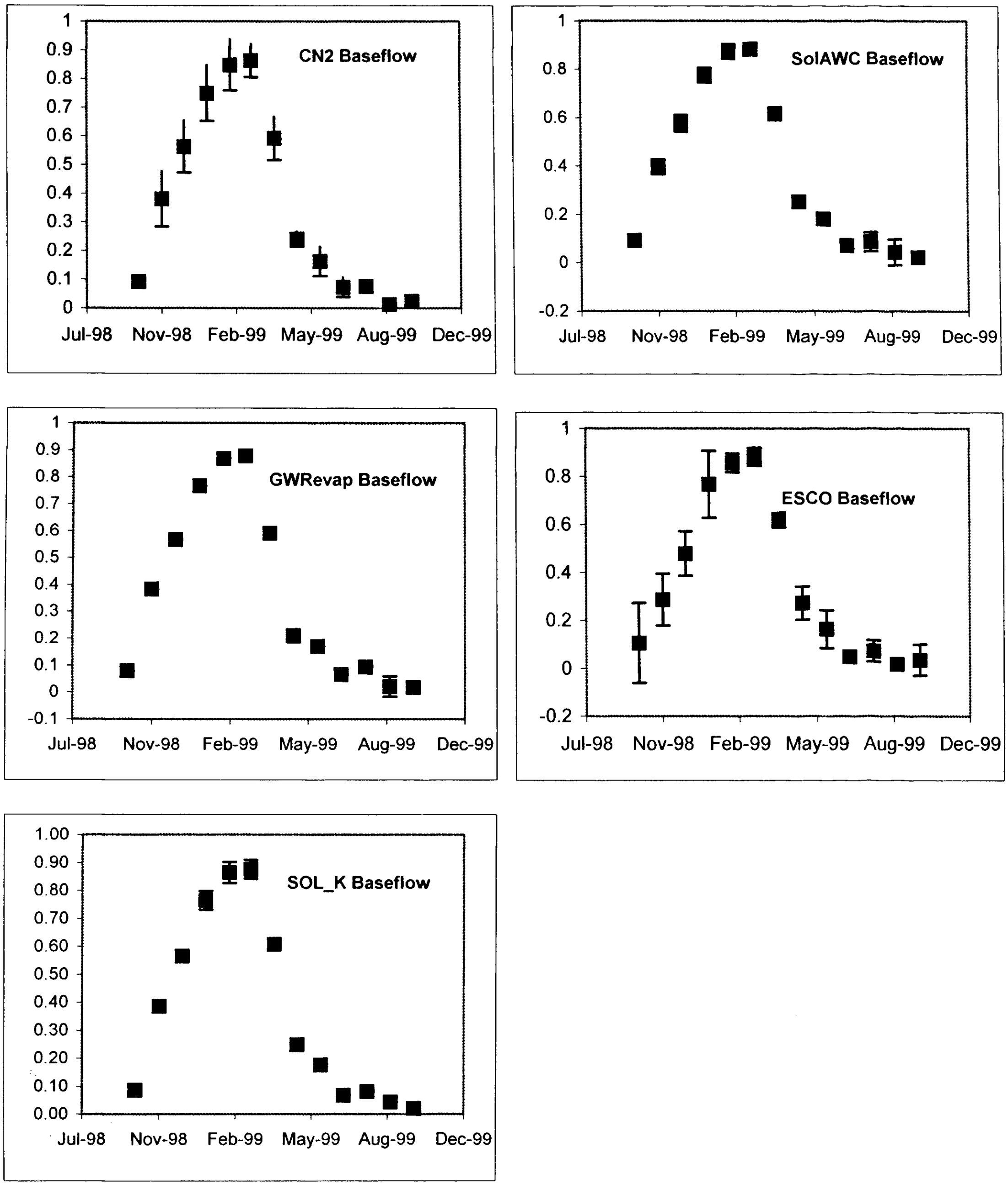

Figure 9.13 Sensitivity plots of monthly baseflow for the five parameters listed in Table 9.1. Error bars denote one standard deviation and units are cumecs.

Results of the sensitivity analyses conducted on stormflow are shown in Figure 9.14. Similar anomalies to those seen in total flow are present in the SOL_AWC and GW_REVAP results indicating these values affect primarily the surface runoff rather than baseflow. CN2 is again the most visually sensitive of all parameters tested. Anomalies exist again in the September values for SOL_AWC and GW_REVAP but otherwise the response of stormflow to these two parameters is low. The ESCO parameter has little effect on the prediction of flow within the river.

Correlation coefficients for CN2 against stormflow are all positively correlated of which only two are not significant – June and July. Of those that are significant, seven are highly significant. The range of response that CN2 illicit in the stormflow predictions is high and is therefore CN2 is considered to be very sensitive and useful for calibration purposes. The response of stormflow to SOL_AWC is again varied with negative and positive significant correlations as well as non-significant negative and positive responses. The range of response is low excepting the anomalies in September in response to both high and low values of SOL_AWC. The months of April and May show significant negative correlations for GW_REVAP. Only September's data are negatively correlated with stormflow, which is for forest and pasture, a period of growth. All other months' data have positive correlations but are not significant. The range of response in the stormflow is low. The correlations between ESCO values and stormflow simulations are largely insignificant but all positive. Only the months November to January are significant. ESCO has had little influence on total and baseflow but does demonstrate some effect on stormflow. Correlations between stormflow predictions and SOL_K parameter values are all highly significant except for the month of October 1999. February and March are positive whilst all other months display negative relationships.

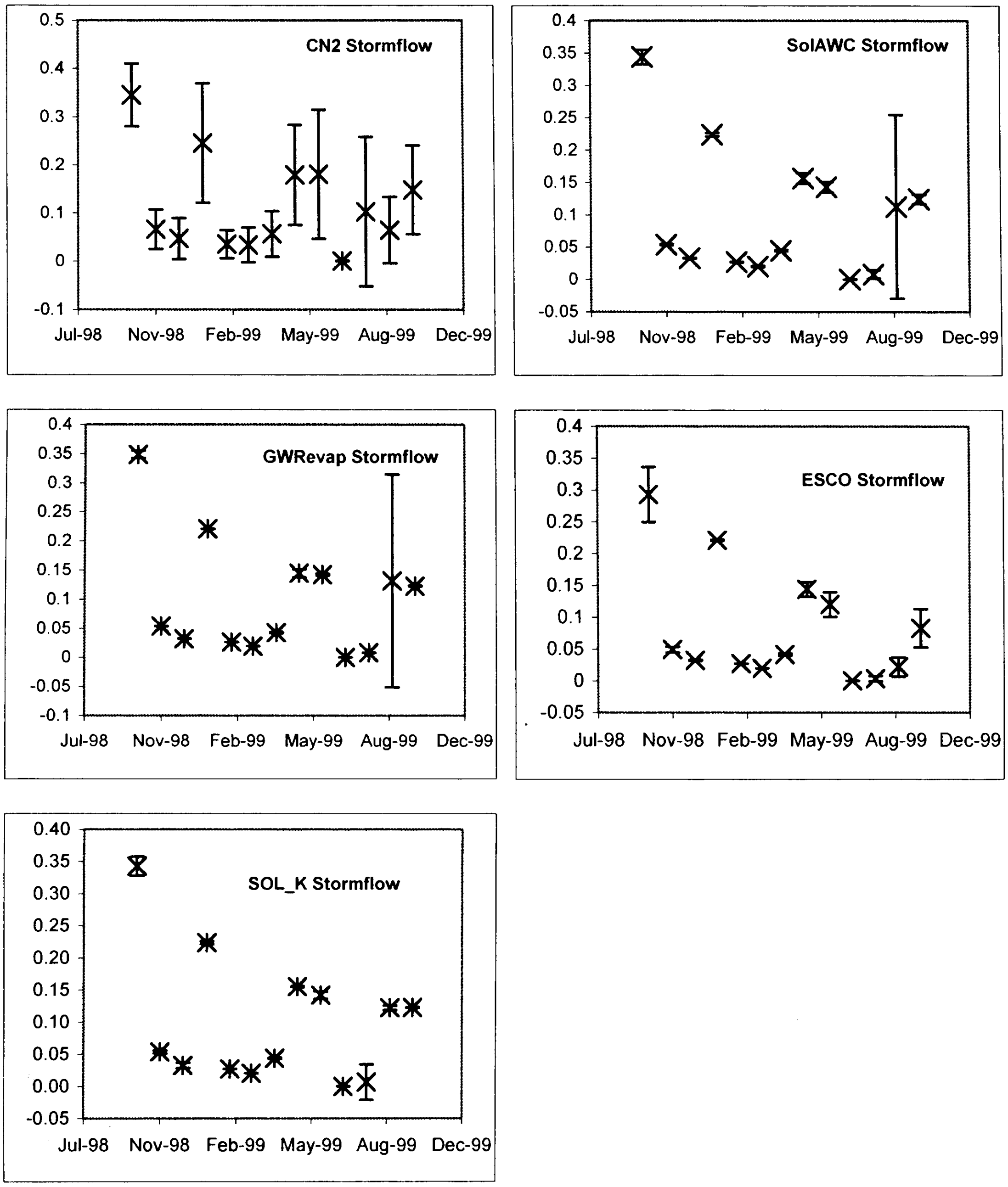

Figure 9.14 Sensitivity plots of monthly baseflow for the five parameters listed in Table 9.1. Error bars denote one standard deviation and units are cumecs.

9.3.2.2 Assessment of phosphorus modelling

Although the hydrological components have been shown to perform poorly an assessment of the P-transport can still be carried out. Simulated P-losses and measured P-losses are shown in Figure 9.15. Notwithstanding the indication above that P-losses are possibly lower than they would have been if stormflow were simulated adequately, the P predictions were an order of magnitude greater than the TP measured in the river. The difference between measured and simulated values of TP loss has a coefficient of variation of 72.43 indicating the match in patterns are better than from AVSWAT99. The mean difference between the two data sets however, is 2723.82 indicating the prediction is adrift by a much larger margin. Phosphorus transport was overestimated by a factor of 13.6. The PBIAS value was -92.6 kg reflecting the gross overestimation of P-loss by AVSWAT2000. Surprisingly the PME value was –94.58 and better than the estimate from AVSWAT99 even though the discrepancy between simulated and measured P-loss was larger. P-loss was however, still inferior in performance than the simple persistence model (PME <0) and therefore, unacceptable.

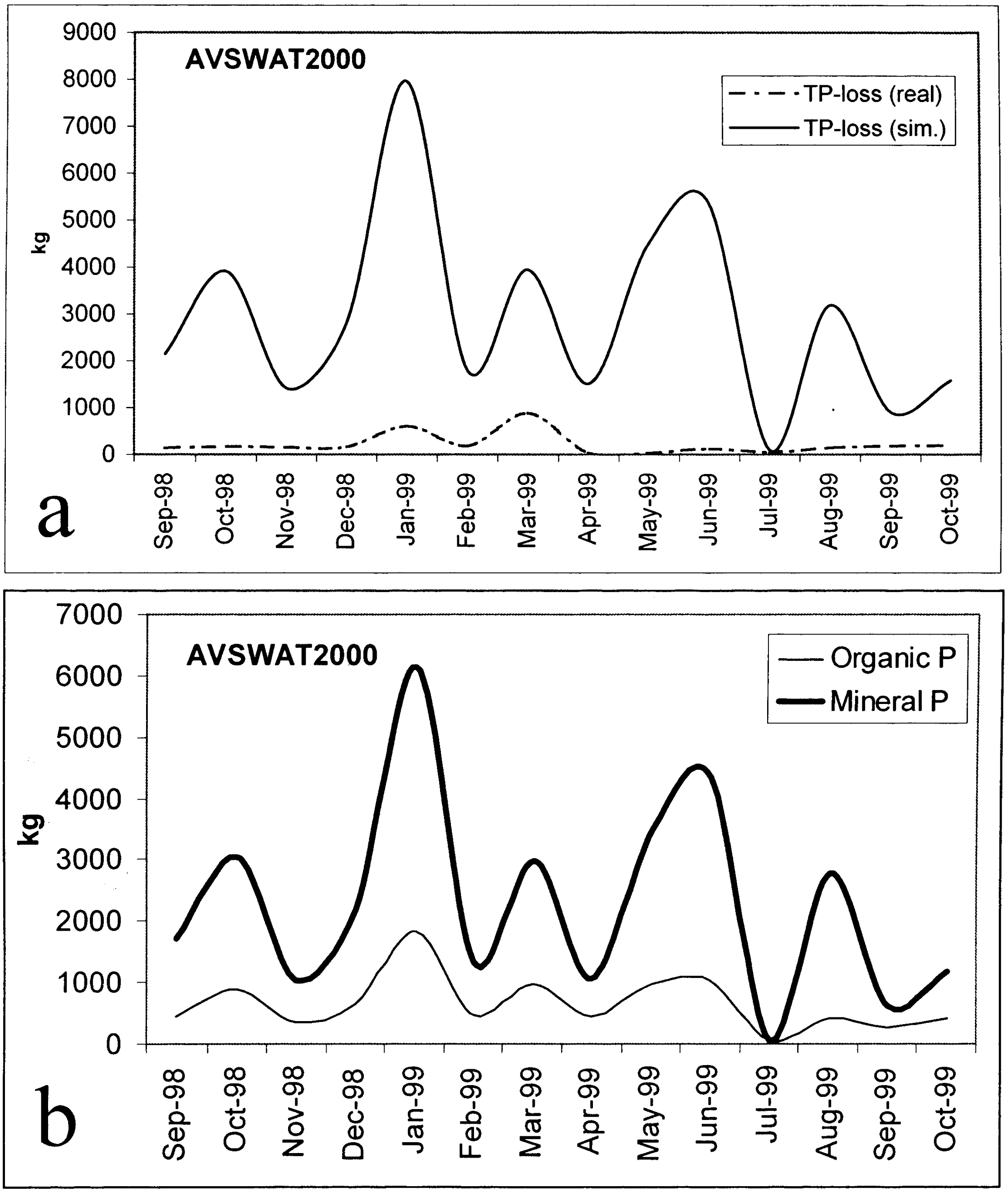

Figure 9.15 Graph a) contains simulated and measured total phosphorus losses, and Graph b) charts the fractionation of mineral and organic P. The simulated losses are overestimated by an order of magnitude, whilst the mineral and organic fractions have a directly proportional relationship. Note the zero values of P-loss coinciding with zero stormflow indicating all P-transport is simulated during runoff events.

P-transport is correlated with runoff events, which would suggest that the P-losses would increase if baseflow were adequate for the given scenario. There are also large predicted P-losses during spring and summer months corresponding with large estimated surface runoff events. Although there are several substantial rainfall events in spring and summer they are not shown in the instream flow. This may be due to the problems in rainfall data as already discussed, but the breakdown in baseflow and surface flow indicates some cause for concern. Vegetation is very mature during this period and should reduce raindrop erosion and increase transpiration. Subsequently, modelled surface sediment transport should contain less sediment. It can be seen in Figure 9.16 that sediment losses are directly proportional to TP-loss.

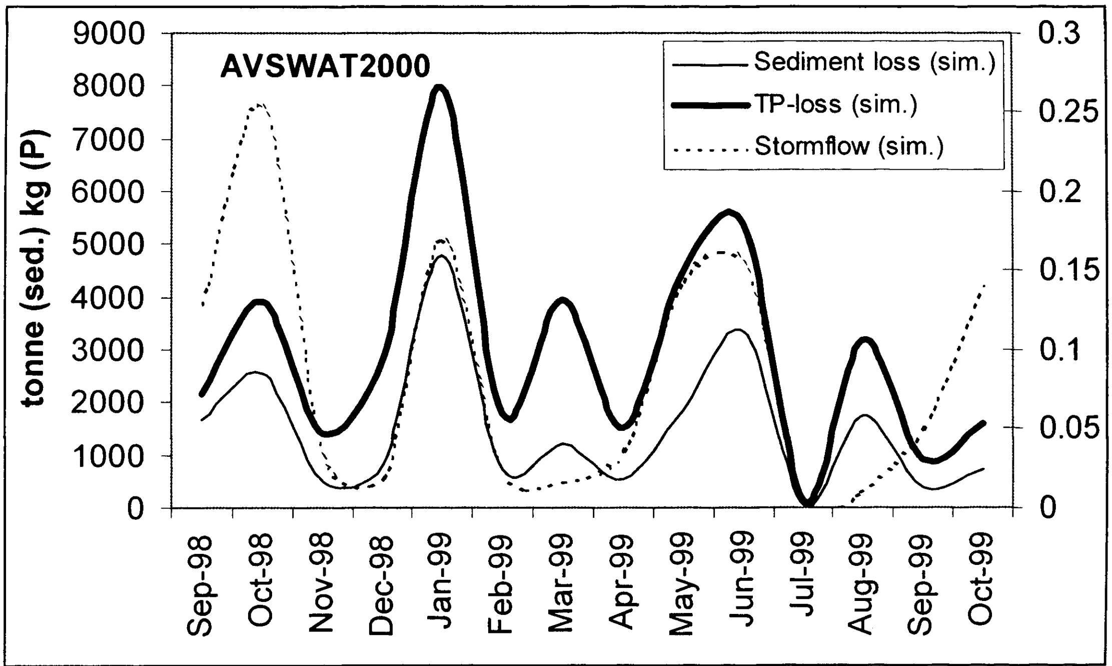

Figure 9.16 Sediment and total P losses plotted against stormflow.

The breakdown of P-losses into mineral and organic P forms provides an insight into how AVSWAT2000 models the transport of these two fractions. The proportions are similar to those reported by Kronvang (1990) but the relationship is too linear. In real systems, the relationship between mineral and organic P is complex, not correlated, and seldom linear (Kronvang, 1990). During high baseflow organic P generally declined in magnitude and inorganic P increased. Figure 9.15b however, displays a very highly significant linear correlation ($F_{0.05,2,13}$: 121.02) between simulated mineral and organic P.

Whilst P-losses are controlled in simulation by sediment loss, sediment losses are not strictly controlled by surface flow as seen in Figure 9.16. Sediment losses corresponding to the first peak in stormflow are proportionately lower than the second. There is however a small peak in sediment and P losses during March indicating some independence of sediment loss with surface runoff. This does not account for the gross overestimation of P-loss. The main problem is therefore due to one or all of the following:

1) Overestimation of surface runoff, which in turn overestimates sediment transported to the river channel

2) Quantity of sediment losses are overestimated which subsequently overestimates the quantity of P transported to the river channel

3) An overestimation of P carried by sediment particles

4) Overestimation of soluble P carried by runoff

These points are now investigated. A probable underestimation of surface runoff has already been demonstrated. P-losses are therefore not directly associated with an overestimation of stormflow, and 1) above can be eliminated. Figure 9.16 shows that sediment transport is largely associated with stormflow but are the sediment losses reasonable? The simulated monthly average sediment loss was 348 kg Ha^{-1}, and the predicted total annual losses from the whole catchment were 17892 tonnes. Catt *et al.* (1998) found values of between 800 and 18000 kg Ha^{-1} for experimental hillslope plots in the UK. Brazier *et al.* (2000) reported average monthly losses of 56.25 kg Ha^{-1} from four hillslope plots in the UK with sandy loam soils. Morgan (2001) gave soil loss values for 24 sites across Denmark, Spain, Greece and Nepal ranging from 330 kg Ha^{-1} to 913 kg Ha^{-1}. The sediment transport estimated by AVSWAT2000 therefore falls within an expected range for a lowland catchment in UK. Assuming a typical sediment P content of 540 mg P kg^{-1} (Chambers *et al.*, 2000), the average monthly sediment loss can be estimated from the measured P-loss. Thus the sediment loss for the Stonton Brook catchment was estimated at 91.17 kg Ha^{-1} per month, or 4682 tonnes annually across the whole of the catchment. AVSWAT2000 therefore overestimates sediment loss by a factor of 3.8. Surface flow is additionally underestimated and this figure therefore is likely to increase on correction of surface flow. Item 2) above therefore is partially responsible but does not account for the majority of P-loss excesses.

The concentration of P on sediment can be calculated using the output variables sediment P (SEDP, kg P Ha^{-1}) and sediment yield (SYLD, tonne Ha^{-1}). Division of the former by the latter and conversion to mg kg^{-1} provides values between 47 and 100 mg P kg^{-1}. These values are much lower than the range found in the literature of between 324 and 1168 mg P kg^{-1} (Chambers *et al.*, 2000). Sediment P is therefore underestimated by a factor of around seven, and point three above can be excluded.

The output variable SOLP (kg Ha^{-1}) records the quantity of soluble P lost. The results show that AVSWAT2000 simulated a maximum of 55 kg of soluble P and a minimum of zero kg per month during the final year of simulation. The soluble P-loss across the catchment for the whole year was 274 kg. Evans (1998) reported that soluble P formed more than 50% of TP. AVSWAT2000 therefore underestimates soluble P transport when compared to the measured TP of 2.59 tonnes. P-loss overestimation therefore must be caused by the quantification of mineral P or organic P (item 4), and is independent of surface runoff or sediment.

The variable ORGP_OUT is reported in kg P, and is the amount of organic P carried by the river in the time step. In this simulation the monthly average organic P-loss for the whole of the catchment was between 49.87 kg P, and 1835 kg P. The lower figure was coincident with zero surface runoff in July and the higher figure for the month of January. Annual predicted loss of organic P from the catchment was 7.89 tonnes compared with measured TP losses of 2.59 tonnes. Annual predicted losses of mineral P (MINP_OUT) was 27.39 tonnes whilst the monthly averages were between 45.46 and 6129 kg P. AVSWAT2000 therefore overestimates TP-loss by excessive quantification of transported mineral and organic P.

9.3.3 RAVSWAT simulations and analyses

The RAVSWAT model was parameterised using exactly the same set of data used in AVSWAT2000 with the exception of rainfall. It has been shown that the Hallaton Croft data most closely matches the pattern of flow in the Stonton Brook. For this reason only rainfall data from Hallaton Croft were used and all other databases were excluded from parameterisation. All choices for model components, e.g. potential evaporation model, were identical to the simulations performed with AVSWAT2000.

9.3.3.1 RAVSWAT hydrological results

Results of flow, baseflow and stormflow are shown in Figure 9.17. The mean difference between simulated and measured flow data was 0.13 cumecs, and is closer to the measured data than from AVSWAT2000. The coefficient of variation was 82.4%. This value is again lower than the value obtained through AVSWAT2000 indicating that the pattern of output matches the instream data more closely. Both values are lower than the results from AVSWAT2000 indicating that improvements have been achieved. PBIAS results for RAVSWAT were slightly higher than AVSWAT2000 at –32.52 cumecs, again indicating slight overestimation. The estimate of PME was better with a value of 0.66, which shows better performance than a simple persistence model (PME >0), and is therefore of an acceptable standard. It is also closer to the optimum value of 1 than AVSWAT99. Simulations of baseflow and stormflow in Figure 9.17b are more realistic than those obtained with AVSWAT2000 in terms of storm differentiation.

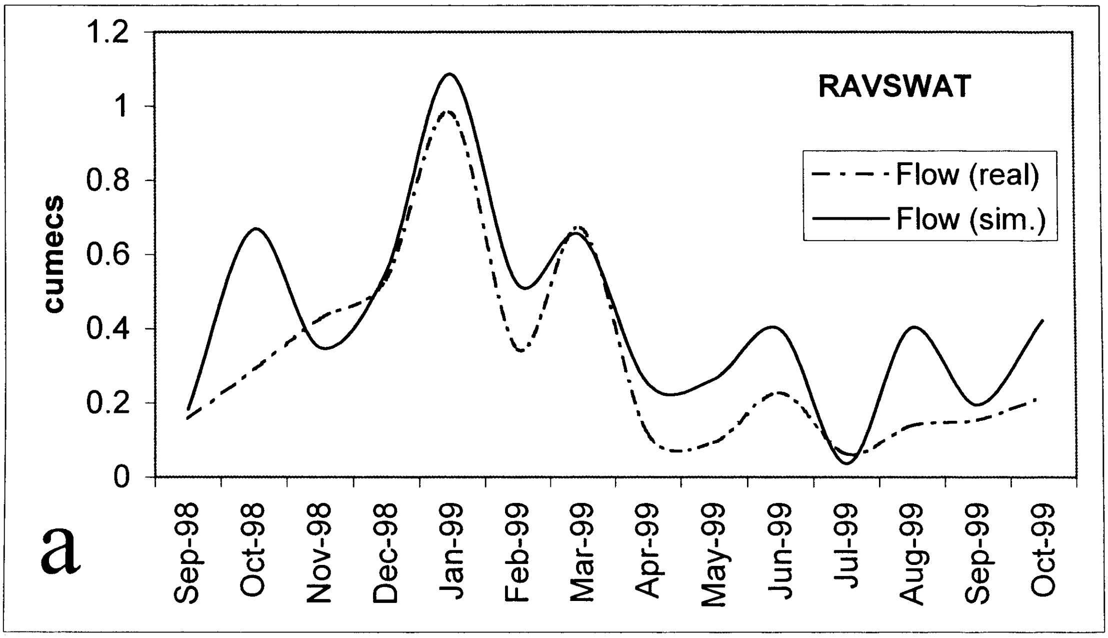

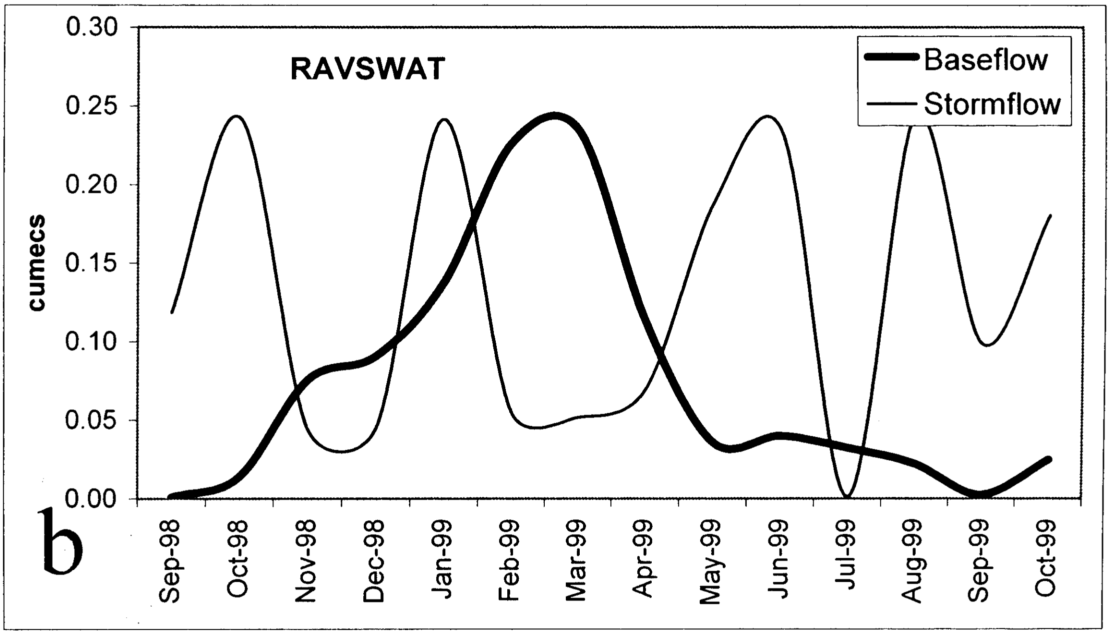

Figure 9.17 Results of simulations using RAVSWAT. Graph a) contains measured and simulated river flow and b) divides simulated flow into baseflow and stormflow.

The simulated and measured magnitudes in the troughs are more similar indicating good baseflow/stormflow differentiation. The intense storms of March 1999 should register in surface runoff but do not. Late spring, early summer and late summer stormflows are overestimated as with AVSWAT2000. There also appears to be a false ceiling to the peaks. All four major peaks fall within 0.01 cumec of each other. A simulation was performed using just rainfall data from Hallaton Croft but had a negligible effect on base and stormflow.

Reasons for the improvements in the hydrological component of RAVSWAT can be seen in Figure 9.18 and 9.19 where LAI and plant biomass are plotted. Plant growth occurs in all years apart from oilseed rape. Additionally, wheat, barley and flax are harvested as specified in the management file. The results still have a few anomalies and may be due to the unavailable additional data required for RAVSWAT.

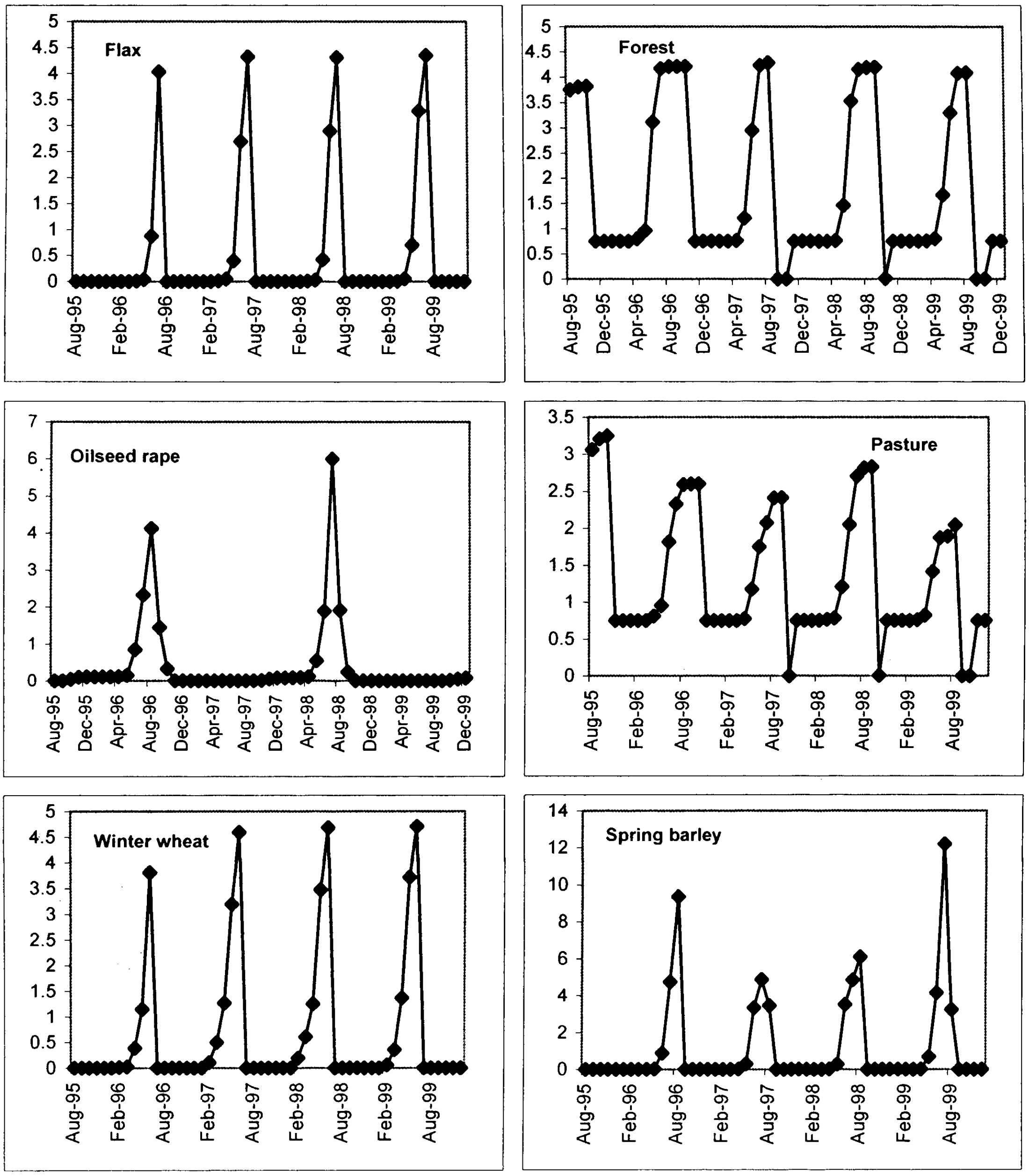

Figure 9.18 LAI curves for six land covers as simulated by RAVSWAT. Units are m^2/m^2.

Oilseed rape is only grown for years one and three and is not harvested in July as specified. Several permutations of oilseed rape management parameters were tried but with little effect on output. Winter growth is not modelled in any of the crop types except for oilseed rape, and does not compare well with the growth curves in Figure 4.2. Perennial growth problems still occur in growth simulations of forest and pasture. The drop of growth and LAI to zero for forest in years 1997, 1998 and 1999 is logical but it does not happen in years 1995 and 1996.

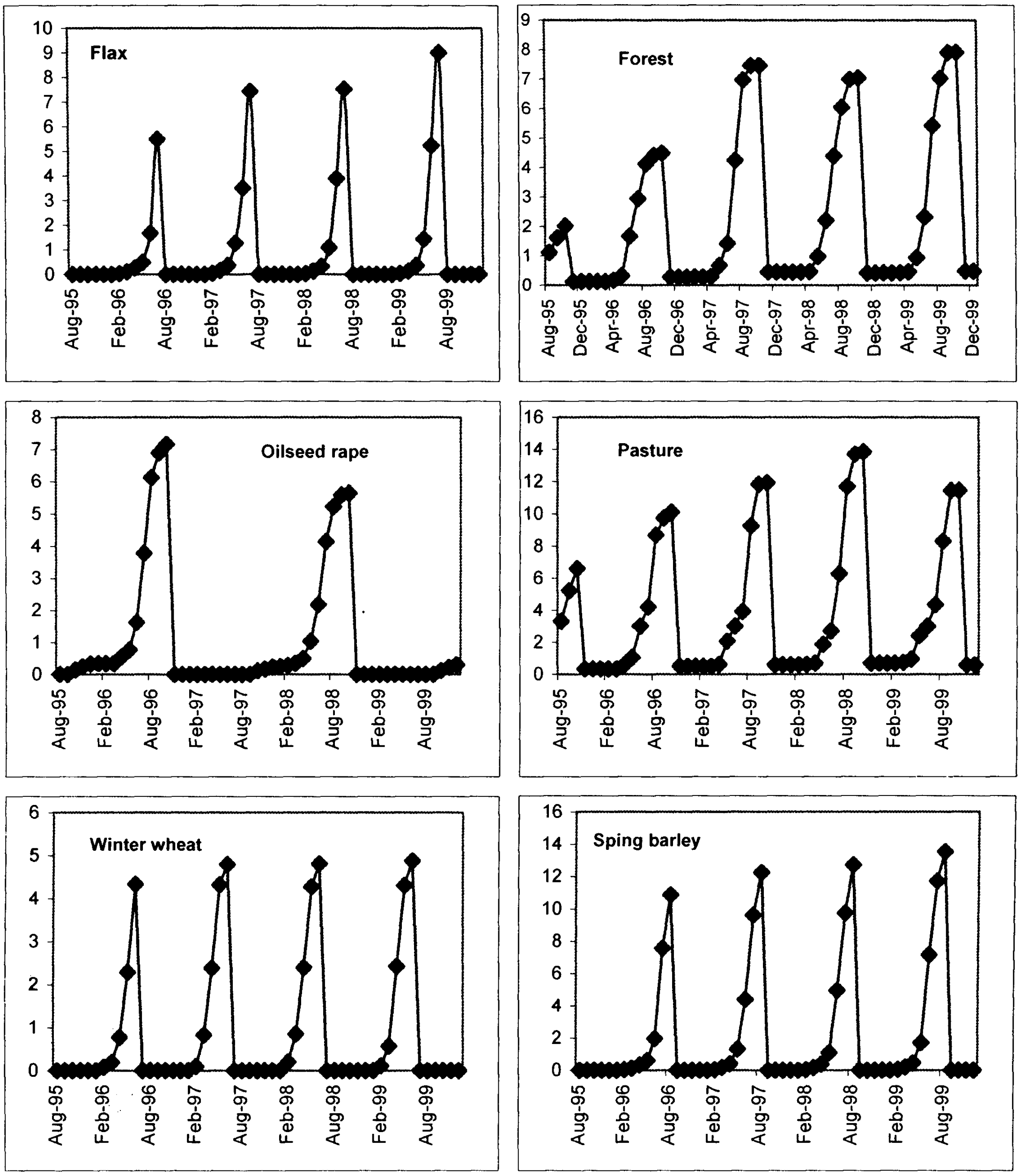

Figure 9.19 Biomass curves for the six commonest land cover types simulated by RAVSWAT. Various options were tried for oilseed rape but the results could not be affected. Units are tonne Ha^{-1}.

Simulated temperature plant stresses for RAVSWAT are plotted in Figure 9.20. Stress across crops appears to have reduced in this simulation, but crop growth season has also been shortened for most crops. Temperature stress for flax and barley appears to be modelled well. Wheat has been modelled with no stress during the winter months but was sown in the autumn along with oilseed rape, which is stressed during the winter. Temperature stress for forest drops during the winter but only for a period of one month.

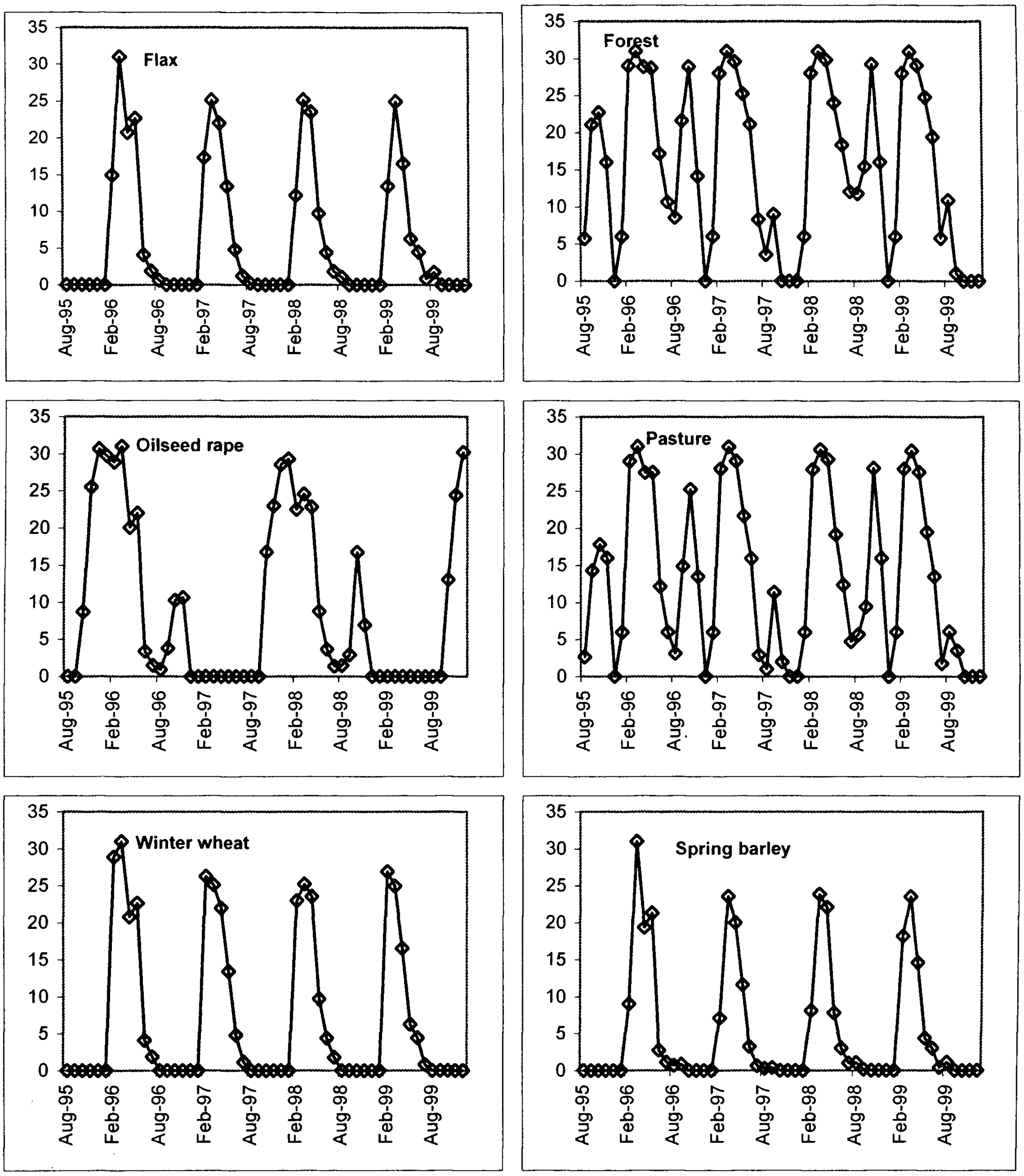

Figure 9.20 Temperature stress modelled by RAVSWAT for six land cover types. Units are days in which plant stress occurred.

Simulated nitrogen stress is shown in Figure 9.21 for six land cover types. All crop stresses appear higher than expected for intensive agricultural management. Forest is the only land cover type that suffers low stresses. A simulation was performed with additions of fertiliser above that given in the literature to force nitrogen stresses down. Twice the amount of fertiliser was added but with no noticeable improvement on the results shown here. P-loss did increase in this simulation. In this additional simulation vegetation growth of wheat was observed to return to a similar pattern of that found in Figures 9.7 and 9.8. The only changes made affected the fertiliser regime.

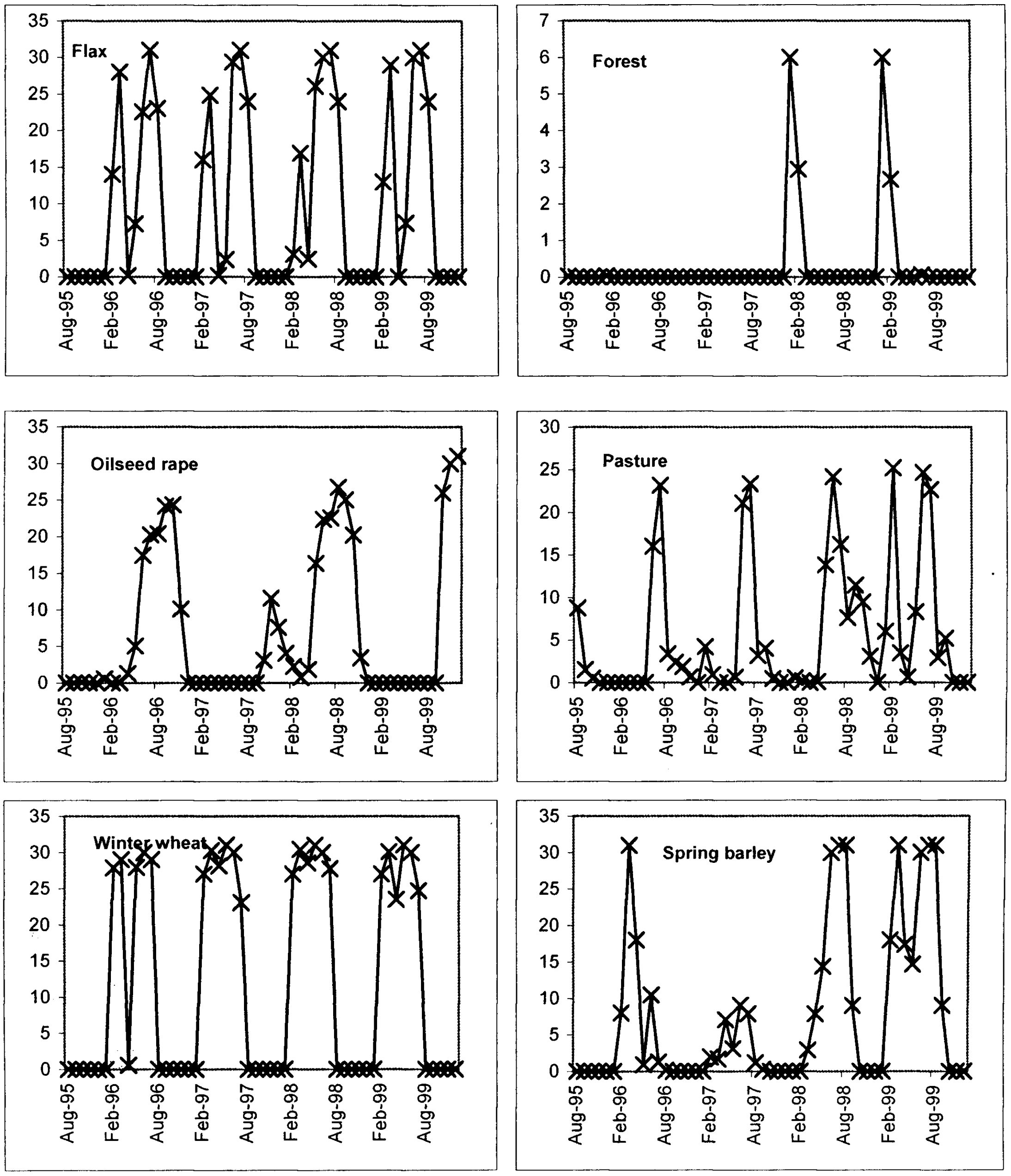

Figure 9.21 Nitrogen stress in six crop types as simulated by RAVSWAT. Units are days in which plant stress occurred.

9.3.3.2 RAVSWAT P transport results

P-losses are overestimated in RAVSWAT by a larger amount than in AVSWAT2000 as shown in Figure 9.22. Surface flow has been altered in RAVSWAT by the correction of baseflow programming errors. Larger amounts of P transport were therefore expected. The mean difference between simulated and measured P-loss was 6774 kg. The coefficient of variation for

RAVSWAT was 72.1% which is marginally closer to the pattern achieved by AVSWAT2000. A PBIAS value of -3134 kg was obtained supporting the large difference between measured and simulated flow. The PME analysis gave a value of –588 indicating an unacceptable prediction, and much worse than from AVSWAT2000.

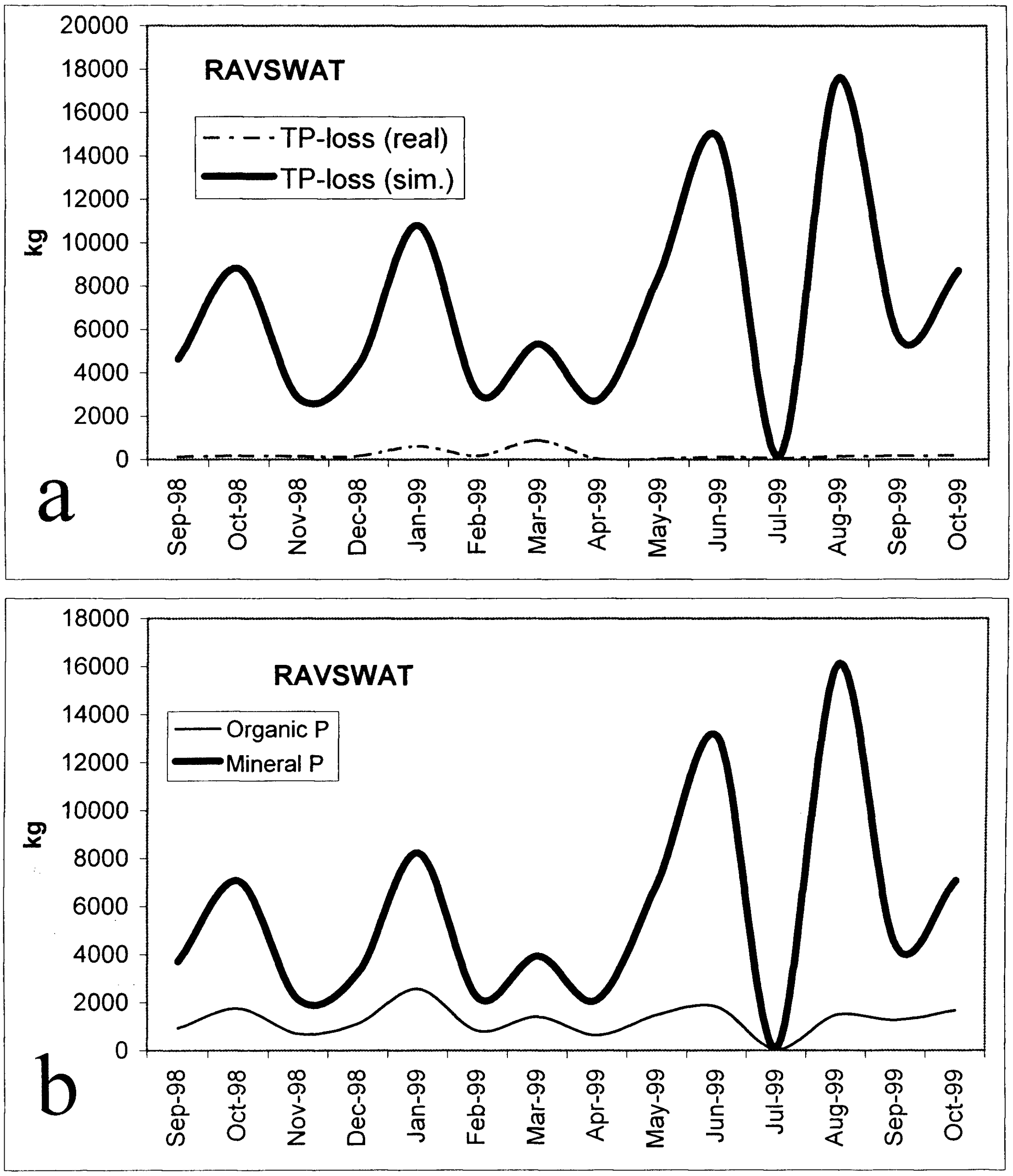

Figure 9.22 Results of total phosphorus loss from simulations using RAVSWAT. Graph a) shows simulations and measured TP loss. Graph b) shows division of mineral and organic P. Note the diminished appearance of measured P-loss in a) compared to the highly overestimated simulation of P-loss.

9.3.4 RAVSWAT simulations with MLE land cover map

The RAVSWAT model was parameterised in precisely the same way as AVSWAT2000 but included the land cover map classified using MLE (Figure 8.9). Flow results are shown in Figure 9.23 and P-loss results are shown in Figure 9.24. Notwithstanding the problems found in Section 9.3.3, analyses were carried out and any changes in model performance were assumed to occur whether the model was performing well or not. Mean difference between simulated and measured flow was 0.131 cumecs and coefficient of variation 72.7%. The mean is slightly higher than that found with RAVSWAT using the land survey map but the lower coefficient of variation indicates a closer match to the pattern. A value of -32.8 cumecs was obtained through PBIAS calculations showing an overestimation of predicted flow. The estimate of PME was 0.68 and is closer to the optimum value of one than previous simulations. RAVSWAT simulates flow more precisely with MLE land cover map but with less accuracy.

The magnitude of stormflow compared with baseflow is slightly higher than in the previous simulation. Baseflow is lower in comparison to stormflow as shown by the magnitude of flow in the troughs of measured flow. P-losses were therefore expected to rise.

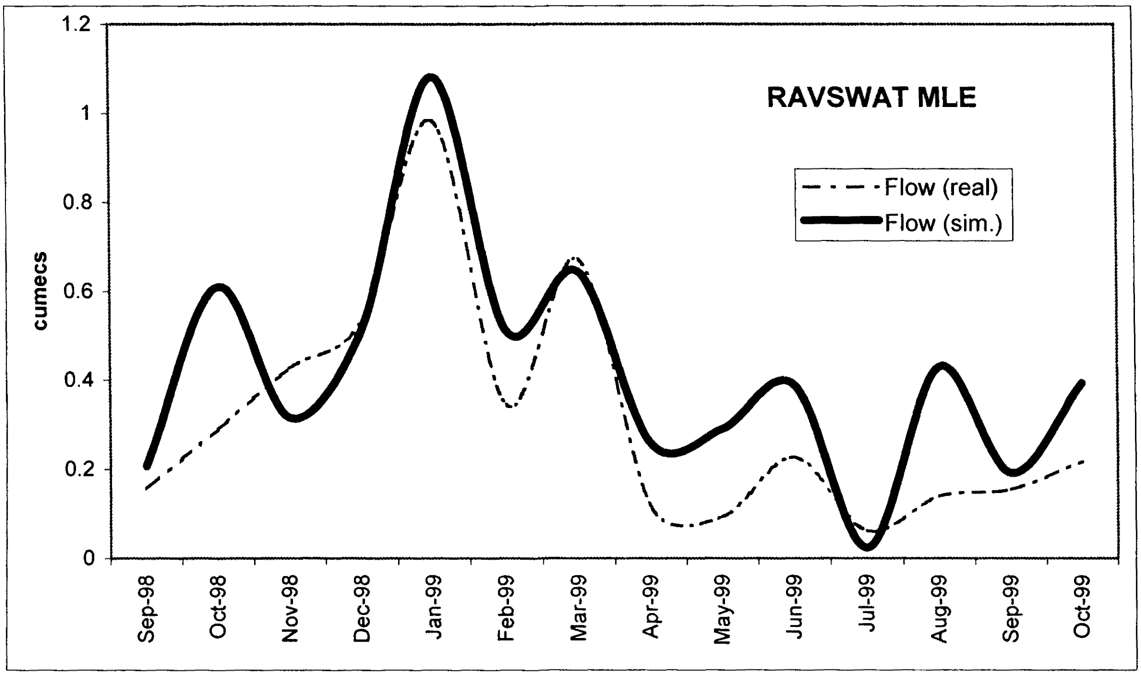

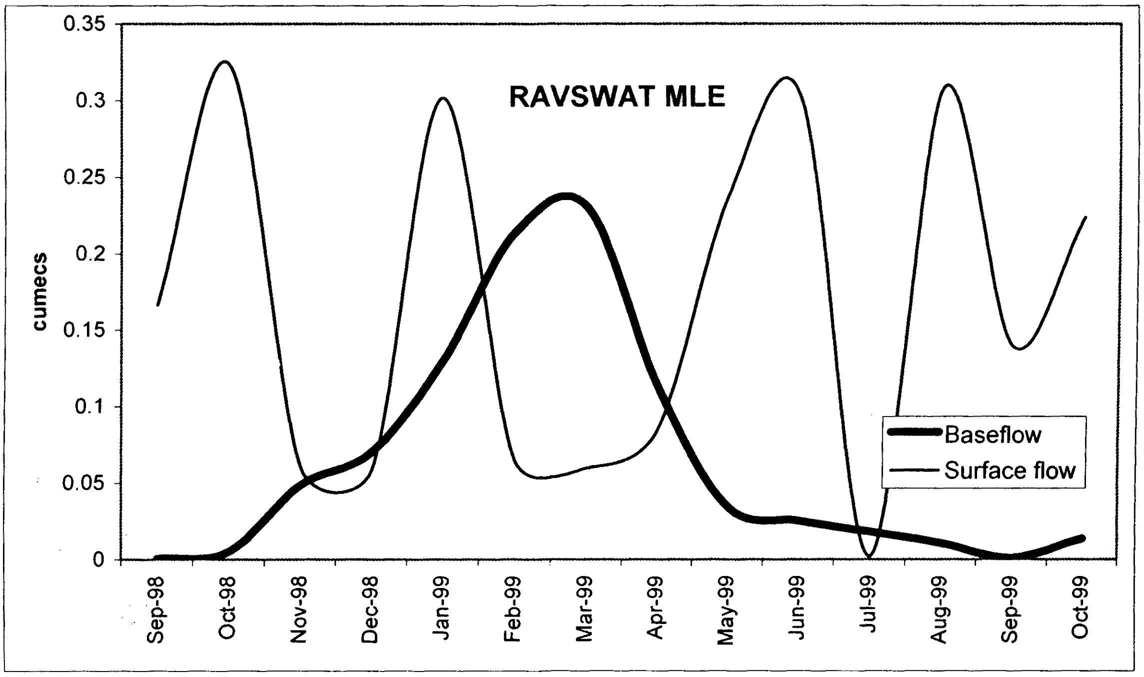

Figure 9.23 Plots of: a) measured and simulated flow and b) baseflow and surface flow using RAVSWAT and MLE classification land cover map.

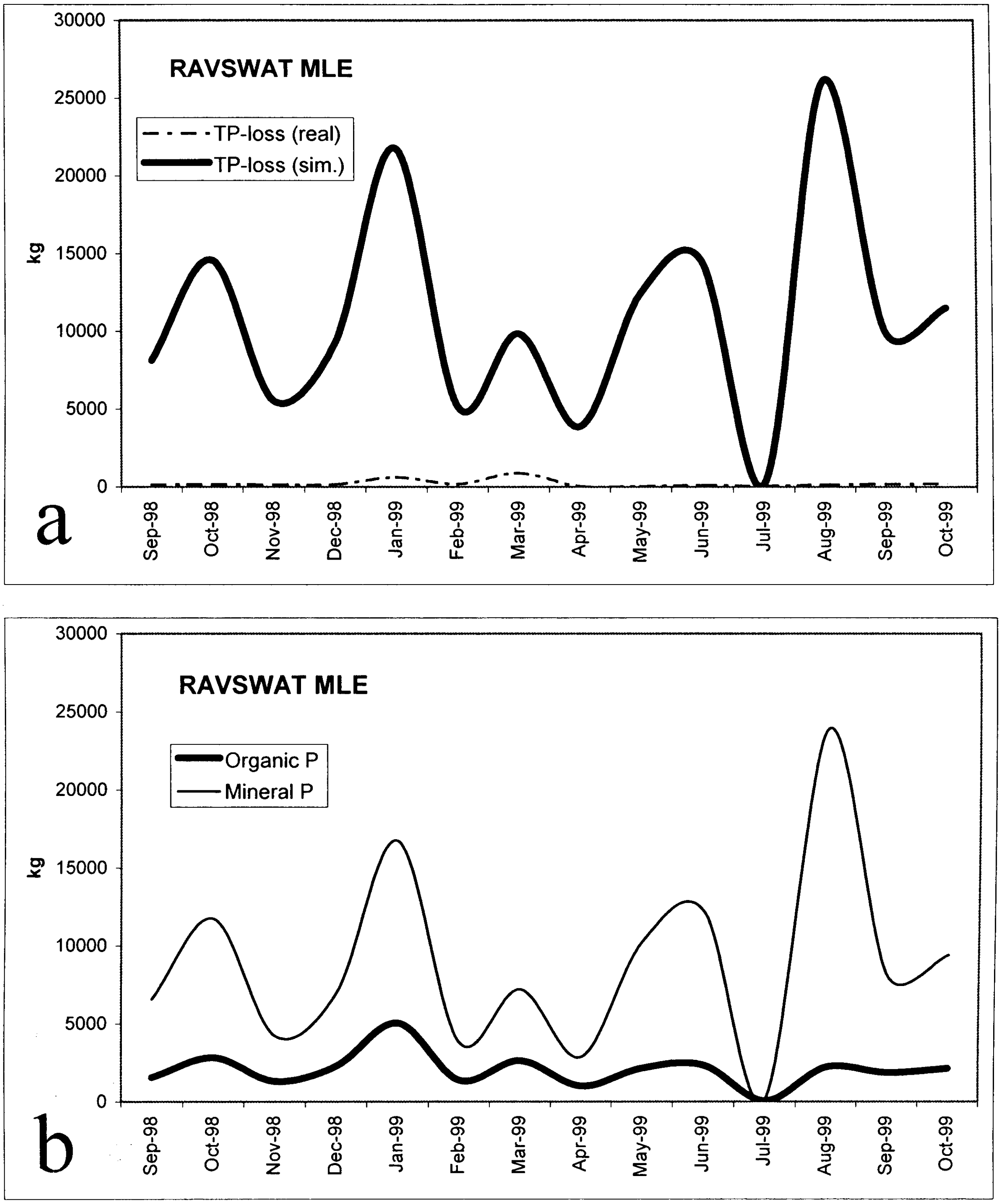

Figure 9.24 Predicted TP-loss plotted against measured. Measured losses are barely discernible across the bottom of graph a).

Differences between measured and predicted P-loss was an average of 10695 kg and had a coefficient of variation of 63.8%. The overestimation of P-loss therefore increased by using the map derived by MLE classification. The PBIAS value of -4898 cumecs reflects the huge discrepancy between measured and simulated P-losses. A negative PME value of –1339 was found indicating the poor and unacceptable performance of RAVSWAT in predicting P-loss.

9.3.5 RAVSWAT simulations with land cover map derived from unsupervised training

The RAVSWAT model was parameterised again using exactly the same set of data and information except for the land cover map. The land cover classification derived from unsupervised training (Figure 8.10) was used in place of the classified map based on MLE. Hallaton Croft rainfall data were used on their own. All choices for model components, e.g. potential evaporation model, were identical to the simulations performed with AVSWAT2000. Results of the flow simulations are shown in Figure 9.25.

The average difference between measured and simulated monthly flow was 0.123 cumecs and is the narrowest of margins yet. Coefficient of variation was 72.14%. The PBIAS calculation gave –30.28 cumecs indicating a smaller overestimation in all but the AVSWAT2000 simulation. The PME value was slightly higher with 0.719. This is closer to 1.0 than all the other values and again indicates the dynamics of flow is modelled better using this land map. Stormflow and baseflow predictions are very similar to the last simulation.

P-loss prediction is lower than the results obtained using the MLE derived map but higher than all others. These results are shown in Figure 9.26. Calculation of PBIAS gave a figure of –4093 cumecs, and PME was calculated as –972.5. Both these figures reflect the gross overestimation of P-loss by RAVSWAT.

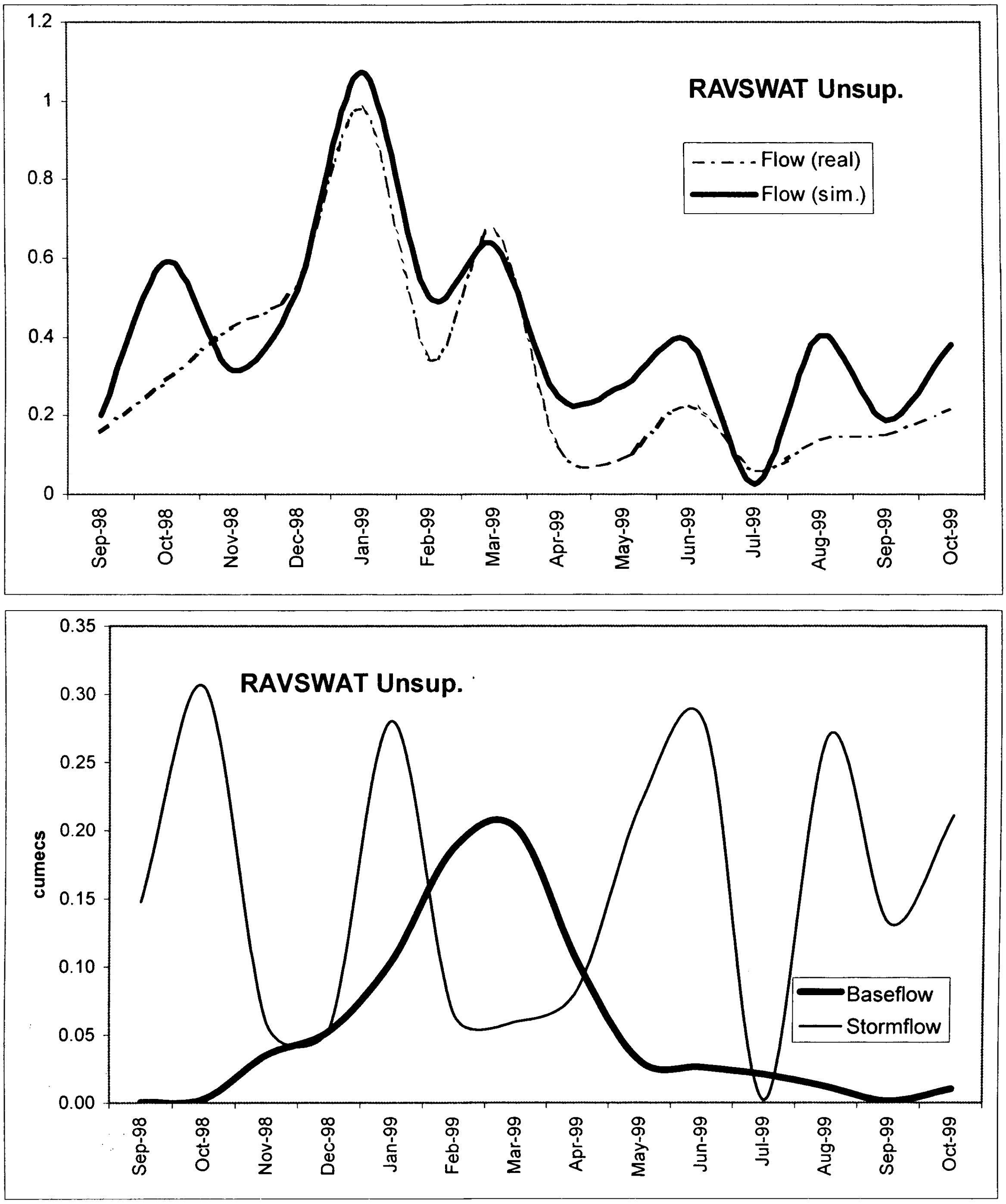

Figure 9.25 Graph a) contains simulated and measured flow and graph b) contains division of flow into baseflow and stormflow. The model was RAVSWAT using the land map derived from unsupervised classification.

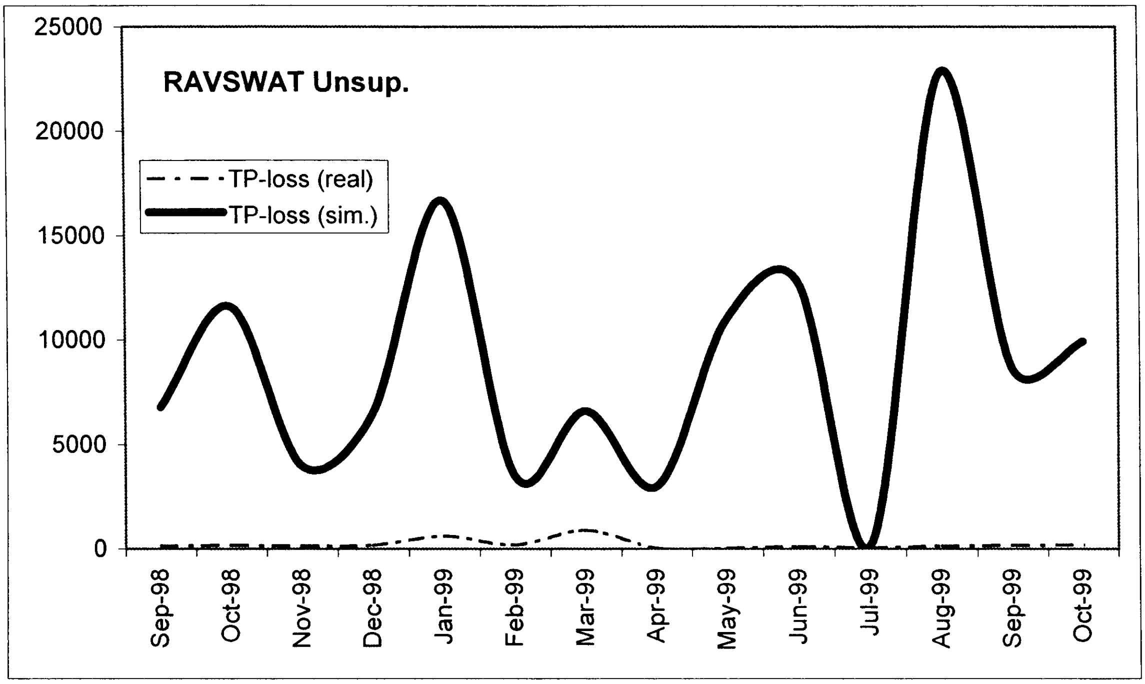

Figure 9.26 P-loss simulation and measurement by RAVSWAT using the unsupervised training derived land cover map. Measured data are dwarfed by the gross overestimation of predicted P-losses.

The PBIAS and PME results for flow from each of the AVSWAT versions are summarised in Figure 9.27. Results from AVSWAT99 are not included as they clearly were poor results. PBIAS indicates overall differences between predicted and measured data whilst PME indicates acceptability of model performance. Values close to zero are preferred in the former whilst values close to 1 preferred in the latter. Ironically AVSWAT2000, the model deemed to provide the least suitable output, obtained the best result in terms of proximity to the measured flow. It obtained the lowest PME value, however, indicating it was the least similar in fit to the measured data. According to the resultant values of PBIAS and PME the best all round performance was found using RAVSWAT based on the map derived from unsupervised training of the multi date SAR image. It had the second best result from PBIAS and the best result from PME. However it is known that the land survey map gave the most accurate image of land cover and these results must be considered within that knowledge.

PBIAS and PME results for the P-loss from each simulation are plotted in Figure 9.28. The best performance came from AVSWAT2000 but was still overestimated by a factor of 12. The other simulations are adrift by a much larger margin and highlight severe failings by the SWAT model to forecast P-losses in a catchment.

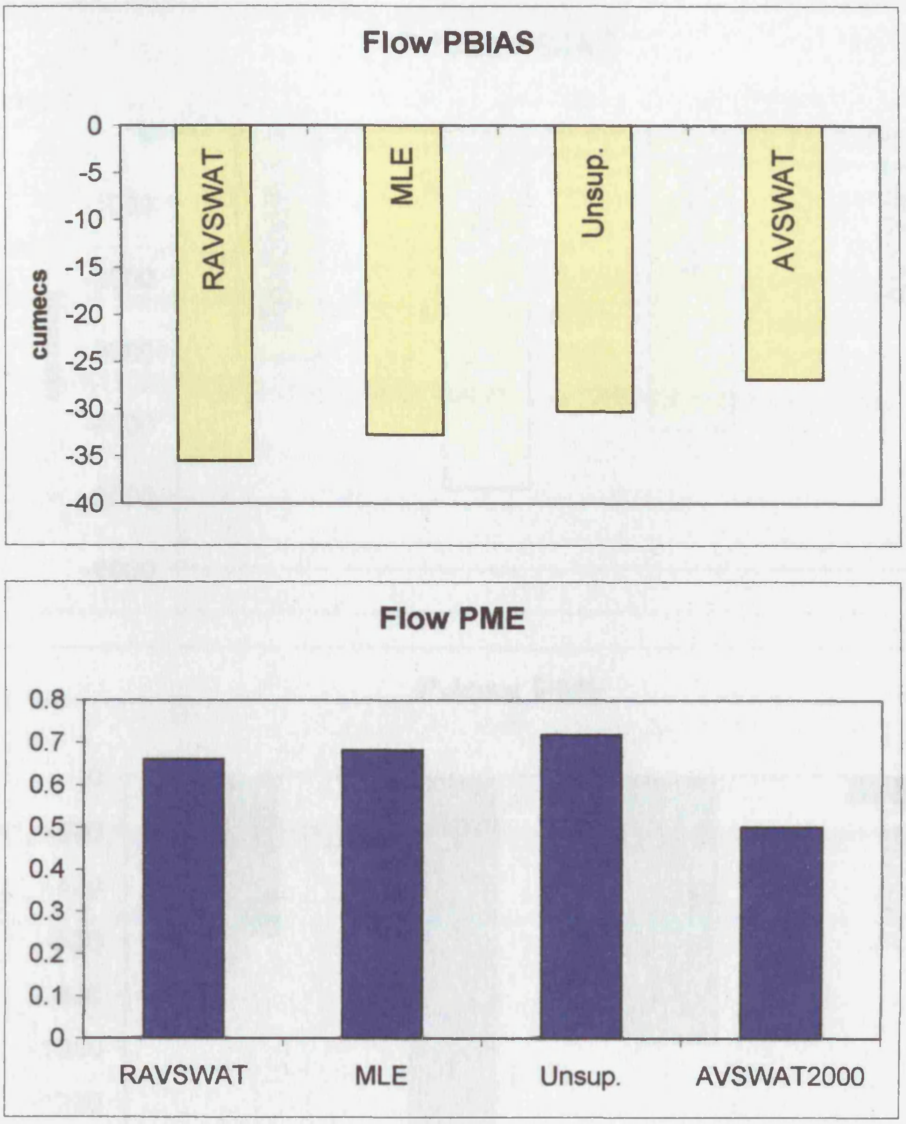

Figure 9.27 Summary of PBIAS and PME analyses for flow simulations.

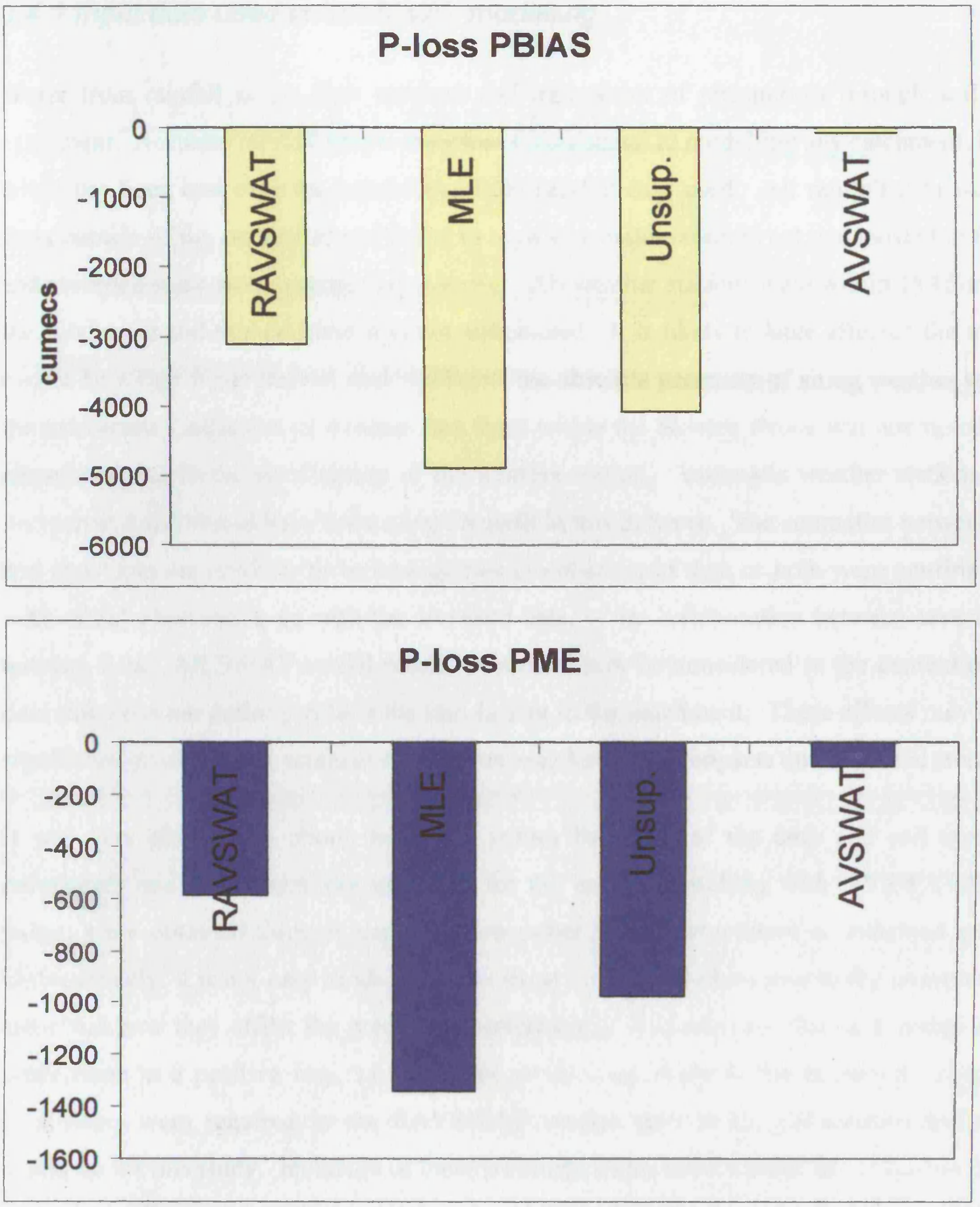

Figure 9.28 Summary of PBIAS and PME analyses for P-loss simulations.

9.4 Discussion

There are three overall aspects within these results that require discussion: the input data which can be broken down into field survey data and remote sensing data; the measured in stream data upon which the model output is compared, and the model itself. It is imperative that all are assessed as each one influences the perception of the model performance. These areas will now be discussed in the following sections.

9.4.1 Input data used in the SWAT modelling

Water from rainfall is the flow medium and transporter of phosphorus through soil and the catchment. Accurate rainfall data is therefore fundamental to modelling any catchment, but some doubt has been cast over the suitability of the rainfall data used. All rainfall data were taken from outside of the catchment and failed to register a major storm event that existed in flow data and recorded some storm events that were not. All weather stations were within 15 kilometres of the catchment and this problem was not anticipated. It is likely to have affected the modelling output by a significant degree, and highlights the absolute necessity of siting weather stations in the catchment. Collection of weather data from within the Stonton Brook was attempted but was abandoned due to the unreliability of the weather station. Automatic weather stations are now inexpensive and would have been a huge benefit in this instance. The anomalies between rainfall and flow data are unlikely to be ambiguities in either set of data as both were confirmed either with visual observation as with the instream data, or by collaboration between several sets of weather data. All SWAT model results must therefore be considered in the context of rainfall data that does not entirely reflect the rain falling in the catchment. These effects may not be so significant in cumulative totals over time, but may have large impacts on individual storm events.

It was very difficult to obtain measured values for many of the crop and soil management parameters and some were not available for the earlier modelling with AVSWAT99. Some values were obtained through improvisation rather than measurement or informed guesswork. Unfortunately, it is not easy to identify how these individual values owe to the uncertainties and error and how they affect the predictive performance. It is possible that such errors affect the predictions in a positive way, i.e. make the predictions closer to the measured values. More parameters were required in the RAVSWAT version than in its predecessors and were not available for this study. Inclusion of these parameters may have worked for or against the model accuracy. There were 905 parameters in AVSWAT and ten or so further coefficients for adjusting output (Neitsch *et al.*, 2002), although not all are applicable to hydrology and phosphorus transport. This project only gathered about 90 of those parameters, and of those, 20 were "best guesses" based on other people's judgement or obtained through standard values from similar crops. Default values in the SWAT databases have also been questioned and it is possible such errors have been overlooked. Saturated conductivity of soil is known to be highly variable and not easy to measure (S. White, Silsoe College, Centre for Environmental Studies). Values for this parameter were obtained through Silsoe Soil Science centre and related to soil associations in the UK. Saturated conductivity in the Stonton Brook could be very different from these "national" values measured from elsewhere. This variable was one of the most sensitive parameters used in this project and could contribute to calibration if required. Without more thorough analyses of the model and the data on which it is based, values such as this could wrongfully parameterise AVSWAT and mislead the importance of parameters or processes. Analyses such as GLUE, FORA or mollifiers must be used to acquire a better understanding of the influence input data has on a model's performance. Identification of the important parameters can then prompt more research into these values. Some optimism must also be derived from such a large model with so many parameters providing an accurate picture of the flow within the river. The most sensitive of parameters and/or processes within the revised SWAT must be robust enough to "ignore" many of the errors identified in this thesis. Conversely, sample size is only "1" in this instance with the single simulation, and the proximity of the predicted flow to measured flow could be by random chance (accuracy). Alternatively, storm events can be seen as being replicated and therefore the pattern of events appears to be robust (precision), but this should be expected since rainfall is the driving force through the model.

The land maps used as input to SWAT also generated interesting responses in the predictions. It is known that the land survey map is the most accurate of all land cover maps but induced a less accurate response from SWAT than the land maps derived from remote sensing. All other conditions entered into SWAT were equal and thus indicates that error in the derived land cover maps forced a reaction in the model towards a more positive outcome i.e. another indication of obtaining good (in this case better) results for the wrong reasons. The land survey map is not without error but its error is less than either of the other two maps as shown in Chapter 8. For this reason the apparent improvements in the results must be treated with some caution. It is acknowledged that error exists in the rainfall data and acceptance of the absolute values of PBIAS and PME should not be accepted blindly. Instead, these values should be considered in terms of proximity to the results obtained with the best information i.e. the land survey map. It is therefore suggested that the land map classified using MLE and supervised training is closer to optimum data than the land map classified using unsupervised training. Although this appears subjective and dismissive of the evidence supplied by Gupta *et al.* (1999), it is based on objective knowledge of the three land cover maps. The improvements in results also indicate that error exists in the other inputs, modelling assumptions, code, or all three, with a resultant total of the discrepancy between the measured and predicted values when parameterised with the land survey map.

The remote sensing exercise has demonstrated through the modelling procedure, that predictions of flow from SWAT, parameterised with land cover maps derived from SAR imagery, can be acceptably close to the optimum method of land cover sampling. Utilising SAR imagery on larger catchments, and therefore more economical scales, is a feasible alternative to walking the catchment and recording each crop in each field. Further improvements in accuracy, and therefore input error, could be achieved through combinations of LandSAT TM and SAR imagery.

9.4.2 Instream data

The flow and phosphorus data have been shown to be reliable and relatively robust in acquisition and analyses. They are considered a good benchmark against performance of the SWAT model. Without such intensively sampled flow and phosphorus data the comparisons between predicted values and measured values would have been much less robust. The instream data have identified the shortcomings of the rainfall data and if used in further analyses such as GLUE or FORA, they would disclose more information about uncertainties and error within the input data or the modelling processes. Without these data it would be impossible to make good comparisons and indicates use on ungauged catchments is unwise.

Only daily data were used in comparison of the modelling due to the prohibitively long simulations based on hourly time steps. Sub-daily data were available from the instream sampling regime and if more time was available or computing power vastly increased, comparisons could have been made at the hourly time step. This could disclose how the model behaves at finer resolutions of time at the sub-storm event scale. Costs of intensive sampling regimes are high but with the increasing flexibility and economy of auto-samplers will become cheaper in future.

9.4.3 SWAT model performance

Early simulations with the AVSWAT model were far from satisfactory. AVSWAT99 was unstable and unpredictable. Parameterisation processes, such as discretisation, did not work as required. The predictions were inaccurate and did not reflect what was happening in the catchment. Flow was underestimated by more than half and P-losses were overestimated by an average of 70%. After the initial simulations with AVSWAT99 more parameter values became available such as SCS curve numbers (Morgan, 2001) and these were used in AVSWAT2000. This may be part of the reason that AVSWAT99 did not perform as well as the later versions. Additionally, many of the values contained within the standard SWAT databases were wrong (S. Anthony, ADAS Wolverhampton), and some of these were only corrected prior to using AVSWAT2000. Additionally, AVSWAT99 did not simulate artificial land drainage and would have resulted in a faster response within flow in the river. It would also have overestimated the P-loss to a greater extent than it did.

For the above reasons AVSWAT2000 was used on release. It was not without problems but was much more consistent and stable compared to AVSWAT99. Most importantly, the various discretisation schemes worked as documented in AVSWAT2000. All requests were performed with ease except for daily output. The data checking routine also proved very useful. Although limits of some parameters are set too low e.g. LAI (<8), it verifies whether parameter values fall outside of their allowed range. Additionally, the model failed to perform at all if required files or images are missing from the project folder. Simulations were performed on the catchment discretised on a grid at the scale of the DEM (50m). No attempt was made to change this scale but it is acknowledged that scale dependent investigations on the SWAT model are required.

After most of the work had been conducted on AVSWAT2000 a revised form became available through K. Karayanan (Institute of Water and Environment, Cranfield University). Various programming errors in the SWAT model had been identified and corrected. The main problem areas were plant growth, crop management and groundwater management. Some of these factors had been corrected in the revised version (RAVSWAT) but not all. Additionally, more crop and agricultural management parameters were required for the new version and were not available for the Stonton Brook. The revised model was used nonetheless and produced better hydrological results. The balance between baseflow and stormflow was improved and improvements were obtained in modelling vegetation growth and plants stresses. There were still anomalies in the results concerning oilseed rape growth and nutrient stress. AVSWAT2000 and RAVSWAT produced results that were inconsistent with the parameter set used. For example, after the sensitivity analysis of AVSWAT2000, saturated soil conductivity values were reset to original, but subsequent results were very different than before sensitivity analyses were performed. No other parameter value had been adjusted. This was rechecked and it must be concluded that AVSWAT contains programming bugs that causes such random and problematic responses. Concern therefore remains about the reliability of AVSWAT and RAVSWAT until the programming code has been checked and verified.

9.4.3.1 Hydrological modelling performance

AVSWAT2000 performed flow simulation adequately according to PBIAS and PME (Gupta *et al.*, 1999). River flow predictions were recognisably similar to measured data but baseflow and stormflow separation did not appear to work well. The latter two fractions of river flow were never measured, but stormflow was too low in comparison with baseflow. Inspection of underlying model components (baseflow, stormflow output, LAI and plant biomass) revealed that AVSWAT2000 was not working in the way it should. Baseflow comprised the vast majority of predicted water flow and stormflow was consequently too low. Vegetation growth was also poorly modelled probably through management events and plant stresses. Both nutrient stress and temperature stresses were high and crop management events such as harvesting were ignored. These components affect both the hydrology and nutrient transport and were therefore important to investigate before modelling and investigating P-loss.

Sensitivity analyses gave no indication of where the model was failing but revealed anomalies in the effects of two of the five parameters used. The adjustment of SOL_AWC and ground water revaporation (GW_REVAP) produced suspicious responses in the flow predictions. Two values either side of zero in SOL_AWC and two isolated values in GW_REVAP produced wayward responses in flow output. The actual causes for these have not been investigated fully but it is unlikely to be caused by the theoretical algorithms given the wealth of model validation that has occurred on the sub-components. Models such as CREAMS (Knisel, 1980), GLEAMS (Leonard *et al.*, 1987) and EPIC (Williams *et al.*, 1984) have been extensively tested and validated, albeit against US datasets. It is the theory from these models that are used within SWAT.

RAVSWAT was shown to perform better than its predecessor in total flow and in the breakdown of hydrological components. Baseflow and stormflow components appeared to be comparatively better, and the PBIAS and PME values indicated better fit between measured and predicted data than for AVSWAT2000. Breakdowns in simulations of plant processes were also much improved indicating the model performed better internally. There were however still some unexplained anomalies in the revised model. Both models handled the land maps adequately and both had similar patterns of performance between the land maps derived from remote sensing.

Although the successful application of SWAT has been reported on numerous occasions (Bingner, 1996; Manguerra and Engel, 1998; Peterson and Hamlett, 1998; Muttiah and Wurbs, 2001) over a period of seven years, the above problems have not. Klemes (1986a and 1986b) and Beven (1993) have questioned the faith that many scientists place on models and the lack of detailed inspection and analyses of forecasts. This thesis has shown that a model can give realistic predictions even though the underlying processes are unrealistic as in the case of AVSWAT2000. Thorough testing and validation of models are therefore essential. Without trust in the modelling theories there must be blind faith in the modelling forecasts (Beven, 1993; Brazier *et al.*, 2000). Development of physically based models can help dispel scientific doubt that inevitably accompanies blind faith. If however, thorough assessments are not carried out it will not be known whether the model and theory is doing what it is supposed to do. Simple breakdowns of variable output can identify potential problems in either model theory or data error when output variables are few and well documented. The problem becomes much greater when there are many output variables spread across the catchment as in the case of HRUs. The investigation into hydrological and flow patterns described in this thesis do not go far enough to define the problem but only in which areas to delve further.

9.4.3.2 Phosphorus modelling performance

The SWAT manual (Neitsch *et al.*, 2002) suggests that surface runoff is the only means of P transport in SWAT. This is wrongly reported. The output variable P_GW records the amount of soluble P transported into the reach by groundwater. Concentration of P in groundwater has to be specified by the user and is a constant. This element was not selected in this project and appears to be included in the model as an oversight. It is however, a useful addition to AVSWAT2000.

Modelling of phosphorus by SWAT, regardless of the version, was poor. Flux in P levels followed the same trends as water flow but were always grossly overestimated. Investigations into variable output relating to P-loss showed that it was the calculation of mineral and organic P that was to blame. This sounds an obvious conclusion but there are various other factors that could be the cause. The SWAT model transports P primarily in association with water and sediment contained in surface flow. The soluble component held within the water was underestimated by SWAT and the sediment content slightly overestimated. Surface flow was slightly overestimated but not by the magnitude needed to produce 35 tonnes of P-loss instead of 2.5 tonnes annually. Sewerage data were incompatible with AVSWAT and therefore, not used in the modelling procedure. Inclusion of this small addition would have only increased the predicted losses. It is anticipated that the processes affecting flux in P levels will be appropriate but that the calculations estimating the amount of P are incorrect. It is therefore essential that the modelling components that simulate P processes be checked. The code has been shown to contain a number of critical errors and therefore there are likely to be more. The SWAT model was employed in good faith and algorithms accepted as being good representatives of the catchment processes. The code is available from the SWAT web site and therefore available for scrutiny. It was not inspected in this project.

The model has performed inadequately in terms of P losses and therefore conclusions cannot be drawn on how the land cover maps have affected P loss. It is however likely to follow similar conclusions to the hydrological component once the code has been revised to account for the above problems.

9.4.4 Modelling Summary

The size of SWAT compounds the investigative work that can be carried out on it. Sensitivity analyses carried out here have isolated two parameters that appear insensitive to flow output. These parameters could be ignored in future sensitivity analyses but many more need assessing. Attempts to carry out sensitivity analyses or calibration will encounter the problems outlined in

Section 2.1.4. Equifinality and overparameterisation will need to be addressed. Simple models would not require such efforts. The effects of overparameterisation are to cause any of the above exercises to become unwieldy and laborious. Equifinality however, could obscure the results of sensitivity analyses and confuse whether some parameters are more influential than they should be or vice-versa. Equifinality can also be confused with natural events and is not simply a problem of data or model artefacts. At various times during the measurement period the instream sampling gave the similar flow and P-levels but with different catchment conditions. It is therefore safe to suggest that if different environmental and catchment conditions can give the same output from the Stonton Brook the main assumption of equifinality (optimum parameter set) is inapplicable. It is acknowledged that these doubts existed when the model was selected for use. Further investigation into P-loss is beyond the scope of this project. It would involve scrutiny of the source code or complete breakdown of the output files. Source code for P-loss spans 30 of 215 programs that make up AVSWAT. In light of the findings from K. Karayanan (Institute of Water and Environment, Cranfield University) checking the source code is essential but beyond the scope of this Ph.D. The output variable files involve: (i) five variables in the channel file (.rch), (ii) seven variables from the HRU file (.bsb) and seven variables from the basins file (.sbs). Each variable would have to be assessed together with regard to each crop type and location in catchment. Multivariate statistics such as discriminant analyses would be applicable and disclose which areas and conditions are most influential for P transport in AVSWAT. This method would not however, identify potentially simple programming errors within the source code.

The problems identified here are blatant problems and may not always be as convenient to identify. Once the model code in AVSWAT has been corrected for all processes the model will still require evaluation. Thorough model assessment is time consuming for simple models and requires high levels of computer resources. Applying the model to smaller catchments will reduce resource demands both in data collection and computing power. Complex models can be assessed fully but are relatively more difficult to carry out.

Sensitivity analysis is also a process used in calibration. Calibration on poorly performing models presumes to hide the inadequacies of the model, and may demonstrate how models can be calibrated to provide the right answer for the wrong reasons (Klemes, 1986a; Beven, 1989). The conclusions from this chapter suggest that calibration should not be used as a development tool in hydrological and nutrient transport modelling and only used by the final user in fine scale adjustment once the model has been adequately field tested.

Chapter 10 Conclusions

10.1 Objectives

The SWAT model has been developed to forecast hydrological, nutrient and pesticide variables in large catchments over long periods. It requires a large data set for land cover, crops, soils and agricultural practices. Remote sensing offers some potential to gather some of those variables from across large catchment areas. SAR can provide images that can be used to simultaneously extract: (i) soils data, (ii) vegetation parameters, and (iii) land cover data. SAR images can be acquired throughout the year in temperate zones and can operate independently from weather. Eight SAR images from the European Space Agency's ERS-2 platform were obtained simultaneously to conducting an extensive data collection and field-sampling regime. The data were then analysed and processed and applied to the SWAT model to meet the following objectives:

1) **To establish and maintain an intense river sampling regime for the whole period of nutrient transport modelling. These data will be the benchmark against which the nutrient transport modelling must be assessed.**

2) **To investigate the extraction of vegetation and soil parameters from ERS-2 SAR that could be used in the nutrient transport model.**

3) **To acquire accurate field boundary maps from aerial photography.**

4) **To extract land cover information from the ERS-2 SAR instrument for use as a land cover map in the nutrient transport model and assess its performance.**

5) **To apply a catchment-scale nutrient transport model to a small catchment in lowland UK. The model must undergo sensitivity analyses and analysis of final output.**

The Stonton Brook catchment in Leicestershire was chosen as the catchment upon which the objectives would be tested. This river is a tributary of the larger River Welland, which is an economically important river in the East Midlands. All field sampling was conducted within the catchment for the acquisition of data for:

- Direct input to the SWAT model

- Instream flow and nutrient data

- Land cover types to create a land cover map and classification of the SAR images

- Modelling of vegetation and soil variables against SAR backscatter

Field sampling was conducted for a period of 13 months from September 1998 to November 1999. Eight SAR images were acquired through the ESA Third Announcement of Opportunity.

10.2 Instream flow and P data acquisition

In Chapter 5 the collection of flow and P-concentration data was described. A data logger and pressure transducer were situated near a disused weir at the outlet of the Stonton Brook. The data logger collected data that could be converted to river depth and thus flow using the weir for calibration. Extreme storm events were calibrated using a concrete bridge 15 m upstream from the weir. Data were recorded at ten-minute intervals and downloaded to a laptop once every 6 weeks. Linear regression equations were used to obtain the relationship between flow at the weir and depth at the logger.

Automatic water samplers were placed near the outlet of the Stonton Brook and at Tinwell on the River Welland, approximately 20 kilometres downstream of the Stonton Brook. Water sub-samples were collected at 3.5 and seven-hour intervals and analysed in the laboratory as concentration of orthophosphate. It was assumed that all P in the samples was digested and that orthophosphate was equivalent to TP. Loadings and P-loss was estimated by combining flow and TP concentration. For three periods during the sampling regime the instream sampling equipment broke down. Estimates of flow and P-concentrations were calculated using a cubic regression equation based on the relationship between flow at Tinwell and flow at the outlet from the Stonton Brook. Some anomalies were shown to occur in the resulting data but overall the flow and TP concentrations were accurate and representative of the flow and P fluxes in the Stonton Brook.

- **Flow and TP concentration data collected from the Stonton Brook were reliable and intensive, and acquired data representative of a small river with dynamic flow and P processes. These data were deemed a good benchmark against which the model output could be adequately tested, thus fulfilling Objective 1.**

10.3 Extraction of vegetation and soil parameters from ERS-2SAR images

In Chapter 8 the extraction of soil and vegetation variables from ERS-2 SAR images was investigated. All images were filtered using the Lee filter across a 7x7 pixel block to reduce the effects of speckle. After speckle suppression the images were converted to backscatter coefficients and then georectified. Primary georectification proved to be insufficient and secondary georectification was performed on the Stonton Brook area only.

Estimates of radar backscatter were then taken from the images to investigate the following soil and vegetation responses of backscatter:

1) Soil moisture, organic matter content and soil surface roughness

2) LAI and plant wet biomass retrieval

3) MIMICS radiative transfer modelling

Soil samples were gathered from 15 sites in November and 12 in February from across the Stonton Brook and analysed in the laboratory to provide mean soil volumetric moisture content and soil organic matter content. Additionally, RMS and correlation coefficients were calculated from use of a profilometer. These values were then regressed with corresponding backscatter values.

- **No significant relationships were found between backscatter values and any of the soil variables.**

Mean plant biomass and LAI data were acquired for oilseed rape from seven sites across the Stonton Brook. These were regressed against backscatter values extracted from SAR images corresponding with the geographical positions of the sampling sites.

- **No significant relationships were found between either LAI and backscatter or plant biomass and backscatter.**

An extensive list of vegetation and underlying soil parameters were acquired for wheat and oilseed rape to satisfy the requirements of the MIMICS radiative transfer model. Samples were obtained in May and July for wheat and May only for oilseed rape, from 12 sites for each crop. The MIMICS model was parameterised using these data and results compared with respective backscatter values from the associated SAR image.

- **A good but non-significant relationship was observed between MIMICS output from simulated backscatter from oilseed rape and SAR backscatter coefficients. MIMICS predictions using green wheat gathered in May did not show any relationship with SAR backscatter. The mature wheat in July had a significant**

relationship between MIMICS backscatter output and backscatter coefficients extracted from SAR images.

The objectives of Item 2 have been achieved albeit with little success. Dry wheat and oilseed rape were only marginally successful when using MIMICS to predict the backscatter response. MIMICS is a research tool only and is not yet in the position to predict vegetation parameters from SAR backscatter data.. All other parameter extraction showed no relationships with SAR backscatter values at all. This was potentially due to several factors including sub-optimal SAR characteristics such as wavelength for the type of data this project was trying to model. Results from this section indicates that SAR data shows no promise for aiding the parameterisation of catchment scale nutrient transport models at this stage. Inclusion of remote sensing imagery utilising visible light may provide better opportunities for extracting variables for the above parameters.

10.4 Production of field boundary map from aerial photography

Aerial photographs were collected from the NERC Navajo Chieftain airborne platform whilst collecting other non-optical data. 19 photographs covered the whole of the Stonton Brook with some overlap. Each photo was scanned at high resolution and georectified using a minimum of 15 GCPs. All processed images were amalgamated into a single mosaic image. This image was shown to have high geographic accuracy and was ideal for producing a field boundary map. All discrete land sections were then manually digitised to produce a single polygon shapefile. This shapefile was given attributes according to the land cover type in each polygon based on a complete survey of all fields and other discrete patches of land.

- **An accurate field boundary map was produced defining each discrete plot of land cover upon which land use maps could be based**

10.5 Extraction of land cover data from multi data SAR images

Single SAR images were collected during the months of May June and August. These were processed independently using speckle suppression, conversion to backscatter coefficient and georectified. Al three images were then overlaid to produce a single multi date composite SAR image that contain three backscatter values per pixel instead of the original one. The single multi data image was processed using two classification methods to define the land cover for each plot of land. Several classification schemes were used to assess the full potential but only two were visually good enough to be used. Supervised MLE was accomplished using 67 field sampling points on the Stonton Brook were selected to include the most common land cover types. Supervised training was used to establish land cover signatures. Each signature was then assigned a given land cover type. Various methods of training were investigated to find the optimum. Whole field based training samples provided the best results. This method recognised all land cover types used in the training apart from standing water.

An unsupervised training method was also performed on the multi date image to divide the images into natural signature groupings. Each signature was then assigned a land cover most commonly associated with known land cover in the area. The two classification schemes were overlaid on the field boundary map and the dominant land cover class in each field polygon attributed to the map. Both SAR classification schemes failed to identify small urban areas and roadways. This was due to the resolution of the image and effects of speckle.

Both classification schemes and both land cover maps were assessed for accuracy against the field survey map using error matrices. The two supervised images achieved lower accuracy values of 46% for MLE and 53% for the unsupervised classification, than the derived land cover maps. The map derived from MLE achieved 58% and the map derived from unsupervised classification achieved a small increase to 54%. These accuracies did not meet the arbitrary minimum set by Thomlinson *et al.* (1999) of 85% but they were reasonable. Both were therefore used in SWAT parameterisation.

- **Two land cover maps were successfully derived from radar remote sensing images. The two methods are different in their approach but both relevant to catchment-scale modelling. This satisfies the requirements of objective number four.**

MLE classification using supervised training can be used where adequate *a priori* data are available about the land cover conditions in the catchment. The classification using unsupervised training methods can be used where information about the proportions of land use types is known rather than specific details about each field or plot. The Agricultural Census data would be such a source.

10.6 Application of a catchment scale nutrient transport model

Three versions of SWAT were used in this project but the first - AVSWAT99 - proved to be unstable and gave very poor modelling results. The second - AVSWAT2000 - was used on release and performed much more reliably. All collected variables from Chapters, 4, 6, 7, and 8 were used to build a parameterisation data set and input into AVSWAT2000. Various permutations of the options in AVSWAT2000 were used to find the optimum settings. To ensure the model worked at the beginning and when specifying particular agricultural events, a coarse resolution of catchment discretisation was used. This allowed quick processing of settings and simulations. Finally, the simulations were performed at the highest resolution achievable in

AVSWAT2000 and all land cover and soil classes were represented in simulations. The Hargreaves method of potential evapotranspiration gave more realistic results than the alternatives.

The following was found:

- **AVSWAT99 did not function well and was a poor predictor of flow and P-loss**
- **AVSWAT2000 simulated flow adequately according to PBIAS and PME calculations. It did not simulate underlying hydrological and crop variables well, and was shown to ignore certain specified crop management events.**
- **Substantial differences between rainfall and flow data were observed suggesting that rainfall records were inappropriate for the Stonton Brook even though the nearest was situated only two km and the furthest 15. This emphasizes the need for weather stations within the boundary of the catchment.**
- **P-loss was heavily overestimated by AVSWAT2000 and was shown to be highly inadequate by PBIAS and PME values. Identification of the P-loss inaccuracies was traced to simple overestimation of mineral and organic P. Surface flow volume, sediment concentration and soluble P transport were shown to be simulated within realistic ranges and were exonerated from the problem.**
- **RAVSWAT simulated flow adequately according to PBIAS and PME and better than AVSWAT2000. Improvements were obtained in baseflow and stormflow simulations. Underlying system processes were shown to work better than the previous version but did show some discrepancies especially with regards to perennial crops and oilseed rape.**
- **RAVSWAT overestimated P-loss with greater differences than before and is afflicted by the same problems that caused overestimation in AVSWAT2000**
- **Flow predictions using RAVSWAT based on the SAR maps were more accurate than simulations based on the field survey map according to PBIAS and PME estimates. It is accepted that the proximity to the results obtained from the field survey map is considered and not the absolute values of PBIAS and PME. SAR data classified using supervised MLE is therefore considered the best alternative to field survey of those used. SAR images classified using an unsupervised method is also acceptable.**

The AVSWAT2000 and RAVSWAT models have successfully modelled river flow in the Stonton Brook. This was achieved without calibration and therefore reflects well on the data and model. Arnold *et al.* (1996) stated that one of the objectives of SWAT is to develop a multi-component catchment-scale tool that can be applied to ungauged catchments. Some doubt still exists about the underlying processes, which must be addressed, but the revised model performed adequately without calibration and therefore supports the claim by Arnold *et al.* (1996). The final objective has therefore been achieved but with mixed successes. Hydrology has been modelled successfully but P transport has not. The source of the problem has been identified but it seems that other anomalies within the SWAT model indicate more problems than those resolved in RAVSWAT. Problems relating to the hydrological components must be resolved fully before SWAT can be used as a nutrient transport model.

10.7 Future work

The most urgent task following from this project is to carry out a thorough examination of the SWAT source code. This is not a small task and would require excellent knowledge of Fortran 70 or 99 and familiarity with SWAT. The question of whether valuable resources should be used on correcting SWAT code must be considered. It has been shown that RAVSWAT can reliably simulate flow within a catchment over a period of time and without necessary calibration. In hydrological terms this is a valuable tool. Although similar results can be shown with much simpler models e.g. TOPMODEL (Beven *et al.*, 1995), they are not linked to nutrient and pesticide sub-routines. If the progress shown in this thesis can be mirrored in the P-transport simulations, and thereafter in the nitrogen and pesticide simulations, RAVSWAT would be an extremely valuable tool.

Further work on output from the corrected model would then be essential. At present the source code appears to be the most important source of error in the model. It may be that the processes upon which P-loss are based may be sub-optimal. Analysis of uncertainty in the data, model and predictions can then be carried out with GLUE or FORA. This would help in understanding the responses of the system with variables that are difficult or impossible to measure accurately e.g. saturated conductivity (Brazier *et al.*, 2000). It would however demand a great deal of computer power and programming time as shown by Brazier *et al.* (2000) on the WEPP model. SAR data are available for the River Welland downstream to Tinwell near Stamford for the same period. Field survey data are not available but land cover maps could be derived using unsupervised training and subsequent classification based on known proportions of crop cover. Weekly P concentrations have been collected by the Environment Agency from Tinwell for many years. Intense flow data are available from Anglian water for the same location. Many weather stations are located within the River Welland catchment and the problems with rainfall data encountered in this project would be avoided. These data could be applied to RAVSWAT to assess the potential at a much greater scale. The SWAT model is reported to perform better on larger catchments than on smaller ones so an improvement may be seen in the predictive output. Karayanan (Institute of Water and Environment, Cranfield University) however, has successfully applied the RAVSWAT on a catchment of less than two kilometres in the UK. In the past this range of scale would have been carried out using several models.

The investigation into extraction of soil and vegetation parameters from SAR data was incomplete in this project. Few crops were included and samples were few. The results given in this thesis should not therefore be taken too seriously. The potential of SAR to acquire relevant physical vegetation and soil parameters still remains. Additionally, the combination of SAR with data relating to the visible spectrum may help in data acquisition.

Bibliography

Abbot, M.B. & Refsgaard, J.C., eds. (1996) *Distributed Hydrological Modelling*. Kluwers Academic Publishers, Dortrecht, Nederlands.

Adamus, C.L. & Bergman, M.J. (1995) Estimating nonpoint source pollution loads with a GIS screening model. *Water Resources Bulletin*, 31, 647-655.

Addiscott, T., Smith, J., & Bradbury, N. (1995) Critical Evaluation of Models and their Parameters. Journal of Environmental Quality, 24, 803-807.

Allen, S.E., Grimshaw, H.M., Parkinson, J.A.R., & Quarmby, C. (1974) Chemical analysis of ecological materials Blackwell Scientific Publications.

Altese, E., Bolognani, O., Mancini, M., & Troch, P.A. (1996) Retrieving soil moisture over bare soil from ERS-1 synthetic aperture radar data: Sensitivity analysis based on a theoretical surface scattering model and field data. Water Resources Bulletin, 32, 653-661.

Anon. (1984) Field Guide to the Animals of Britain The Reader's Digest Association Ltd., London.

Arnold, J.G., Srinivasan, R., & King, K.W. (1996) *SWAT: Soil and Water Assessment Tool* USDA, ARS, Temple Texas.

Arnold, J.G., Williams, J.R., Srinivasan, R., & King, K.W. (1999) SWAT, Soil and Water Assessment Tool USDA, Agricultural Research Service, Temple Texas.

Atkinson, P.M. (2001). Geostatistical Regularisation in Remote Sensing. In Modelling Scale in Geographical Information Science (eds N.J. Tate & P.M. Atkinson), pp. 237-260. John Wiley & Sons Ltd., Chichester, England.

Attema, E.P.W. & Ulaby, F.T. (1978) Vegetation modelled as a water cloud. Radio Science, 13, 357-364.

Avery, B.W. (1990) Soils of the British Isles C.A.B. International, Wallingford.

BADC (2002) Met Office - Land Surface Observation Stations Data http://badc.nerc.ac.uk/data/surface, British Atmospheric Data Centre.

Baghdadi, N., Gaultier, S., & King, C. (2002a) Retrieving surface roughness and soil moisture from synthetic aperture radar (SAR) data using neural networks. Canadian Journal of Remote Sensing, 28, 701-711.

Baghdadi, N., King, C., Bourguignon, A., & Remond, A. (2002c) Potential of ERS and Radarsat data for surface roughness monitoring over bare agricultural fields: application to catchments in Northern France. International Journal of Remote Sensing, 23, 3427-3442.

Baghdadi, N., King, C., Chanzy, A., & Wigneron, J.P. (2002b) An empirical calibration of the integral equation model based on SAR data, soil moisture and surface roughness measurement over bare soils. International Journal of Remote Sensing, 23, 4325-4340.

Bastin, L., Edwards, M., & Fisher, P. (2000) Tracking the positional uncertainty in 'ground truth'. In Proceedings of the 4th International Symposium on Spatial Accuracy Assessment in Natural Resources and Environmental Sciences (eds G.B.M. Heuvelink & M.J.P.M. Lemmens), pp. 39-42. Delft University Press, Delft.

Beasley, D.B., Huggins, L.F., & Monke, E.J. (1980) ANSWERS: a model for watershed planning. *Transactions of the ASAE*, 23, 938-944.

Benallegue, M., Normand, M., Galle, S., Dechambre, M., Taconet, O., Vidal-Madjar, D., & Prevot, L. (1994) Soil moisture assessment at a basin scale using active microwave remote sensing: the Agriscatt '88 Airborne Campaign on the Orgeval watershed. International Journal of Remote Sensing, 15, 645-656.

Beven, K., Calver, A., & Morris, E. (1987). *The Institute of Hydrology Distributed Model*, Rep. No. Report Number 98. Institute of Hydrology, Wallingford, UK.

Beven, K., J. & Jakeman, A.J. (1990) Complexity and Uncertainty in Predictive Models. In International Symposium on Water Quality and Modelling of Non-point Sources, (eds D.G. DeCoursey, A.S. Donigian & P.C.S. Rao), pp. 555-599.

Beven, K.J. (1989) Changing ideas in hydrology - the case of physically-based models. *Journal of Hydrology*, 105, 157-172.

Beven, K.J. (1993) Prophecy, reality and uncertainty in distributed hydrological modelling. *Advances in Water Resources*, 16, 41-51.

Beven, K.J. (1996). A discussion of distributed hydrological modelling. In *Distributed Hydrological Modelling* (eds M.B. Abbott & J.C. Refsgaard). Kluwer Academic Publishers, Dortrecht, Nederlands.

Beven, K.J., Lamb, R., Quinn, P., Romanowicz, R., & Freer, J. (1995). TOPMODEL. In *Computer Models of Watershed Hydrology* (ed V.P. Singh). Water Resources Publications, Colorado, US.

Bingner, R.L. (1996) Runoff Simulated from Goodwin Creek Watershed Using SWAT. *Transactions of the ASAE*, 39, 85-90.

Biot, Y. & Lu, X.X. (1995) Loss of yield caused by sandy soils in the UK. Soil Use and Management, 11, 157-162.

Boardman, J., Favis-Mortlock, D.T., & Evans, R., eds. (1992) Modelling soil erosion under future climates, pp 195, Newcastle upon Tyne, England, UK.

Bowling, L.C. & Baker, P.D. (1996) Major cyanobacterial bloom in the Barwon-Darling River, Australia, in 1991, and underlying limnological conditions. Marine and Freshwater Research, 47, 643-657.

Bouman, B.A.M., van Kraalingen, D.W.G., Stol, W., & van Leeuwen, H.J.C. (1999) An agroecological modelling approach to explain ERS SAR radar backscatter of agricultural crops. Remote Sensing of the Environment, 67, 137-146.

Boutwell, S.H., Brown, S.M., Roberts, B.R., & Atwood, D.F. (1985). *Modelling remedial actions at uncontrolled hazardous waste sites*, Rep. No. EPA/540/2-85/001. Anderson-Nichols and Co., Inc. Prepared for Environmental Protection Agency, Hazardous Waste Engineering Research Laboratory, Cincinnati, OH, Palo Alto, CA.

Bradford, M.E. & Peters, R.H. (1987) The relationship between chemically analyzed phosphorus fractions and bioavailable phosphorus. 32.

Brady, N.C. (1990) The Nature and Properties of Soils, 10th edn. Macmillan Publishing Company Ltd., New York.

Brazier, R.E., Beven, K.J., Freer, J., & Rowan, J.S. (2000) Equifinality and uncertainty in physically based soil erosion models: application of the GLUE methodology to WEPP - the Water Erosion Prediction Project - for sites in the UK and USA. Earth Surface Processes and Landforms, 25, 825-845.

Brook, A.J. (1964). The phytoplankton of the Scottish freshwater locks. In The Vegetation of Scotland (ed A.J. Burnett), pp. 290-305. Oliver and Boyd, Edinburgh.

Brookes, P.C., Heckrath, G., De Smet, J., Hofman, G., & Vanderdeelen, J. (1998). Losses of phosphorus in drainage water. In Phosphorus Loss from Soil to Water (eds H. Tunney, O.T. Carton, P.C. Brookes & A.E. Johnston). CAB International, Wallingford.

Burn, D.H. (1991) Water quality sampling for nutrient loading estimation. In *Water Pollution: Modelling, Measuring and Prediction.* Proceedings of the First International Conference on Water Pollution: Modelling, Measuring and Prediction (eds L.C. Wrobel & C.A. Brebbia). Elsevier Applied Science.

Burt, T.P. & Heathwaite, A.L. (1993). A scale-dependent approach to the study of nutrient export from basins, Rep. No. 120. *Institute of Hydrology Report.*

Catt, J.A., Howse, K.R., Farina, R., Brockie, D., Todd, A., Chambers, B.J., Hodgkinson, R., Harris, G.L., & Quinton, J.N. (1998) Phosphorus losses from arable land in England. Soil Use and Management, 14, 168-174.

CEH (2003) 31017 - Stonton Brook at Welham Road Bridge http://www.nwl.ac.uk/ih/nrfa/station_summaries/031/017.html Accessed January 2003. Centre for Ecology and Hydrology.

Chaler Navarro, S. (2002) Soil Erosion Risk Assessment using Crystal Ball: A Case Study in a Sub-Catchment of the River Flitt, Mid Bedfosrdshire, England. M.Sc., Cranfield University, Silsoe, Cranfield.

Chambers, B.J., Garwood, T.W.D., & Unwin, R.J. (2000) Controlling soil water erosion and phosphorus losses from arable land in England and Wales. Journal of Environmental Quality, 29, 145-150.

Chen, K.S., Yen, S.K., & Huang, W.P. (1995) A simple model for retrieving bare soil moisture from radar-scattering coefficients. Remote Sensing of Environment, 54, 121-126.

Colston, A. & Balbi, T. (1995). The River Welland a Vision for the Flood Plain Summary Report. Wildlife Trust for Northamptonshire, Northampton.

Congalton, R.G. (1991) A review of assessing the accuracy of classifications of remotely sensed data. Remote Sensing of Environment, 37, 35-46.

Congalton, R.G. & Green, K.M. (1999) Assessing the Accuracy of Remotely Sensed Data: Principles and Practices Lewis Publishing, Boca Raton.

Cooke, G.W. (1976) A review of the effects of agriculture on the chemical composition and quality of surface and underground waters. Technical Bulletin for the Ministry of Agriculture Fisheries and Food, 32, 5-57.

Cox, N.J. (1983) On the estimation of spatial autocorrelation in geomorphology. *Earth surface processes and landforms*, 8, 89-93.

Curran, P.J., Foody, G.M., Kondratyev, K.Y., Kozoderov, V.V., & Fedchenko, P.P. (1990) *Remote Sensing of Soils and Vegetation in the USSR* Taylor and Francis, London.

Curtis, L.F., Courtney, F.M., & Trudgill, S.T. (1976) Soils in the British Isles, Longman Group Ltd., New York.

Dam Kofoed, D.A. (1985). Pathways of nitrate and phosphate to ground and surface waters. In Environment and Chemicals in Agriculture (ed F.P.W. Winteringham), pp. 27-69. Elsevier, London, New York.

Dawson, M.S., Fung, A.K., & Manry, M.T. (1997) A robust statistical-based estimator for soil moisture retrieval from radar measurements. IEEE Transactions on Geoscience and Remote Sensing, 35, 57-66.

de Jong, S.M. (1994). *Applications of Reflective Remote Sensing for Land Degradation Studies in a Mediterranean Environment*, Rep. No. 177. Netherlands Geographical Studies.

de Troch, F.P., Troch, P.A., Su, Z., & Lin, D.S. (1996). Application of remote sensing for hydrological modelling. In *Distributed Hydrological Modelling* (eds M.B. Abbott & J.C. Refsgaard). Kluwer Academic Publishers, Dortrecht, Nederlands.

de Willigen, P., Bergström, L., & Gerritse, R.G. (1990) Leaching models of the unsaturated zone: their potential use for management and planning. In *Proceedings of an International Symposium on Water Quality Modelling of Agricultural Non-Point source Pollution* (ed D.G. Decoursey), Vol. ARS-81. USDA-ARS, Washington DC, Logan, UT.

Deckers, F. & Te Stroet, C.B.M. (1996). Use of GIS and database with distributed modelling. In *Distributed Hydrological Modelling* (eds M.B. Abbott & J.C. Refsgaard). Kluwer Academic Publishers, Dortrecht, Nederlands.

Di Luzio, M., Srinivasan, R., Arnold, J.G., & Neitsch, S.L. (2002). ArcView Interface for SWAT2000, Rep. No. TR-193. Texas Water Resources Institute, College Station, Texas, College Station.

Djodjic, F., Bergström, L., & Ulén, B. (2002) Phosphorus losses from a structured clay soil in relation to tillage practices. Soil Use and Management, 18, 79-83.

Dobson, M.C., Ulaby, F.T., LeLoan, T., Bedoin, A., Kasischke, E.S., & Christensen, N. (1992) Dependence of radar backscatter on coniferous forest biomass. IEEE Transactions on Geoscience and Remote Sensing, 30, 412-415.

Dobson, M.C., Ulaby, F.T., & Pierce, L.E. (1995) Land cover classification and estimation of terrain attributes using synthetic aperture radar. Remote Sensing of Environment, 51, 199-214.

Dong, Y., Milne, A.K., & Forster, B.C. (2001) Segmentation and classification of vegetated areas using polarimetric SAR image data. IEEE Transactions on Geoscience and Remote Sensing, 39, 321-329.

Donigian, A.S. & Rao, P.S.C. (1990) Selection, application and validation of environmental models. In Proceedings International Symposium on Water Quality Modelling of Agricultural Non-Point Sources (ed D.G. Decoursey), Vol. ARS-81. USDA-ARS, Washington D.C., Logan, UT.

Drayton, R.S., Wilde, B.M., & Harris, J.H.K. (1992) Geographical information system approach to distributed modelling. Hydrological Processes, 6, 361-368.

Dubois, P.C., van Zyl, J., & Engman, T. (1995) Measuring soil moisture with imaging radars. IEEE Transactions on Geoscience and Remote Sensing, 33, 915-926.

Dungan, J.L. (2001). Scaling Up and Scaling Down: the Relevance of the Support Effect on Remote Sensing of Vegetation. In Modelling Scale in Geographical Information Science (eds N.J. Tate & P.M. Atkinson), pp. 221-235. John Wiley & Sons Ltd., Chichester, England.

Durand, J.M., Gimonet, B.J., & Perbos, J.R. (1987) SAR data filtering for classification. IEEE Transactions on Geoscience and Remote Sensing, GE-25, 629-637.

Dutra, L.V. & Huber, R. (1999) Feature Extraction and selection for ERS-1/2 InSAR classification. International Journal of Remote Sensing, 20, 993-1016.

EA (1997). Local Environment Agency Plan, Welland Consultation Report. Environment Agency.

EA (2000). Aquatic eutrophication in England and Wales: a management strategy. Environment Agency, Peterborough.

Edwards, A.C. & Withers, P.J.A. (1998) Soil phosphorus management and water quality: a UK perspective. Soil Use and Management, 14, 124-130.

EEA (1995). Europe's Environment: The Dobris Assessment. European Environment Agency, Copenhagen, Denmark.

EEA (1999). The Environment in the European Union at the turn of the Century. European Environment Agency, Copenhagen, Denmark.

Eisenreich, S.J., Bannerman, R.T., & Armstrong, D.E. (1975) A simplified phosphorus analysis technique. Environmental Letters, 9, 43-53.

Elachi, C. (1988) Spaceborne Radar Remote Sensing: Applications and Techniques IEEE Press, New York.

Elosegui, A., Arana, X., Basaguren, A., & Pozo, J. (1995) Self-purification processes along a medium sized stream. Environmental Management, 19, 931-939.

Elser, J.J., Marzolf, E.R., & Goldman, C.R. (1990) Phosphorus and nitrogen limitation of phytoplankton growth in the freshwaters of North America: a review and critique of experimental enrichments. *Canadian Journal of Fisheries and Aquatic Science*, 47, 1468-1477.

Elvidge, C.D. & Chen, Z. (1994) Comparison of broad-band and narrow band red and near-infrared vegetation indices. *Remote Sensing of the Environment*, 54, 38-48.

Enell, M. (1980) The Phosphorus economy of a hypertrophic seepage lake in Scania, south Sweden Limnologiska Institutionen, Lunds Universitet, Lunds.

Eom, H.J. & Fung, A.K. (1984) A scatter model for vegetation up to Ku-band. Remote Sensing of Environment, 15, 185-200.

ERDAS (1997a) ERDAS Imagine Tour Guide Version 8.3 ERDAS, Atlanta, Georgia.

ERDAS (1997b) ERDAS Imagine Field Guide Version 8.3 ERDAS, Atlanta, Georgia.

ERDAS (1997c) Orthoradar Tour Guide ERDAS Inc., Atlanta.

ESA (2000) ERS SAR PRI: ERS-1/ Synthetic Aperture Radar (SAR) Precision Image Product. European Space Agency.

Evans, G.L. (1999) Phosphorus and its Biological Effect in Lowland Rivers. Ph.D., University of Leicester, Leicester.

Farres, P. (1978) The role of time and aggregate size in the crusting process. Earth Surface Processes, 3, 243-254.

Ferrazzoli, P., Paloscia, S., Pampaloni, P., Schiavon, G., Sigismondi, S., & Solimini, D. (1997) The potential of multi frequency polarimetric SAR in assessing Agricultural and arboreous biomass. IEEE Transactions on Geoscience and Remote Sensing, 35, 5-17.

Ferro-Famil, L. & Pottier, E. (2001) Multi frequency polarimetric SAR data classification. Annales des Telecommunications, 56, 510-522.

Fisher, P., Abrahart, R.J., & Herbinger, W. (1997) The sensitivity of two distributed non-point source pollution models to the spatial arrangement of the landscape. *Hydrological Processes*, 11, 241-252.

FMA (1999). The British Survey of Fertiliser Practice, Fertiliser Use on Farm Crops for Crop Year 1998. Peterborough, Fertiliser Manufacturers' Association.

Foody, G.M. (2002) Status of land classification accuracy assessment. Remote Sensing of Environment, 80, 185-201.

Foody, G.M., McCulloch, M.B., & Yates, W.B. (1994) Crop classification from C-band polarimetric radar data. International Journal of Remote Sensing, 15, 2871-2885.

Fox, I. & Malati, M.A. (1985). Cycling of Phosphorus in Rivers, Rep. No. PECD 7/7/039. Department of the Environment.

Foy, R.H. & Withers, P.J.A. (1995) The contribution of agricultural phosphorus to eutrophication The Fertiliser Society.

Froelich, P.N. (1988) Kinetic control of dissolved phosphate in natural rivers and estuaries: A primer on the phosphate buffer mechanism. Limnology and Oceanography, 33, 649-668.

Fung, A. & Ulaby, F. (1978) A scatter model for leafy vegetation. IEEE Transactions on Geoscience and Remote Sensing, GE-16, 281-286.

Fung, A.K., Li, Z., & Chen, K.S. (1992) Backscattering from a randomly rough dielectric surface. IEEE Transactions on Geoscience and Remote Sensing, 30, 356-369.

Gardner, R.H., O'Neill, R.V., Mankin, J.B., & Carney, J.H. (1981) A comparison of sensitivity and error analysis based on a stream ecosystem model. Ecological Modeling, 12, 173-190.

Gibson, C.E. (1998). The Dynamics of Phosphorus in Freshwater and Marine Environments. In Phosphorus Loss from Soil to Water (eds H. Tunney, O.T. Carton, P.C. Brookes & A.E. Johnston), pp. 119-135. CAB International, Wallingford.

Gill, H. (1996) Industrial water resource management. In Multiple Land Use and Catchment Management (eds M. Cresser & K. Pugh), pp. 23-25. The Macaulay Land Use Research Institute, Aberdeen, Scotland.

Golterman, H.L. & de Oude, N.T. (1991). Eutrophication of rivers, lakes and coastal seas. In The Handbook of Environmental Chemistry (ed O. Hutzinger), Vol. 5, pp. 79-124. Springer-Verlag, Berlin.

Grant, D.M. & Dawson, B.D. (1978) ISCO Open Channel Flow Measurement Handbook, Fourth Edition edn. ISCO, Lincoln, Nebraska, USA.

Grimm, V. (1994) Mathematical Models and Understanding in Ecology. Ecological Modelling, 75/76, 641-651.

Grover, K., Quegan, S., & da Costa Freitas, C. (1999) Quantitative estimation of Tropical forest cover by SAR. IEEE Transactions on Geoscience and Remote Sensing, 37, 479-490.

Gupta, H.V., Sorooshian, S., & Yapo, P.O. (1999) Status of automatic calibration for hydrologic models: comparison with multilevel expert calibration. Journal of Hydrologic Engineering, ASCE, 4, 135-143.

Harper, D. & Evans, G. (1998). Sources of soluble and particulate phosphorus in surface water in eastern England: relative importance of agricultural versus small point sources. In Phosphorus Loss from Soil to Water (eds H. Tunney, O.T. Carton, P.C. Brookes & A.E. Johnston), pp. 385-391. CAB International, Wallingford, UK.

Harper, D.M. (1992) *Eutrophication of Freshwaters: Principles Problems and Restoration* Chapman and Hall, London.

Harper, D.M. & Pacini, N. (1995). *Eutrophication Control Methodologies.* National Rivers Authority Report.

Haygarth, P.M., Ashby, C.D., & Jarvis, S.C. (1995) Short-term Changes in the Molybdate Reactive Phosphorus of Stored Soil Waters. Journal of Environmental Research, 24, 1133-1140.

Haygarth, P.M., Hepworth, L., & Jarvis, S.C. (1998) Forms of phosphorus transfer in hydrological pathways from soil under grazed grassland. European Journal of Soil Science, 49, 65-72.

Haygarth, P.M. & Jarvis, S.C. (1997) Transfer of Phosphorus from Agricultural Soils. Advances in Agronomy, 1-54.

He, C., Riggs, J.F., & Kang, Y.-T. (1993) Integration of geographic information systems and a computer model to evaluate impacts of agricultural runoff on water quality. Water Resources Bulletin, 29, 891-900.

Heathwaite, A.L. (1998). Sources and pathways of phosphorus loss from agriculture. In Phosphorus Loss from Soil to Water (eds H. Tunney, O.T. Carton, P.C. Brookes & A.E. Johnston). CAB International, Wallingford.

Heathwaite, A.L., Burt, B.T., & Trudgill, S.T. (1990). The effect of land use on nitrogen, phosphorus and suspended sediment delivery to streams in a small catchment in south-west England. In *Vegetation and Erosion* (ed J.B. Thornes). John Wiley and Sons Ltd, Chichester, England.

Heathwaite, A.L., Johnes, P.J., & Peters, N.E. (1996) Trends in Nutrients. Hydrological Processes, 10, 263-293.

Heckrath, G., Brookes, P.C., Poulton, P.R., & Goulding, K.W.T. (1995) Phosphorus leaching from soils containing different phosphorus concentrations in the Broadbalk experiment. Journal of Environmental Quality, 24, 904-910.

Higgs, B., Johnston, A.E., Salter, J.L., & Dawson, C.J. (2000) Some aspects of achieving sustainable phosphorus use in agriculture. Journal of Environmental Quality, 29, 80-87.

Holtan, H., Kamp-Nielsen, L., & Stuanes, A.O. (1988) Phosphorus in soil, water and sediment: an overview. Hydrobiologia, 170, 19-34.

House, W.A. & Denison, F.H. (1998) Phosphorus dynamics in a lowland river. Water Research, 32, 1819-1830.

House, W.A., Jickells, T.D., Edwards, A.C., Praska, K.E., & Denison, F.H. (1998) Reactions of phosphorus with sediments. Soil Use and Management, 14, 139-146.

Huber, W.C. & Dickinson, R.E. (1988) Storm Water Management Model, Version 4: User's Manual U.S. Environmental Protection Agency, Athens G.A.

Huang, C. & Bradford, J.M. (1990) Portable laser scanner for measuring soil surface roughness. Journal of the Soil Science Society of America, 54, 1402-1406.

Hunt, R. (1990) Basic growth analysis Unwin Hyman, London.

ICWE (1992) The Dublin Statement and report of the conference. In International Conference on Water and the Environment: Development issues for the 21st century, pp. 26-31, Dublin, Ireland.

Jackson, T.J. (1993) Measuring surface soil moisture using passive microwave remote sensing. *Hydrological Processes*, 7, 139-152.

Jørgensen, S.E. (1994) Fundamentals of Ecological Modelling Elsevier Science Ltd.

Keyzer, M.A. & Sonneveld, B.G.J.S. (1997) Using the mollifier-method to characterise data sets and models: the case of the Universal Soil Loss Equation. ITC Journal, 97-4, 1-23.

Klemes, V. (1986a) Dilettantism in Hydrology: Transition or Destiny? *Water Resources Research*, 22, 177S-188S.

Klemes, V. (1986b) Operational testing of hydrological simulation models. Journal des Hydrologiques, 31, 13-25.

Knisel, W.G. (1980). *CREAMS: A Field Scale Model for Chemicals, Runoff, and Erosion from Agricultural Management Systems*, Rep. No. 20. USDA-ARS, Washington DC.

Krokowski, J.T. (1998) *An Investigation into Nutrient Fluxes in a Lowland, Pumped-Storage Reservoir During Ferric Sulphate Dosing*. Ph.D., University of Leicester, Leicester.

Kronvang, B. (1990). Sediment-associated phosphorus transport from two intensively farmed catchment areas. In Soil Erosion on Agricultural Land (eds J. Boardman, I.D.L. Foster & J.A. Dearing). John Wiley and Sons Ltd, New York.

Kurvonen, L., Pulliainen, J., & Hallikainen, M. (1999) Retrieval of biomass in boreal forest from multi-temporal ERS-1 and JERS-1 SAR images. IEEE Transactions on Geoscience and Remote Sensing, 37, 198-205.

Landis, J. & Koch, G. (1977) The measurement of observer agreement for categorical data. Biometrica, 33.

Lane, L.J. & Nearing, M.A. (1989). *USDA-Water Erosion Prediction Project: Hillslope profile model documentation*, Rep. No. NSERL Report No.2. USDA-ARS, National Soil Erosion Research Laboratory, West Lafayette, Indiana 47907.

Laur, H., Bally, P., Meadows, P., Sanchez, J., Schaettler, B., Lopinto, E., & Esteban, D. (1998). ERS SAR Calibration: Derivation of the Backscattering Coefficient Sigma0 in ESA ERS SAR PRI Products, Rep. No. ES-TN-RS-PM-HL09. European Space Agency.

Lee, G.F. (1992) Role of phosphorus in eutrophication and diffuse source control. Pergamon Press, 7, 111-128.

Leicestershire County Council (2003) Harborough Mid-Year Parish Population Estimates
http://www.leicestershire.gov.uk/p_t/policy_research/population/parish_harborough.htm, Accessed January 2003. Leicestershire County Council.

Lennox, S.D., Foy, R.H., Smith, R.V., & Jordan, C. (1998). Estimating the contribution from agriculture to the phosphorus load in surface water. In Phosphorus Loss from Soil to Water (eds H. Tunney, O.T. Carton, P.C. Brookes & A.E. Johnston). CAB International, Wallingford.

Leonard, R.A., Knisel, W.G., & Still, D.A. (1987) GLEAMS: Groundwater Loading Effects of Agricultural Management Systems. *Transactions of the ASAE*, 30, 1403-1418.

Loumagne, C., Normand, M., Riffard, M., Weisse, A., Quesney, A., Le Hegarat-Mascle, S., & Alem, F. (2001) Integration of remote sensing data into hydrological models for reservoir management. Hydrological Sciences Journal, 46, 89-102.

Lowrance, R., Leonard, R., & Sheridan, J. (1985) Managing riparian ecosystems to control nonpoint pollution. Journal of Soil and Water Conservation, 40, 87-97.

MAFF (1991). Code of good agricultural practice for the protection of water. Ministry of Agriculture, Fisheries and Food, London.

MAFF (1993). Code of good agricultural practice for the protection of soil. Ministry of Agriculture, Fisheries and Food, London.

MAFF (1999). Fertiliser Recommendations for Agricultural and Horticultural Crops (RB209). London, The Stationery Office.

MAFF (1999). Controlling Soil Erosion: A Manual for the Assessment and Management of Agricultural Land at Risk of Water Erosion in Lowland England. Ministry of Agriculture, Fisheries and Food, London.

Mainstone, C.P., Davis, R.D., House, A., & Parr, W. (1996). A Review of Methods for Assessing and Controlling Non-point Sources of Phosphorus. National Rivers Authority, Bristol.

Mather, P.M. (1987) *Computer Processing of Remotely Sensed Images* Wiley, Chichester.

Matthews, P.J. (1985). Phosphate in Water - is it really a problem? An English Water Authority Over-View.

McColl, R.H.S. (1974) Self-purification of small freshwater streams: phosphate, nitrate and ammonia removal. New Zealand Journal of Marine Freshwater Research, 8, 375-388.

MacDonald, D.W., ed. (2001) The New Encyclopedia of Mammals, pp 930. Oxford University Press, Oxford.

Manguerra, H.B. & Engel, B.A. (1998) Hydrologic Parameterization of Watersheds for Runoff Prediction Using SWAT. Journal of the American Water Resources Association, 34, 1149-1163.

McDowell, R., Sharpley, A.N., & Folmar, G. (2001) Phosphorus export from an agricultural watershed: linking source and transport mechanisms. Journal of Environmental Quality, 30, 1587-1595.

McGarrigle, M.L. (1993) Aspects of river eutrophication in Ireland. *Annals of Limnology*, 29, 355-364.

McKelvie, I.D., Peat, D.M.W., & Worsfold, P.J. (1995). Techniques for the Quantification and Specification of Phosphorus in Natural Waters. In Analytical Proceedings Including Analytical Communications, Vol. 32, pp. 437-445.

Melching, C.S. & Yoon, C.G. (1996) Key sources of uncertainty in QUAL2E model of Passaic River. Journal of Water Resources Planning and Management, 122, 105-113.

Michelson, D.B., Liljeberg, B.M., & Pilesjo, P. (2000) Comparison of algorithms for classifying Swedish land cover using Landsat TM and ERS-1 SAR data. Remote Sensing of Environment, 71, 1-15.

Millward, R. (1985) Leicestershire and Rutland: a History Phillimore and Co. Ltd.

Morgan, M.A. (1998). The behaviour of soil and fertiliser phosphorus. In Phosphorus Loss from Soil to Water (eds H. Tunney, O.T. Carton, P.C. Brookes & A.E. Johnston). CAB International, Wallingford.

Morgan, R.P.C. (2001) A simple approach to soil loss prediction: a revised Morgan-Morgan-Finney model. Catena, 44, 305-322.

Morse, G., Eatherall, A., & Jenkins, A. (1994) Managing agricultural pollution using a linked Geographical Information System and Non-Point Source Pollution Model. *Journal of the Institute of Water and Environmental Management*, 8, 277-286.

Morse, G.K., Lester, J.N., & Perry, R. (1993) The Economic and Environmental Impact of Phosphorus Removal from Wastewater in the European Community Selper Publications.

Moss, B. (1988) Ecology of Fresh Waters, 2nd edn. Blackwell Scientific Publications, Oxford.

Moss, B., Irvine, K., & Stansfield, J. (1988) Approaches to the restoration of shallow eutrophicated lakes in England.

Moss, B., Johnes, P.J., & Phillips, G. (1996) The Monitoring of Ecological Quality and the Classification of Standing Waters in Temperate Regions: A review based on a worked scheme for British Waters. Biological Reviews, 71, 301-339.

Moss, B., Johnes, P.J., & Phillips, G. (1998) The monitoring and classification of standing waters in temperate regions by state-changed schemes – a discussion and a proposal based upon a worked scheme for British waters. in press.

Murphy, J. & Riley, J.P. (1962) A modified single solution method for the determination of phosphate in natural waters. Analytica Chimica Acta, 27, 31-36.

Muttiah, R.S. & Wurbs, R.A. (2002) Scale-dependent soil and climate variability effects on watershed water balance of the SWAT model. Journal of Hydrology, 256, 264-285.

Nasset, E. (1995) A method to test for systematic differences between maps and reality using error matrices. International Journal of Remote Sensing, 16, 3147-3156.

Nearing, M.A., Lane, L.J., Alberts, E.E., & Laflen, J.M. (1986) Prediction Technology for Soil Erosion by Water: Status and Research Needs. Soil Science Society, 54, 1702-1711.

Neitsch, S.L., Arnold, J.G., Kiniry, J.R., Srinivasan, R., & Williams, J.R. (2002b). Soil and Water Assessment Tool, User's Manual, Rep. No. TR-192. Texas Water Resources Institute, College Station, Texas, College Station.

Neitsch, S.L., Arnold, J.G., Kiniry, J.R., Williams, J.R., & King, K.W. (2002a). Soil and Water Assessment Tool, Theoretical Documentation, Rep. No. TR-191. Texas Water Resources Institute, College Station, Texas, College Station.

Neitsch, S.L., Arnold, J.G., & Williams, J.R. (1999) Soil and Water Assessment Tool, User's Manual Grassland, Soil and Water Research Laboratory, Agricultural Research Service., Temple Texas.

Newman, E.I. (1995) Phosphorus inputs to terrestrial ecosystems. Journal of Ecology, 83, 713-726.

Newson, M. (1996) Land, water and development: key themes driving international policy on catchment management. In Multiple Land Use and Catchment Management (eds M. Cresser & K. Pugh), pp. 11-21. The Macaulay Land Use Research Institute, Aberdeen, Scotland.

Nishii, R. & Tanaka, S. (1999) Accuracy and inaccuracy assessments in land cover classification. IEEE Transactions on Geoscience and Remote Sensing, 37, 491-498.

NRA (1991) Chemistry Laboratory Procedures Manual, Number 2 edn. National Rivers Authority, Peterborough.

NRA (1994). Lake restoration: the role of biomanipulation. National Rivers Authority and the Broads Authority.

Odum, E.P. (1971) Fundamentals of Ecology, Third edn. Saunders, Philadelphia.

OECD (1982) Eutrophication of waters, monitoring, assessment and control Organisation for Economic Co-operation and Development, Paris.

Oh, Y. & Kay, Y.-C. (1998) Condition for precise measurement of soil surface roughness. IEEE Transactions on Geoscience and Remote Sensing, 36, 691-695.

Oh, Y., Sarabandi, K., & Ulaby, F.T. (1992) An empirical model and an inversion technique for radar scattering from bare soil surfaces. IEEE Transactions on Geoscience and Remote Sensing, 30, 370-381.

Oliver, G., Burt, J., & Solomon, R. (1990) The use of surface runoff models for water quality decisions-a user's perspective. In *Proceedings of an International Symposium on Water Quality Modelling of Agricultural Non-Point source Pollution* (ed D.G. Decoursey), Vol. ARS-81. USDA-ARS, Washington DC, Logan, UT.

Owens, M. & Wood, G. (1968) Some aspects of the eutrophication of water. Water Research, 2, 151-159.

Paloscia, S. (2002) A summary of experimental results to assess the contribution of SAR for mapping vegetation biomass and soil moisture. Canadian Journal of Remote Sensing, 28, 246-261.

Peters, R.H. (1991) A Critique for Ecology Cambridge University Press, Cambridge.

Peterson, J.R. & Hamlett, J.M. (1998) Hydrological calibration of the SWAT model in a watershed containing fragipan soils. Journal of the American Water Resources Association, 34, 531-545.

Peuquet, D., Davis, J.R., & Cuddy, S. (1993). Geographic Information Systems and Environmental Modelling. In Modelling Change in Environmental Systems (eds A.J. Jakeman, M.B. Beck & M.J. McAleer), pp. 543-556. John Wiley & Sons Ltd.

Philip, J.R. (1991) Soils, Natural Science and Models. Soil Science, 151, 91-98.

Pionke, H.B., Gburek, W.J., Sharpley, A.N., & Zollweg, J.A. (1998). Hydrological and chemical controls on phosphorus loss from catchments. In Phosphorus loss from soil to water (eds H. Tunney, O.T. Carton, P.C. Brookes & A.A. Johnston), pp. 225-242. CAB International, Wallingford.

Plate, E.J. & Duckstein, L. (1990) Stochastic aspects of water quality modelling for nonpoint sources. In *Proceedings of an International Symposium on Water Quality Modelling of Agricultural Non-Point source Pollution* (ed D.G. Decoursey), Vol. ARS-81. USDA-ARS, Washington DC, Logan, UT.

Popper, K.R. (1959) The logic of scientific discovery Hutchinson, London.

Preedy, N., McTiernan, K., Matthews, R., Heathwaite, A.L., & Haygarth, P.M. (2001) Rapid incidental phosphorus transfers from grassland. Journal of Environmental Quality, 30, 2105-2112.

Prevot, L., Dechambre, M., Taconet, O., Vidal-Madjar, D., Normand, M., & Galle, S. (1993) Estimating the characteristics of vegetation canopies with airborne radar measurements. International Journal of Remote Sensing, 14, 2803-2818.

Pulliainen, J., Kurvonen, L., & Hallikainen, M. (1999) Multitemporal behaviour of L- and C-band SAR observations of boreal forests. IEEE Transactions on Geoscience and Remote Sensing, 37, 927-937.

Quinn, P., Anthony, S., Lord, E., & Turner, S. (1996) Nitrate modelling for the UK: a Minimum Information Requirement (MIR) approach. Hydrologie Dans Les Pays Celtique, 215-223.

Quinn, P.F. & Beven, K.J. (1993) Spatial and temporal predictions of soil moisture dynamics, runoff, variable source areas and evapotranspiration for Plynlimon, mid-Wales. *Hydrological Processes*, 7, 425-448.

Ragg, J.M., Beard, G.R., George, H., Heaven, F.W., Hollis, J.M., Jones, R.J.A., Palmer, R.C., Reeve, M.J., Robson, J.D., & Whitfield, W.A.D. (1984) Soils and Their Use in Midland and Western England Harpenden.

Refsgaard, J.C. & Storm, B. (1996). Construction, calibration and validation of hydrological models. In Distributed Hydrological Modelling (eds M.B. Abbott & J.C. Refsgaard), pp. 41-54. Kluwer Academic Publishers.

Refsgaard, J.C., Storm, B., & Abbott, M.B. (1996). Comment on "A discussion of distributed hydrological modelling" by K. Beven. In *Distributed Hydrological Modelling* (eds M.B. Abbott & J.C. Refsgaard). Kluwer Academic Publishers, Dortrecht, Nederlands.

Reid, I., Parkinson, R., Twomlow, S., & Clark, A. (1990). The impact of agricultural land use changes on soil conditions and drainage. In Vegetation and Erosion (ed J.B. Thornes), pp. 199-215. John Wiley & Sons Ltd, Chichester, England.

Rekolainen, S. (1989) Phosphorus and nitrogen load from forest and agricultural areas in Finland. Aqua Fennica, 19, 95-107.

Rignot, E., Salas, W.A., & Skole, D.L. (1997) Mapping deforestation and secondary growth in Rondonia, Brazil, using imaging radar and thematic mapper data. Remote Sensing of Environment, 59, 167-179.

Rijckenberg, G.J. (1997) Inversion Techniques in Radar Remote Sensing of Agricultural Fields; Case Studies on Sugar Beet and Winter Wheat. Ph.D., Agricultural University Wageningen, Wageningen, The Netherlands.

Rose, C.W., Dickinson, W.T., Ghadiri, H., & Jørgensen, S.E. (1990) Agricultural nonpoint-source runoff and sediment yield water quality (NPSWQ) models: modeller's perspective. In *Proceedings of an International Symposium on Water Quality Modelling of Agricultural Non-Point source Pollution* (ed D.G. Decoursey), Vol. ARS-81. USDA-ARS, Washington DC, Logan, UT.

Rowland, A.P. & Haygarth, P.M. (1997) Determination of Total Dissolved Phosphorus in Soil Solutions. Journal of Environmental Quality, 26, 410-415.

Russell, M.A., Walling, D.E., & Hodgkinson, R.A. (2001) Suspended sediment sources in two small lowland agricultural catchments in the UK. Journal of Hydrology, 252, 1-24.

Rykiel Jr., E.J. (1996). Testing ecological models: the meaning of validation. In Ecological Modelling 90, pp. 229-244. Elsevier Science B.V.

Saich, P.J., Cordey, R.A., Quegan, S., Williams, M.L., Baker, J.R., Luckman, A., Wielogorska, A., & Wooding, M.G. (1995). SAR Retrieval Algorithms for Land Applications, Rep. No. 10644/93/NL/NB. ESA.

Schotten, C.G.J., van Rooy, W.W.L., & Janssen, L.L.F. (1995) Assessment of the capabilities of multi-temporal ERS-1 SAR data to discriminate between agricultural crops. International Journal of Remote Sensing, 16, 2619-2637.

Scion Corporation. (1998) Scion Image http://www.scioncorp.com:8080/Downloads/fr_login.htm, Accessed August 1998. Scion Corporation.

Schultz, G.A. (1988) Remote sensing in hydrology. *Journal of Hydrology*, 100, 239-265.

Sharpley, A.N. (1985) The selective erosion of plant nutrients in runoff. Journal of the American Society of Soil Sciences, 49, 1527-1534.

Sharpley, A.N., Chapra, S.C., Wedepohl, R., Sims, J.T., Daniel, T.C., & Reddy, K.R. (1994) Managing agricultural phosphorus for protection of surface waters: issues and options. Journal of Environmental Quality, 23, 437-451.

Sharpley, A.N., Foy, R.H., & Withers, P.J.A. (2000) Practical and innovative measures for the control of agricultural phosphorus losses to water: an overview. Journal of Environmental Quality, 29, 1-9.

Sharpley, A.N. & Rekolainen, S. (1998). Phosphorus in Agriculture and its Environmental Implications. In Phosphorus Loss from Soil to Water (eds H. Tunney, O.T. Carton, P.C. Brookes & A.E. Johnston), pp. 1-53. CAB International, Wallingford.

Sharpley, A.N. & Smith, S.J. (1990). Phosphorus transport in agricultural runoff: The role of soil erosion. In Soil Erosion on Agricultural Land (eds J. Boardman, I.D.L. Foster & J.A. Dearing). John Wiley & Sons Ltd, New York.

Shaw, R.R. & Falco, J.W. (1990) A management perspective on water quality models for agricultural nonpoint sources of pollution. In Proceedings of an International

Symposium on Water Quality Modelling of Agricultural Non-Point source Pollution (ed D.G. Decoursey), Vol. ARS-81. USDA-ARS, Washington DC, Logan, UT.

Shi, J., van Zyl, J.J., Soares, J.V., & Engman, E.T. (1992) Development of soil moisture retrieval algorithm for L-band SAR measurements. IGARSS, 495-497.

Simard, R.R., Beauchemin, S., & Haygarth, P.M. (2000) Potential for preferential pathways for phosphorus transport. Journal of Environmental Quality, 29, 97-105.

Skinner, R.J. & Chambers, B.J. (1996) A survey to assess the extent of soil water erosion in lowland England and Wales. Soil Use and Management, 12, 214-220.

Sonzongoni, G., Chesters, D.R., Jeffs, D.N., Konrad, J.C., Ostry, R.C., & Robinson, J.B. (1980) Pollution from land runoff. Environmental Science and Technology, 14, 148-153.

Steglik, O. (1982) A technique for retrieving soil erosion based on remote sensing data. *Studies of the Earth from Space*, 3, 92-95.

Stehman, S.V. (1996) Estimating the Kappa coefficient and its variance under stratified random sampling. Photogrammetric Engineering and Remote Sensing, 62, 401-407.

Styczen, M. & Nielsen, S.A. (1989) A view of soil erosion theory, process-research and model building: possible interactions and future developments. Quaderni Di Scienza Del Suolo, 2, 27-45.

Su, Z. & Troch, P.A. (1996) Soil Surface parameters and radar backscattering. In 21st General Assembly of the European Geophysical Society, The Hague, Belgium.

Svoray, T., Shoshany, M., Curran, P.J., Foody, G.M., & Perevolotsky, A. (2001) Relationship between green leaf biomass volumetric density and ERS-2 SAR backscatter of four vegetation formations in the semi-arid zone of Israel. International Journal of Remote Sensing, 22, 1601-1607.

Swain, C.H. (2001) The MAFF Method for Soil Erosion Risk Assessment on National Trust Farms. M.Sc., Cranfield University, Silsoe, Cranfield.

Taconet, O., Vidal-Madjar, D., Emblanch, C., & Normand, M. (1996) Taking into account vegetation effects to estimate soil moisture from C-band radar measurements. Remote Sensing of the Environment, 56, 52-56.

Tané, H. (1996) The case for integrated river catchment management. In Multiple Land Use and Catchment Management (eds M. Cresser & K. Pugh), pp. 5-10. The Macaulay Land Use Research Institute, Aberdeen, Scotland.

Tansey, K.J. (1999) Monitoring and retrieval of biophysical parameters in north-east Jordan using ERS SAR data. Ph.D., University of Leicester, Leicester.

Tansey, K.J., Millington, A.C., White, K., & Battikhi, A. (1997) Comparison of modelled backscatter response and ERS-1 SAR data for desert surfaces, the eastern Badia of Jordan. In Proceedings Third ERS Symposium on Space at the Service of our Environment, Vol. Vol. 1, pp. 21-26. ESA SP-414, Florence.

Taylor, A.W., Edwards, W.M., & Simpson, E.C. (1971) Nutrients in streams draining woodland and farmland near Coschocton, Ohio. Water Resources Research, 7, 81-90.

The World Bank (1993) Water Resources Management International Bank for Reconstruction and Development, Washington D.C.

Thomann, R.V. & Mueller, J.A. (1987) *Principles Of Surface Water Quality Modeling And Control* Harper and Row, New York.

Thomlinson, J.R., Bolstad, P.V., & Cohen, W.B. (1999) Coordinating methodologies for scaling land cover classifications from site-specific to global: steps toward validating global map products. Remote Sensing of Environment, 70, 16-28.

Thorsen, M., Feyen, J., & Styczen, M. (1996) Agrochemical modelling. In *Distributed Hydrological Modelling* (eds M.B. Abbott & J.C. Refsgaard). Kluwer Academic Publishers, Dortrecht, Nederlands.

Tim, U.S. (1996a) Emerging technologies for hydrologic and water quality modelling research. Transactions of the ASAE, 39, 465-476.

Tim, U.S. (1996b) Coupling vadose zone models with GIS: emerging trends and potential bottlenecks. Journal of Environmental Quality, 25, 535-544.

Tim, U.S. & Jolly, R. (1994) Evaluating agricultural nonpoint-source pollution using integrated GIS and hydrological/water quality model. Journal of Environmental Quality, **23**, 25-35.

Touré, A., Thompson, K.P.B., Edwards, G., Brown, R.J., & Brisco, B.G. (1994) Adaptation of the MIMICS backscattering model to the agricultural context - wheat and canola at L and C bands. IEEE transactions on Geoscience and Remote Sensing, 32, 47-61.

Tsang, L. & Kong, J. (1981) Applications of strong fluctuation random medium theory to scattering from vegetation-like half space. IEEE Transactions on Geoscience and Remote Sensing, GE-19, 62-69.

Tso, B. & Mather, P.M. (1999) Crop discrimination using multi-temporal SAR imagery. International Journal of Remote Sensing, 20, 2443-2460.

Turner, B.L. & Haygarth, P.M. (2000) Phosphorus forms and concentrations in leachate under four grassland soil types. Soil Science Society of America Journal, 64, 1090-1099.

Ulaby, F.T. (1998) SAR biophysical retrievals: lessons learned and challenges to overcome. In Retrieval of bio- and geo-physical parameters from SAR data for land applications workshop. ESA-ESTEC.

Ulaby, F.T., Dubois, P.C., & van Zyl, J. (1996) Radar mapping of surface soil moisture. Journal of Hydrology, 184, 57-84.

Ulaby, F.T. & El Rays, M.A. (1987) Microwave dielectric spectrum of vegetation. Transactions on Geoscience and Remote Sensing, 25, 541-549.

Ulaby, F.T. & Elachi, C. (1990) Radar Polarimetry for Geoscience Applications Dedham, MA, Artech House, Inc.

Ulaby, F.T., Sarabandi, K., McDonald, K., Whitt, M., & Dobson, M.C. (1990) Michigan microwave canopy scattering model. *International Journal of Remote Sensing*, 11, 1223-1253.

USDA (1999) ArcView Interface for SWAT 99.2, User's Guide United States Department of Agriculture, Agricultural Research Service, Temple, Texas.

Uunk, E.J.B. (1991). Eutrophication of Surface Waters and the Contribution to of Agriculture, Rep. No. Proceedings Number 303. The Fertiliser Society, Peterborough.

Van Beek, P., Watson, R.D., & Maxwell, T.J. (1996) Making research work for the community: workshop report. In Multiple Land Use and Catchment Management (eds M. Cresser & K. Pugh), pp. 147-155. The Macaulay Land Use Research Institute, Aberdeen, Scotland.

van Genuchten, M.T., Gorelick, S.M., & Yeh, W.W.-G. (1990) Application of Parameter estimation techniques to solute transport studies. In *Proceedings of an International Symposium on Water Quality Modelling of Agricultural Non-Point source Pollution* (ed D.G. Decoursey). ARS-81 USDA-ARS, Washington DC, Logan, UT.

van Leeuwen, H.J.C. (1996) Methodology for Combining Optical and Microwave Remote Sensing in Agricultural Crop Monitoring; The Sugar Beet Crop as a Special Case. Ph.D., Agricultural University Wageningen, Wageningen, The Netherlands.

van Oevelen, P.J. & Hoekman, D.H. (1999) Radar backscatter inversion techniques for estimation of surface soil moisture: EFEDA-Spain and HAPEX-Sahel case studies. IEEE Transactions on Geosciences and Remote Sensing, 37, 113-123.

Vauchad, G., Vauclin, M., & Addiscott, T.M. (1990) Solute transport in the vadose zone: a review of models. In *Proceedings of an International Symposium on Water Quality Modelling of Agricultural Non-Point source Pollution* (ed D.G. Decoursey). ARS-81 USDA-ARS, Washington DC, Logan, UT.

Venables, W.N. & Ripley, B.D. (1999) Modern Applied Statistics with S-Plus Springer-Verlag, New York.

Viessman, W. & Lewis, G.L. (1996) Introduction to Hydrology, 4th edn. Harper Collins, New York.

Viner, A.B. (1987) Nutrients transported on silt in rivers. Arch. Hydrobiol. Beih. Ergebn. Limnol., 28, 63-71.

Wheater, H.S., Jakeman, A.J., & Beven, K.J. (1993). Progress and Directions in Rainfall-runoff Modelling. In Modelling Change in Environmental Systems (ed A.J. Jakeman), pp. 101-131. John Wiley & Sons Ltd.

Wigneron, J.P., Fouilhoux, M., Prevot, L., Chanzy, A., Olioso, A., Baghdadi, N., & King, C. (2002) Monitoring sunflower crop development from C-band radar observations. Agronomie, 22, 587-595.

Williams, J.R. (1969) Flood routing with variable travel time or variable storage coefficients. Transactions of the ASAE, 12, 100-103.

Williams, J.R. (1975) Sediment routing for agricultural watersheds. Water Resources Bulletin, 11, 965-974.

Williams, J.R., Jones, C.A., & Dyke, P.T. (1984) A modeling approach to determining the relationship between erosion and soil productivity. Transactions of the ASAE, 27, 129-144.

Williams, J.R., Nicks, A.D., & Arnold, J.G. (1985) Simulator for Water Resources in Rural Basins. *ASCE Journal of Hydraulic Engineering*, 111, 970-986.

Wischmeier, W.H. & Smith, D.D. (1965) Predicting Rainfall-erosion Losses from Cropland East of the Rocky Mountains USDA-ARS.

Wischmeier, W.H. & Smith, D.D. (1978) Predicting Rainfall Losses: A Guide to Conservation Planning U.S. Government Print Office, Washington D.C.

Withers, P.J.A. (1994) The Significance of Agriculture as a Source of Phosphorus Pollution to Inland and Coastal Waters in the UK ADAS Bridgets, Winchester.

Withers, P.J.A., Davidson, I.A., & Foy, R.H. (2000) Prospects for controlling nonpoint phosphorus loss to water: a UK perspective. Journal of Environmental Quality, 29, 167-175.

Wood, J. (1999) LandSerf http://www.landserf.org/, accessed 1999. City University, London.

Woolhiser, D.A., Jury, W.A., & Nielsen, D.R. (1990) Effects of spatial and temporal variability on water quality model development. In Proceedings International Symposium on Water Quality Modelling of Agricultural Non-Point Sources (ed D.G. DeCoursey), Vol. ARS-81. USDA-ARS, Washington D.C., Logan, UT.

Yeh, K.-C. & Tung, Y.-K. (1993) Uncertainty and sensitivity analyses of pit-migration model. Journal of Hydrological Engineering, ASCE, 119, 252-283.

Young, R.A., Onstad, C.A., Bosch, D.D., & Anderson, W.P. (1989) AGNPS: A nonpoint-source pollution model for evaluating agricultural watersheds. Journal of Soil and Water, 168-173.

Young, R.A. & Wiersma, J.L. (1973) The role of rainfall impact in soil detachment and transport. Water Resources Research, 9, 1629-1636.

Zar, J.H. (1984) Biostatistical Analysis, Second edn. Prentice-Hall, Englewood Cliffs, New Jersey.

Zribi, M. & Dechambre, M. (2003) A new empirical model to retrieve soil moisture and roughness from C-band radar data. Remote Sensing of Environment, 84, 42-52.

Zribi, M., Taconet, O., Ciarletti, V., & Vidal-Madjar, D. (2002) Effect of row structures on radar microwave measurements over soil surface. International Journal of Remote Sensing, 23, 5211-5224.

Appendices

Appendix A Example of vegetation data collected from the Stonton Brook for inclusion in SWAT model and comparison with plant growth simulation

Table A1 Wheat.

Date	Dry biomass (kg/m^2)	Dry biomass (tonne Ha^{-1})	LAI (m^2/m^2)
06-Nov-98	0.001519	0.015194	0.012837
19-Dec-98	0.012312	0.123117	0.274924
14-Feb-99	0.016905	0.169053	0.392631
23-Mar-99	0.12989	1.2989	1.397681
31-May-99	0.883354	8.833543	6.981849
05-Jul-99	1.025467	10.25467	7.11962
13-Aug-99			
18-Oct-99	0.011459	0.114593	0.230137

Table A2 Oilseed rape.

Date	Dry biomass (kg/m^2)	Dry biomass (tonne Ha^{-1})	LAI (m^2/m^2)
10-Oct-98	0.123092	1.230923	0.039396
06-Nov-98	0.071999	0.719992	0.529212
08-Dec-98	0.129013	1.290131	1.054389
15-Jan-99	0.205508	2.055084	1.486
14-Feb-99	0.353224	3.53224	2.0462
23-Mar-99	0.467428	4.674285	2.860078
31-May-99	2.533661	25.33661	3.155871
05-Jul-99	3.32952	33.2952	0.219872

Appendix B Example of field survey data used in remote sensing exercise

Table B1 Data collected from wheat fields relevant to May and July 1999

Site no.	Soil % Sand	Silt	Clay	RMS (cm)	Soil correlation (cm)
1a	5	45	50	3.656021	4.5
1b	0	48	52	1.732374	3.5
2a	4	57	39	4.16832	4.75
2b	5	54	41	4.294209	18.5
3a	22	40	37	2.8369675	9.125
3b	17	52	31	2.0088675	14
4a	27	44	29	0.8304955	18.5
4b	40	27	33	1.1581255	11.75
5a	32	35	33	1.439792	5.25
5b	37	35	28	1.164592	3.25
6a	24	39	37	3.656021	6
6b	24	40	36	3.1510245	7

Table B2 Vegetation and soil data collected from wheat in May 1999

Site no.	Total wet wt. (g)	Trunk wt. (g)	Trunk ht. (m)	Trunk width (cm)	LA (cm^2)	Crown ht. (m)	Soil moisture
1a	8.02±0.9	5.60±0.7	0.39±0.04	0.45±0.03	119.13±9.9	0.751	26.8%
1b	10.25±1.1	7.16±0. 9	0.44±0.03	0.52±0.02	144.4±9.4	0.806	28.9%
2a	11.54±0.8	7.04±0.4	0.61±0.02	0.48±0.01	158.9±40.2	0.864	28.7%
2b	10.84±0.9	7.00±0.5	0.56±0.02	0.51±0.02	145.2±6.1	0.786	26.2%
3a	9.51±0.9	7.06±0.8	0.51±0.02	0.48±0.02	129.3±5.1	0.769	23.1%
3b	7.16±1.5	5.24±1.2	0.36±0.05	0.44±0.04	99.2±13.4	0.752	21.3%
4a	8.76±0.9	6.07±0.6	0.56±0.03	0.44±0.02	121.0±7.4	0.788	21.5%
4b	9.00±1.2	5.74±0.8	0.53±0.05	0.44±0.02	125.9±11.8	0.799	27.1%
5a	9.78±0.8	6.81±0.6	0.53±0.02	0.47±0.03	118.5±6.7	0.801	22.7%
5b	10.85±1.0	7.38±0.5	0.53±0.03	0.52±0.02	119.42±8.3	0.827	21.7%
6a	7.45±0.9	4.92±0.7	0.39±0.03	0.47±0.03	130.29±9.7	0.675	25.3%
6b	8.67±0.9	5.78±0.7	0.39±0.02	0.54±0.02	148.43±3.9	0.675	26.5%

Table B3 Derivatives from data in Table 4.2 for wheat in May

Site no.	Leaf grav. moisture	Leaf density	LAI	Trunk grav. moisture	Trunk dry density	Leaf dry density	Soil vol. moisture
1a	0.7933	3716	0.146	0.8471	0.1430	0.1975	0.2680
1b	0.8129	3242	0.13	0.8337	0.1277	0.1850	0.2887
2a	0.8420	2910	0.125	0.8257	0.1085	0.1480	0.2867
2b	0.8277	3495	0.136	0.8130	0.1152	0.1530	0.2615
3a	0.8042	3809	0.136	0.8440	0.1175	0.1728	0.2311
3b	0.8228	3150	0.193	0.8287	0.1673	0.1411	0.2131
4a	0.9382	4150	0.134	0.8240	0.1247	0.0426	0.2150
4b	0.8277	4715	0.11	0.8158	0.1279	0.1628	0.2711
5a	0.7990	3270	0.154	0.8427	0.1165	0.1703	0.2272
5b	0.7991	3635	0.137	0.8229	0.1157	0.2361	0.2172
6a	0.80143	4103	0.137	0.8256	0.1241	0.1790	0.2532
6b	0.7433	4158	0.12	0.8255	0.1128	0.2323	0.2648

Table B4 Dielectric constants for vegetation in Table 1

Site no	Trunks		Leaves	
	r	-j	r	-j
1a	70.013	26.53	30.881	11.726
1b	53.55	20.292	32.256	12.242
2a	37.416	14.187	34.357	13.028
2b	36.469	13.828	33.316	12.639
3a	52.069	19.731	31.642	12.012
3b	84.058	31.859	32.958	12.505
4a	46.29	17.543	41.823	15.815
4b	44.484	16.86	33.313	12.638
5a	50.534	19.149	31.276	11.874
5b	40.434	15.328	32.969	12.509
6a	46.666	17.685	31.447	11.939
6b	39.816	15.094	27.53	10.467

Appendix C.1 Acid Hydrolysis and Determination of Orthophosphate (Based on method from Rowland and Haygarth, 1997).

This protocol to be used in conjunction with record sheet LRS1

Materials Preparation.

1.0 0.5M Sulphuric Acid
Slowly add 27ml of concentrated sulphuric acid (S.G. 1.84) to 800ml deionised water and stir. Make up to 1000ml with deionised water. Store in glass bottle.

2.0 Dry 2 batches of 1g potassium dihydrogen orthophosphate from separate sources for two hours in oven at 105°C for 2 hours (oven in Room 209).

3.0 100mg $P.l^{-1}$ Phosphate Stock Standard
Weigh out accurately 0.4394g of potassium dihydrogen orthophosphate from each batch of 2 above. Transfer each measure to separate 1000ml flasks and dissolve in deionised water, then make up to 1000ml. Mark each flask stock A and stock B. Store in dark at 4-6°C and REPLACE MONTHLY.

4.0 Working standards.
Make up serial dilutions as agreed with BS using following amounts of Stock Standard (Stock A and B from 3.0 above) in 500 ml volumetric flask and dilute to the mark.

1.0 mg:	5ml stock to 500ml.
0.9 mg:	4.5ml stock to 500ml.
0.8 mg:	4ml stock to 500ml.
0.7 mg:	3.5ml stock to 500ml.
0.6 mg:	3ml stock to 500ml.
0.5 mg:	2.5ml stock to 500ml.
0.4 mg:	2ml stock to 500ml.
0.3 mg:	1.5ml stock to 500ml.
0.2 mg:	1ml stock to 500ml.
0.1 mg:	0.5ml stock to 500ml.

PREPARE FRESHLY AS REQUIRED.

Two sets of standards must be prepared one from Stock A and one from Stock B.

5.0 Mixed Reagent

5.1 Acid-molybdate reagent.

Dissolve 0.57g antimony potassium (+)-tartrate in water, warming if necessary, and dilute to 500ml. Carefully add whilst stirring and cooling, 45ml concentrated sulphuric acid.

Separately, dissolve 8.52g ammonium molybdate in 400ml deionised water.

Mix both solutions together and dilute to 1000 ml. Store in refrigerator.

☐

5.2 Persulphate colorimetric reagent

On day of analysis complete colorimetric reagent by dissolving 0.31g L-ascorbic acid in 50ml of acid-molybdate reagent.

Analytical Procedure. ☐

The following equipment will be required:

40 X 60 ml polyethylene bottles with screw tops.

dropper and various pipettes/Gilson tips

All regularly used equipment must be cleaned using detergent/ascorbic acid wash and pre-cleaned by soaking overnight in 10% nitric acid solution and rinsed three times in deionised water. Between samples and QC solutions pipettes, flasks, measuring cylinders and spectrophotometer cells must be rinsed well in deionised water and allowed to drain as thoroughly as possible.

A Transfer 25ml of each sample to marked polyethylene bottles. Repeat with 25ml blank (deionised water) and agreed pre-digest QC phosphate working standards. ☐

B Add 0.17g ammonium persulphate and 1.25ml 0.5M sulphuric acid to each tube and swirl to mix. In addition, a blank without persulphate but inclusive of acid; with persulphate but without acid, and one with neither in, also needs to be prepared: ☐

C **<u>Ensure caps are placed loosely on bottles</u>** and autoclave for one hour at 121°C and 1.05 bar. Remove from autoclave and allow to cool. ☐

D Prepare two post-digest blanks one only of water and one inclusive of persulphate and acid. ☐

E Add 1ml persulphate colorimetric reagent and leave for 12 minutes. ☐

F Set-up spectrophotometer at 880nm. Zero for deionised water and note absorbance of samples blanks and standards ensuring that no bubbles exist on the inside of the glass. ☐

NOTE: the spectrophotometer in the lab has an intermittent cut-out fault. If left for longer than necessary the machine can switch itself off. Re-zeroing is then required which renders previous absorbancies incompatible. Always ensure that you can complete the analysis without moving from the bench.

G Construct a graph of concentration against absorbance and note deviation from linearity. ☐

NOTE: Should the sample be turbid and total phosphorus expected above 1mg $P.l^{-1}$, dilutions must be applied. Discuss with Barry if absorbance is above highest quality control standard's.

Appendix C.2 Protocol for Determination of Soil Moisture Content and Organic Matter Content (Loss on Ignition).

This protocol to be read in conjunction with record sheet LRS2

Soil Moisture Content

Equipment:

Porcelain basins or crucibles.

Oven capable of 105°C

Muffle furnace capable of 250 and 450°C

Method

1. Remove stones > 3mm from samples.
2. Weigh empty crucibles (A) and place appropriate amount of soil sample (approx 25gm) in marked crucible and reweigh (B).
3. Place in oven at 105°C for 17 hours or until weight remains constant $\Delta < + 0.15$gm. Weighing must be carried out on cool samples.
4. Cool in desiccator and reweigh. Note oven-dry weight (C).

Organic Matter Content (Loss on Ignition)

Materials:

Porcelain bowls or crucibles.

Furnace capable of 500°C.

Method

5. Lightly break up aggregates from samples from 4 above and remove stones >3mm
6. Replace in crucibles, reweigh (D) and place in furnace at 220°C for 16 hours
7. Cool in a desiccator and reweigh. Note mass of soil (E)
8. Heat crucibles slowly to 450°C and maintain for 4 hours. Allow to cool substantially before moving to a desiccator. Reweigh and note final mass (F)

Notes:

i. As many replicates as possible must be used to ensure fair representation of variation. Both these variables are highly erratic.

Appendix D Example data Input to MIMICS model

Table D1 May data collection

Site no.	Total wet weight (g)	Trunk weight (g)	Trunk height (m)	Trunk width (cm)	LA (cm^2)	Crown ht. (m)	Soil moisture %
1a	8.02±0.88	5.60±0.66	0.39±0.04	0.45±0.03	119.13±9.93	0.7513	26.8
1b	10.25±1.13	7.16±0.89	0.44±0.03	0.52±0.02	144.4±9.36	0.8063	28.9
2a	11.54±0.80	7.04±0.44	0.61±0.02	0.48±0.01	158.9±40.2	0.8638	28.7
2b	10.84±0.87	7.00±0.52	0.56±0.02	0.51±0.02	145.2±6.05	0.786	26.2
3a	9.51±0.91	7.06±0.81	0.51±0.02	0.48±0.02	129.3±5.08	0.769	23.1
3b	7.16±1.45	5.24±1.17	0.36±0.05	0.44±0.04	99.2±13.42	0.752	21.3
4a	8.76±0.88	6.07±0.55	0.56±0.03	0.44±0.02	121.0±7.43	0.788	21.5
4b	9.00±1.24	5.74±0.81	0.53±0.05	0.44±0.02	125.9±11.77	0.799	27.1
5a	9.78±0.82	6.81±0.55	0.53±0.02	0.47±0.03	118.5±6.66	0.801	22.7
5b	10.85±1.02	7.38±0.54	0.53±0.03	0.52±0.02	119.42±8.29	0.827	21.7
6a	7.45±0.91	4.92±0.68	0.39±0.03	0.47±0.03	130.29±9.74	0.675	25.3
6b	8.67±0.85	5.78±0.70	0.39±0.02	0.54±0.02	148.43±3.91	0.675	26.5

Table D2 Derived May data. Values are derived from the measurements in Table D1 above.

Site no.	Leaf grav. moisture	Leaf density	LAI	Trunk grav. moisture	Dry density trunk	Dry density leaf	Soil vol. moisture
1a	0.7933	3716	0.1464	0.8471	0.1430	0.1975	0.2680
1b	0.8129	3242	0.1296	0.8337	0.1277	0.1850	0.2887
2a	0.8420	2910	0.1252	0.8257	0.1085	0.1480	0.2867
2b	0.8277	3495	0.1363	0.8130	0.1152	0.1530	0.2615
3a	0.8042	3809	0.1359	0.8440	0.1175	0.1728	0.2311
3b	0.8228	3150	0.1933	0.8287	0.1673	0.1411	0.2131
4a	0.9382	4150	0.1339	0.8240	0.1247	0.0426	0.2150
4b	0.8277	4715	0.1097	0.8158	0.1279	0.1628	0.2711
5a	0.7990	3270	0.1537	0.8427	0.1165	0.1703	0.2272
5b	0.7991	3635	0.1365	0.8229	0.1157	0.2361	0.2172
6a	0.80143	4103	0.1367	0.8256	0.1241	0.1790	0.2532
6b	0.7433	4158	0.1200	0.8255	0.1128	0.2323	0.2648

Table D3 Dielectric constants

Site no	Trunks		Leaves	
	r	-j	r	-j
1a	70.013	26.53	30.881	11.726
1b	53.55	20.292	32.256	12.242
2a	37.416	14.187	34.357	13.028
2b	36.469	13.828	33.316	12.639
3a	52.069	19.731	31.642	12.012
3b	84.058	31.859	32.958	12.505
4a	46.29	17.543	41.823	15.815
4b	44.484	16.86	33.313	12.638
5a	50.534	19.149	31.276	11.874
5b	40.434	15.328	32.969	12.509
6a	46.666	17.685	31.447	11.939
6b	39.816	15.094	27.53	10.467

Appendix E List of parameters in SWAT model (From Neitsch *et al.*, 2002)

A 3 x 3 matrix of elements defined to ensure serial and cross correlation of generated temperature and radiation values $A = M_1 \cdot M_0^{-1}$
A_{ch} Cross-sectional area of flow in the channel (m^2)
$A_{ch,bnkfull}$ Cross-sectional area of flow in the channel when filled to the top of the bank (m^2)
A_s Area of sediment-water interface (m^2)
A_{surf} Amplitude of the surface fluctuations in soil temperature (°C)
AGP Algal growth potential (mg l^{-1})
$Area$ Subbasin area (km^2 or ha)
AU Astronomical unit (1 AU = 1.496 x 10^8 km)
AWC Available water capacity (mm H_2O)
AWC_{ly} Available water capacity for layer ly (mm H_2O)
B 3 x 3 matrix of elements defined to ensure serial and cross correlation of generated temperature and radiation values $B \cdot B^T = M_0 - M_1 \cdot M_0^{-1} \cdot M_1^T$
BFD Number of baseflow days for the watershed
C Runoff coefficient in peak runoff rate calculation
$C1$ Coefficient in Muskingum flood routing equation
$C2$ Coefficient in Muskingum flood routing equation
$C3$ Coefficient in Muskingum flood routing equation
C_{CH} Channel cover factor
C_{NH4} Concentration of ammonium in the reach (mg N/L).
C_{NO3} Concentration of nitrate in the reach (mg N/L)
$C_{solidphase}$ Concentration of the pesticide sorbed to the solid phase (mg chemical/kg solid material)
C_{solP} Concentration of phosphorus in solution in the reach (mg P/L)
$C_{solution}$ Concentration of the pesticide in solution (mg chemical/L solution)
C_{USLE} USLE cover and management factor
$C_{USLE,aa}$ Average annual C factor for the land cover
$C_{USLE,mn}$ Minimum value for the cover and management factor for the land cover
$CFRG$ Coarse fragment factor
$Chla$ Chlorophyll *a* concentration (•g/L)
$Chla_{co}$ User-defined coefficient to adjust predicted chlorophyll *a* concentration
CN Curve number
CN_1 Moisture condition I curve number
CN_2 Moisture condition II curve number
CN_{2s} Moisture condition II curve number adjusted for slope
CN_3 Moisture condition III curve number
CO_2 Concentration of carbon dioxide in the atmosphere (ppmv)
CO_{2amb} Ambient atmospheric CO_2 concentration (330 ppmv)
CO_{2hi} Elevated atmospheric CO_2 concentration (ppmv)
CV Total aboveground biomass and residue present on current day (kg ha^{-1})
D_a Oxygen deficit above the structure (mg O_2/L)
D_b Oxygen deficit below the structure (mg O_2/L)
D_g Gas molecular diffusion coefficient (m^2/day)
D_l Liquid molecular diffusion coefficient (m^2/day)
D_m Molecular diffusion coefficient for oxygen (m^2/day)
D_{sed} Depth of the active sediment layer (m)
DA HRU drainage area (km^2)
E Depth rate evaporation (mm d^{-1})
E_0 Eccentricity correction factor of earth $(r_0/r)^2$

E_a Actual amount of evapotranspiration on a given day (mm H_2O)
E_{can} Amount of evaporation from free water in the canopy on a given day (mm H_2O)
E_{ch} Evaporation from the reach for the day (m^3 H_2O)
E_o Potential evapotranspiration (mm d^{-1})
E'_o Potential evapotranspiration adjusted for evaporation of free water in the canopy (mm H_2O)
E_s Maximum sublimation/soil evaporation on a given day (mm H_2O)
E'_s Maximum sublimation/soil evaporation adjusted for plant water use on a given day (mm H_2O)
E''_s Maximum soil water evaporation on a given day (mm H_2O)
$E_{soil,ly}$ Evaporative demand for layer *ly* (mm H_2O)
$E'_{soil,ly}$ Evaporative demand for layer *ly* adjusted for water content (mm H_2O)
$E''_{soil,ly}$ Amount of water removed from layer *ly* by evaporation (mm H_2O)
$E_{soil,z}$ Evaporative demand at depth *z* (mm H_2O)
E_{storm} Total storm energy (0.0017 m-metric ton/m^2),
E_{sub} Amount of sublimation on a given day (mm H_2O)
E_t Transpiration rate (maximum) (mm d^{-1})
$E_{t,act}$ Actual amount of transpiration on a given day (mm H_2O)
EI_{USLE} Rainfall erosion index (0.017 m-metric ton cm/(m^2 hr))
EL Elevation (m)
EL_{band} Mean elevation in the elevation band (m)
EL_{gage} Elevation at the precipitation, temperature, or weather generator data recording gage (m)
F_d Fraction of total pesticide in the dissolved phase
$F_{d,sed}$ Fraction of total sediment pesticide in the dissolved phase
F_{inf} Cumulative infiltration at time *t* (mm H_2O)
F_p Fraction of total pesticide in the particulate phase
$F_{p,sed}$ Fraction of total sediment pesticide in the particulate phase
FC Water content of soil profile at field capacity (mm H_2O)
FC_{ly} Water content of layer *ly* at field capacity (mm H_2O)
FL Algal growth attenuation factor for light for the water column
FL_z Algal growth attenuation factor for light at depth *z*
FN Algal growth limitation factor for nitrogen
FP Algal growth limitation factor for phosphorus
G Heat flux density to the ground (MJ m^{-2} d^{-1})
H_0 Extraterrestrial daily irradiation (MJ m^{-2} d^{-1})
H_b Net outgoing long-wave radiation (MJ m^{-2} d^{-1})
H_{day} Solar radiation reaching ground on current day of simulation (MJ m^{-2} d^{-1})
H_e Henry's constant (atm m^3 $mole^{-1}$)
H_L Long-wave radiation (MJ m^{-2} d^{-1})
H_{MX} Maximum possible solar radiation (MJ m^{-2} d^{-1})
H_{net} Net radiation on day (MJ m^{-2} d^{-1})
H_o Saturated thickness normal to the hillslope at the outlet expressed as a fraction of the total thickness (mm/mm)
H_{phosyn} Intercepted photosynthetically active radiation on a given day (MJ m^{-2})
H_R Radiant energy (MJ m^{-2} d^{-1})
HI Potential harvest index for a given day
HI_{act} Actual harvest index
HI_{min} Harvest index for the plant in drought conditions and represents the minimum harvest index allowed for the plant

HI_{opt} Potential harvest index for the plant at maturity given ideal growing conditions
HI_{trg} Target harvest index
HU Number of heat units accumulated on a given day where base temperature is dependant on the plant species (heat units)
HU_0 Number of base zero heat units accumulated on a given day (heat units)
I_0 Extraterrestrial daily irradiance incident on a horizontal surface (MJ m^{-2} d^{-1})
I_{0n} Extraterrestrial daily irradiance incident on a normal surface (MJ m^{-2} d^{-1})
I_{30} Maximum 30 minute intensity (mm/hr)
I_a Initial abstractions which includes surface storage, interception and infiltration prior to runoff (mm H_2O)
I_{frac} Fraction of daily solar radiation falling during specific hour on current day of simulation
I_{hr} Solar radiation reaching ground during specific hour on current day of simulation (MJ m^{-2} h^{-1})
$I_{phosyn,hr}$ Photosynthetically-active solar radiation reaching ground during specific hour on current day of simulation (MJ m^{-2} h^{-1})
$I_{phosyn,z}$ Photosynthetically-active light intensity at a depth z below the water surface (MJ/m^2 -hr)
I_{SC} Solar constant (4.921 MJ m^{-2} h^{-1})
$\bar{I}_{phosyn,hr}$ Daylight average photosynthetically-active light intensity (MJ/m^2 -hr)
J_i Jet index used to calculate channel erodibility
K Storage time constant for the reach (s)
$K_{0.1bnkfull}$ Storage time constant calculated for the reach segment with one-tenth of the bankfull flows (s)
K_1 Dimension coefficient in Penman-Monteith equation
$K_{bnkfull}$ Storage time constant calculated for the reach segment with bankfull flows (s)
K_{ch} Effective hydraulic conductivity of the channel alluvium (mm/hr)
K_{CH} Channel erodibility factor
K_d Pesticide partition coefficient (m^3 /g)
K_e Effective hydraulic conductivity (mm/hr)
K_g Mass-transfer velocity in the gaseous laminar layer (m/day)
K_l Mass-transfer velocity in the liquid laminar layer (m/day)
K_L Half-saturation coefficient for light (MJ/m^2 -hr)
$K_{l,O2}$ Oxygen transfer coefficient (m/day)
K_N Michaelis-Menton half-saturation constant for nitrogen (mg N/L)
K_{oc} Soil adsorption coefficient normalized for soil organic carbon content (ml/g or (mg kg^{-1})/(mg l^{-1}) or L/kg)
K_p Soil adsorption coefficient ((mg/kg)/(mg l^{-1}))
K_P Michaelis-Menton half-saturation constant for phosphorus (mg P l^{-1})
K_{sat} Saturated hydraulic conductivity (mm/hr)
K_{USLE} USLE soil erodibility factor (0.013 metric ton m^2 hr/(m^3 -metric ton cm))
L Channel length from the most distant point to the subbasin outlet (km)
L_c Average flow channel length for the subbasin (km)
L_{cen} Distance along the channel to the subbasin centroid (km)
L_{ch} Length of main channel (km)

L_{gw} Distance from the ridge or subbasin divide for the groundwater system to the main channel (m)
L_{hill} Hillslope length (m)
L_{slp} Subbasin slope length (m)
LAI Leaf area index of the canopy
LAI_{evap} Leaf area index at which no evaporation occurs from the water surface
LAI_{mx} Maximum leaf area index for the plant
LS_{USLE} USLE topographic factor
M Particle-size parameter for estimation of USLE K factor
M_0 3 x 3 matrix of correlation coefficients between maximum temperature, minimum temperature and solar radiation on same day
M_1 3 x 3 matrix of correlation coefficients between maximum temperature, minimumn temperature and solar radiation on consecutive days
M_{flowin} Mass of nutrient entering water body on the given day (kg)
$M_{initial}$ Initial mass of nutrient in water body for the given day (kg)
M_s Mass of the solids (Mg)
M_{sed} Mass of solid phase in the sediment layer (g)
$M_{settling}$ Mass of nutrient lost via settling on a given day (kg)
M_{stored} Mass of nutrient in water body at end of previous day (kg)
MW Molecular weight of the pesticide compound
N Time lapsed since the start of the recession (days)
$N_{actualup,ly}$ Actual nitrogen uptake for layer ly (kg N/ha)
$N_{dec,ly}$ Nitrogen decomposed from the fresh organic N pool (kg N/ha)
N_{demand} Nitrogen uptake demand not met by overlying soil layers (kg N/ha)
$N_{denit,ly}$ Amount of nitrogen lost to denitrification (kg N/ha)
N_{evap} Amount of nitrate moving from the first soil layer to the soil surface zone (kg N/ha)
N_{fix} Amount of nitrogen added to the plant biomass by fixation (kg N/ha)
$N_{mina,ly}$ Nitrogen mineralized from the humus active organic N pool (kg N/ha)
$N_{minf,ly}$ Nitrogen mineralized from the fresh organic N pool (kg N/ha)
$N_{nit,ly}$ Amount of nitrogen converted from NH_4^+ to NO^-_3 in layer ly (kg N/ha)
$N_{nit|vol,ly}$ Amount of ammonium converted via nitrification and volatilization in layer ly (kg N/ha)
N_{rain} Nitrate added by rainfall (kg N/ha)
$N_{trns,ly}$ Amount of nitrogen transferred between the active and stable organic pools (kgN/ha)
N_{up} Potential nitrogen uptake (kg N/ha)
$N_{up,ly}$ Potential nitrogen uptake for layer ly (kg N/ha)
$N_{up,z}$ Potential nitrogen uptake from the soil surface to depth z (kg N/ha)
$N_{up,zl}$ Potential nitrogen uptake from the soil surface to the lower boundary of the soil layer (kg N/ha)
$N_{up,zu}$ Potential nitrogen uptake from the soil surface to the upper boundary of the soil layer (kg N/ha)
$N_{vol,ly}$ Amount of nitrogen converted from NH_4^+ to NH_3 in layer ly (kg N/ha)
ND_{targ} Number of days required for the reservoir to reach target storage
$NH4$ Ammonium content of the soil profile (kg NH_4-N/ha)

$NH4_{fert}$ Amount of ammonium added to the soil in the fertilizer (kg N/ha)
$NH4_{ly}$ Ammonium content of layer *ly* (kg NH_4-N/ha)
$NH4_{str}$ Ammonium concentration in the stream (mg N/L)
$NO2_{str}$ Nitrite concentration in the stream (mg N/L)
$NO3$ Nitrate content of the soil profile (kg NO_3-N/ha)
$NO3_{conc,z}$ Concentration of nitrate in the soil at depth *z* (mg/kg or ppm)
$NO3_{fert}$ Amount of nitrate added to the soil in the fertilizer (kg N/ha)
$NO3'_{lat}$ Amount of lateral flow nitrate generated in HRU on a given day (kg N/ha)
$NO3_{lat,ly}$ Nitrate removed in lateral flow from a layer (kg N/ha)
$NO3_{latstor,i-1}$ Lateral flow nitrate stored or lagged from the previous day (kg N/ha)
$NO3_{ly}$ Nitrate content of soil layer *ly* (kg NO_3-N/ha)
$NO3_{perc,ly}$ Nitrate moved to the underlying layer by percolation (kg N/ha)
$NO3_{str}$ Nitrate concentration in the stream (mg N/L)
$NO3_{surf}$ Nitrate removed in surface runoff (kg N/ha)
$NO3'_{surf}$ Amount of surface runoff nitrate generated in HRU on a given day (kg N/ha)
$NO3_{surstor,i-1}$ Surface runoff nitrate stored or lagged from the previous day (kg N/ha)
OM Percent organic matter (%)
Ox_{sat} Saturation oxygen concentration (mg O_2/L)
Ox_{str} Dissolved oxygen concentration in the stream (mg O_2/L)
Ox_{surf} Dissolved oxygen concentration in surface runoff (mg O_2/L)
P Atmospheric pressure (kPa)
$P_{actualup,ly}$ Actual phosphorus uptake for layer *ly* (kg P/ha)
$P_{act|sta,ly}$ Amount of phosphorus transferred between the active and stable mineral pools (kg P/ha)
P_{ch} Wetted perimeter for a given depth of flow (m)
$P_{dec,ly}$ Phosphorus decomposed from the fresh organic P pool (kg P/ha)
P_{demand} Phosphorus uptake demand not met by overlying soil layers (kg P/ha)
$P_i(D/D)$ Probability of a dry day on day *i* given a dry day on day *i* -1
$P_i(D/W)$ Probability of a dry day on day *i* given a wet day on day *i* -1
$P_i(W/D)$ Probability of a wet day on day *i* given a dry day on day *i* -1
$P_i(W/W)$ Probability of a wet day on day *i* given a wet day on day *i* -1
$P_{mina,ly}$ Phosphorus mineralized from the humus active organic P pool (kg P/ha)
$P_{minf,ly}$ Phosphorus mineralized from the fresh organic P pool (kg P/ha),
P_{perc} Amount of phosphorus moving from the top 10 mm into the first soil layer (kg P/ha)
$P_{solution,fert}$ Amount of phosphorus in the solution pool added to the soil in the fertilizer (kg P/ha)
$P_{solution,ly}$ Phosphorus content of soil solution in layer *ly* (kg P/ha)
$P_{sol|act,ly}$ Amount of phosphorus transferred between the soluble and active mineral pool(kg P/ha)
$P_{stor,i-1}$ Solution P loading stored or lagged from the previous day (kg P/ha)
P_{surf} Amount of soluble phosphorus lost in surface runoff (kg P/ha)

P'_{surf} Amount of solution P loading generated in HRU on a given day (kg P/ha)
P_{up} Potential phosphorus uptake (kg P/ha)
$P_{up,ly}$ Potential phosphorus uptake for layer *ly* (kg P/ha)
$P_{up,z}$ Potential phosphorus uptake from the soil surface to depth *z* (kg P/ha)
$P_{up,zl}$ Potential phosphorus uptake from the soil surface to the lower boundary of the soil layer (kg P/ha)
$P_{up,zu}$ Potential phosphorus uptake from the soil surface to the upper boundary of the soil layer (kg P/ha)
P_{USLE} USLE support practice factor
PHU Potential heat units or total heat units required for plant maturity where base temperature is dependent on the plant species (heat units)
PHU_0 Total base zero heat units or potential base zero heat units (heat units)
Q Volumetric flow rate for water exiting water body (m^3 H_2O/day)
Q_{gw} Groundwater flow, or base flow, into the main channel (mm H_2O)
$Q_{gw,0}$ Groundwater flow at the start of the recession (mm H_2O)
$Q_{gw,N}$ Groundwater flow on day *N* (mm H_2O)
Q_{lat} Lateral flow; water discharged from the hillslope outlet (mm H_2O/day)
$Q_{latstor,i-1}$ Lateral flow stored or lagged from the previous day (mm H_2O)
Q_{stor} Surface runoff stored or lagged (mm H_2O)
Q_{surf} Surface runoff on a given day (mm H_2O)
R Universal gas constant (8.206×10^{-52} atm m^3 (K mole)$^{-1}$)
$R_{0.5sm}$ Smoothed maximum half-hour rainfall for a given month (mm H_2O)
$R_{0.5x}$ Extreme maximum half-hour rainfall for the specified month (mm H_2O)
$R_{\Delta t}$ Amount of rain falling during the time step (mm H_2O)
R_{band} Precipitation falling in the elevation band (mm H_2O)
R_{ch} Hydraulic radius for a given depth of flow (m)
R_{day} Amount of rainfall on a given day (mm H_2O)
R'_{day} Amount of precipitation on a given day before canopy interception is removed (mm H_2O)
R_h Average relative humidity for the day
R_{hDmon} Average relative humidity of the month on dry days
R_{hLmon} Smallest relative humidity value that can be generated on a given day in the month
R_{hmon} Average relative humidity for the month
R_{hUmon} Largest relative humidity value that can be generated on a given day in the month
R_{hWmon} Average relative humidity for the month on wet days
R_{INT} Amount of free water held in the canopy on a given day (mm H_2O)
R_{NO3} Concentration of nitrogen in the rain (mg N/L)
R_{tc} Amount of rain falling during the time of concentration (mm H_2O)
RUE Radiation-use efficiency of the plant (kg/ha·(MJ/m^2)$^{-1}$ or 10^{-1} g/MJ)
RUE_{amb} Radiation-use efficiency of the plant at ambient atmospheric CO_2 concentration (kg/ha·(MJ/m^2)$^{-1}$ or 10^{-1} g/MJ)
RUE_{hi} Radiation-use efficiency of the plant at the elevated atmospheric CO_2 concentration, CO_{2hi}, (kg/ha·(MJ/m^2)$^{-1}$ or 10^{-1} g/MJ)
$RUE_{vpd=1}$ Radiation-use efficiency for the plant at a vapor pressure deficit of 1 kPa

(kg/ha·(MJ/m^2)$^{-1}$ or 10^{-1} g/MJ)

S Retention parameter in SCS curve number equation (mm)
S_3 Retention parameter for the moisture condition III curve number
S_{frz} Retention parameter adjusted for frozen conditions (mm)
S_{max} Maximum value the retention parameter can achieve on any given day (mm)
SA Surface area of the water body (m^2)
SA_{em} Surface area of the reservoir/pond when filled to the emergency spillway (ha)
SA_{mx} Surface area of the wetland when filled to the maximum water level (ha)
SA_{nor} Surface area of the wetland when filled to the normal water level (ha)
SA_{pr} Surface area of the reservoir/pond when filled to the principal spillway (ha)
SAT Amount of water in the soil profile when completely saturated (mm H_2O),
SAT_{ly} Amount of water in the soil layer when completely saturated (mm H_2O)
SC Storage coefficient for variable storage flow routing
SD Secchi-disk depth (m)
SD_{co} User-defined coefficient to adjust predicted secchi-disk depth
SED Solid build-up (kg/curb km)
SED_{mx} Maximum accumulation of solids possible for the urban land type (kg/curb km)
SND_{day} Standard normal deviate for the day
SNO Water content of snow cover on current day (mm H_2O)
SNO_{100} Amount of snow above which there is 100% cover (mm H_2O)
SNO_{mlt} Amount of snow melt on a given day (mm H_2O)
SW Amount of water in soil profile (mm H_2O)
SW_{ly} Soil water content of layer *ly* (mm H_2O)
$SW_{ly,excess}$ Drainable volume of water stored layer (mm H_2O)
T_{bare} Temperature of soil surface with no cover (°C)
T_{base} Plant's base or minimum temperature for growth (°C)
T_{DL} Daylength (h)
$T_{DL,mn}$ Minimum daylength for the watershed during the year (hrs)
$T_{DL,thr}$ Threshold daylength to initiate dormancy (hrs)
T_{hr} Air temperature during hour (°C)
T_K Mean air temperature in Kelvin (273.15 + °C)
T_{mlt} Threshold temperature for snow melt (°C)
T_{mn} Minimum air temperature for day (°C)
$T_{mn,band}$ Minimum daily temperature in the elevation band (°C)
T_{mx} Maximum air temperature for day (°C)
$T_{mx,band}$ Maximum daily temperature in the elevation band (°C)
T_{opt} Plant's optimal temperature for growth (°C)
T_{s-r} Rain/snow boundary temperature (°C)
T_{snow} Snow pack temperature on a given day (°C)
T_{soil} Soil temperature (°C)
$T_{soil,ly}$ Temperature of layer *ly* (°C)
T_{SR} Time of sunrise in solar day (h)
T_{SS} Time of sunset in solar day (h)
T_{ssurf} Soil surface temperature (°C)
$T_{wat,K}$ Water temperature in Kelvin (273.15+°C)
T_{water} Average daily water temperature (°C)

$\overline{T}_{AA}$ Average annual soil temperature (°C)
$\overline{T}_{AAair}$ Average annual air temperature (°C)
$\overline{T}_{av}$ Mean air temperature for day (°C)
$\overline{T}_{av,band}$ Mean daily temperature in the elevation band (°C)
$\overline{T}_{water}$ Average water temperature (°C)
TN Total Kjeldahl nitrogen load (moles)
TP Total phosphorus load (moles)
TT Travel time (s)
TT_{lag} Lateral flow travel time (days)
TT_{perc} Travel time for percolation (hrs)
V Volume of water in water body (m^3 H_2O)
V_A Volume of air (m^3)
V_{bnk} Volume of water added to the reach via return flow from bank storage (m^3 H_2O)
V_{ch} Volume of water stored in the channel (m^3)
V_{em} Volume of water held in the reservoir when filled to the emergency spillway (m^3 H_2O)
V_{evap} Volume of water removed from the water body by evaporation during the day (m^3 H_2O)
V_{flowin} Volume of water entering water body on given day (m^3 H_2O)
$V_{flowout}$ Volume of water flowing out of the water body during the day (m^3 H_2O)
$V'_{flowout}$ Initial estimate of the volume of water flowing out of the water body during the day (m^3 H_2O).
V_{in} Volume of inflow during the time step (m^3 H_2O)
$V_{initial}$ Initial volume of water in water body on given day (m^3 H_2O)
V_{mx} Volume of water held in the wetland when filled to the maximum water level (m^3 H_2O)
V_{nor} Volume of water held in the wetland when filled to the normal water level (m^3 H_2O)
V_{out} Volume of outflow during the time step (m^3 H_2O)
V_{pcp} Volume of precipitation falling on the water body during the day (m^3 H_2O)
$V_{pot,mx}$ Maximum amount of water that can be stored in the pothole (m^3 H_2O)
V_{pr} Volume of water held in the reservoir when filled to the principal spillway (m^3 H_2O)
V_S Volume of solids (m^3)
V_{sed} Volume of solids in the sediment layer (m^3)
V_{seep} Volume of water lost from the water body by seepage (m^3 H_2O)
V_{stored} Volume of water stored in water body or channel (m^3 H_2O)
V_T Total soil volume (m^3)
V_{targ} Target reservoir volume for a given day (m^3 H_2O)
V_{tot} Total volume of the sediment layer (m^3)
V_W Volume of water (m^3)
V_{wtr} Volume of water in the sediment layer (m^3)
W Width of channel at water level (m)
$W(t)$ Rate of nutrient loading (kg/day)
$W_{bnkfull}$ Top width of the channel when filled with water (m)
W_{btm} Bottom width of the channel (m)
$W_{btm,fld}$ Bottom width of the flood plain (m)
WP Water content at wilting point (mm H_2O)
WP_{ly} Water content of layer *ly* at wilting point (mm H_2O)
X Weighting factor in Muskingum routing
Y Total constituent load (kg)
Y_{sed} Cumulative amount of solids washed off at time *t* (kg/curb km)

a Constant in equation used to calculate the cloud cover adjustment factor
a_1 Constant in equation used to calculate net emissivity
a_r Unit channel regression intercept (m^3)
a_x Regression intercept for a channel of length L and width W (m^3)
aa Exponent between 0 and 1 that varies with atmospheric stability and surface roughness that is used in calculating wind speed at different heights
$adj_{0.5}$. Peak rate adjustment factor
adj_{hmd} Change in relative humidity expressed as a fraction
adj_{pcp} % change in rainfall
adj_{rad} Change in radiation (MJ m^{-2} d^{-1})
adj_{tmp} Change in temperature (°C)
$algae$ Algal biomass concentration (mg alg/L)
ap_{ef} Pesticide application efficiency
aq_{dp} Amount of water stored in the deep aquifer (mm H_2O)
aq_{sh} Amount of water stored in the shallow aquifer (mm H_2O)
$aq_{shthr,q}$ Threshold water level in shallow aquifer for base flow (mm H_2O)
$area_{hru}$ HRU area (ha or km^2)
b Constant in equation used to calculate the cloud cover adjustment factor
b_1 Constant in equation used to calculate net emissivity
b_H Scaling factor that controls the degree of deviation in relative humidity caused by the presence or absence of precipitation
b_{mlt} Melt factor for the day (mm H_2O/day–°C)
b_{mlt6} Melt factor for June 21 (mm H_2O/day–°C)
b_{mlt12} Melt factor for December 21 (mm H_2O/day–°C)
b_r Unit channel regression slope
b_R Scaling factor that controls the degree of deviation in solar radiation caused by the presence or absence of precipitation
b_T Scaling factor that controls the degree of deviation in temperature caused by the presence or absence of precipitation
b_x Regression slope for a channel of length L and width W
$bact_{lpsol,fert}$ Amount of less persistent bacteria in the solution pool added to the soil in the fertilizer (# bact/ha)
$bact_{lpsorb,fert}$ Amount of less persistent bacteria in the sorbed pool added to the soil in fertilizer (# bact/ha)
$bact_{psol,fert}$ Amount of persistent bacteria in the solution pool added to the soil in the fertilizer (# bact/ha)
$bact_{psorb,fert}$ Amount of persistent bacteria in the sorbed pool added to the soil in fertilizer (# bact/ha)
bcv Weighting factor for impact of ground cover on soil surface temperature
bio Total plant biomass on a given day (kg/ha)
bio_{ag} Aboveground biomass on the day of harvest (kg ha^{-1})
bio_N Actual mass of nitrogen stored in plant material (kg N/ha)
$bio_{N,opt}$ Optimal mass of nitrogen stored in plant material for the growth stage (kg N/ha)
bio_P Actual mass of phosphorus stored in plant material (kg P/ha)
$bio_{P,opt}$ Optimal mass of phosphorus stored in plant material for the current growth stage (kg P/ha)
bio_{trg} Target biomass specified by the user (kg/ha)
bnk Total amount of water in bank storage (m^3 H_2O)

bnk_{in} Amount of water entering bank storage (m^3 H_2O)
$bnk_{revap,mx}$ Maximum amount of water moving into the unsaturated zone in response to water deficiencies (m^3 H_2O)
c Concentration of nutrient in the water (kg/m^3 H_2O)
c_k Celerity corresponding to the flow for a specified depth (m/s)
c_p Specific heat of moist air at constant pressure (1.013×10^{-3} MJ kg^{-1} $°C^{-1}$)
c_{perm} Profile-permeability class
$c_{soilstr}$ Soil-structure code used in soil classification
c_{sp} Coefficient in sediment transport equation
can_{day} Maximum amount of water that can be trapped in the canopy on a given day (mm H_2O)
can_{mx} Maximum amount of water that can be trapped in the canopy when the canopy is fully developed (mm H_2O)
$cbod$ Carbonaceous biological oxygen demand concentration (mg CBOD/L)
$cbod_{surq}$ CBOD concentration in surface runoff (mg CBOD/L)
$chla$ Chlorophyll *a* concentration (μg chla/L)
$coef_1$ Weighting coefficient for storage time constant calculation
$coef_2$ Weighting coefficient for storage time constant calculation
$coef_a$ Empirical water quality factor
$coef_b$ Empirical dam aeration coefficient
$coef_{crk}$ Adjustment coefficient for crack flow
$coef_{ev}$ Evaporation coefficient
$conc_N$ Concentration of nitrogen in a layer (mg/kg or ppm)
$conc_{NO3,mobile}$ Concentration of nitrate in the mobile water for a given layer (kg N/mm H_2O)
$conc_{orgN}$ Concentration of organic nitrogen in the soil surface top 10 mm (g N/ metric ton soil)
$conc_P$ Concentration of phosphorus in a layer (mg/kg or ppm)
$conc_{pst,flow}$ Concentration of pesticide in the mobile water (kg pst/ha-mm H_2O)
$conc_{sed}$ Concentration of sediment in lateral and groundwater flow (mg l^{-1})
$conc^*_{sed}$ "Concentration" of solid particles in the sediment layer (g/m^3)
$conc_{sed,ch,I}$ Initial sediment concentration in the reach (kg/L or ton/m^3)
$conc_{sed,ch,mx}$ Maximum concentration of sediment that can be transported by the water (kg/L or ton/m^3)
$conc_{sed,eq}$ Equilibrium concentration of suspended solids in the water body (Mg/m^3)
$conc_{sed,surq}$ Concentration of sediment in surface runoff (Mg sed/m^3 H_2O)
$conc_{sedP}$ Concentration of phosphorus attached to sediment in the top 10 mm (g P/metric ton soil)
cov_1 Snow cover areal depletion curve shape coefficient
cov_2 Snow cover areal depletion curve shape coefficient
cov_{sol} Soil cover index
crk Total crack volume for the soil profile on a given day (mm)
crk_{ly} Crack volume for the soil layer on a given day expressed as a depth (mm)
$crk_{ly,d-1}$ Crack volume for the soil layer on the previous day (mm)
$crk_{ly,I}$ Initial crack volume calculated for the soil layer on a given day expressed as a depth (mm)

crk_{max} Potential crack volume for the soil profile expressed as a fraction of the total volume
$crk_{max,ly}$ Maximum crack volume possible for the soil layer (mm)
d Zero plane displacement of the wind profile (cm)
d_{50} Median particle size of the inflow sediment (µm)
d_n Day number of year, 1 on January 1 and 365 on December 31
$days_{dry}$ Number of dry days in the month
$days_{tot}$ Total number of days in the month
$days_{wet}$ Number of wet days in the month
dd Damping depth (mm)
dd_{max} Maximum damping depth (mm)
$depth$ Depth of water in the channel (m)
$depth_{bnkfull}$ Depth of water in the channel when filled to the top of the bank (m)
$depth_{dcut}$ Amount of downcutting (m)
$depth_{fld}$ Depth of water in the flood plain (m)
$depth_{ly}$ Depth of the soil layer (mm)
df Depth factor used in soil temperature calculations
div Volume of water added or removed from the reach for the day through diversions (m^3 H_2O)
dt Length of time step (1 day)
dur_{flw} Duration of flow (hr)
e Actual vapor pressure on a given day (kPa)
e_{mon} Actual vapor pressure at the mean monthly temperature (kPa)
e^o Saturation vapor pressure on a given day (kPa)
e^o_{mon} Saturation vapor pressure at the mean monthly temperature (kPa)
$epco$ Plant uptake compensation factor
$esco$ Soil evaporation compensation coefficient
$expsa$ Exponent for impoundment surface area calculation
f Coefficient
f_{cl-si} Factor that gives low soil erodibility factors for soils with high clay to silt ratios
f_{cld} Factor to adjust for cloud cover in net long-wave radiation calculation
f_{csand} Factor that gives low soil erodibility factors for soils with high coarse-sand contents and high values for soils with little sand
f_{gr} Growth stage factor in nitrogen fixation equation
f_{hisand} Factor that reduces soil erodibility for soils with extremely high sand contents
f_{inf} Infiltration rate (mm/hr)
f_{NH4} Preference factor for ammonia nitrogen
f_{no3} Soil nitrate factor in nitrogen fixation equation
f_{orgc} Factor that reduces soil erodibility for soils with high organic carbon content
f_{sw} Soil water factor in nitrogen fixation equation
$fert$ Amount of fertilizer applied (kg/ha)
$fert_{eff}$ Fertilizer application efficiency assigned by the user
$fert_{lpbact}$ Concentration of less persistent bacteria in the fertilizer (# bact/kg fert)
$fert_{minN}$ Fraction of mineral nitrogen in the fertilizer
$fert_{minP}$ Fraction of mineral P in the fertilizer
$fert_{NH4}$ Fraction of mineral N in the fertilizer that is ammonium
$fert_{orgN}$ Fraction of organic N in the fertilizer
$fert_{orgP}$ Fraction of organic P in the fertilizer
$fert_{pbact}$ Concentration of persistent bacteria in the fertilizer (# bact/kg fert)

fr_{actN} Fraction of humic nitrogen in the active pool
fr_{av} Fraction of the curb length available for sweeping (the availability factor)
fr_{bnd} Fraction of subbasin area within the elevation band
fr_{DL} Fraction of daylight hours
$fr_{g,mx}$ Fraction of the maximum stomatal conductance, $g_{\square,mx}$, achieved at the vapor pressure deficit, vpd_{fr}
fr_{imp} Fraction of the subbasin area draining into the impoundment
$fr_{LAI,1}$ Fraction of the maximum plant leaf area index corresponding to the 1 st point on the optimal leaf area development curve
$fr_{LAI,2}$ Fraction of the maximum plant leaf area index corresponding to the 2 nd point on the optimal leaf area development curve
fr_{LAImx} Fraction of the plant's maximum leaf area index corresponding to a given fraction of potential heat units for the plant
fr_{N} Optimal fraction of nitrogen in the plant biomass for current growth stage
$fr_{N,1}$ Normal fraction of nitrogen in the plant biomass at emergence
$fr_{N,2}$ Normal fraction of nitrogen in the plant biomass at 50% maturity
$fr_{N,3}$ Normal fraction of nitrogen in the plant biomass at maturity
$fr_{N,\sim3}$ Normal fraction of nitrogen in the plant biomass near maturity
$fr_{N,yld}$ Fraction of nitrogen in the yield
fr_{NH4} Fraction of algal nitrogen uptake from ammonium pool
$fr_{nit,ly}$ Estimated fraction of nitrogen lost by nitrification
fr_{P} Fraction of phosphorus in the plant biomass
$fr_{P,1}$ Normal fraction of phosphorus in the plant biomass at emergence
$fr_{P,2}$ Normal fraction of phosphorus in the plant biomass at 50% maturity
$fr_{P,3}$ Normal fraction of phosphorus in the plant biomass at maturity
$fr_{P,\sim3}$ Normal fraction of phosphorus in the plant biomass near maturity
$fr_{P,yld}$ Fraction of phosphorus in the yield
fr_{phosyn} Fraction of solar radiation that is photosynthetically active
fr_{PHU} Fraction of potential heat units accumulated for the plant on a given day in the growing season
$fr_{PHU,1}$ Fraction of the growing season corresponding to the 1 st point on the optimal leaf area development curve
$fr_{PHU,2}$ Fraction of the growing season corresponding to the 2 nd point on the optimal leaf area development curve
$fr_{PHU,50\%}$ Fraction of potential heat units accumulated for the plant at 50% maturity ($fr_{PHU,50\%}$=0.5)
$fr_{PHU,100\%}$ Fraction of potential heat units accumulated for the plant at maturity ($fr_{PHU,100\%}$=1.0)
$fr_{PHU,sen}$ Fraction of growing season at which senescence becomes the dominant growth process
fr_{pot} Fraction of the HRU area draining into the pothole
fr_{root} Fraction of total biomass in the roots on a given day in the growing season
fr_{trns} Fraction of transmission losses partitioned to the deep aquifer

$fr_{vol,ly}$ Estimated fraction of nitrogen lost by volatilization

fr_{wsh} Wash-off fraction for the pesticide

$fr_{.t}$ Fraction of the time step in which water is flowing in the channel

g Exponent

$g_{\square}$ Leaf conductance (m s^{-1})

$g_{\square,mx}$ Maximum conductance of a single leaf (m s^{-1})

g_{mon} Skew coefficient for daily precipitation in the month

gc Fraction of the ground surface covered by plants

h_c Canopy height (cm)

$h_{c,mx}$ Plant's maximum canopy height (m)

h_{fall} Height through which water falls (m)

h_{wtbl} Water table height (m)

$harv_{eff}$ Efficiency of the harvest operation

hr Hour of day (1-24)

I Rainfall intensity (mm/hr)

i_{mx} Maximum rainfall intensity (mm/hr)

imp_{con} Fraction of the HRU area that is impervious and hydraulically connected to the drainage system

imp_{dcon} Fraction of the HRU area that is impervious but not hydraulically connected to the drainage system

imp_{tot} Fraction of the HRU area that is impervious (both connected and disconnected)

irr Amount of irrigation water added on a given day (m^3 H_2O)

k Von Kármán constant

k_{bact} Bacterial partition coefficient

$k_{d,perc}$ Phosphorus percolation coefficient (10 m^3/Mg)

$k_{d,surf}$ Phosphorus soil partitioning coefficient (m^3 /Mg)

k_i Decay constant for rainfall intensity (hr)

$k_{\square}$ Light extinction coefficient

$k_{\square,0}$ Non-algal portion of the light extinction coefficient (m^{-1})

$k_{\square,1}$ Linear algal self shading coefficient (m^{-1} (µg-chla/L)$^{-1}$)

$k_{\square 1,2}$ Nonlinear algal self shading coefficient (m^{-1} (µg-chla/L)$^{-2/3}$)

$k_{p,aq}$ Rate constant for degradation or removal of pesticide in the water (1/day)

$k_{p,foliar}$ Rate constant for degradation or removal of the pesticide on foliage (1/day)

$k_{p,sed}$ Rate constant for degradation or removal of pesticide in the sediment (1/day)

$k_{p,soil}$ Rate constant for degradation or removal of the pesticide in soil (1/day)

k_r Decay factor (m^{-1} km^{-1})

k_s Sediment settling decay constant (1/day)

kk Coefficient in urban wash off equation

m Exponential term in USLE LS factor calculation

m_c Percent clay content

m_s Percent sand content

m_{silt} Percent silt content (0.002-0.05 mm diameter particles)

m_{vfs} Percent very fine sand content (0.05-0.10 mm diameter particles)

$minN_{app}$ Amount of mineral nitrogen applied (kg N/ha)

$minN_{app,mx}$ Maximum amount of mineral N allowed to be applied on any one day (kg N/ha)

$minN_{app,mxyr}$ Maximum amount of mineral N allowed to be applied during a year (kg N/ha)
$minP_{act,ly}$ Amount of phosphorus in the active mineral pool (mg/kg or kg P/ha)
$minP_{sta,ly}$ Amount of phosphorus in the stable mineral pool (mg/kg or kg P/ha)
mon Month of the year
$mon_{fld,beg}$ Beginning month of the flood season
$mon_{fld,end}$ Ending month of the flood season
n Manning's roughness coefficient for the subbasin or channel
n_1 First shape coefficient in plant nitrogen equation
n_2 Second shape coefficient in plant nitrogen equation
$nstrs$ Nitrogen stress for a given day
$orgC_{ly}$ Amount of organic carbon in the layer (%)
$orgC_{surq}$ Organic carbon in surface runoff (kg orgC),
$orgN_{act,fert}$ Amount of nitrogen in the active organic pool added to the soil in the fertilizer (kg N/ha)
$orgN_{act,ly}$ Nitrogen in the active organic pool (mg/kg or kg N/ha)
$orgN_{frsh,fert}$ Amount of nitrogen in the fresh organic pool added to the soil in the fertilizer (kg N/ha)
$orgN_{frsh,surf}$ Nitrogen in the fresh organic pool in the top 10mm (kg N/ha)
$orgN_{hum,ly}$ Humic organic nitrogen in the layer (mg/kg or kg N/ha)
$orgN_{sta,ly}$ Nitrogen in the stable organic pool (mg/kg or kg N/ha)
$orgN_{stor,i-1}$ Surface runoff organic N stored or lagged from the previous day (kg N/ha)
$orgN_{str}$ Organic nitrogen concentration in the stream (mg N/L)
$orgN_{surf}$ Amount of organic nitrogen transport to the main channel in surface runoff (kg N/ha)
$orgN'_{surf}$ Amount of surface runoff organic N generated in HRU on a given day (kg N/ha)
$orgP_{act,ly}$ Amount of phosphorus in the active organic pool (kg P/ha)
$orgP_{frsh,fert}$ Amount of phosphorus in the fresh organic pool added to the soil in the fertilizer (kg P/ha)
$orgP_{frsh,ly}$ Phosphorus in the fresh organic pool in layer *ly* (kg P/ha)
$orgP_{hum,fert}$ Amount of phosphorus in the humus organic pool added to the soil in the fertilizer (kg P/ha)
$orgP_{hum,ly}$ Amount of phosphorus in humic organic pool in the layer (mg/kg or kg P/ha)
$orgP_{sta,ly}$ Amount of phosphorus in the stable organic pool (kg P/ha)
$orgP_{str}$ Organic phosphorus concentration in the stream (mg P/L)
p Total phosphorus concentration (μg P/L)
p_1 First shape coefficient in plant phosphorus equation
p_2 Second shape coefficient in plant phosphorus equation
pai Phosphorus availability index
$pest$ Actual amount of pesticide applied (kg pst/ha)
$pest'$ Effective amount of pesticide applied (kg pst/ha)
$pest_{fol}$ Amount of pesticide applied to foliage (kg pst/ha)
$pest_{surf}$ Amount of pesticide applied to the soil surface (kg pst/ha)
$plaps$ Precipitation lapse rate (mm H2O/km)
prf Peak rate adjustment factor

pst_{bur} Amount of pesticide removed via burial (mg pst)
$pst_{deg,sed}$ Amount of pesticide removed from the sediment via degradation (mg pst)
$pst_{deg,wtr}$ Amount of pesticide removed from the water via degradation (mg pst)
pst_{dif} Amount of pesticide transferred between the water and sediment by diffusion (mg pst)
pst_{f} Amount of pesticide on the foliage (kg pst/ha)
$pst_{f,wsh}$ Amount of pesticide on foliage that is washed off the plant and onto the soil surface on a given day (kg pst/ha)
pst_{flow} Amount of pesticide removed in the flow (kg pst/ha)
pst_{in} Pesticide added to the water body via inflow (mg pst)
pst'_{lat} Amount of lateral flow soluble pesticide generated in HRU on a given day (kg pst/ha)
$pst_{lat,ly}$ Pesticide removed in lateral flow from a layer (kg pst/ha)
$pst_{latstor,i-1}$ Lateral flow pesticide stored or lagged from the previous day (kg pst/ha)
pst_{lksed} Amount of pesticide in the sediment (mg pst)
pst_{lkwtr} Amount of pesticide in the water (mg pst)
$pst_{perc,ly}$ Pesticide moved to the underlying layer by percolation (kg pst/ha)
pst_{rchsed} Amount of pesticide in the sediment (mg pst)
pst_{rchwtr} Amount of pesticide in the water (mg pst)
$pst_{rsp,wtr}$ Amount of pesticide removed from sediment via resuspension (mg pst)
$pst_{s,ly}$ Amount of pesticide in the soil (kg pst/ha)
pst_{sed} Amount of sorbed pesticide transported to the main channel in surface runoff (kg pst/ha)
pst'_{sed} Sorbed pesticide loading generated in HRU on a given day (kg pst/ha)
$pst_{sedstor,i-1}$ Sorbed pesticide stored or lagged from the previous day (kg pst/ha)
pst_{sol} Solubility of the pesticide in water (mg l^{-1})
$pst_{sol,o}$ Amount of dissolved pesticide removed via outflow (mg pst)
$pst_{sorb,o}$ Amount of particulate pesticide removed via outflow (mg pst)
$pst_{stl,wtr}$ Amount of pesticide removed from the water due to settling (mg pst)
pst_{surf} Pesticide removed in surface runoff (kg pst/ha)
pst'_{surf} Amount of surface runoff soluble pesticide generated in HRU on a given day (kg pst/ha)
$pst_{surstor,i-1}$ Surface runoff soluble pesticide stored or lagged from the previous day (kg pst/ha)
$pst_{vol,wtr}$ Amount of pesticide removed via volatilization (mg pst)
$pstrs$ Phosphorus stress for a given day
q^*_0 Unit source area flow rate (mm hr^{-1})
q_{ch} Average channel flow rate (m^3 s^{-1})
q^*_{ch} Average channel flow rate (mm hr^{-1})
$q_{ch,pk}$ Peak flow rate (m^3 /s)
q_{in} Inflow rate (m^3 /s)
q_{out} Outflow rate (m^3 /s)
q_{ov} Average overland flow rate (m^3 s^{-1})
q_{peak} Peak runoff rate (m^3 /s or mm/hr)
$q_{peak,f}$ Peak rate after transmission losses (m^3 /s)
$q_{peak,I}$ Peak rate before accounting for transmission losses (m^3 /s)
q_{rel} Average daily principal spillway release rate (m^3 /s)
$q_{rel,mn}$ Minimum average daily outflow for the month (m^3 /s)
$q_{rel,mx}$ Maximum average daily outflow for the month (m^3 /s)

q_{tile} Average daily tile flow rate (m^3 /s)
r Actual earth-sun distance (AU)
r_0 Mean earth-sun distance, 1 AU
r_1 First shape coefficient for radiation-use efficiency curve
r_2 Second shape coefficient for radiation-use efficiency curve
r_a Diffusion resistance of the air layer (aerodynamic resistance) (s m^{-1})
r_c Plant canopy resistance (s m^{-1})
r_g Gaseous surface renewal rate (1/day)
r_l Liquid surface renewal rate (1/day)
$r_{\sqsubset}$ Minimum effective resistance of a single leaf (s m^{-1})
$r_{\sqsubset\text{-}ab}$ Minimum abaxial stomatal leaf resistance (s m^{-1})
$r_{\sqsubset\text{-}ad}$ Minimum adaxial stomatal leaf resistance (s m^{-1})
$ratio_{WD}$ Channel width to depth ratio
reff Removal efficiency of the sweeping equipment
rexp Exponent for exponential precipitation distribution
rnd_1 Random number between 0.0 and 1.0
rnd_2 Random number between 0.0 and 1.0
rock Percent rock in soil layer (%)
rsd_{ly} Residue in layer *ly* (kg/ha)
rsd_{surf} Material in the residue pool for the top 10mm of soil on day *i* (kg ha^{-1})
sed Sediment yield on a given day (metric tons)
sed_{ch} Amount of suspended sediment in the reach (metric tons)
sed_{deg} Amount of sediment reentrained in the reach segment (metric tons)
sed_{dep} Amount of sediment deposited in the reach segment (metric tons)
sed_{flowin} Amount of sediment added to the water body with inflow (metric tons)
$sed_{flowout}$ Amount of sediment transported out of the water body (metric tons)
sed_{lat} Sediment loading in lateral and groundwater flow (metric tons)
sed_{out} Amount of sediment transported out of the reach (metric tons)
sed_{stl} Amount of sediment removed from the water by settling (metric tons)
$sed_{stor,i-1}$ Sediment stored or lagged from the previous day (metric tons)
sed_{wb} Sediment in the water body (metric tons)
$sedP_{stor,i-1}$ Sediment-attached P stored or lagged from the previous day (kg P/ha)
$sedP_{surf}$ Amount of phosphorus transported with sediment to the main channel in surface runoff (kg P/ha)
$sedP'_{surf}$ Amount of sediment-attached P loading generated in HRU on a given day (kg P/ha)
slp Average slope of the subbasin (% or m/m)
slp_{ch} Average channel slope along channel length (m m^{-1})
sno_{cov} Fraction of the HRU area covered by snow
spexp Exponent in sediment transport equation
starg Target reservoir volume specified for a given month (m^3 H_2O)
surlag Surface runoff lag coefficient
t Number of hours before (+) or after (-) solar noon
$t_{1/2,aq}$ Aqueous half-life for the pesticide (days)
$t_{1/2,f}$ Half-life of the pesticide on foliage (days)
$t_{1/2,s}$ Half-life of the pesticide in the soil (days)

$t_{1/2,sed}$ Sediment half-life for the pesticide (days)
t_{half} Length of time needed for solid build up to increase from 0 kg/curb km to ½ SED_{mx} (days)
t_{ch} Time of concentration for channel flow (hr)
t_{conc} Time of concentration for a subbasin (hr)
t_{dorm} Dormancy threshold (hrs)
t_{drain} Time required to drain the soil to field capacity (hrs)
t_i Solar time at the midpoint of the hour i
t_{ov} Time of concentration for overland flow (hr)
$tile_{lag}$ Drain tile lag time (hrs).
$tile_{wtr}$ Amount of water removed from the layer on a given day by tile drainage (mm H_2O)
$tlaps$ Temperature lapse rate (°C/km)
$tloss$ Channel transmission losses (m^3 H_2O)
$trap_{ef}$ Fraction of the constituent loading trapped by the filter strip
$trap_{ef,bact}$ Fraction of the bacteria loading trapped by the filter strip
$tstrs$ Temperature stress for a given day expressed as a fraction of optimal plant growth
u_z Wind speed at height zw (m s^{-1})
u_{z1} Wind speed (m s^{-1}) at height $z1$
u_{z2} Wind speed (m s^{-1}) at height $z2$
urb_{coef} Wash off coefficient (mm^{-1})
vb Pesticide burial velocity (m/day)
vc Average channel velocity (m s^{-1})
$v_{ch,pk}$ Peak channel velocity (m/s)
vd Pesticide rate of diffusion or mixing velocity (m/day)
v_{lat} Velocity of flow at the hillslope outlet (mm·h^{-1})
v_{ov} Overland flow velocity (m s^{-1})
v_r Pesticide resuspension velocity (m/day)
v_s Pesticide settling velocity (m/day)
v_{surf} Surface runoff flow rate (m^3/s)
v_v Pesticide volatilization mass-transfer coefficient (m/day)
$vol_{Qsurf,f}$ Volume of runoff after transmission losses (m^3)
$vol_{Qsurf,I}$ Volume of runoff prior to transmission losses (m^3)
vol_{thr} Threshold volume for a channel of length L and width W (m^3)
vpd Vapor pressure deficit (kPa)
vpd_{fr} Vapor pressure deficit corresponding to frg,mx (kPa)
vpd_{thr} Threshold vapor pressure deficit above which a plant will exhibit reduced leaf conductance or reduced radiation-use efficiency (kPa)
w_1 Shape coefficient in retention parameter adjustments for soil moisture content
w_2 Shape coefficient in retention parameter adjustments for soil moisture content
$w_{actualup}$ Total plant water uptake for the day (mm H_2O)
$w_{actualup,ly}$ Actual water uptake for layer ly (mm H_2O)
$w_{crk,btm}$ Amount of water flow past the lower boundary of the soil profile due to bypass flow (mm H_2O)
w_{deep} Amount of water percolating from the shallow aquifer into the deep aquifer (mm H_2O)
$w_{deep,mx}$ Maximum amount of water moving into the deep aquifer on day i (mm H_2O)
w_{demand} Water uptake demand not met by overlying soil layers (mm H_2O)
w_{inf} Amount of water entering the soil profile on a given day (mm H_2O)
w_{mobile} Amount of mobile water in the layer (mm H_2O)

$w_{perc,ly}$ Amount of water percolating to the underlying soil layer on a given day (mm H_2O)
$w_{pump,dp}$ Amount of water removed from the deep aquifer by pumping (mm H_2O)
$w_{pump,sh}$ Amount of water removed from the shallow aquifer by pumping (mm H_2O)
w_{rchrg} Amount of water entering the aquifer via recharge (mm H_2O)
w_{revap} Amount of water moving into the soil zone in response to water deficiencies (mm H_2O)
$w_{revap,mx}$ Maximum amount of water moving into the soil zone in response to water deficiencies on day i (mm H_2O)
w_{seep} Total amount of water exiting the bottom of the soil profile (mm H_2O)
$w_{up,ly}$ Potential water uptake for layer ly (mm H_2O)
$w'_{up,ly}$ Adjusted potential water uptake for layer ly (mm H2O)
$w''_{up,ly}$ Potential water uptake when the soil water content is less than 25% of plant available water (mm H_2O)
$w_{up,z}$ Potential water uptake from the soil surface to a specified depth, z, on a given day (mm H_2O)
$w_{up,zl}$ Potential water uptake for the profile to the lower boundary of the soil layer (mm H_2O)
$w_{up,zu}$ Potential water uptake for the profile to the upper boundary of the soil layer (mm H_2O)
$width_{filtstrip}$ Width of filter strip (m)
$wstrs$ Water stress for a given day expressed as a fraction of total water demand
yld Crop yield (kg/ha)
yld_{act} Actual yield (kg ha^{-1})
$yld_{est,N}$ Nitrogen yield estimate (kg N/ha)
$yld_{est,Nprev}$ Nitrogen yield estimate from the previous year (kg N/ha)
yld_N Amount of nitrogen removed in the yield (kg N/ha)
yld_P Amount of phosphorus removed in the yield (kg P/ha)
$yld_{yr,N}$ Nitrogen yield target for the current year (kg N/ha)
yr_{sim} Year of simulation (1 - yr_{tot})
yr_{tot} Total number of calendar years simulated
yrs Number of years of rainfall data used to obtain values for monthly extreme half-hour rainfalls
z Depth below soil surface (mm)
z_1 Height of wind speed measurement (cm)
z_2 Height of wind speed measurement (cm)
z_{ch} Inverse of the channel side slope
z_{fld} Inverse of the flood plain side slope
z_g Thickness of the gas film (m)
z_l Thickness of the liquid film (m)
$z_{l,ly}$ Depth from the surface to the bottom of the soil layer (mm)
$z_{mid,ly}$ Depth from the soil surface to the middle of the layer (mm)
z_{om} Roughness length for momentum transfer (cm)
z_{ov} Roughness length for vapor transfer (cm)
z_p Height of the humidity (psychrometer) and temperature measurements (cm)
z_{root} Depth of root development in the soil (mm)
$z_{root,mx}$ Maximum depth for root development in the soil (mm)
z_{tot} Depth to bottom of soil profile (mm)
z_w Height of the wind speed measurement (cm)
zd Ratio of depth in soil to damping depth
α Short-wave reflectance or albedo

α_0 Ratio of chlorophyll *a* to algal biomass (µg chla/mg alg)

$\alpha_{0.5}$ Maximum half-hour rainfall expressed as a fraction of daily rainfall

$\alpha_{0.5L}$ Smallest half-hour rainfall fraction that can be generated on a given day

$\alpha_{0.5mon}$ Average maximum half-hour rainfall fraction for the month

$\alpha_{0.5U}$ Largest half-hour rainfall fraction that can be generated on a given day

α_1 Fraction of algal biomass that is nitrogen (mg N/mg alg biomass),

α_2 Fraction of algal biomass that is phosphorus (mg P/mg alg biomass)

α_3 Rate of oxygen production per unit of algal photosynthesis (mg O_2/mg alg)

α_4 Rate of oxygen uptake per unit of algae respired (mg O_2/mg alg)

α_5 Rate of oxygen uptake per unit NH_4+ oxidation (mg O_2/mg N)

α_6 Rate of oxygen uptake per unit NO_2 oxidation (mg O_2/mg N)

α_{bnk} Bank flow recession constant or constant of proportionality

α_{gw} Baseflow recession constant

α_{hill} Slope of the hillslope segment (degrees)

α_{pet} Coefficient in Priestley-Taylor equation

α_{plant} Plant albedo (set at 0.23)

α_{soil} Soil albedo

α_{tc} Fraction of daily rainfall that occurs during the time of concentration

$\bullet_0$ Coefficient for USGS regression equations for urban loadings

$\bullet_1$ Coefficient for USGS regression equations for urban loadings

$\bullet_2$ Coefficient for USGS regression equations for urban loadings

$\bullet_3$ Coefficient for USGS regression equations for urban loadings

$\bullet_4$ Coefficient for USGS regression equations for urban loadings

$\bullet_{deep}$ Aquifer percolation coefficient

$\bullet_{eqP}$ Slow equilibration rate constant (0.0006 d^{-1})

$\bullet_{min}$ Rate coefficient for mineralization of the humus active organic nutrients

$\bullet_n$ Nitrogen uptake distribution parameter

$\bullet_{N,1}$ Rate constant for biological oxidation of ammonia nitrogen (day^{-1} or hr^{-1})

$\bullet_{N,1,20}$ Rate constant for biological oxidation of ammonia nitrogen at 2°C (day^{-1} or hr^{-1})

$\bullet_{N,2}$ Rate constant for biological oxidation of nitrite to nitrate (day^{-1} or hr^{-1})

$\bullet_{N,2,20}$ Rate constant for biological oxidation of nitrite to nitrate at 2°C (day^{-1} or hr^{-1})

$\bullet_{N,3}$ Rate constant for hydrolysis of organic nitrogen to ammonia nitrogen (day-1 or hr-1)

$\bullet_{N,3,20}$ Local rate constant for hydrolysis of organic nitrogen to NH_4+ at 2°C
(day^{-1} or hr^{-1})
$\bullet_{NO3}$ Nitrate percolation coefficient
$\bullet_{p}$ Phosphorus uptake distribution parameter
$\bullet_{P,4}$ Rate constant for mineralization of organic phosphorus (day^{-1} or hr^{-1})
$\bullet_{P,4,20}$ Local rate constant for organic phosphorus mineralization at 2°C
(day^{-1} or hr^{-1})
$\bullet_{pst}$ Pesticide percolation coefficient
$\bullet_{rev}$ Revap coefficient
$\bullet_{rsd}$ Rate coefficient for mineralization of the residue fresh organic nutrients
$\bullet_{sa}$ Coefficient for impoundment surface area equation
$\bullet_{trns}$ Rate constant for nitrogen transfer between active and stable organic pools (1x10^{-5})
$\bullet_{w}$ Water-use distribution parameter
$\chi_i(j)$ 3x1 matrix for day *i* whose elements are residuals of maximum temperature *(j* =1), minimum temperature *(j* = 2) and solar radiation *(j* = 3),
Δ Slope of the saturation vapor pressure curve (kPa °C^{-1})
$\Delta algae$ Change in algal biomass concentration (mg alg/L)
Δbio Potential increase in total plant biomass on a given day (kg/ha)
Δbio_{act} Actual increase in total plant biomass on a given day (kg/ha)
$\Delta g_{\square dcl}$ Rate of decline in leaf conductance per unit increase in vapor pressure deficit (ms^{-1} kPa^{-1})
ΔLAI_i Leaf area added on day *i* (potential)
$\Delta LAI_{act,I}$ Actual leaf area added on day *i*
$\Delta NH4_{str}$ Change in ammonium concentration (mg N/L)
$\Delta NO2_{str}$ Change in nitrite concentration (mg N/L)
$\Delta orgN_{str}$ Change in organic nitrogen concentration (mg N/L)
$\Delta orgP_{str}$ Change in organic phosphorus concentration (mg P/L)
ΔOx_{str} Change in dissolved oxygen concentration (mg O_2/L)
Δpst_{lkwtr} Change in pesticide mass in the water layer (mg pst)
Δpst_{lksed} Change in pesticide mass in the sediment layer (mg pst)
Δpst_{rchwtr} Change in pesticide mass in the water layer (mg pst)
Δpst_{rchsed} Change in pesticide mass in the sediment layer (mg pst)
Δrsd Biomass added to the residue pool on a given day (kg ha^{-1})
Δrue_{dcl} Rate of decline in radiation-use efficiency per unit increase in vapor pressure deficit (kg/ha·(MJ/m^2)$^{-1}$·kPa^{-1} or (10^{-1} g/MJ)·kPa^{-1})
$\Delta solP_{str}$ Change in solution phosphorus concentration (mg P/L)
Δt Length of the time step (s)
δ Solar declination (radians)
δ_{gw} Delay time or drainage time for aquifer recharge (days)
$\delta_{ntr,ly}$ Residue decay rate constant
ε Emissivity
ε' Net emittance
ε_a Atmospheric emittance
$\varepsilon_{C:N}$ Residue C:N ratio in the soil layer

$\varepsilon_{C:P}$	Residue C:P ratio in the soil layer
$\varepsilon_{C:sed}$	Carbon enrichment ratio
ε_{I}	3x1 matrix of independent random components
$\varepsilon_{N:sed}$	Nitrogen enrichment ratio
$\varepsilon_{P:sed}$	Phosphorus enrichment ratio
$\varepsilon_{pst:sed}$	Pesticide enrichment ratio
ε_{sr}	Radiation term for bare soil surface temperature calculation
ε_{vs}	Vegetative or soil emittance
ϕ	Latitude in radians
ϕ_{d}	Drainable porosity of the soil (mm/mm)
ϕ_{fc}	Porosity of the soil layer filled with water when the layer is at field capacity water content (mm/mm)
ϕ_{soil}	Porosity of the soil (mm/mm)
γ	Psychrometric constant (kPa °C^{-1})
$\gamma_{ntr,ly}$	Nutrient cycling residue composition factor for layer ly
γ_{reg}	Plant growth factor (0.0-1.0)
$\gamma_{sw,ly}$	Nutrient cycling water factor for layer *ly*
$\gamma_{tmp,ly}$	Nutrient cycling temperature factor for layer *ly*
γ_{wu}	Water deficiency factor
η	Evaporation coefficient (0.6)
$\eta_{midz,ly}$	Volatilization depth factor
$\eta_{nit,ly}$	Nitrification regulator
$\eta_{sw,ly}$	Nitrification soil water factor
$\eta_{tmp,ly}$	Nitrification/volatilization temperature factor
$\eta_{vol,ly}$	Volatilization regulator
φ	Scaling factor for impact of soil water on damping depth
φ_{n}	Scaling factor for nitrogen stress equation
φ_{p}	Scaling factor for phosphorus stress equation
κ_{1}	CBOD deoxygenation rate (day^{-1} or hr^{-1})
$\kappa_{1,20}$	CBOD deoxygenation rate at 20°C (day^{-1} or hr^{-1})
κ_{2}	Reaeration rate for Fickian diffusion (day^{-1} or hr^{-1})
$\kappa_{2,20}$	Reaeration rate at 20°C (day^{-1} or hr^{-1})
κ_{3}	Settling loss rate of CBOD (day^{-1} or hr^{-1})
$\kappa_{3,20}$	Settling loss rate of CBOD at 20°C (day^{-1} or hr^{-1})
κ_{4}	Sediment oxygen demand rate (mg O_2/(m^2· day))
$\kappa_{4,20}$	Sediment oxygen demand rate at 20°C (mg O_2/(m^2· day) or mg O_2/(m^2· hr))
λ	Latent heat of vaporization (MJ kg^{-1})
[	Lag coefficient that controls influence of previous day's temperature on current day's temperature
$[_{1}$	First shape coefficient for optimal leaf area development curve
$[_{2}$	Second shape coefficient for optimal leaf area development curve
$[_{crk}$	Lag factor for crack development during drying
$[_{sno}$	Snow temperature lag factor
μ	Specific yield of the shallow aquifer (m/m)
μ_{10m}	Mean wind speed for the day at height of 10 meters (m s^{-1})
μ_{a}	Local specific growth rate of algae (day^{-1})

$\mu_{a,20}$ Local specific algal growth rate at 20°C (day^{-1} or hr^{-1})
μ_{max} Maximum specific algal growth rate (day^{-1} or hr^{-1})
μ_{mon} Mean daily rainfall (mm H_2O) for the month
μdew_{mon} Average dew point temperature for the month (°C)
μDmx_{mon} Average daily maximum temperature of the month on dry days (°C)
$\mu Drad_{mon}$ Average daily solar radiation of the month on dry days (MJ m^{-2})
μmn_{mon} Average daily minimum temperature for the month (°C)
μmx_{mon} Average daily maximum temperature for the month (°C)
μrad_{mon} Average daily solar radiation for the month (MJ m^{-2})
μtmp_{mon} Mean air temperature for the month (°C)
μ_w Wind speed (m/s)
μWmx_{mon} Average daily maximum temperature of the month on wet days (°C)
μwnd_{mon} Average wind speed for the month (m s^{-1})
$\mu Wrad_{mon}$ Average daily solar radiation of the month on wet days (MJ m^{-2})
ν Apparent settling velocity (m/day)
θ_e Fraction of water volume that excludes anions
θ_v Volumetric moisture content (mm/mm)
θ_z Zenith angle (radians)
$\rho_0(j,k)$ Correlation coefficient between variables j and k on the same day where j and k may be set to 1 (maximum temperature), 2 (minimum temperature) or 3 (solar radiation)
$\rho_1(j,k)$ Correlation coefficient between variable j and k with variable k lagged one day with respect to variable j
ρ_a Local respiration rate of algae (day^{-1})
$\rho_{a,20}$ Local algal respiration rate at 20°C (day^{-1} or hr^{-1})
ρ_{air} Air density (kg m^{-3})
ρ_b Soil bulk density (Mg m^{-3})
ρ_s Particle density (Mg m^{-3})
ρ_w Density of water (1 Mg m^{-3})
σ Stefan-Boltzmann constant (4.903×10^{-9} MJ m^{-2} K^{-4} d^{-1})
σ_1 Local settling rate for algae (m/day)
$\sigma_{1,20}$ Local algal settling rate at 20°C (m/day or m/hr)
σ_2 Benthos (sediment) source rate for soluble P (mg P/m^2-day or mg P/m^2-hr)
$\sigma_{2,20}$ Benthos (sediment) source rate for soluble phosphorus at 20°C (mg P/m^2-day or mg P/m^2-hr)
σ_3 Benthos (sediment) source rate for ammonium (mg N/m^2-day or mg N/m^2-hr)
$\sigma_{3,20}$ Benthos (sediment) source rate for ammonium nitrogen at 20°C (mg N/m^2-day or mg N/m^2-hr)
σ_4 Rate coefficient of organic nitrogen settling (day^{-1}or hr^{-1})
$\sigma_{4,20}$ Local settling rate for organic nitrogen at 20°C (day^{-1}or hr^{-1})
σ_5 Rate coefficient for organic phosphorus settling (day^{-1}or hr^{-1})

$\sigma_{5,20}$ Local settling rate for organic phosphorus at 20°C (day^{-1}or hr^{-1})
σ_{mon} Standard deviation of daily rainfall (mm H_2O) for the month
σmn_{mon} Standard deviation for daily minimum temperature during the month (°C)
σmx_{mon} Standard deviation for daily maximum temperature during the month (°C)
σrad_{mon} Standard deviation for daily solar radiation during the month (MJ m^{-2})
ω Angular velocity of the earth's rotation (0.2618 radians h^{-1})
ω_{tmp} Angular frequency in soil temperature variation
Ψ_{wf} Wetting front matric potential (mm)